UNIVERSITY OF CALIFORNIA, SAN DIEGO

Understanding and improving the mechanical stability of semiconducting polymers for flexible and stretchable electronics

A Dissertation submitted in partial satisfaction of the requirements for the degree of Doctor of Philosophy

in

NanoEngineering

by

Adam David Printz

Committee in charge:

Professor Darren Lipomi, Chair
Professor Joseph Wang, Co-Chair
Professor Justin Opatkiewicz
Professor Yu Qiao
Professor Shyni Varghese

2015

This Dissertation of Adam David Printz is approved, and it is acceptable in quality and form for publication on microfilm and electronically:

_____

_____

_____

_____
Co-Chair

_____
Chair

University of California, San Diego

2015

DEDICATION

To Catherine

TABLE OF CONTENTS

LIST OF FIGURES

LIST OF TABLES

ACKNOWLEDGEMENTS

As the first graduate student member of the Lipomi Group, I have had the distinct privilege of seeing the entirety of the growth that the group has undergone. It has been a great pleasure to call many tremendous students my colleagues, and while I owe a debt to every single group member, there are several I feel compelled to specifically acknowledge. Suchol Savagatrup has been my partner in crime on many projects, and I can honestly say that I would not have been nearly as productive without him. I look forward to seeing the trajectory of his career and expect nothing but greatness. Aliaksandr Zaretski has been the genesis of countless interesting conversations regarding graphene, scientific philosophy, and life in general. His creativity is unbounded and I can only hope some of it has rubbed off on me. I would like to thank Daniel Burke for stimulating my interest in polymer chemistry. I also greatly appreciate his advice on dealing with administrative tasks. I am grateful to Timothy O'Connor for taking our research on fundamentals and using it to push the boundaries on devices. None of this work means anything without people like you making tangible devices. Daniel Rodriquez has been a terrific resource for discussions about the mechanical properties of organic semiconductors. I wish him the best of luck in his research, but I know he will not need it. Although our collaborations never worked out, Brandon Marin has always been a source of interesting and insightful conversations. I also would like to take this opportunity to deny whatever ridiculous quote he attributes to me in his dissertation. Thanks to Sam Root for demonstrating the potential of simulations in predicting the mechanical properties of polymers, Kirtana Rajan for helping me with circuit design, and Julian Ramirez for always being the first to volunteer for the dirty jobs.

I would not have graduated on time without the help of Esther Chan, Celine Liong, Rachel Owyeung, and especially Andrew Chiang, who played critical roles in my last two projects. I appreciate the relentless work ethic you all demonstrated, and I only hope that you learned as much from me as I did from you. I wish nothing but the best for all of you.

In addition to my labmates, there are several others I would like to thank. I would like to thank Joseph Wang, Justin Opatkiewicz, Shyni Varghese, and Yu Qiao for serving on my Senate and defense committees. I am also eternally indebted to Jan Talbot, who is the reason I joined the NanoEngineering department. Without her advice and encouragement, I am not sure where I would be today, but I certainly would not be as passionate about my work. Chris Emerson and David Szeto, you made my first year much more enjoyable. I am proud to call you friends. Amay Bandodkar, thank you for all of the help you have offered over the years. Anna Shonle, thank you for always finding time to answer my questions. Thank you Dana Jimenez for not only being great at your job, but also for being so positive while doing it.

The day Darren Lipomi hired me, my life changed for the better. His mentorship has shaped me into the best version of me I could possibly be at this stage of my career. Long after I graduate, his innovativeness, experimental rigor, and emphasis on transparent communication will continue to influence me. Perhaps most importantly, he is proof that nice guys do not finish last. If some of those praises sound familiar to you, Darren, they should. You did indeed pay it forward. It has been an absolute honor and privilege.

Finally, I would like to thank my family. My mother and father, Dianne and Edward, and my brother and sister, Kip and Carmita, have supported and encouraged me

throughout my long (and winding) journey to this point. Last, but certainly not least, I would like to thank my amazing wife Catherine. You inspire me every single day.

I also include the following acknowledgements below as required by the University of California, San Diego.

Chapter 1, in part is currently being prepared for submission for publication of the material by **Adam D. Printz** and Darren J. Lipomi. The dissertation author was the primary investigator and author of this material.

Chapter 2, in full, is a reprint of the material as it appears in *Macromolecules*, 2014, 47, 1981. American Chemical Society, 2014. Suchol Savagatrup,[†] **Adam D. Printz**,[†] Daniel Rodriquez, and Darren J. Lipomi. ([†] Equal contribution). The dissertation author was the primary investigator and author of this paper.

Chapter 3, in full, is a reprint of the material as it appears in *Synthetic Metals*, 2015, 203, 208. Elsevier B.V., 2015. Suchol Savagatrup,[†] **Adam D. Printz**,[†] Haosheng Wu, Kirtana Rajan, Eric J. Sawyer, Aliaksandr V. Zaretski, Christopher J. Bettinger, and Darren J. Lipomi, Darren J. ([†] Equal contribution). The dissertation author was the primary investigator and author of this paper.

Chapter 4, in full, is a reprint of the material as it appears in *RSC Advances*, 2014, 4, 13635. The Royal Society of Chemistry, 2014. **Adam D. Printz**,[†] Suchol Savagatrup,[†] Daniel J. Burke, Trevor N. Purdy, and Darren J. Lipomi. ([†] Equal contribution). The dissertation author was the primary investigator and author of this paper.

Chapter 5, in full, is a reprint of the material as it appears in *Solar Energy Materials & Solar Cells*, 2015, 134, 62. Elsevier B.V., 2015. **Adam D. Printz**, Suchol Savagatrup,

Daniel Rodriquez, and Darren J. Lipomi. The dissertation author was the primary investigator and author of this paper.

Chapter 6, in full, is a reprint of the material as it appears in *ACS Applied Materials & Interfaces*, 2015, 7, 23257. American Chemical Society, 2015. **Adam D. Printz**, Aliaksandr V. Zaretski, Suchol Savagatrup, Andrew S.-C. Chiang, and Darren J. Lipomi. The dissertation author was the primary investigator and author of this paper.

Chapter 7, in part is currently being prepared for submission for publication of the material. **Adam D. Printz**, Andrew S.-C. Chiang, Suchol Savagatrup, and Darren J. Lipomi. The dissertation/thesis author was the primary investigator and author of this material.

Appendix C, in full, is a reprint of the material as it appears in *PLoS ONE*, 2013, 8, e83939. **Adam D. Printz**, Esther Chan, Celine Liong, René Martinez, and Darren J. Lipomi. The dissertation author was the primary investigator and author of this paper.

VITA

2003	Bachelor of Science in Finance, University of Maryland, College Park
2011	Teaching Assistant, Department of NanoEngineering, University of California, San Diego
2012	Teaching Assistant, Department of Mechanical Engineering, University of California, San Diego
2012	Master of Science in NanoEngineering, University of California, San Diego
2012–2015	Graduate Researcher, University of California, San Diego
2015	Teaching Assistant, Department of NanoEngineering, University of California, San Diego
2015	Doctor of Philosophy in NanoEngineering, University of California, San Diego

PUBLICATIONS

T. F. O'Connor, A. V. Zaretski, S. Savagatrup, **A. D. Printz**, C. D. Wilkes, M. I. Diaz, D. J. Lipomi, "Wearable organic solar cells with high cyclic bending stability: Materials selection criteria," *Solar Energy Materials & Solar Cells*, 2015, 144, 438.

A. D. Printz, A. V. Zaretski, S. Savagatrup, A. S-C. Chiang, and D. J. Lipomi, "Yield Point of Semiconducting Polymer Films on Stretchable Substrates Determined by Onset of Buckling," *ACS Applied Materials & Interfaces,* 2015, 7, 23257.

P. B. Landon, A. H. Mo, **A. D. Printz**, C. Emerson, C. Zhang, W. Janetanakit, D. A. Colburn, S. Akkiraju, S. Dossou, B. Chong, G. Glinsky, and R. Lal, "Asymmetric Colloidal Janus Particle Formation is Core Size Dependent," *Langmuir*, 2015, 31, 9148.

S. Savagatrup, D. Rodriquez, **A. D. Printz**, A. B. Sieval, J. C. Hummelen, and D. J. Lipomi, "[70]PCBM and Incompletely Separated Grades of Methanofullerenes Produce Bulk Heterojunctions with Increased Robustness for Ultra-Flexible and Stretchable Electronics," *Chemistry of Materials*, 2015, 27, 3902.

T. F. O'Connor, K. M. Rajan, **A. D. Printz**, and D. J. Lipomi, "Toward Organic Electronics with Properties Inspired by Biological Tissue," *Journal of Materials Chemistry B*, 2015, 3, 4947.

S. Savagatrup[†], **A. D. Printz**[†], H. Wu, K. M. Rajan, E. J. Sawyer, A. V. Zaretski, C. J. Bettinger, and D. J. Lipomi, "Viability of Stretchable Poly(3-heptylthiophene) (P3HpT) for Organic Solar Cells and Field-Effect Transistors," *Synthetic Metals*, 2015, 203, 208. ([†] *Equal contribution*)

A. V. Zaretski, H. Moetazedi, C. Kong, E. J. Sawyer, S. Savagatrup, E. Valle, T. F. O'Connor, **A. D. Printz**, and D. J. Lipomi, "Metal-Assisted Exfoliation (MAE): Green, Roll-to-Roll Compatible Method for Transferring Graphene to Flexible Substrates," *Nanotechnology*, 2015, 26, 045301.

A. D. Printz, S. Savagatrup, D. Rodriquez, and D. J. Lipomi, "Role of Molecular Mixing on the Stiffness of Polymer:Fullerene Bulk Heterojunction Films," *Solar Energy Materials & Solar Cells*, 2015, 134, 62.

S. Savagatrup, E. Chan, S. M. Renteria-Garcia, **A. D. Printz**, A. V. Zaretski, T. F. O'Connor, D. Rodriquez, E. Valle, and D. J. Lipomi, "Plasticization of PEDOT:PSS by Common Additives for Mechanically Robust Devices and Wearable Sensors," *Advanced Functional Materials*, 2015, 4, 13635.

S. Savagatrup, **A. D. Printz**, T. F. O'Connor, A. V. Zaretski, D. Rodriquez, E. J. Sawyer, K. Rajan, R. I. Acosta, S. E. Root, and D. J. Lipomi, "Mechanical Degradation and Stability of Organic Solar Cells: Molecular and Microstructural Determinants," *Energy and Environmental Science*, 2015, 8, 55.

E. J. Sawyer, S. Savagatrup, T. F. O'Connor, A. S. Makaram, D. J. Burke, A. V. Zaretski, **A. D. Printz**, D. J. Lipomi, "Toward Intrinsically Stretchable Organic Semiconductors: Mechanical Properties of High-Performance Conjugated Polymers," *Proc. SPIE 9185, Organic Field-Effect Transistors XIII; and Organic Semiconductors in Sensors and Bioelectronics VII, 91850U (October 7, 2014); doi:10.1117/12.2059098*

P. B. Landon, A. H. Mo, C. Zhang, C. Emerson, **A. D. Printz**, A. F. Gomez, C. J. DeLaTorre, D. A. M. Colburn, P. Anzenberg, M. Eliceiri, C. O'Connell, and R. Lal, "Designing Hollow Nano Gold Golf Balls," *ACS Applied Materials & Interfaces*, 2014, 6, 9937.

S. Savagatrup, **A. D. Printz**, T. F. O'Connor, A. V. Zaretski, and D. J. Lipomi, "Molecularly Stretchable Electronics," *Chemistry of Materials*, 2014, 26, 3028.

S. Savagatrup[†], **A. D. Printz**[†], D. Rodriquez, and D. J. Lipomi, "Best of Both Worlds: Conjugated Polymers Exhibiting Good Photovoltaic Properties and High Tensile Elasticity," *Macromolecules*, 2014, 47, 1981. ([†] *Equal contribution*)

A. D. Printz[†], S. Savagatrup[†], D. J. Burke, T. N. Purdy, and D. J. Lipomi, "Increased Elasticity of a Low-Bandgap Conjugated Polymer by Random Segmentation for Mechanically Robust Solar Cells," *RSC Advances*, 2014, 4, 13635. ([†] *Equal contribution*)

T. F. O'Connor, A. V. Zaretski, B. A. Shiravi, S. Savagatrup, **A. D. Printz**, M. I. Diaz, and D. J. Lipomi, "Stretching and Conformal Bonding of Organic Solar Cells to Non-Planar Substrates," *Energy & Environmental Science*, 2014, 7, 370.

A. D. Printz, E. Chan, C. Liong, R. S. Martinez, and D. J. Lipomi, "Photoresist-Free Patterning by Mechanical Abrasion of Water-Soluble Lift-Off Resists and Bare Substrates: Toward Green Fabrication of Transparent Electrodes," *PLoS One*, 2013, 8, e83939.

ABSTRACT OF THE DISSERTATION

Understanding and improving the mechanical stability of semiconducting polymers for flexible and stretchable electronics

by

Adam David Printz

Doctor of Philosophy in NanoEngineering

University of California, San Diego, 2015

Professor Darren J. Lipomi, Chair
Professor Joseph Wang, Co-Chair

Polymeric semiconductors offer the promise of low-cost, printable, and mechanically robust electronic devices for use in outdoor, portable, and wearable applications such as organic photovoltaics, biosensors, and electronic skins. However,

many organic semiconductors are unable to accommodate the mechanical stresses these applications require, and it is therefore important to understand the factors and parameters that govern the mechanical stability of these materials. Chapter 1 provides a gentle introduction to the electronic and mechanical properties relevant to flexible and stretchable organic semiconductor devices. The idea of inherent competition between electronic performance and mechanical robustness is explored. Chapter 2 investigates the inherent competition between good electronic performance and mechanical robustness in poly(3-alkylthiophene)s. A key finding is a critical alkyl side-chain length that allows for good electronic performance and mechanical compliance. Chapter 3 and Appendix A are further studies on the properties of poly(3-alkylthiophene)s with side-chains close to the critical length to gain better understanding of the transition from good electronic properties and poor mechanical properties to poor electronic properties and good mechanical properties. Chapter 4 and Appendix B detail the effects on mechanical and electronic properties of statistical incorporation of unlike monomer into a low-bandgap polymer backbone in an effort to disrupt aggregation and improve mechanical compliance. Chapter 5 explores how the extent of molecular mixing of polythiophenes and fullerenes—materials common in organic photovoltaics—affects their mechanical properties. Chapter 6 describes the invention of a new technique to determine the yield point of thin films. A dependence on the alkyl-side chain length is observed, as well as a critical film thickness below which the yield point increases substantially. In Chapter 7, the weakly interacting H-aggregate model—a spectroscopic model which estimates the quantity and quality of aggregates in a polymer film—is used to determine how the microstructure of a semiconducting polymer thin film evolves with repetitive strain. Samples strained below the yield point undergo

little microstructural evolution, while samples strained above the yield point exhibit a significant decrease in aggregation and tensile modulus. Appendix C describes the invention of an environmentally-friendly fabrication technique, abrasion lithography.

Chapter 1

Competition between deformability and charge transport in organic semiconducting polymers for flexible and stretchable electronics

Adam D. Printz and Darren J. Lipomi

Department of NanoEngineering, University of California, San Diego

9500 Gilman Drive, Mail Code 0448, La Jolla, CA 92093-0448

Abstract

The primary goal of the field concerned with organic semiconductors is to produce devices with performance approaching that of silicon electronics, but with the deformability—flexibility and stretchability—of conventional plastics. However, an inherent competition between deformability and charge transport has long been observed in these materials, and achieving the extreme (or even moderate) deformability implied by the word "plastic" concurrently with high charge transport may be elusive. This competition arises because the properties needed for high carrier mobilities—e.g., rigid chains in π-conjugated polymers and high degrees of crystallinity in the solid state—are antithetical to deformability. On the device scale, this competition leads to low-mobility, yet mechanically robust devices, or high-mobility devices that fail catastrophically (e.g., cracking, cohesive failure, and delamination) under strain. There are, however, some observations that contradict the notion of the mutual exclusivity of electronic and mechanical performance. These observations suggest that this problem may not be a fundamental trade-off, but rather an inconvenience that may be negotiated by a logical selection of materials and processing conditions. For example, the selection of the poly(3-alkylthiophene) with a critical side-chain length—poly(3-heptylthiophene) (n = 7)—married the high deformability of poly(3-octylthiophene) (n = 8) with the high electronic performance (as manifested in photovoltaic efficiency) of poly(3-hexylthiophene) (n = 6). This review explores the relationship between deformability and charge transport in organic semiconductors. The principal conclusions are that to reduce the competition between these two parameters, the following design rules are identified: (1) decreasing the T_g of the polymer, with one possible route being the lengthening of alkyl side-chains

to a critical length, *n*, (2) mixing highly deformable materials with high-mobility materials, (3) promotion of moderate disorder in the solid state, and (4) the introduction of additives that behave as plasticizers. The aim of this review is to describe the current state of knowledge of the molecular determinants of deformability and charge transport, what morphological factors are critical for each, and how to decouple their mutual incompatibility. Such an understanding would allow for rational design of materials for applications requiring large-area, low-cost, printable devices that are ultra-flexible or stretchable, such as organic photovoltaic devices and wearable, conformable, or implantable sensors.

1.1 Introduction

Organic semiconductors have recently exhibited hole mobilities over 40 $cm^2\ V^{-1}\ s^{-1}$ in organic field effect transistors (OFETs)[1] and power conversion efficiencies (*PCE*) over 10% in organic photovoltaics (OPVs).[2–4] Organic semiconductors also promise high flexibility and stretchability which allows for many applications previously impossible (or much more expensive) with stiffer inorganic materials.[5–8] Inorganic materials can be patterned to allow for stretchability (e.g., sinusoidal buckles),[9–11] however replacing these patterned materials with those with intrinsic stretchability would allow for simplification of the fabrication and increase functionality by using materials that can be tailored on the molecular scale.[12–14] However, there is an apparent competition between good electronic performance—as manifested in charge-carrier mobility and photovoltaic efficiency—and desirable mechanical properties such as high deformability and elastic range.[7,15–17]

Overcoming this apparent competition and coupling good electronic performance and deformability into a single material would facilitate high performance, yet low-cost,[18–20] printable,[21–25] wearable,[26,27] and mechanically robust devices.[28,29] It is therefore important to understand what parameters affect these properties and determine if it is indeed possible to co-optimize desirable properties. Parameters that are frequently studied are the rigidity of the organic semiconductor backbone,[30,31] the length and branching of the solubilizing side-chains (required because unsubstituted conjugated polymers are insoluble in common solvents),[7,13,32–34] processing conditions such as solvent evaporation rate[16] and annealing,[35–39] and molecular orientation.[40–45]

The most studied family of conjugated polymers in the literature are poly(3-alkylthiophene)s (P3ATs, **Figure 1.1**), because they are a simple model system with a repeat unit composed of a thiophene moiety and a solubilizing alkyl side-chain substituted at the 3-position. P3ATs have been the subject of studies including the effects of molecular weight,[46–51] processing conditions including solvent deposited from,[52,53] film thickness,[54] film morphology,[55,56] alkyl side-chain length,[38,57,58] and regioregularity.[59] Another group of commonly studied polymers are those based on diketopyrrolopyrrole (DPP) units.[41,60–64] DPP-based polymers are of interest, in part, because they have a narrow bandgap, meaning they can absorb light at longer wavelengths (and therefore better overlap with the solar spectrum), which ideally leads to better photovoltaic performance than P3ATs (and other materials with relatively higher bandgaps).[60] DPP-based polymers incorporating both electron donor and electron acceptor units along the backbone have also exhibited hole mobilities above 12 $cm^2\ V^{-1}\ s^{-1}$.[61] Small molecules, and specifically fullerene derivatives, such as [6,6]-phenyl-C61-

butyric acid methyl ester ($PC_{61}BM$) and [6,6]-phenyl-C71-butyric acid methyl ester ($PC_{71}BM$), are commonly blended with polymers and act as electron acceptors in photovoltaic devices. They have high embodied energy and generally embrittle films,[20,65] which has led to many researchers looking to replace fullerenes with small molecule[66] or polymer electron acceptors[67–69] such as in block copolymers with PFTBT.[70]

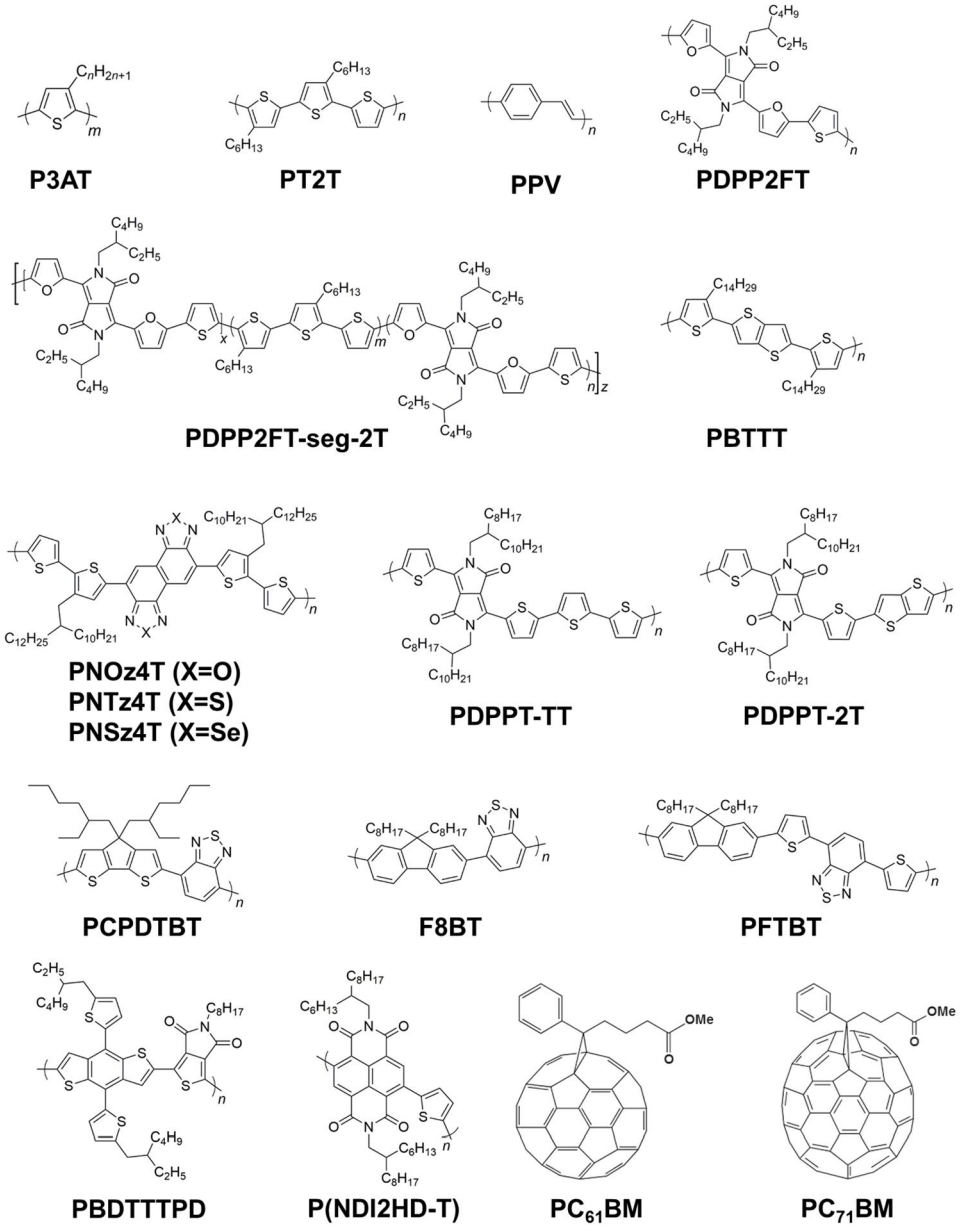

Figure 1.1. Molecular structures of the organic semiconductors discussed in this review.

The aim of this review is to bridge the knowledge of the fields interested in electronic properties and mechanical properties of organic semiconductors. We do this with the hope that researchers will focus on the likely applications for organic semiconductors: printable, wearable, and implantable devices, which require not only good electronic performance, but frequently good deformability and robustness as well. In the following sections, we have included brief introductions to the measurement of electronic and mechanical properties relevant in organic electronic devices. Due to the limited literature on the mechanical properties of small molecules, the scope of this review is focused on polymer and, because of their relevance to organic photovoltaics, polymer:fullerene composites.

1.2 Device physics

Charge transport and the factors governing it in organic semiconductors have been studied extensively.[71–73,44,74,75] Organic semiconductors conduct charge because of their molecular conjugation—the alternation of single and double bonds between carbon atoms—which results in the delocalization of electrons. In general, electronic performance in organic semiconductors depends on their solid-state packing structure.[72] Packing dictates intermolecular electronic coupling (which is determined by the wavefunction overlap or the π-π stacking distance) and thus the charge transport.[72] Aggregates and crystallites typically have a smaller π-π stacking distance than amorphous polymer, and therefore tend to have higher mobilities.[74] While these crystallites and aggregates are frequently required for high electronic performance, they are stiffer than

disordered amorphous polymer and therefore tend to decrease deformability of films. Aggregates of planar polymers and small molecules such as poly(3-hexylthiophene) (P3HT) generally exhibit anisotropy along three axes (**Figure 1.2**). The a-axis is the lamellar stacking axis and it is the direction of the slowest charge transport. The b-axis is the π-π stacking axis and has relatively fast charge transport. The c-axis is along the conjugated backbone and because of the covalently linked conjugated units, charge transport is highest in this direction.[74,76,77]

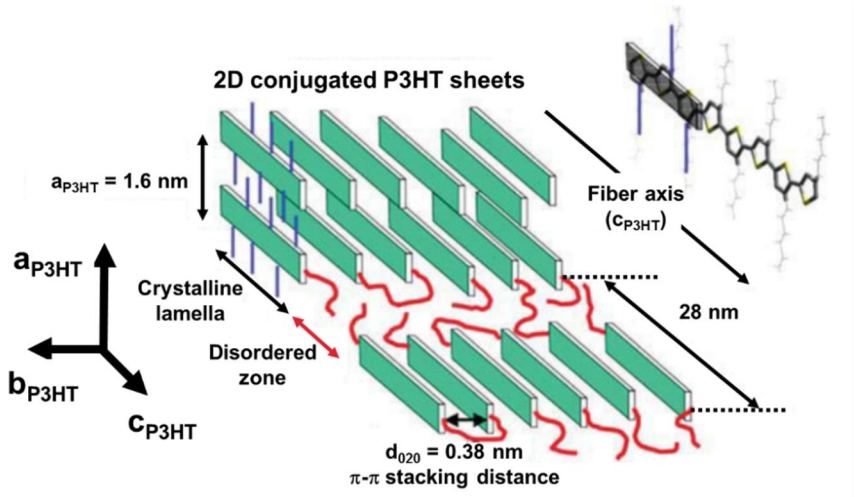

Figure 1.2. The stacking structure of P3HT. Charge mobility is highest along the fiber axis or backbone (c_{P3HT}) and lower in the π-π stacking direction (b_{P3HT}). Negligible transport occurs in the a_{P3HT} direction. Reproduced with permission from ref. 77. Copyright 2011, Wiley-VCH Verlag GmbH & Co. KGaA.

Transfer of charge through a film requires a percolated network of conjugation, usually through well-ordered polymer aggregates (whose presence in some materials is correlated with stiffness and brittleness).[74,78,79] Aggregates are required for charge transport because of their greater conjugation when compared to less ordered or completely amorphous regions (where kinks lead to disruption of conjugation).[79,80] However, at the boundary of each aggregate is amorphous polymer which can disrupt

charge transport due to the lack of conjugation, and in non-percolated networks, the disruption in charge transport by amorphous polymer would be the limiting factor in charge-carrier mobility.[81] To bypass these amorphous regions, aggregates in percolated films are connected by polymer chains with intact conjugation—or "tie-chains"—allowing charge to be transported efficiently from aggregate to aggregate, resulting in a high mobility.[74] This high mobility leads to enhanced performance of organic electronic devices, specifically organic field effect transistors (OFETs) and organic photovoltaic (OPV) devices.

In OFETs, current is controlled by voltage and is dependent on the carrier mobility in the semiconducting layer. There are three general classes of transistors: p-channel, n-channel, and ambipolar. The charge carriers are holes in p-channel transistors, and electrons in n-channel transistors, while the charge carriers can be holes or electrons depending on operating parameters—that is, the source-drain and source-gate voltages—in ambipolar transistors. OFETs can have many different architectures, but in typically they comprise a source (or charge-injecting) electrode and drain (or charge-extracting) electrode lying in the same plane, a semiconductor layer filling the channel between the source and drain, a gate dielectric layer atop or below the semiconductor, and a gate electrode in contact with the dielectric layer (but not the semiconductor). An example of a bottom-gate coplanar OFET is shown in **Figure 1.3a**. Briefly, transistors operate in the following manner. A voltage is applied between the source and the gate electrodes, V_G, which causes a mobile layer of charge to form in the semiconductor at the interface of the dielectric. The number of mobile charges is proportional to V_G and the capacitance of the dielectric, C_d. There are also deep trap states that must be filled before the induced

charges can be mobile and the bias required to fill these trap states is the threshold voltage, V_{Th}. Therefore, the effective voltage that the mobile carriers are proportional to is $V_G - V_{Th}$. In the case of a p-channel transistors—*e.g.*, semiconductor layers of P3HT or PBTTT—V_G is much lower than 0 V and the highest occupied molecular orbital (HOMO) and lowest unoccupied molecular orbital (LUMO) bands of the semiconductor bend up, resulting in the accumulation of holes at the semiconductor/dielectric interface (**Figure 1.3b, left**). In n-channel transistors—*e.g.*, semiconductor layers of poly(9,9-dioctylfluorene-alt-benzothiadiazol) (F8BT) or poly(p-phenylene-vinylene) (PPV)[82]—V_G is greater than 0 V and the HOMO and LUMO bands of the semiconductor bend down, resulting in the accumulation of electrons at the semiconductor/dielectric interface (**Figure 1.3b, right**). In p-channel transistors, the energy barrier between the HOMO of the semiconductor and the Fermi energy level (E_F) of the source and drain must be as small as possible, or in other words, the ionization potential (IP) of the semiconductor should be similar to the work function (WF) of the source and drain. In n-channel transistors, it is instead desirable for the energy barrier between the LUMO (rather than the HOMO) and the E_F of the source and drain to be small as possible, that is, the electron affinity (EA) of the semiconductor should be similar to the WF of the source and drain. An additional voltage is applied between the source and drain, V_{DS}, which offsets the energy levels of the source and drain and bends the HOMO and LUMO levels of the semiconductor (**Figure 1.3c**). When $0 < V_{DS} << V_G$, a linear gradient of charge density occurs from the source to drain. The potential at the source is 0 and increases linearly through the channel until it reaches V_{DS} at the drain. The current flowing through the channel from source to drain, I_{DS}, is proportional to V_{DS} in this "linear regime." When

V_{DS} is increased, at some point, it will be equal to $V_G - V_{Th}$.[83] At the drain, the channel is "pinched off" because the difference between the local potential and the gate voltage is below the threshold voltage. A depletion region results and its high electric field allows current to be swept across to the drain at a saturation current $I_{DS,sat}$. As V_{DS} is increased further, there is no (substantial) increase in current, and instead the depletion region expands and the channel becomes slightly shorter. This regime, where the current remains constant as V_{DS} is increased is the "saturation regime."

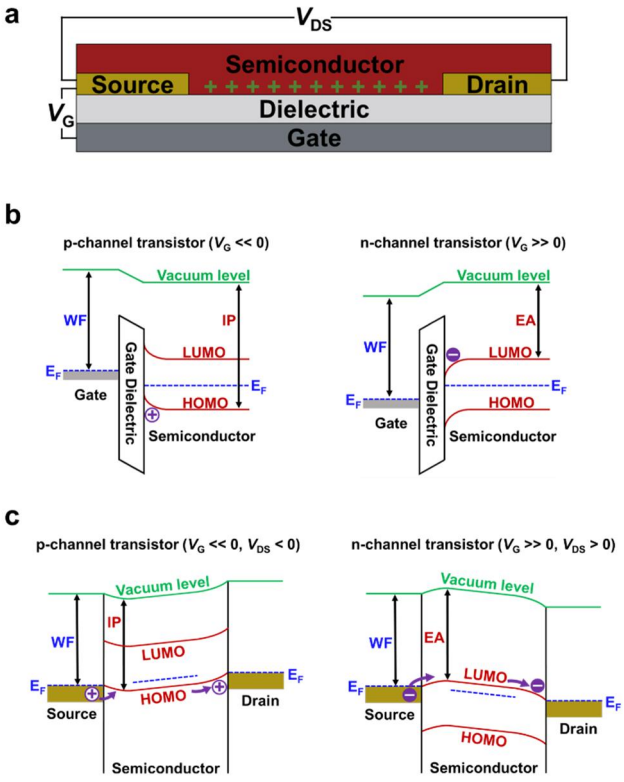

Figure 1.3. Organic field effect transistor (OFET) operation. (a) A bottom-gate (inverted) coplanar OFET. This is a p-channel transistor with holes accumulating at the interface of the semiconductor and dielectric due to the gate voltage, V_G. (b) Energy-level diagrams across the semiconductor/dielectric interface of p-channel and n-channel transistors. Holes accumulate at the semiconductor/dielectric interface in p-channel transistors (left) and electrons accumulate at the interface in n-channel transistors (right). (c) Energy-level diagrams of the carrier channel for p-channel and n-channel transistors. Holes travel from the source to drain through the semiconductor in the p-channel transistor (left), while electrons travel from the source to drain in the n-channel transistor (right). Abbreviations: WF: work function; IP: ionization potential; EA: electron affinity; LUMO: lowest unoccupied molecular orbital; HOMO: highest occupied molecular orbital; E_F: Fermi energy level. (b) and (c) Reproduced with permission from ref. 84. Copyright 2010, The Royal Society of Chemistry.

Typically, OFET data is plotted as the source-drain current versus the source-drain voltage—*i.e.*, the output plot—or the source-drain current versus the gate voltage—*i.e.*, the transfer plot. In the output plot (**Figure 1.4a**), the source-drain current initially increases with the source-drain voltage linearly (the linear regime). In the linear regime, when $V_{DS} << V_G$ (**Figure 1.4b**), the field-effect mobility, μ_{lin}, can be extracted from the linear fit of the slope of I_{DS} vs. V_G using equation 1:

$$I_{DS} = \mu_{lin} C_d \frac{W}{L} (V_G - V_{Th}) V_{DS} \quad (\mathbf{1})$$

where W and L are the semiconductor channel width and length, respectively (remember that C_d is the dielectric capacitance). The onset voltage, V_{on}, or the voltage at which I_{DS} increases quickly can be found in the log(I_{DS}) vs. V_G plot (**Figure 1.4b**). In the saturation regime, $V_{DS} > V_G - V_{Th}$ (**Figure 1.4c**), the field effect-mobility, μ_{sat}, can be extracted from the slope of the linear fit in the saturation regime on the plot of $(I_{DS,sat})^{1/2}$ vs. V_G, and the threshold voltage, V_{Th}, can be extracted from the interception of the linear fit and the x-axis using equation 2:[85,86]

$$I_{DS,sat} = \mu_{sat} C_d \frac{W}{2L} (V_G - V_{Th})^2 \quad (\mathbf{2})$$

In addition to charge-carrier mobility, the other important material parameter for OFETs is the on/off ratio, which is the ratio of the maximum drain current in the on-state of the transistor to the minimum drain current in the off-state of the transistor. A high on/off ratio is desirable since it is essentially the signal-to-noise ratio for a transistor.

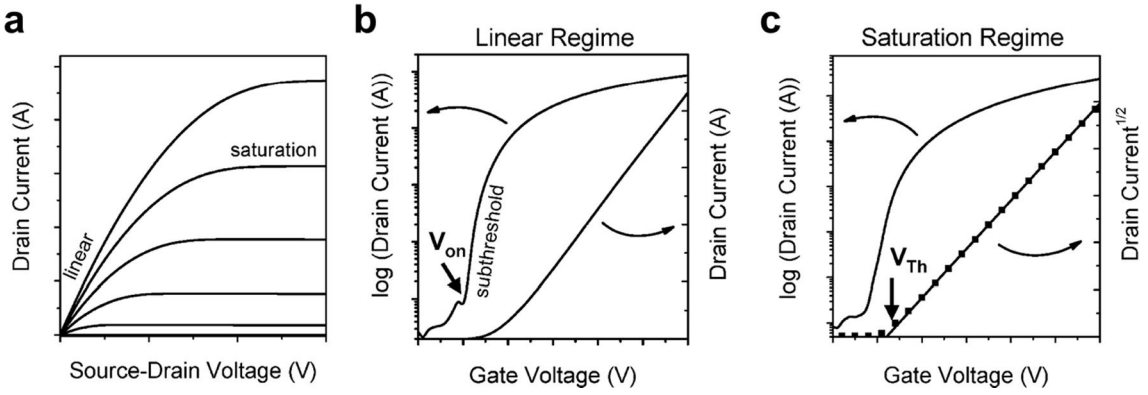

Figure 1.4. Hypothetical output and transfer plots for an OFET. (a) Output plot of the source-drain current versus the source-drain voltage. (b) Transfer plot of the source-drain current versus the gate voltage for a typical OFET in the linear regime. (c) Transfer plot of the source-drain current versus the gate voltage for a typical OFET in the saturation regime. Reproduced with permission from ref. 83. Copyright 2007, American Chemical Society.

Charge transport in OPV devices manifests principally in the short-circuit current and fill factor (and thus in the power conversion efficiency). Typically, the device architecture of OPVs is a stack comprising an electrode, an active layer consisting of an intimately mixed electron donating material with an electron accepting material—known as a bulk heterojunction (BHJ)—and a transparent electrode (**Figure 1.5a**). Depending on the molecular components, the bulk heterojunction can take on many different morphologies. For polymer-fullerene bulk heterojunctions, these morphologies include a molecularly mixed amorphous composite, a ternary blend with pure or enriched phases separated by mixed phases, or a well ordered blend with bimolecular crystallization (**Figure 1.5a**).[87] The operation of OPVs is detailed in **Figure 1.5b**. In step (1), light is absorbed by the BHJ—typically by the electron donor—and it excites an electron from the HOMO to the LUMO. Upon excitation of the electron to the LUMO, there in an absence of an electron in the HOMO level, which is known as a hole. This electron-hole pair—or exciton—is tightly bound because of the relatively low dielectric constant of organic photovoltaics. (In inorganic devices, the dielectric constant is higher and

effectively screens the charges of the electron and hole, allowing them to separate and diffuse through the device).[88] (2) Excitons diffuse through the film until they reach an interface of the electron donor and acceptor, or until they recombine. The exciton diffusion length is on the order of 10 nm, so ideally donor and acceptor phases will be sufficiently small to allow for excitons to diffuse to interfaces before they have the opportunity to recombine.[89] (3) In the case where an interface is reached, if the energetics are favorable, the electron will transfer to the electron acceptor; the exciton binding energy is ~0.3-0.5 eV, so an offset of the LUMOs of the donor and the acceptor of at least 0.3 eV is usually required to allow for charge separation.[88] (4), (5) Once the charges separate at the donor/acceptor interface, the electrons will travel through the acceptor toward the cathode (the electrode with the relatively lower work function), and the holes will travel through the donor toward the anode (the electrode with the relatively higher work function).

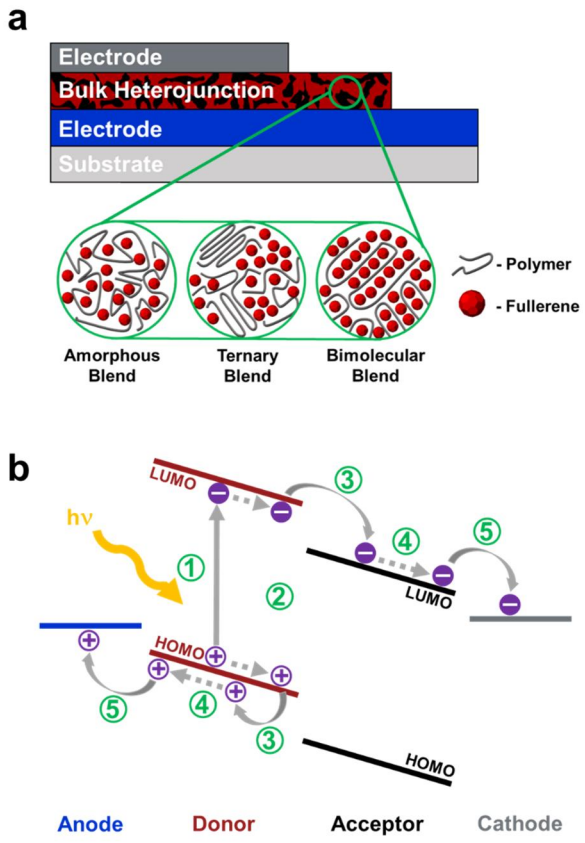

Figure 1.5. Organic photovoltaic (OPV) operation. (a) A conventional OPV architecture with a polymer:fullerene bulk heterojunction (BHJ) active layer. The three potential morphologies of the BHJ are highlighted: an amorphous blend of electron donor and acceptor; a ternary blend with pure or enriched phases of donor or acceptor surrounded by disordered blends of the two; an intimately mixed bimolecular blend, with the fullerene aligning along the chains of the polymer. (b) Hypothetical energy-level diagrams for the OPV device in (a). Light is absorbed and a tightly bound electron-hole pair (exciton) is created in step 1, followed by diffusion of the exciton to the donor/acceptor interface in step 2. The charges then separate with the electron jumping to the acceptor and the hole able to freely move in the donor (step 3). The charges then drift towards the electrodes (the holes toward the anode and the electrons toward the cathode, step 4) and then finally are transferred to the electrodes (step 5).

Device measurements are typically made by sweeping the electrode voltage, V, and plotting it against the current density, J. A hypothetical J-V curve of an OPV device is shown in **Figure 1.6**. The points of interest are the short-circuit current density, J_{SC}, which is the current density when the device is at zero voltage, the open-circuit voltage, V_{OC}, which is the voltage when there is no current flowing, and the maximum power point, P_{max}, which is the point at which the product of the current density and voltage is at

its maximum. The current density and voltage at P_{max} are J_{max} and V_{max}, respectively, and these can be used to determine the fill factor, *FF*, by equation 3:

$$FF = \frac{J_{max}V_{max}}{J_{SC}V_{OC}} \quad (\mathbf{3})$$

The ideal *J-V* curve is a rectangle, and as the experimental curve becomes more rectangular (assuming J_{max} approaches J_{SC} and V_{max} approaches V_{OC}), the *FF* approaches unity. However, in practice, losses due to resistance in the electrodes and contacts (*i.e.*, series resistance, R_{series}) and shunting due to defects in the film (represented by the shunt resistance, R_{shunt}) prevent a *FF* of unity. The power conversion efficiency, which is the ratio of power output of the device to the power incident (the amount of power contributed by the sunlight), P_{inc}, (100 mW cm^{-2} at AM 1.5G), can then be calculated by equation 4:

$$PCE = \frac{P_{max}}{P_{inc}} = \frac{J_{SC}V_{OC}FF}{P_{inc}} \quad (\mathbf{4})$$

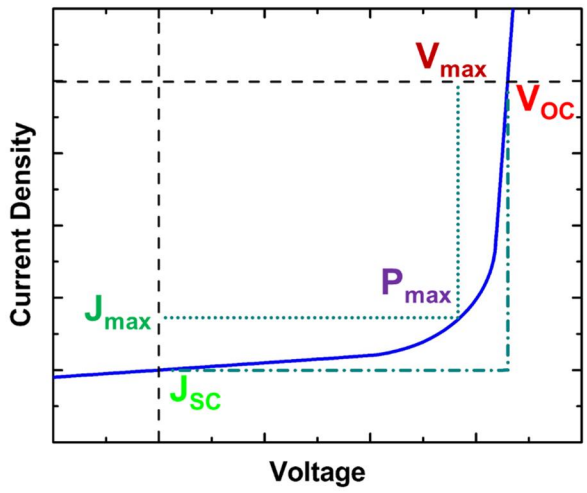

Figure 1.6. Hypothetical *J-V* curve for an organic photovoltaic. The short-circuit current density, J_{SC}, is the current when the voltage across the cell is zero (the dashed black lines), and the open-circuit voltage, V_{OC}, is the voltage when the current is zero. J_{max} and V_{max} are the current density and voltage at the point of maximum power point, P_{max}. The fill-factor, *FF*, is the ratio of the rectangle created from the origin to J_{max} and V_{max} (dotted line) to the rectangle created from the origin to J_{SC} and V_{OC} (dash-dot line).

While the *PCE* is not a measurement of only the semiconductor charge transport properties due to contributions from the contacts, it is a reasonable method to obtain a qualitative understanding of electronic performance for similar materials and device architecture.

Increasing aggregation and crystallinity of the organic semiconductors frequently play a role in improving the charge transport properties of the film. X-ray diffraction is often utilized to determine ordering of organic semiconductor films, and improved ordering has been correlated to improved charge-carrier mobility in many different systems (but also to a reduction in compliance and ductility).[46,90,91] The microstructure of films of P3HT have shown to contribute greatly to mobility. For example, the hole mobility, μ_h, of poorly ordered regiorandom P3HT is several orders of magnitude lower than more ordered films of highly regioregular P3HT.[84] In another example, Kawashima and coworkers recently reported that increased disorder in naphthobischalcogenadiazole-based π-conjugated polymers dramatically affected μ_h.[91] The polymers studied were PNOz4T, which consists of a naphtho[1,2-c:5,6-c′]bis[1,2,5]oxadiazole flanked by 4 thiophenes (with the two thiophenes directly flanking the napthooxadiazole having alkyl side-chains in the 3-position), and PNSz4T, which replaces the oxadiazole with a selenadiazole. 2D GIXD showed that PNSz4T was mostly amorphous—which was coupled with a low μ_h, 0.01 $cm^2\ V^{-1}\ s^{-1}$—while PNOz4T exhibited greater order (and a much higher μ_h of 1 $cm^2\ V^{-1}\ s^{-1}$).[91] The increased order in PNOz4T compared to PNSz4T was attributed to the selenium atom of PNSz4T being much larger than oxygen in PNOz4T and causing steric repulsion between neighboring polymer chains.

Another technique for quantifying the order in polymer thin films is fitting the weakly interacting H-aggregate model developed by Spano to UV-vis absorption spectra.[52,76,80,92,93] The absorption by a polymer is the convolution of absorption by the ordered aggregates as well as the disordered amorphous regions of the film. The weakly interacting H-aggregate model calculates the absorption by the different vibronic states in the polymer aggregates—which when added together gives the total absorption by the aggregates—based on Gaussian fits to the experimental spectra using equation 5:

$$A(E) \propto \sum_{m=0} \left(\frac{S^m}{m!}\right) \times \left(1 - \frac{We^{-S}}{2E_{\mathrm{p}}} \sum_{n \neq m} \frac{S^n}{n!\,(n-m)}\right)^2 \times exp\left(\frac{-\left(E - E_{00} - mE_{\mathrm{p}} - \frac{1}{2}WS^m e^{-S}\right)^2}{2\,\sigma^{\,2}}\right) \quad (\mathbf{5})$$

where A is the absorption by an aggregate as a function of the photon energy (E). S is the Huang-Rhys factor, which is calculated from absorption and emission spectra.[80] E_{p} is the intermolecular vibration energy and is determined by Raman spectroscopy. The variables W, σ, E_{00}, and a scaling factor are then adjusted to fit the model to the experimental spectrum. E_{00} is the energy of the 0→0 vibronic transition, which is allowed assuming some disorder in the aggregates.[80] W is the free exciton bandwidth, which is related to the nearest neighbor interchain excitonic coupling. Upon coupling, a dispersion of the energies occurs, the width of which is equal to W (which is four times the nearest neighbor coupling). σ is the Gaussian linewidth and the terms m and n are the ground- and excited state vibrational levels.

Once the absorption by the aggregates is calculated, it can then be subtracted from an experimental spectrum to determine the amount of absorption by the amorphous regions of the film. This information can then be used to estimate the proportion of

aggregates in the films. Additional information about the quality of the aggregates (*e.g.*, *W*, which is inversely related to conjugation length) can also be determined from the weakly interacting H-aggregate model. This model has been used to look at the effects of solvents,[52] solvent evaporation rates,[16] annealing temperature,[93] and side-chain length.[7]

1.3 Deformability

Mechanical properties of organic semiconductors are challenging to measure by traditional bulk measurement techniques such as tensile testing because laboratory-scale synthesis of new materials may obtain only a few hundred milligrams. Even in the case of large-batch production, tensile testing would not be ideal because of the difficulty associated with isolating and manipulating a film of sub-micron thickness. To overcome these problems and measure the mechanical properties of thin films, several non-bulk techniques have been developed. Many of these techniques rely on film-on-elastomer (FOE) systems, in which a thin film is either coated directly or transferred onto an elastomeric substrate. Properties such as the tensile modulus,[7,16,32,94] the failure point (or crack-onset strain),[16,32,95] and the yield point,[96–98] can be readily measured by these techniques. The tensile modulus, E_{film}, is a measure of how a material accommodates strain in the elastic (or linear) regime of its stress-strain response. A low tensile modulus (highly deformable in the elastic regime) is prerequisite for applications requiring conformal bonding such as wearable[99–102] or implantable biosensors,[103,104] or more generally, any applications in which deformation occurs in two or three dimensions,[28] such as bonding to objects with geometries that are neither planar nor cylindrical. The crack-onset strain (*CoS*), or the strain at which a device fractures and fails, is a measure

of material ductility and is a significant parameter to consider when designing devices.[32,95] When creating devices for applications where high strain is required, selection of a material that cannot undergo much strain before cracking would be a poor design choice. Likewise, knowledge of the yield point is driven by the same argument. The yield point, which is the strain at which the material begins to plastically or permanently deform, is also associated with changes in the electronic performance.[43,105] While plastic deformation can lead to chain alignment and improved mobility parallel to the axis of strain while the film is in the strained state, it has deleterious effects perpendicular to the strain.[43] Upon relaxation of the strain, the chain alignment is not permanent, and the increased disorder from the plastic deformation most likely has deleterious effects on device performance. A stress-strain curve for a hypothetical polymer is shown in **Figure 1.7**. Properties that can be easily measured by film-on-elastomer techniques (discussed below) are highlighted in green. Adhesion and cohesion of device layers are also important properties for mechanical robustness, but they are not measured by traditional stress-strain responses.[106–108]

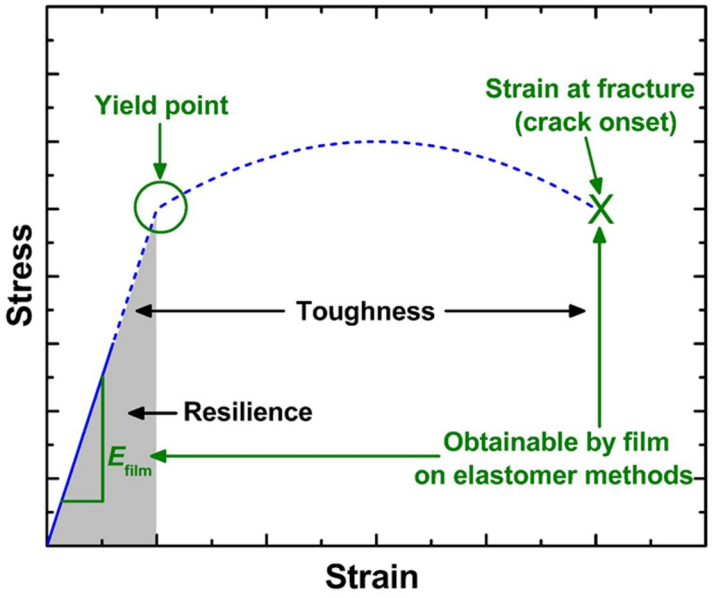

Figure 1.7. The stress-strain response for a hypothetical polymer. The tensile modulus, E_f, the yield point, and the strain at fracture are obtainable by film on elastomer methods. Reproduced with permission from ref. 98. Copyright 2015, American Chemical Society.

Stafford et al. developed a buckling-based metrology to measure the tensile modulus for FOE systems such as polystyrene and poly(methyl methacrylate).[94,109,110] In one implementation of this technique, the material of interest is spun onto a glass slide and then transferred to an elastomeric substrate that has been strained by a few percent before the film transfer. The strain is then released and the film then forms sinusoidal buckles out of plane **(Figure 1.8a**). The wavelength of the buckles is determined by the energy balance between the amount of energy it takes to deform the relatively soft elastomeric substrate and the amount of energy it takes to bend the relatively stiff thin film. The buckling wavelength has a linear dependence on the film thickness (*e.g.*, thicker films are more rigid, which leads to a higher buckling wavelength). The tensile modulus of the film, E_{film}, can then be related to the buckling wavelength, λ_b, and the film

thickness, d_f, as well as the tensile modulus of the elastomeric substrate, E_s, and the Poisson's ratios of the thin film, ν_f, and the substrate, ν_s, by equation 6:[94]

$$E_{film} = 3E_s\left(\frac{1-\nu_f^2}{1-\nu_s^2}\right)\left(\frac{\lambda_b}{2\pi d_f}\right)^3 \quad (\mathbf{6})$$

This method has been used to determine the E_{film} of many polymers, including polystyrene and poly(methyl methacrylate),[94,110,111] poly(3-alkylthiophene)s,[7,16,32,57] diketopyrrolopyrrole (DPP) based polymers.[30,112] Tahk and coworkers were the first to use this technique to measure the tensile modulus of conjugated polymers, including poly(3,4-ethylenedioxythiophene):poly(4-styrenesulfonate) (PEDOT:PSS), pentacene, P3HT, and P3HT:PCBM.[113] The modulus of PEDOT:PSS was reported to be 2.26 ± 0.05 GPa (**Figure 1.8b,c**), while pentacene, P3HT, and P3HT:PCBM were 16.09 ± 2.83, 1.33 ± 0.01, and 6.02 ± 0.03 GPa, respectively.[113] The much higher tensile modulus of pentacene when compared to the other materials tested was attributed to its polycrystallinity, while the others are only semicrystalline. Another early buckling-based study on conjugated polymers explored the effect of the modification of the polymer backbone on the tensile modulus,[30] The modulus of DPPT-TT, a polymer with a repeat unit of DPP flanked by two thiophene rings and thienothiophene, was compared to DPPT-2T, which had a similar structure but replaced the thienothiophene unit with two thiophene rings.[30] The authors found that the DPPT-TT had a higher modulus (0.99 GPa) than did DPPT-2T (0.74 GPa) and attributed this observation to the fact that the stiffness of the fused rings of the thienothiophene unit in DPPT-TT was greater than that of the isolated rings of the bithiophene unit DPPT-2T.[15,30]

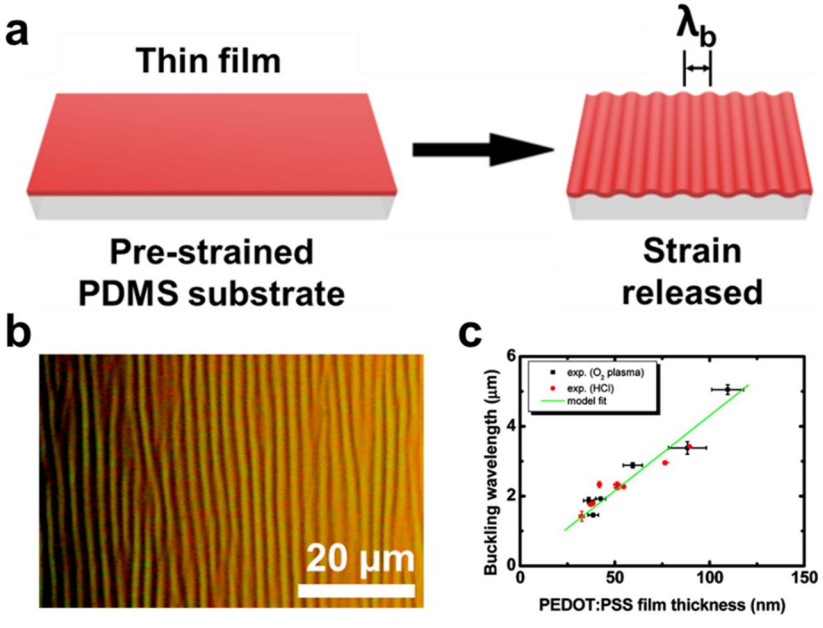

Figure 1.8. Determination of the tensile modulus by the buckling-based metrology. (a) Schematic of one variation of the buckling procedure. A polymer thin film is transferred to a pre-strained polydimethylsiloxane (PDMS) substrate. The strain is released and the polymer buckles. The wavelength, $\lambda_{b,}$ is related to the film stiffness and thickness. (b) Micrograph of a buckled film of PEDOT:PSS on PDMS. (c) Experimental data of buckling wavelength as a function of PEDOT:PSS film thickness. (b) and (c) Reproduced with permission from ref. 113. Copyright 2009, American Chemical Society.

While the buckling method described above works well for materials with tensile moduli up to a few GPa, some materials are too stiff and crack upon transfer or upon the compression due to the prestrained elastomeric substrate being relaxed.[65,87,109] In this case, an intermediate layer—a more deformable material with a known E_{film}—can be used between the soft substrate and the more rigid film, and the effective tensile modulus, E_{eff}, can be calculated by equation 7:[65,109]

$$E_{eff} = \frac{1 + m^2n^4 + 2mn(2n^2 + 3n + 2)}{(1+n)^3(1+mn)}E_1 \quad where \quad m = \frac{E_{film,2}}{E_{film,1}}, \; n = \frac{h_2}{h_1} \qquad (7)$$

where $E_{film,1}$ and $E_{film,2}$ are the moduli of the two films and h_1 and h_2 are the thicknesses of the two films. The authors previously used this bilayer method to measure the E_{film} of fullerenes, and found moduli between 5.1 and 25.6 GPa for technical grade $PC_{71}BM$ and 99% purity $PC_{61}BM$, respectively.[65,87]

In addition to the tensile modulus, other mechanical properties such as the failure point (*i.e.*, crack-onset) and the yield point can be measured by FOE methods. The *CoS* can be determined by observing the formation of cracks in a thin film on elastomer under increasing strain.[29,95] The *CoS*, though not an exact measurement of the failure point of a material—due to contributions from interlayer adhesion and the stress-strain response of the underlying substrate—is a qualitative measurement of ductility of materials and has been well correlated to the tensile modulus of materials.[32] The yield point of a material, which is the strain at which it begins to plastically (*i.e.*, permanently) deform, can be measured by two FOE techniques. The first involves the delamination of the film from the substrate and measurement of the curvature to determine the yield.[96] The FOE is compressed to force delamination before the strain is relaxed; the film is then annealed and at the point of delamination, a bump forms. The curvature of the bump and the thickness of the film are then used to calculate the yield point. Gurmessa used this method to determine the yield point of thin films of polystyrene and poly(2-vinylpyridine) (P2VP) homopolymers and block copolymers.[96,97] Another method to determine the yield point was recently proposed by Printz et al. by determining the onset of thin-film buckling using diffraction of light from a laser. This method—laser detection of yield point (LADYP)—subjects a polymer film on an elastic substrate to cycles of tensile strain that incrementally increase in steps of 1% (*i.e.*, 0% $\rightarrow$ 1% $\rightarrow$ 0% $\rightarrow$ 2% $\rightarrow$

0% → 3% → 0% etc.).[98] The formation of buckles manifests as a diffraction pattern obtained using a laser, and represents the onset of plastic deformation, or the yield point of the polymer. With LADYP, a correlation between side-chain length and yield point was found in P3ATs, ranging from 5% strain for P3PT to 18% strain for P3OT.[98]

In addition to FOE methods, there are other techniques available to measure mechanical properties of thin films. The tensile modulus is commonly measured by nanoindentation, in which a film is indented with a cantilever tip.[114] The load applied to and the displacement of the tip into the film are measured, and upon unloading of the tip, the slope of the load-displacement line is correlated to E_{film}. However, the tips have a very small radius of curvature, resulting in measurements that are localized and not necessarily descriptive of the properties of the entire film. For example, if the indentation occurred on an aggregate, the local tensile modulus will be much higher than the global tensile modulus of the film, while conversely, the indentation occurred in a highly disordered region, the local tensile modulus would be much lower than the global tensile modulus. Nanoindentation can also be complicated by effects of the substrate and also the viscoelasticity of the polymer itself.[115] Another method to measure the mechanical properties of thin films was developed by Kim and coworkers that mimics traditional tensile testing; a thin film is floated upon a liquid—water in the published studies—and a high resolution linear actuator strains the film while a highly sensitive load cell measures the stress.[59,116] A complete stress-strain curve can then be built from this information, however, but the method may be limited in certain instances due to the requirements that the liquid have high surface tension and low viscosity and that the thin film must be compatible with the liquid.[116] This method was used to measure the tensile moduli of

P3HT and copolymers of P3HT and P2VP and their blends with the fullerene derivative OXCBA.[116] Complete stress-strain curves were later measured for P3HT films with varying regioregularity.[59] The authors found that as the regioregularity of the P3HT increased, the E_{film} increased as did the brittleness. These observations were attributed to the fact that polymer with higher regioregularity more readily formed aggregates, which are stiffer than the disorder polymer. Recently, Kim and coworkers used this same measurement technique to demonstrate that organic photovoltaics comprising an active layer blend of poly[4,8-bis(5-(2-ethylhexyl)thiophen-2-yl)benzo[1,2-b:4,5-b′]dithiophene-*alt*-1,3-bis(thiophen-2-yl)-5-(2-hexyldecyl)-4*H*-thieno[3,4-c]pyrrole-4,6(5*H*)-dione] (PBDTTTPD) and poly[[*N*,*N*′-bis(2-hexyldecyl)-naphthalene-1,4,5,8-bis(dicarboximide)-2,6-diyl]-*alt*-5,5′-thiophene] (P(NDI2HD-T)) exhibited a significant improvement in elongation at the point of fracture over blends of PBDTTTPD with PCBM (7.16% and 0.3%, respectively).[117]

1.4 Inherent competition between deformability and charge transport

It has frequently been reported that there is an inherent competition between good electronic performance and high deformability or robustness.[15,16,59] O'Connor et al. reported an increase in mobility was coupled with an increase in stiffness in the polythiophenes P3HT and PBTTT.[15] PBTTT was found to have higher mobility and stiffness than P3HT, which was attributed to differences in the side chain interactions. P3HT has side chains on every conjugated ring, while PBTTT has a thienothiophene spacer without sidechains which allows sidechain intercalation. The sidechain

intercalation results in better vertical registry and aggregation, and while these aggregates improve charge-carrier mobility, they also are more stiff than amorphous regions of the film. The ordering effect is increased by annealing films of PBTTT at 180 °C, and both the mobility and tensile modulus increased further (**Figure 1.9a**).[15,76,118] Processing conditions also affect the mechanical and electronic properties of organic semiconductors, and in blends of P3HT with the fullerene PCBM, their inherent competition has also been observed. Awartani et al. reported a simultaneous increase in photovoltaic *PCE* and E_{film} in films spun at lower spin speeds.[16] At a lower spin speed, the evaporation rate of the solvent is lower than at higher spin speeds, and this lower evaporation rate results in improved film ordering as determined by the weakly interacting H-aggregate model.[16] Another study, performed by Kim and coworkers explored the effect of regioregularity of P3HT on its properties and found that higher regioregularity led to higher mobility and tensile modulus—as well as higher brittleness—which was attributed to the improved order (**Figure 1.9b**).[59] The E_{film} ranged from 13 MPa for 64% regioregular P3HT to 287 MPa for 98% regioregularity, while the hole mobility ranged from 4.84×10^{-8} to 1.81×10^{-1} $cm^2\ V^{-1}\ s^{-1}$.[59]

Another parameter known to affect the electronic and mechanical properties of polymers—the alkyl side-chain length—was previously studied by our group.[7,28,32,57] In P3ATs, we observed an increase in deformability and ductility with increasing side-chain length. The largest decrease in E_{film} was found between P3HT, $n = 6$, and P3OT, $n = 8$ from 1.09 ± 0.15 GPa to 0.15 ± 0.05 GPa (**Figure 1.10a**).[32] To better understand the practical implications of the observed modulus reduction, thin films comprising 1:1 blends of P3HT and P3OT with fullerenes were then stretched over glass hemispheres.[28]

Finite element analysis calculated that these films would be required to accommodate 24% strain. While devices with the P3OT:PCBM active layer accommodated the strain without fracturing, devices with the P3HT:PCBM active layer fractured radially resulting in shorting (**Figure 1.10b,c**). However, even though P3OT:PCBM could accommodate the strain, its *PCE* was too low ($\eta = 0.36\%$) to be commercially viable.[28]

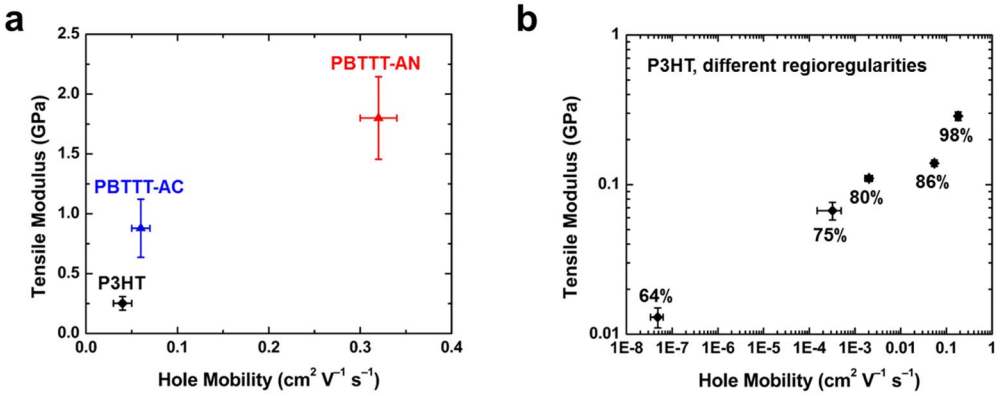

Figure 1.9. Tensile modulus vs. hole mobility for polythiophenes. (a) The tensile modulus and hole mobility of P3HT are lower than that of PBTTT. Both the stiffness and hole mobility of increase when as cast PBTTT (PBTTT-AC) is annealed at 180 °C (PBTTT-AN). The increase in tensile modulus and mobility of PBTTT compared to P3HT is attributed to improved order in PBTTT. Further ordering occurs in PBTTT when it is annealed, also leading to improved mobility and increased stiffness. (b) The tensile modulus and hole mobility of P3HT simultaneously increase with increasing regioregularity of the side-chains. The increase in both properties is likely due to the increased ability of regioregular P3HT to form ordered aggregates, which have improved charge transport properties, but are also stiff. (a) Reproduced with permission from ref. 15. Copyright 2010, American Chemical Society.

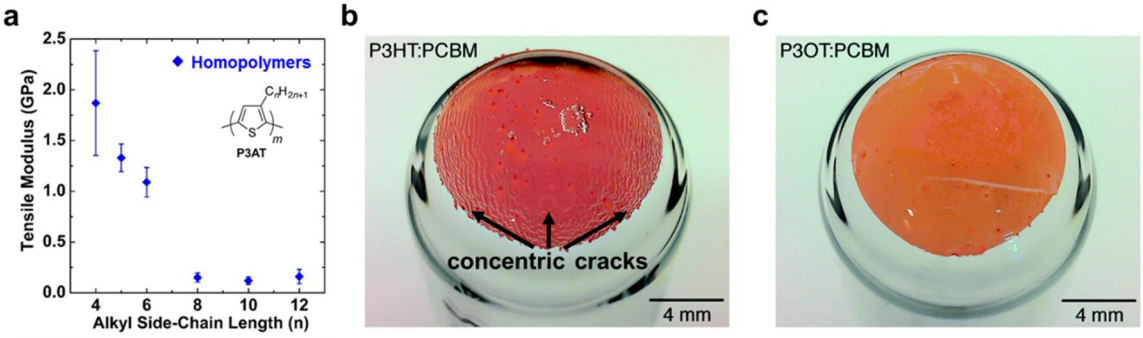

Figure 10. Deformability of P3ATs and its blends with PCBM. (a) The tensile modulus of P3ATs decreased with increasing side-chain length. The largest observed decrease was between P3HT and P3OT. (b) When the relatively stiff P3HT was blended 1:1 with PCBM and transferred to a hemisphere requiring 24% strain accommodation, the film cracked radially. (c) 1:1 P3OT:PCBM did not crack when transferred because of its higher deformability. (b) and (c) Reproduced with permission from ref. 28. Copyright 2014, The Royal Society of Chemistry.

1.5 Improving deformability without sacrificing electronic performance

Ideally, organic semiconductors would demonstrate both high electronic performance and mechanical robustness (*e.g.*, a low tensile modulus and high crack-onset, yield point, resilience, and toughness). To date, a few strategies have been uncovered as potential pathways for achieving co-optimization of electronic performance and deformability. As discussed above, Savagatrup et al. found that in P3ATs as the side-chain length increased, the tensile modulus decreased, but so did the power conversion efficiency.[7,32] We thus sought to combine the favorable properties of P3HT and P3OT in an effort to co-optimize deformability and electronic performance by exploring P3ATs with an average side-chain length, n = 7. We synthesized 1:1 block and random co-polymers of P3HT and P3OT, and also explored the properties of a physical blend of P3HT and P3OT, as well as the homopolymers poly(3-heptylthiophene) (P3HpT, n = 7) (**Figure 1.11a**).[7] **Figure 1.11b** is a graph of the *PCE* against the tensile moduli of these polymers. The properties of the block copolymer, P3HT-*b*-P3OT, are seemingly an average of those properties of the two homopolymers. The random copolymer, P3HT-*co*-P3OT, and the homopolymers blend, P3HT:P3OT, lie slightly above the average of the homopolymers and towards the more favorable region of the properties. P3HpT, however, lies well above the average of the homopolymers and has the favorable deformability of P3OT and photovoltaic performance of P3HT.[7] Interestingly, the μ_h of P3HpT is 0.0005 $cm^2\ V^{-1}\ s^{-1}$, over an order of magnitude lower than that of P3HT (0.011 $cm^2\ V^{-1}\ s^{-1}$), and of the same order of magnitude as P3OT (0.0001 $cm^2\ V^{-1}\ s^{-1}$).[57] However, upon blending in a 1:1 ratio with PCBM, the μ_h of P3HpT increases to 0.004 $cm^2\ V^{-1}\ s^{-1}$, which is on the same order of magnitude as the blend of P3HT:PCBM (0.010

$cm^2\ V^{-1}\ s^{-1}$).[57] This increase in mobility upon addition of PCBM is likely why P3HpT performs similarly in photovoltaic devices as P3HT. Additionally, we attributed the low tensile modulus to the T_g of P3HpT, which at -5 °C (as measured by DSC), is similar to P3OT (-10 °C) and much lower than P3HT (12 °C), which is close to room temperature.[57]

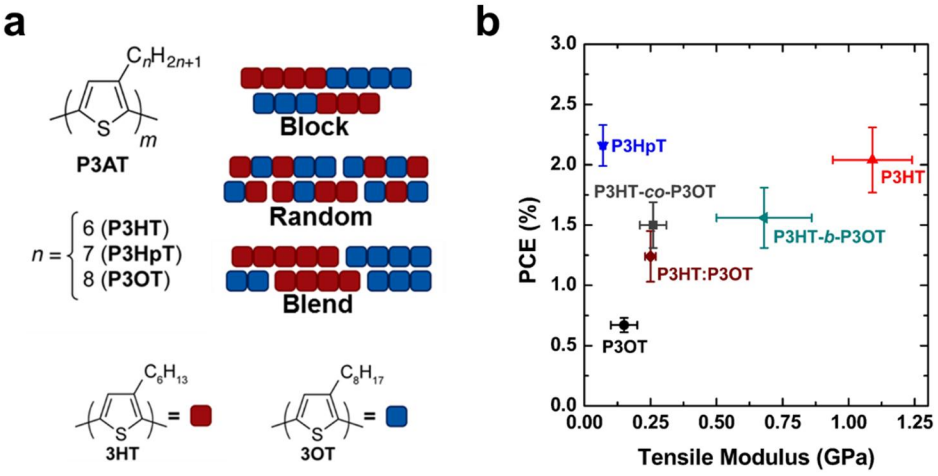

Figure 1.11. Finding co-optimization of electronic properties and deformability in P3ATs. (a) P3ATs with an average side-chain length of n = 7 were tested, including a block and random copolymer of P3HT (n = 6) and P3OT (n = 8), a physical blend of the two homopolymers, and P3HpT (n = 7). (b) OPV power conversion efficiency (*PCE*) versus the tensile modulus of the P3ATs. OPV devices were fabricated with a PEDOT:PSS bottom electrode, an active layer comprising a 1:1 polymer:$PC_{61}BM$ blend, and a eutectic Gallium-Indium (eGaIn) liquid metal as the top electrode. Reproduced with permission from ref. 7. Copyright 2014, American Chemical Society.

Another demonstrated path to co-optimization is covalently linking blocks of softer material to the semiconductor. Müller and coworkers found that diblock copolymers of P3HT and the insulating polyethylene—which both form well-ordered domains—demonstrated not only improved mechanical properties, but also improved μ_h of OFETs.[5] Transistors with the semiconductor comprising diblock copolymers of 35:65 (**Figure 1.12a**) and 10:90 P3HT:PE exhibited mobilities of 0.05 and 0.02 $cm^2\ V^{-1}\ s^{-1}$, respectively, which transistors with P3HT homopolymer only had a mobility of 0.01 cm^2

V^{-1} s^{-1}.[5] In addition to this improvement in mobility, the ductility of the diblock copolymers was also significantly higher; the *CoS* increased from 13% for the pure P3HT to over 600% for both of the diblock copolymers (**Figure 1.12b**).[5] It should be noted that while films of the diblock copolymers were significantly more ductile than those of the P3HT homopolymer, they were also much stiffer. Interestingly, the tensile modulus of the diblock copolymers (240 MPa for the 35:65 copolymer) was about an order of magnitude higher than that of the P3HT homopolymer (28 MPa).[5] Kim and coworkers found that adding 5% block and graft copolymers of P3HT and P2VP to P3HT (and P3HT:fullerene) films actually resulted in a reduction of tensile modulus (and improved cohesive fracture energy) when compared to P3HT homopolymer films, without deleterious effects on the performance in polymer:fullerene OPV devices (**Figure 1.12c–e**).[116] Recently, Qiu and coworkers made ABA triblock copolymer of P3HT (A) and poly(methyl acrylate) (B) and reported the material had a tensile modulus of only 6 MPa, an elongation at break of 140%, and a mobility of 9×10^{-4} cm^2 V^{-1} s^{-1} (compared to 4.5×10^{-4} cm^2 V^{-1} s^{-1} for P3HT homopolymer).[119] Although the authors did not report any measurements of the mechanical properties of P3HT homopolymer, the tensile modulus and elongation at break were below the P3HT values reported by Müller and coworkers.[5]

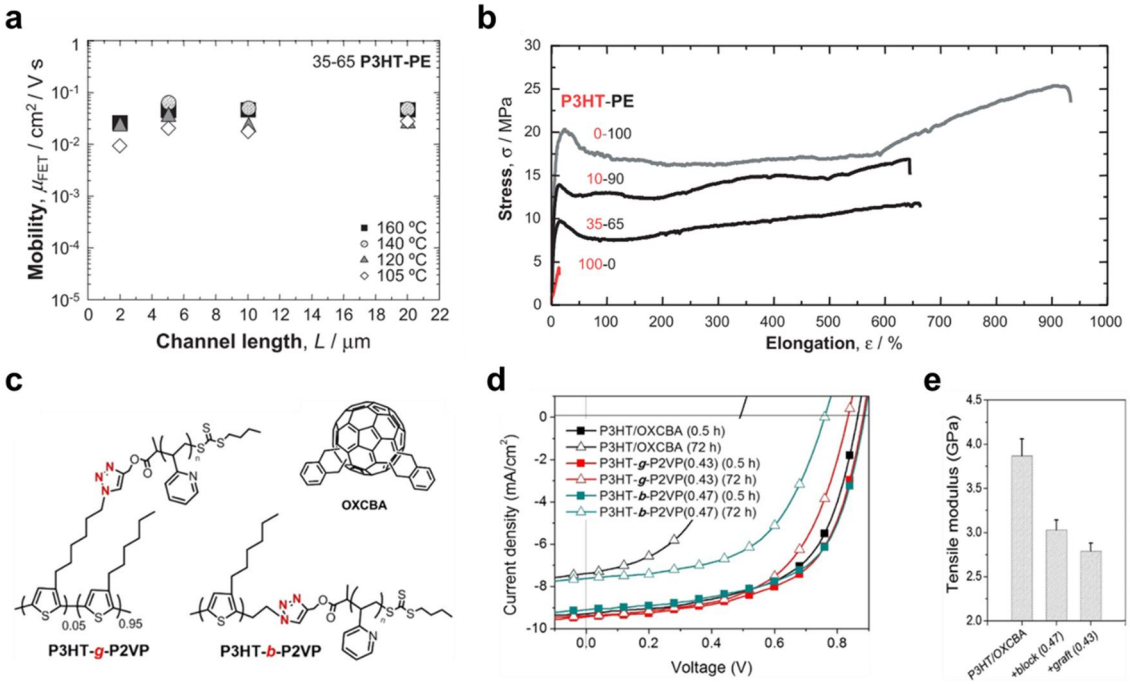

Figure 1.12. Copolymerization of P3HT and its effects on electronic and mechanical properties. (a) The hole mobility in a 35:65 block copolymer of P3HT and PE as a function of OFET channel length. (b) Stress-strain responses of bulk P3HT-*b*-PE copolymers. (c) The molecular structures of the graft copolymer, P3HT-*g*-P2VP, and the block copolymer, P3HT-*b*-P2VP, and the fullerene o-xylenyl C_{60} bis-adduct (OXCBA). (d) *J*-*V* curves of devices made with BHJs of P3HT:OXCBA as well as with 5% copolymer added. The numbers in parenthesis following P2VP are the volume fraction of P3HT in the P3HT-*g*-P2VP and P3HT-*b*-P2VP. (e) The decreasing tensile modulus of polymer:OXCBA blends with the addition of the copolymers of P3HT and P2VP. (a) and (b) Reproduced with permission from ref. 5. Copyright 2007, Wiley-VCH Verlag GmbH & Co. KGaA. (c)–(e) Reproduced with permission from ref. 116. Copyright 2014, American Chemical Society.

While P3ATs are terrific model systems due to their simplicity, they are unlikely to be commercially viable because of their relatively low mobilities and power conversion efficiencies. In the field of organic photovoltaics, low-bandgap polymers, comprising donor and acceptor units covalently bound, have become a primary focus because they absorb more of the solar spectrum than do homopolymers. DPP units are commonly the basis for these low-bandgap polymers, however, because of their fused aromatic rings, they are stiff. We hypothesized that slightly disrupting the aggregation of these polymers would reduce their stiffness. To that end, we introduced random segments

of unlike monomer—a terthiophene with two rings with alkyl side-chain substituents and a third unsubstituted thiophene ring—into the polymer PDPP2FT, which consisted of a DPP unit flanked by two furans and a thiophene.[112] The addition of these random segments decreased the E_{film} from 2.17 GPa for the pure PDPP2FT to 0.93 GPa without having a deleterious effect on the *PCE*.[112]

A potential strategy for co-optimizing properties that warrants further exploration is the addition of plasticizing additives into semiconducting layers. Additives such as 1,8-diiodooctane (DIO) and low molecular weight PDMS have been shown to improve OPV performance. While there were no studies on both the mechanical and electronic properties of the same material with the addition of additives, there were reports that suggesting it as a viable pathway to co-optimization of properties. Lee et al. showed that the addition of DIO to blends of 2,6-(4,4-bis(2-ethylhexyl)-4H-cyclopenta[2,1-b;3,4-b′]-dithiophene)-alt-4,7-(2,1,3-benzothiadiazole) (PCPDTBT) with $PC_{71}BM$ improved the photovoltaic device efficiency from 3.35% to 5.12%.[120] Reynolds and coworkers showed that the addition of small concentrations of low molecular weight PDMS (~0.1 mg mL^{-1}) to a thiophene and isoindigo-based small molecule improved the photovoltaic efficiency of its blend with $PC_{61}BM$ from 1.25% to 2.16%.[121] These additives were also found to decrease the tensile modulus of blends of P3HT:$PC_{61}BM$, from 1.23 GPa for the additive-free blend to 0.88 GPa with the PDMS additive and 0.38 with the DIO additive.[32] The decrease in tensile modulus observed by the authors was attributed to the plasticizing effects, or increasing free volume.

1.6 Conclusion and future directions

A key advantage of organic semiconductors is the potential for intrinsic deformability and robustness, allowing them to be ideal candidates for integration into wearable, implantable, and roll-to-roll printable devices. The integration of organic semiconductors into devices that will undergo bending, stretching, and/or conformal bonding requires anticipation of not only the electronic performance of these materials but also their mechanical performance. We stress that researchers should not assume mechanical robustness and deformability of organic semiconductors and instead verify these properties when developing new materials. To bridge these areas of research, we provided a gentle introduction to some of the important electronic and mechanical properties and measurement techniques for organic electronic devices. We also explored the inherent competition between good electronic performance and mechanical robustness (and specifically deformability), and highlighted several strategies for overcoming this undesirable competition. Pathways to co-optimization include: (1) decreasing the T_g of the polymer, with one possible route being the lengthening of alkyl side-chains to a critical length, n, (2) mixing highly deformable materials with high-mobility materials, (3) promotion of disorder in aggregation, and (4) the introduction of additives that behave as plasticizers.

Co-optimization of electronic performance and deformability and robustness is likely to continue to be a rich area of research for the foreseeable future. For instance, although pathways to co-optimization have been identified, it is still unknown whether or not these effects apply universally to organic semiconductors, or to just a few specific families. Further work also needs to be performed in the identification of additional

design rules for co-optimization, especially in OPV as researchers move away from the use of fullerene electron acceptors and towards new polymers and small molecules, which will likely have different intermolecular interactions with common electron donors. Ideally, these design rules could then be developed into a predictive model for properties of new or not yet synthesized organic semiconductors. This predictive modeling would allow scientists and engineers to easily design or select the best material for specific applications. Ultimately, the goal of this review is to stimulate further research in an area of increasing importance as research in organic semiconductors matures to device design and implementation.

Acknowledgements

This work was supported by the Air Force Office of Scientific Research (AFOSR) Young Investigator Program, Grant FA9550-13-1-0156 and laboratory startup funds from the University of California.

Chapter 1, in part is currently being prepared for submission for publication of the material by Adam D. Printz and Darren J. Lipomi. The dissertation author was the primary investigator and author of this material.

References

(1) Yuan, Y.; Giri, G.; Ayzner, A. L.; Zoombelt, A. P.; Mannsfeld, S. C. B.; Chen, J.; Nordlund, D.; Toney, M. F.; Huang, J.; Bao, Z. Ultra-High Mobility Transparent Organic Thin Film Transistors Grown by an Off-Centre Spin-Coating Method. *Nat. Commun.* **2014**, *5*, 3005.

(2) He, Z.; Zhong, C.; Su, S.; Xu, M.; Wu, H.; Cao, Y. Enhanced Power-Conversion Efficiency in Polymer Solar Cells Using an Inverted Device Structure. *Nat. Photonics* **2012**, *6*, 593–597.

(3) Dou, L.; You, J.; Hong, Z.; Xu, Z.; Li, G.; Street, R. A.; Yang, Y. 25Th Anniversary Article: A Decade of Organic/Polymeric Photovoltaic Research. *Adv. Mater.* **2013**, *25*, 6642–6671.

(4) Riede, M.; Uhrich, C.; Widmer, J.; Timmreck, R.; Wynands, D.; Schwartz, G.; Gnehr, W. M.; Hildebrandt, D.; Weiss, A.; Hwang, J.; Sundarraj, S.; Erk, P.; Pfeiffer, M.; Leo, K. Efficient Organic Tandem Solar Cells Based on Small Molecules. *Adv. Funct. Mater.* **2011**, *21*, 3019–3028.

(5) Müller, C.; Goffri, S.; Breiby, D. W.; Andreasen, J. W.; Chanzy, H. D.; Janssen, R. A. J.; Nielsen, M. M.; Radano, C. P.; Sirringhaus, H.; Smith, P.; Stingelin-Stutzmann, N. Tough, Semiconducting Polyethylene-poly(3-Hexylthiophene) Diblock Copolymers. *Adv. Funct. Mater.* **2007**, *17*, 2674–2679.

(6) Kaltenbrunner, M.; White, M. S.; Głowacki, E. D.; Sekitani, T.; Someya, T.; Sariciftci, N. S.; Bauer, S. Ultrathin and Lightweight Organic Solar Cells with High Flexibility. *Nat. Commun.* **2012**, *3*, 770.

(7) Savagatrup, S.; Printz, A. D.; Rodriquez, D.; Lipomi, D. J. Best of Both Worlds: Conjugated Polymers Exhibiting Good Photovoltaic Behavior and High Tensile Elasticity. *Macromolecules* **2014**, *47*, 1981–1992.

(8) Savagatrup, S.; Printz, A. D.; O'Connor, T. F.; Zaretski, A. V.; Lipomi, D. J. Molecularly Stretchable Electronics. *Chem. Mater.* **2014**, *26*, 3028–3041.

(9) Li, T.; Suo, Z.; Lacour, S. P.; Wagner, S. Compliant Thin Film Patterns of Stiff Materials as Platforms for Stretchable Electronics. *J. Mater. Res.* **2005**, *20*, 3274–3277.

(10) Kim, D. H.; Lu, N. S.; Ma, R.; Kim, Y. S.; Kim, R. H.; Wang, S. D.; Wu, J.; Won, S. M.; Tao, H.; Islam, A.; Yu, K. J.; Kim, T.; Chowdhury, R.; Ying, M.; Xu, L.; Li, M.; Chung, H.-J.; Keum, H.; McCormick, M.; Liu, P.; Zhang, Y.-W.; Omenetto, F. G.; Huang, Y.; Coleman, T.; Rogers, J. A. Epidermal Electronics. *Science (80-.).* **2011**, *333*, 838–844.

(11) Polywka, A.; Jakob, T.; Stegers, L.; Riedl, T.; Görrn, P. Facile Preparation of High-Performance Elastically Stretchable Interconnects. *Adv. Mater.* **2015**, *27*, 3755–3759.

(12) Yu, Z.; Niu, X.; Liu, Z.; Pei, Q. Intrinsically Stretchable Polymer Light-Emitting Devices Using Carbon Nanotube-Polymer Composite Electrodes. *Adv. Mater.* **2011**, *23*, 3989–3994.

(13) Mei, J.; Bao, Z. Side Chain Engineering in Solution-Processable Conjugated Polymers. *Chem. Mater.* **2014**, *26*, 604–615.

(14) Bouffl, P.; Han, Y.; Fei, Z.; Treat, N. D.; Li, R.; Smilgies, D.; Stingelin, N.; Anthopoulos, T. D.; Heeney, M. Using Molecular Design to Increase Hole Transport : Backbone Fluorination in the Benchmark Material. **2015**, 1–11.

(15) O'Connor, B.; Chan, E. P.; Chan, C.; Conrad, B. R.; Richter, L. J.; Kline, R. J.; Heeney, M.; McCulloch, I.; Soles, C. L.; DeLongchamp, D. M. Correlations between Mechanical and Electrical Properties of Polythiophenes. *ACS Nano* **2010**, *4*, 7538–7544.

(16) Awartani, O.; Lemanski, B. I.; Ro, H. W.; Richter, L. J.; DeLongchamp, D. M.; O'Connor, B. T. Correlating Stiffness, Ductility, and Morphology of Polymer:Fullerene Films for Solar Cell Applications. *Adv. Energy Mater.* **2013**, *3*, 399–406.

(17) Shin, M.; Song, J. H.; Lim, G. H.; Lim, B.; Park, J. J.; Jeong, U. Highly Stretchable Polymer Transistors Consisting Entirely of Stretchable Device Components. *Adv. Mater.* **2014**, *26*, 3706–3711.

(18) Po, R.; Carbonera, C.; Bernardi, A.; Tinti, F.; Camaioni, N. Polymer- and Carbon-Based Electrodes for Polymer Solar Cells: Toward Low-Cost, Continuous Fabrication over Large Area. *Sol. Energy Mater. Sol. Cells* **2012**, *100*, 97–114.

(19) Espinosa, N.; Hösel, M.; Angmo, D.; Krebs, F. C. Solar Cells with One-Day Energy Payback for the Factories of the Future. *Energy Environ. Sci.* **2012**, *5*, 5117–5132.

(20) Anctil, A.; Babbitt, C. W.; Raffaelle, R. P.; Landi, B. J. Cumulative Energy Demand for Small Molecule and Polymer Photovoltaics. *Prog. Photovolt Res. Appl.* **2013**, *21*, 1541–1554.

(21) Krebs, F. C. Fabrication and Processing of Polymer Solar Cells: A Review of Printing and Coating Techniques. *Sol. Energy Mater. Sol. Cells* **2009**, *93*, 394–412.

(22) Søndergaard, R. R.; Hösel, M.; Krebs, F. C. Roll-to-Roll Fabrication of Large Area Functional Organic Materials. *J. Polym. Sci. Part B Polym. Phys.* **2013**, *51*, 16–34.

(23) Becerril, H. A.; Mao, J.; Liu, Z.; Stoltenberg, R. M.; Bao, Z.; Chen, Y. Evaluation of Solution-Processed Reduced Graphene Oxide Films as Transparent Conductors. *ACS Nano* **2008**, *2*, 463–470.

(24) Diao, Y.; Zhou, Y.; Kurosawa, T.; Shaw, L.; Wang, C.; Park, S.; Guo, Y.; Reinspach, J. A.; Gu, K.; Gu, X.; Tee, B. C.-K.; Pang, C.; Yan, H.; Zhao, D.; Toney, M. F.; Mannsfeld, S. C. B.; Bao, Z. Flow-Enhanced Solution Printing of All-Polymer Solar Cells. *Nat. Commun.* **2015**, *6*, 7955.

(25) De La Fuente Vornbrock, A.; Sung, D.; Kang, H.; Kitsomboonloha, R.; Subramanian, V. Fully Gravure and Ink-Jet Printed High Speed pBTTT Organic Thin Film Transistors. *Org. Electron. physics, Mater. Appl.* **2010**, *11*, 2037–2044.

(26) Krebs, F. C.; Biancardo, M.; Winther-Jensen, B.; Spanggard, H.; Alstrup, J. Strategies for Incorporation of Polymer Photovoltaics into Garments and Textiles. *Sol. Energy Mater. Sol. Cells* **2006**, *90*, 1058–1067.

(27) Schwartz, G.; Tee, B. C.-K.; Mei, J.; Appleton, A. L.; Kim, D. H.; Wang, H.; Bao, Z. Flexible Polymer Transistors with High Pressure Sensitivity for Application in Electronic Skin and Health Monitoring. *Nat. Commun.* **2013**, *4*, 1859.

(28) O'Connor, T. F.; Zaretski, A. V.; Shiravi, B. A.; Savagatrup, S.; Printz, A. D.; Diaz, M. I.; Lipomi, D. J. Stretching and Conformal Bonding of Organic Solar Cells to Hemispherical Surfaces. *Energy Environ. Sci.* **2014**, *7*, 370–378.

(29) Savagatrup, S.; Printz, A. D.; O'Connor, T. F.; Zaretski, A. V.; Rodriquez, D.; Sawyer, E. J.; Rajan, K. M.; Acosta, R. I.; Root, S. E.; Lipomi, D. J. Mechanical Degradation and Stability of Organic Solar Cells: Molecular and Microstructural Determinants. *Energy Environ. Sci.* **2015**, *8*, 55–80.

(30) Lipomi, D. J.; Chong, H.; Vosgueritchian, M.; Mei, J.; Bao, Z. Toward Mechanically Robust and Intrinsically Stretchable Organic Solar Cells: Evolution of Photovoltaic Properties with Tensile Strain. *Sol. Energy Mater. Sol. Cells* **2012**, *107*, 355–365.

(31) Bruner, C.; Miller, N. C.; McGehee, M. D.; Dauskardt, R. H. Molecular Intercalation and Cohesion of Organic Bulk Heterojunction Photovoltaic Devices. *Adv. Funct. Mater.* **2013**, *23*, 2863–2871.

(32) Savagatrup, S.; Makaram, A. S.; Burke, D. J.; Lipomi, D. J. Mechanical Properties of Conjugated Polymers and Polymer-Fullerene Composites as a Function of Molecular Structure. *Adv. Funct. Mater.* **2014**, *24*, 1169–1181.

(33) Sajjad, M. T.; Ward, A. J.; Kästner, C.; Ruseckas, A.; Samuel, I. D. W.; Hoppe, H.; Samuel, I. D. W. Controlling Exciton Diffusion and Fullerene Distribution in

Photovoltaic Blends by Side Chain Modification. *J. Phys. Chem. Lett.* **2015**, *6*, 3054–3060.

(34) Himmelberger, S.; Duong, D. T.; Northrup, J. E.; Rivnay, J.; Koch, F. P. V.; Beckingham, B. S.; Stingelin, N.; Segalman, R. a.; Mannsfeld, S. C. B.; Salleo, A. Role of Side-Chain Branching on Thin-Film Structure and Electronic Properties of Polythiophenes. *Adv. Funct. Mater.* **2015**, *25*, 2616–2624.

(35) Li, G.; Yao, Y.; Yang, H.; Shrotriya, V.; Yang, G.; Yang, Y. "Solvent Annealing" Effect in Polymer Solar Cells Based on Poly(3-Hexylthiophene) and Methanofullerenes. *Adv. Funct. Mater.* **2007**, *17*, 1636–1644.

(36) Nguyen, L. H.; Hoppe, H.; Erb, T.; Günes, S.; Gobsch, G.; Sariciftci, N. S. Effects of Annealing on the Nanomorphology and Performance of Poly(alkylthiophene):Fullerene Bulk-Heterojunction Solar Cells. *Adv. Funct. Mater.* **2007**, *17*, 1071–1078.

(37) Verploegen, E.; Mondal, R.; Bettinger, C. J.; Sok, S.; Toney, M. F.; Bao, Z. Effects of Thermal Annealing Upon the Morphology of Polymer-Fullerene Blends. *Adv. Funct. Mater.* **2010**, *20*, 3519–3529.

(38) Salammal, S.; Mikayelyan, E.; Grigorian, S.; Pietsch, U.; Koenen, N.; Scherf, U.; Brinkmann, M.; Kayunkid, N. Impact of Thermal Annealing on the Semicrystalline Nanomorphology of Spin-Coated Thin Films of Regioregular Poly (3-Alkylthiophene) S as Observed by High-Resolution Transmission Electron Microscopy and Grazing Incidence X-Ray Diffraction. *Macromolecules* **2012**, *45*, 5575–5585.

(39) Huang, W.; Gann, E.; Cheng, Y.-B.; McNeill, C. R. In-Depth Understanding of the Morphology–Performance Relationship in Polymer Solar Cells. *ACS Appl. Mater. Interfaces* **2015**, *7*, 14026–14034.

(40) Brinkmann, M.; Wittmann, J.-C. Orientation of Regioregular Poly(3-Hexylthiophene) by Directional Solidification: A Simple Method to Reveal the Semicrystalline Structure of a Conjugated Polymer. *Adv. Mater.* **2006**, *18*, 860–863.

(41) Zhang, X.; Richter, L. J.; Delongchamp, D. M.; Kline, R. J.; Hammond, M. R.; McCulloch, I.; Heeney, M.; Ashraf, R. S.; Smith, J. N.; Anthopoulos, T. D.; Schroeder, B.; Geerts, Y. H.; Fischer, D. A.; Toney, M. F. Molecular Packing of High-Mobility Diketo Pyrrolo-Pyrrole Polymer Semiconductors with Branched Alkyl Side Chains. *J. Am. Chem. Soc.* **2011**, *133*, 15073–15084.

(42) Liu, J.; Sun, Y.; Gao, X.; Xing, R.; Zheng, L.; Wu, S.; Geng, Y.; Han, Y. Oriented poly(3-Hexylthiophene) Nanofibril with the Π-Π Stacking Growth Direction by Solvent Directional Evaporation. *Langmuir* **2011**, *27*, 4212–4219.

(43) O'Connor, B.; Kline, R. J.; Conrad, B. R.; Richter, L. J.; Gundlach, D.; Toney, M. F.; DeLongchamp, D. M. Anisotropic Structure and Charge Transport in Highly Strain-Aligned Regioregular Poly(3-Hexylthiophene). *Adv. Funct. Mater.* **2011**, *21*, 3697–3705.

(44) Gargi, D.; Kline, R. J.; DeLongchamp, D. M.; Fischer, D. A.; Toney, M. F.; O'Connor, B. T. Charge Transport in Highly Face-On Poly(3-Hexylthiophene) Films. *J. Phys. Chem. C* **2013**, *117*, 17421–17428.

(45) Kitchen, B.; Awartani, O.; Kline, R. J.; McAfee, T.; Ade, H.; O'Connor, B. T. Tuning Open-Circuit Voltage in Organic Solar Cells with Molecular Orientation. *ACS Appl. Mater. Interfaces* **2015**, *7*, 13208–13216.

(46) Himmelberger, S.; Vandewal, K.; Fei, Z.; Heeney, M.; Salleo, A. Role of Molecular Weight Distribution on Charge Transport in Semiconducting Polymers. *Macromolecules* **2014**, *47*, 7151–7157.

(47) Kline, R. J.; McGehee, M. D.; Kadnikova, E. N.; Liu, J.; Fréchet, J. M. J. Controlling the Field-Effect Mobility of Regioregular Polythiophene by Changing the Molecular Weight. *Adv. Mater.* **2003**, *15*, 1519–1522.

(48) Zen, A.; Saphiannikova, M.; Neher, D. Effect of Molecular Weight on the Structure and Crystallinity of Poly (3-Hexylthiophene). *Macromolecules* **2006**, *39*, 2162–2171.

(49) Zhang, R.; Li, B.; Iovu, M. C.; Jeffries-el, M.; Sauve, G.; Cooper, J.; Jia, S.; Tristram-Nagle, S.; Smilgies, D. M.; Lambeth, D. N.; McCullough, R. D.; Kowalewski, T. Nanostructure Dependence of Field-Effect Mobility in Regioregular Poly (3-Hexylthiophene) Thin Film Field Effect Transistors Nanostructure Dependence of Field-Effect Mobility in Regioregular. *J. Am. Chem. Soc.* **2006**, *128*, 3480–3481.

(50) Zhao, K.; Khan, H. U.; Li, R.; Su, Y.; Amassian, A. Entanglement of Conjugated Polymer Chains Influences Molecular Self-Assembly and Carrier Transport. *Adv. Funct. Mater.* **2013**, *23*, 6024–6035.

(51) Tummala, N. R.; Risko, C.; Bruner, C.; Dauskardt, R. H.; Brédas, J.-L. Entanglements in P3HT and Their Influence on Thin-Film Mechanical Properties: Insights from Molecular Dynamics Simulations. *J. Polym. Sci. Part B Polym. Phys.* **2015**, *53*, 934–942.

(52) Clark, J.; Chang, J.-F.; Spano, F. C.; Friend, R. H.; Silva, C. Determining Exciton Bandwidth and Film Microstructure in Polythiophene Films Using Linear Absorption Spectroscopy. *Appl. Phys. Lett.* **2009**, *94*, 163306.

(53) Chang, J.; Sun, B.; Breiby, D. W.; Nielsen, M. M.; Solling, T. I.; Giles, M.; McCulloch, I.; Sirringhaus, H. Enhanced Mobility of Poly (3-Hexylthiophene) Transistors by Spin-Coating from High-Boiling-Point Solvents. *Chem. Mater.* **2004**, *16*, 4772–4776.

(54) Jia, H.; Gowrisanker, S.; Pant, G. K.; Wallace, R. M.; Gnade, B. E. Effect of Poly (3-Hexylthiophene) Film Thickness on Organic Thin Film Transistor Properties. *J. Vac. Sci. Technol. A Vacuum, Surfaces, Film.* **2006**, *24*, 1228–1232.

(55) Majewski, L. A.; Kingsley, J. W.; Balocco, C.; Song, A. M. Influence of Processing Conditions on the Stability of poly(3- Hexylthiophene)-Based Field-Effect Transistors. *Appl. Phys. Lett.* **2006**, *88*, 2004–2007.

(56) Surin, M.; Leclére, P.; Lazzaroni, R.; Yuen, J. D.; Wang, G.; Moses, D.; Heeger, A. J.; Cho, S.; Lee, K. Relationship between the Microscopic Morphology and the Charge Transport Properties in poly(S-Hexylthiophene) Field-Effect Transistors. *J. Appl. Phys.* **2006**, *100*, 033712.

(57) Savagatrup, S.; Printz, A. D.; Wu, H.; Rajan, K. M.; Sawyer, E. J.; Zaretski, A. V.; Bettinger, C. J.; Lipomi, D. J. Viability of Stretchable poly(3-Heptylthiophene) (P3HpT) for Organic Solar Cells and Field-Effect Transistors. *Synth. Met.* **2015**, *203*, 208–214.

(58) Park, Y. D.; Kim, D. H.; Jang, Y.; Cho, J. H.; Hwang, M.; Lee, H. S.; Lim, J. A.; Cho, K. Effect of Side Chain Length on Molecular Ordering and Field-Effect Mobility in poly(3-Alkylthiophene) Transistors. *Org. Electron. physics, Mater. Appl.* **2006**, *7*, 514–520.

(59) Kim, J.-S.; Kim, J.-H.; Lee, W.; Yu, H.; Kim, H. J.; Song, I.; Shin, M.; Oh, J. H.; Jeong, U.; Kim, T.-S.; Kim, B. J. Tuning Mechanical and Optoelectrical Properties of Poly(3-Hexylthiophene) through Systematic Regioregularity Control. *Macromolecules* **2015**, *48*, 4339–4346.

(60) Wienk, M. M.; Turbiez, M.; Gilot, J.; Janssen, R. A. J. Narrow-Bandgap Diketo-Pyrrolo-Pyrrole Polymer Solar Cells: The Effect of Processing on the Performance. *Adv. Mater.* **2008**, *20*, 2556–2560.

(61) Kang, I.; Yun, H.-J.; Chung, D. S.; Kwon, S.-K.; Kim, Y.-H. Record High Hole Mobility in Polymer Semiconductors via Side-Chain Engineering. *J. Am. Chem. Soc.* **2013**, *135*, 14896–14899.

(62) Ryu, G.-S.; Park, K. H.; Park, W.-T.; Kim, Y.-H.; Noh, Y.-Y. High-Performance Diketopyrrolopyrrole-Based Organic Field-Effect Transistors for Flexible Gas Sensors. *Org. Electron.* **2015**, *23*, 76–81.

(63) Pouliot, J.-R.; Sun, B.; Leduc, M.; Najari, A.; Li, Y.; Leclerc, M. A High Mobility DPP-Based Polymer Obtained via Direct (hetero)arylation Polymerization. *Polym. Chem.* **2015**, *6*, 278–282.

(64) Han, A.-R.; Dutta, G. K.; Lee, J.; Lee, H. R.; Lee, S. M.; Ahn, H.; Shin, T. J.; Oh, J. H.; Yang, C. E-Branched Flexible Side Chain Substituted Diketopyrrolopyrrole-Containing Polymers Designed for High Hole and Electron Mobilities. *Adv. Funct. Mater.* **2015**, *25*, 247–254.

(65) Savagatrup, S.; Rodriquez, D.; Printz, A. D.; Sieval, A. B.; Hummelen, J. C.; Lipomi, D. J. [70]PCBM and Incompletely Separated Grades of Methanofullerenes Produce Bulk Heterojunctions with Increased Robustness for Ultra-Flexible and Stretchable Electronics. *Chem. Mater.* **2015**, *27*, 3902–3911.

(66) Schmidt-Mende, L.; Fechtenkotter, A.; Mullen, K.; Moons, E.; Friend, R. H.; Mackenzie, J. D. Self-Organized Discotic Liquid Crystals for High-Ef Ciency Organic Photovoltaics. *Science (80-.).* **2001**, *293*, 1119–1122.

(67) Zhan, X.; Tan, Z.; Domercq, B.; An, Z.; Zhang, X.; Barlow, S.; Li, Y.; Zhu, D.; Kippelen, B.; Marder, S. R. A High-Mobility Electron-Transport Polymer with Broad Absorption and Its Use in Field-Effect Transistors and All-Polymer Solar Cells. *J. Am. Chem. Soc.* **2007**, *129*, 7246–7247.

(68) Friedel, B.; McNeill, C. R.; Greenham, N. C. Influence of Alkyl Side-Chain Length on the Performance of Poly(3-alkylthiophene)/Polyfluorene All-Polymer Solar Cells. *Chem. Mater.* **2010**, *22*, 3389–3398.

(69) Choi, J.; Kim, K.-H.; Yu, H.; Lee, C.; Kang, H.; Song, I.; Kim, Y.; Oh, J. H.; Kim, B. J. Importance of Electron Transport Ability in Naphthalene Diimide-Based Polymer Acceptors for High-Performance, Additive-Free All-Polymer Solar Cells. *Chem. Mater.* **2015**, *27*, 5230–5237.

(70) Guo, C.; Lin, Y.-H.; Witman, M. D.; Smith, K. a; Wang, C.; Hexemer, A.; Strzalka, J.; Gomez, E. D.; Verduzco, R. Conjugated Block Copolymer Photovoltaics with near 3% Efficiency through Microphase Separation. *Nano Lett.* **2013**, *13*, 2957–2963.

(71) Sirringhaus, H.; Brown, P. J.; Friend, R. H.; Nielsen, M. M.; Bechgaard, K.; Spiering, A. J. H. Two-Dimensional Charge Transport in Conjugated Polymers. *Nature* **1999**, *401*, 685–688.

(72) Coropceanu, V.; Cornil, J.; da Silva Filho, D. A.; Olivier, Y.; Silbey, R.; Bredas, J.-L. Charge Transport in Organic Semiconductors. *Chem. Rev.* **2007**, *107*, 926–952.

(73) Kim, J. Y.; Frisbie, C. D. Correlation of Phase Behavior and Charge Transport in Conjugated Polymer/Fullerene Blends. *J. Phys. Chem. C* **2008**, *112*, 17726–17736.

(74) Noriega, R.; Rivnay, J.; Vandewal, K.; Koch, F. P. V; Stingelin, N.; Smith, P.; Toney, M. F.; Salleo, A. A General Relationship between Disorder, Aggregation and Charge Transport in Conjugated Polymers. *Nat. Mater.* **2013**, *12*, 1038–1044.

(75) Peter, F.; Koch, V.; Rivnay, J.; Foster, S.; Müller, C.; Downing, J. M.; Buchaca-domingo, E.; Westacott, P.; Yu, L.; Yuan, M.; Baklar, M.; Fei, Z.; Luscombe, C.; McLachlan, M. A.; Heeney, M.; Rumbles, G.; Silva, C.; Salleo, A.; Nelson, J.; Smith, P.; Stingelin, N. The Impact of Molecular Weight on Microstructure and Charge Transport in Semicrystalline Polymer Semiconductors–Poly(3-Hexylthiophene), a Model Study. *Prog. Polym. Sci.* **2013**, *38*, 1978–1989.

(76) Salleo, A.; Kline, R. J.; DeLongchamp, D. M.; Chabinyc, M. L. Microstructural Characterization and Charge Transport in Thin Films of Conjugated Polymers. *Adv. Mater.* **2010**, *22*, 3812–3838.

(77) Brinkmann, M. Structure and Morphology Control in Thin Films of Regioregular poly(3-Hexylthiophene). *J. Polym. Sci. Part B Polym. Phys.* **2011**, *49*, 1218–1233.

(78) Clarke, T. M.; Durrant, J. R. Charge Photogeneration in Organic Solar Cells. *Chem. Rev.* **2010**, *110*, 6736–6767.

(79) Mollinger, S. A.; Krajina, B. A.; Noriega, R.; Salleo, A.; Spakowitz, A. J. Percolation, Tie-Molecules, and the Microstructural Determinants of Charge Transport in Semicrystalline Conjugated Polymers. *ACS Macro Lett.* **2015**, *4*, 708–712.

(80) Spano, F. C. Modeling Disorder in Polymer Aggregates: The Optical Spectroscopy of Regioregular poly(3-Hexylthiophene) Thin Films. *J. Chem. Phys.* **2005**, *122*, 234701.

(81) Roehling, J. D.; Batenburg, K. J.; Swain, F. B.; Moulé, A. J.; Arslan, I. Three-Dimensional Concentration Mapping of Organic Blends. *Adv. Funct. Mater.* **2013**, *23*, 2115–2122.

(82) Chua, L.-L.; Zaumseil, J.; Chang, J.-F.; Ou, E. C.-W.; Ho, P. K.-H.; Sirringhaus, H.; Friend, R. H. General Observation of N-Type Field-Effect Behaviour in Organic Semiconductors. *Nature* **2005**, *434*, 194–199.

(83) Zaumseil, J.; Sirringhaus, H. Electron and Ambipolar Transport in Organic Field-Effect Transistors. *Chem. Rev.* **2007**, *107*, 1296–1323.

(84) Klauk, H. Organic Thin-Film Transistors. *Chem. Soc. Rev.* **2010**, *39*, 2643–2666.

(85) Giri, G.; Verploegen, E.; Mannsfeld, S. C. B.; Atahan-Evrenk, S.; Kim, D. H.; Lee, S. Y.; Becerril, H. A.; Aspuru-Guzik, A.; Toney, M. F.; Bao, Z. Tuning Charge Transport in Solution-Sheared Organic Semiconductors Using Lattice Strain. *Nature* **2011**, *480*, 504–508.

(86) Bettinger, C. J.; Bao, Z. Organic Thin-Film Transistors Fabricated on Resorbable Biomaterial Substrates. *Adv. Mater.* **2010**, *22*, 651–655.

(87) Printz, A. D.; Savagatrup, S.; Rodriquez, D.; Lipomi, D. J. Role of Molecular Mixing on the Stiffness of Polymer:fullerene Bulk Heterojunction Films. *Sol. Energy Mater. Sol. Cells* **2015**, *134*, 64–72.

(88) Piliego, C.; Loi, M. A. Charge Transfer State in Highly Efficient Polymer–fullerene Bulk Heterojunction Solar Cells. *J. Mater. Chem.* **2012**, *22*, 4141–4150.

(89) Menke, S. M.; Holmes, R. J. Exciton Diffusion in Organic Photovoltaic Cells. *Energy Environ. Sci.* **2014**, *7*, 499–512.

(90) Rivnay, J.; Mannsfeld, S. C. B.; Miller, C. E.; Salleo, A.; Toney, M. F. Quantitative Determination of Organic Semiconductor Microstructure from the Molecular to Device Scale. *Chem. Rev.* **2012**, *112*, 5488–5519.

(91) Kawashima, K.; Osaka, I.; Takimiya, K. Effect of Chalcogen Atom on the Properties of Naphthobischalcogenadiazole-Based Π-Conjugated Polymers. *Chem. Mater.* **2015**, *27*, 6558–6570.

(92) Clark, J.; Silva, C.; Friend, R.; Spano, F. Role of Intermolecular Coupling in the Photophysics of Disordered Organic Semiconductors: Aggregate Emission in Regioregular Polythiophene. *Phys. Rev. Lett.* **2007**, *98*, 206406.

(93) Turner, S. T.; Pingel, P.; Steyrleuthner, R.; Crossland, E. J. W.; Ludwigs, S.; Neher, D. Quantitative Analysis of Bulk Heterojunction Films Using Linear Absorption Spectroscopy and Solar Cell Performance. *Adv. Funct. Mater.* **2011**, *21*, 4640–4652.

(94) Stafford, C. M.; Harrison, C.; Beers, K. L.; Karim, A.; Amis, E. J.; VanLandingham, M. R.; Kim, H.-C.; Volksen, W.; Miller, R. D.; Simonyi, E. E. A Buckling-Based Metrology for Measuring the Elastic Moduli of Polymeric Thin Films. *Nat. Mater.* **2004**, *3*, 545–550.

(95) Lu, N.; Wang, X.; Suo, Z.; Vlassak, J. Metal Films on Polymer Substrates Stretched beyond 50%. *Appl. Phys. Lett.* **2007**, *91*, 221909.

(96) Gurmessa, B. J.; Croll, A. B. Onset of Plasticity in Thin Polystyrene Films. *Phys. Rev. Lett.* **2013**, *110*, 074301.

(97) Gurmessa, B.; Croll, A. B. Influence of Thin Film Confinement on Surface Plasticity in Polystyrene and Poly(2-Vinylpyridine) Homopolymer and Block Copolymer Films. *Macromolecules* **2015**, *48*, 5670–5676.

(98) Printz, A. D.; Zaretski, A. V.; Savagatrup, S.; Chiang, A. S.-C.; Lipomi, D. J. Yield Point of Semiconducting Polymer Films on Stretchable Substrates Determined by Onset of Buckling. *ACS Appl. Mater. Interfaces* **2015**, *7*, 23257–23264.

(99) Tee, B. C.-K.; Wang, C.; Allen, R.; Bao, Z. An Electrically and Mechanically Self-Healing Composite with Pressure- and Flexion-Sensitive Properties for Electronic Skin Applications. *Nat. Nanotechnol.* **2012**, *7*, 825–832.

(100) Kaltenbrunner, M.; Sekitani, T.; Reeder, J.; Yokota, T.; Kuribara, K.; Tokuhara, T.; Drack, M.; Schwödiauer, R.; Graz, I.; Bauer-Gogonea, S.; Bauer, S.; Someya, T. An Ultra-Lightweight Design for Imperceptible Plastic Electronics. *Nature* **2013**, *499*, 458–463.

(101) Savagatrup, S.; Chan, E.; Renteria-Garcia, S. M.; Printz, A. D.; Zaretski, A. V.; O'Connor, T. F.; Rodriquez, D.; Valle, E.; Lipomi, D. J. Plasticization of PEDOT:PSS by Common Additives for Mechanically Robust Organic Solar Cells and Wearable Sensors. *Adv. Funct. Mater.* **2015**, *25*, 427–436.

(102) Chou, H.-H.; Nguyen, A.; Chortos, A.; To, J. W. F.; Lu, C.; Mei, J.; Kurosawa, T.; Bae, W.-G.; Tok, J. B.-H.; Bao, Z. A Chameleon-Inspired Stretchable Electronic Skin with Interactive Colour Changing Controlled by Tactile Sensing. *Nat. Commun.* **2015**, *6*, 8011.

(103) Ghezzi, D.; Antognazza, M. R.; Maccarone, R.; Bellani, S.; Lanzarini, E.; Martino, N.; Mete, M.; Perile, G.; Bisti, S.; Lanzani, G.; Benfenati, F. A Polymer Optoelectronic Interface Restores Light Sensitivity in Blind Rat Retinas. *Nat. Photonics* **2013**, *7*, 400–406.

(104) Hammock, M. L.; Chortos, A.; Tee, B. C.-K.; Tok, J. B.-H.; Bao, Z. 25th Anniversary Article: The Evolution of Electronic Skin (E-Skin): A Brief History, Design Considerations, and Recent Progress. *Adv. Mater.* **2013**, *25*, 5997–6038.

(105) O'Connor, B. T.; Reid, O. G.; Zhang, X.; Kline, R. J.; Richter, L. J.; Gundlach, D. J.; Delongchamp, D. M.; Toney, M. F.; Kopidakis, N.; Rumbles, G. Morphological

Origin of Charge Transport Anisotropy in Aligned Polythiophene Thin Films. *Adv. Funct. Mater.* **2014**, *24*, 3422–3431.

(106) Dauskardt, R. H.; Lane, M.; Ma, Q.; Krishna, N. Adhesion and Debonding of Multi-Layer Thin Film Structures. *Eng. Fract. Mech.* **1998**, *61*, 141–162.

(107) Brand, V.; Bruner, C.; Dauskardt, R. H. Cohesion and Device Reliability in Organic Bulk Heterojunction Photovoltaic Cells. *Sol. Energy Mater. Sol. Cells* **2012**, *99*, 182–189.

(108) Dupont, S. R.; Voroshazi, E.; Heremans, P.; Dauskardt, R. H. Adhesion Properties of Inverted Polymer Solarcells: Processing and Film Structure Parameters. *Org. Electron.* **2013**, *14*, 1262–1270.

(109) Stafford, C. M.; Guo, S.; Harrison, C.; Chiang, M. Y. M. Combinatorial and High-Throughput Measurements of the Modulus of Thin Polymer Films. *Rev. Sci. Instrum.* **2005**, *76*, 062207.

(110) Stafford, C. M.; Vogt, B. D.; Harrison, C.; Julthongpiput, D.; Huang, R. Elastic Moduli of Ultrathin Amorphous Polymer Films. *Macromolecules* **2006**, *39*, 5095–5099.

(111) Lee, J.-H.; Chung, J. Y.; Stafford, C. M. Effect of Confinement on Stiffness and Fracture of Thin Amorphous Polymer Films. *ACS Macro Lett.* **2012**, *1*, 122–126.

(112) Printz, A. D.; Savagatrup, S.; Burke, D. J.; Purdy, T. N.; Lipomi, D. J. Increased Elasticity of a Low-Bandgap Conjugated Copolymer by Random Segmentation for Mechanically Robust Solar Cells. *RSC Adv.* **2014**, *4*, 13635–13643.

(113) Tahk, D.; Lee, H. H.; Khang, D.-Y. Elastic Moduli of Organic Electronic Materials by the Buckling Method. *Macromolecules* **2009**, *42*, 7079–7083.

(114) Zeng, K.; Chen, Z. K.; Shen, L.; Liu, B. Study of Mechanical Properties of Light-Emitting Polymer Films by Nano-Indentation Technique. *Thin Solid Films* **2005**, *477*, 111–118.

(115) VanLandingham, M. R.; Villarrubia, J. S.; Guthrie, W. F.; Meyers, G. F. Nanoindentation of Polymers: An Overview. *Macromol. Symp.* **2001**, *167*, 15–43.

(116) Kim, H. J.; Kim, J.; Ryu, J.; Kim, Y.; Kang, H.; Lee, W. B.; Kim, T.; Kim, B. J. Architectural Engineering of Rod-Coil Compatibilizers for Producing Mechanically and Thermally Stable Polymer Solar Cells. *ACS Nano* **2014**, *8*, 10461–10470.

(117) Kim, T.; Kim, J.-H.; Kang, T. E.; Lee, C.; Kang, H.; Shin, M.; Wang, C.; Ma, B.; Jeong, U.; Kim, T.-S.; Kim, B. J. Flexible, Highly Efficient All-Polymer Solar Cells. *Nat. Commun.* **2015**, *6*, 8547.

(118) Mcculloch, I.; Heeney, M.; Bailey, C.; Genevicius, K.; Macdonald, I.; Shkunov, M.; Sparrowe, D.; Tierney, S.; Wagner, R.; Zhang, W.; Chabinyc, M. L.; Kline, J. R.; McGehee, M. D.; Toney, M. F. Liquid-Crystalline Semiconducting Polymers with High Charge-Carrier Mobility. *Nat. Mater.* **2006**, *5*, 328–333.

(119) Peng, R.; Pang, B.; Hu, D.; Chen, M.; Zhang, G.; Wang, X.; Lu, H.; Cho, K.; Qiu, L. An ABA Triblock Copolymer Strategy for Intrinsically Stretchable Semiconductors †. *J. Mater. Chem. C* **2015**, *3*, 3599–3606.

(120) Lee, J. K.; Ma, W. L.; Brabec, C. J.; Yuen, J.; Moon, J. S.; Kim, J. Y.; Lee, K.; Bazan, G. C.; Heeger, A. J. Processing Additives for Improved Efficiency from Bulk Heterojunction Solar Cells. *J. Am. Chem. Soc.* **2008**, *130*, 3619–3623.

(121) Graham, K. R.; Mei, J.; Stalder, R.; Shim, J. W.; Cheun, H.; Steffy, F.; So, F.; Kippelen, B.; Reynolds, J. R. Polydimethylsiloxane as a Macromolecular Additive for Enhanced Performance of Molecular Bulk Heterojunction Organic Solar Cells. *ACS Appl. Mater. Interfaces* **2011**, *3*, 1210–1215.

Chapter 2

Best of both worlds: Conjugated polymers exhibiting good photovoltaic behavior and high tensile elasticity

Adam D. Printz,[†] Suchol Savagatrup,[†] Daniel Rodriquez, and Darren J. Lipomi

([†] Equal contribution)

Department of NanoEngineering, University of California, San Diego

9500 Gilman Drive, Mail Code 0448, La Jolla, CA 92093-0448

Abstract

This paper examines a series of poly(3-alkylthiophene)s (P3ATs), a class of materials for which mechanical compliance and electronic performance have been observed to be in competition. P3ATs with longer alkyl side chains ($n \geq 8$) have high elasticity and ductility, but poor electronic performance (as manifested in photovoltaic efficiency in blends with fullerenes); P3ATs with shorter chains ($n \leq 6$) exhibit the opposite characteristics. A series of four polymer films in which the average length of the side chain is $n = 7$ is tested using mechanical, spectroscopic, microscopic, and photovoltaic device-based measurements to determine whether or not it is possible, in principle, to maximize both mechanical and electronic performance in a single organic semiconductor (the "best of both worlds"). The four polymer samples are (1) a physical blend of equal parts P3HT and P3OT (P3HT:P3OT, $n = 6$ and $n = 8$); (2) a block copolymer (P3HT-*b*-P3OT); (3) a random copolymer (P3HT-*co*-P3OT); and (4) poly(3-heptylthiophene) (P3HpT, $n = 7$). The tensile moduli obtained by mechanical buckling correlate well with spectroscopic evidence (using the weakly interacting H-aggregate model) of a well-ordered microstructure of the polymers. The block copolymer was the stiffest of the hybrid samples (680 ± 180 MPa), while P3HpT exhibited maximum compliance (70 ± 10 MPa) and power conversion efficiency in a 1:1 blend with the fullerene $PC_{61}BM$ using stretchable electrodes ($PCE = 2.16 \pm 0.17\%$) that was similar to that of P3HT:$PC_{61}BM$. These analyses may permit the design of organic semiconductors with improved mechanical and electronic properties for mechanically robust and stretchable applications.

2.1. Introduction and background

There is an apparent competition between electronic performance and mechanical compliance in semiconducting polymers.[1–4] We previously observed the increase in elasticity in a series of regioregular poly(3-alkylthiophene)s (P3ATs) with increasing side-chain length (from n = 4 to 12, **Figures 2.1 and 2.2**).[1,2] Various groups have reported the decrease in electronic and photovoltaic properties with increasing side-chain length, including field-effect mobilities[5,6] and power conversion efficiency (*PCE*) in bulk heterojunctions (BHJs) when paired with a polyfluorene copolymer[7] and fullerene.[8] O'Connor and coworkers had reported a similar trend in competition between field-effect mobilities and tensile moduli of various conjugated polymers.[3] This competition has been attributed to the rigid, π-conjugated main chains and the three-dimensionally ordered crystallites generally regarded as beneficial for charge transport.[1–4] These crystallites, however, are correlated with high stiffness and low ductility of the highest-performing pure polymers and—for organic solar cells (OSCs)—polymer:fullerene composites.[1–4] The competing attributes of compliance and performance have significant consequences for the environmental stability of ultra-thin OSCs[9] and devices based on organic thin-film transistors (OTFTs).[10] Beyond the near-term goal of rendering devices already known in the literature more mechanically stable, intrinsically elastic and ductile ("stretchable") semiconductors could find applications in new types of systems, such as wearable and implantable biomedical sensors[11] and in soft robotics.[12] This paper represents an attempt to find the "best of both worlds"—i.e., to co-engineer the mechanical compliance and photovoltaic efficiencies—in a series of regioregular poly(3-alkylthiophene)s (P3ATs), the most-studied class of materials in the field of organic electronics.[13] The lengths of the

alkyl side-chains in P3ATs have very large effects on virtually all mechanical and electronic properties of the materials.[1,5,14] The largest increase in mechanical compliance occurs in a series of P3ATs having between six and eight carbon atoms—poly(3-hexylthiophene) (P3HT) and poly(3-octylthiophene) (P3OT). We thus sought to determine the effect of the length of alkyl side-chain in the "sweet spot" on the elasticity and photovoltaic performance and to attempt to maximize the two parameters. Toward this goal, we obtained or synthesized a series of four materials exhibiting an average side-chain length of n = 7: (1) a physical blend (P3HT:P3OT); (2) a block copolymer (P3HT-*b*-P3OT); (3) a random copolymer (P3HT-*co*-P3OT); and (4) poly(3-heptylthiophene) (P3HpT), whose side chain contains exactly seven carbon atoms (**Figure 2.1**) and its field effect mobility had been reported between those of P3HT and P3OT.[6]

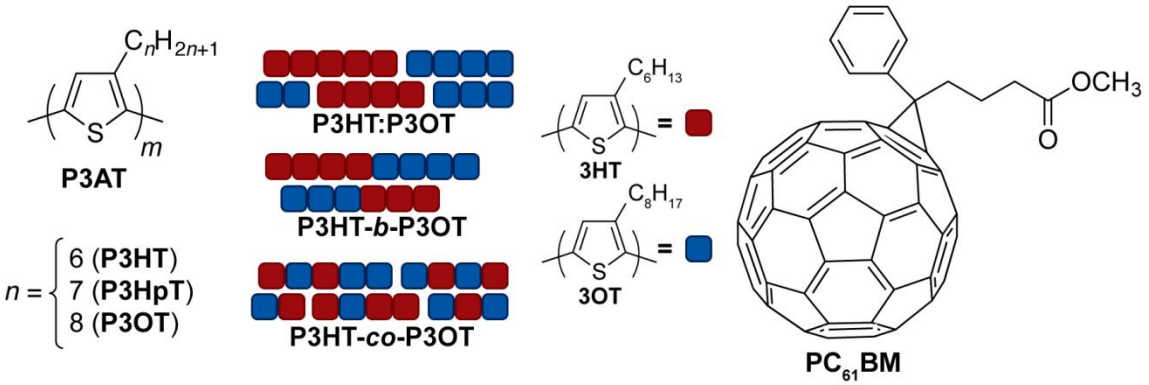

Figure 2.1. Chemical structures and schematic diagrams of the organic semiconductors examined in this paper.

Plastic electronics. The vision of organic electronics has always been to fabricate traditional semiconductor devices using inexpensive materials that can be processed from solution in a roll-to-roll manner.[15–17] The thinness of the active layers (≤200 nm) required to realize applications such as OSCs, OTFTs, and organic light-emitting devices

(OLEDs) permits extremely small bending radii and substantial overall flexibility, as long as the device is fabricated on a sufficiently thin substrate (OSCs with a total thickness of 2 μm have been demonstrated).[16] The strains imposed on materials under bending are rarely >2%, however, and for a material to accommodate substantial tensile strain for integration with ultra-thin substrates,[18] textiles,[19] the moving parts of machines and portable devices,[20] medical prostheses and implants,[11] robotics,[21] and three-dimensional surfaces other than cones and cylinders,[2] significantly more mechanical robustness is required of these nominally plastic semiconductors.[22] The best-performing organic semiconductors—including pentacene, poly[2,5-bis(3-tetradecylthiophen-2-yl)thieno[3,2-*b*]thiophene] (PBTTT), and P3HT:PCBM blends—are stiff (elastic moduli >1 GPa) and brittle (crack-onset strain on elastomeric substrates <2%)[3,23,24]

Electronic properties for organic electronic materials and devices have surpassed or are approaching those of their inorganic counterparts.[25–27] Semiconducting polymers now exhibit ambipolar field-effect mobilities greater than those of amorphous silicon,[25] and organic solar cells have reached efficiencies over ten percent.[28] Studies on roll-to-roll manufacturing suggest that modules can be made at low-cost.[29] While some of the most impressive demonstrations have used high-mobility, low-bandgap polymers,[30] regioregular P3HT is still the archetypal conjugated polymer and serves as a reference point for comparing the properties of new materials.[13] Even though the photovoltaic properties of structurally complex, donor-acceptor copolymers have surpassed those of P3HT (though perhaps not by much[31]), P3HT has significant advantages including synthetic accessibility[32] and low embodied energy,[33] facile functionalization by side-

chain engineering,[14] amenability to block copolymerization,[34] and a band gap that is complementary to modern donor-acceptor copolymers for tandem cells.[26]

While the power conversion efficiency (*PCE*) is frequently the focal point for studies of organic solar cells, the mechanical resiliency is often overlooked. Despite its good photovoltaic performance under ideal conditions,[31] P3HT—especially when combined with $PC_{61}BM$—has been shown to fracture at relatively low applied strains.[1,4,23,24] Our laboratory has shown that small changes in the structure of a conjugated polymer,[35] such as varying the length of the alkyl side chains, can significantly alter the electronic and mechanical properties of the poly(3-alkylthiophene)s (P3ATs).[1,2] For example, increasing the length of the side chain of P3AT from butyl to hexyl decreases the tensile modulus from 1.87 GPa to 1.09 GPa; increasing it further to octyl decreases the modulus to 150 MPa **(Figure 2.2)**.[1] The extreme compliance of P3OT—even in a blend with PCBM[1]—permits it to be strained to conform to hemispherical objects without wrinkling.[2] The elasticity and ductility of P3OT, however, come at a cost of significantly degraded field-effect mobility and photovoltaic efficiency compared to P3HT.[2,5]

Elasticity and ductility are regarded as antithetical to electronic performance; several studies are consistent with this perception. O'Connor et al. noted a correlation between stiffness and charge-carrier mobility in two types of polythiophenes, P3HT and PBTTT.[3] Intercalation of the side-chains in the case of PBTTT led to good vertical registration and a highly crystalline morphology.[3] This ordered microstructure was correlated with good charge transport properties (although high crystallinity is not always a prerequisite for good photovoltaic performance[36]). Poor vertical registration in the case

of P3HT, whose side chains are liquid-like at room temperature, produces a semicrystalline film that is relatively stretchable but has a field-effect mobility that is no longer considered state-of-the art.[3] In another system, Awartani et al. showed that slow evaporation of the solvent during casting of P3HT:$PC_{61}BM$ blends led to greater order of the polymer (as determined by applying the weakly interacting H-aggregate model to UV-vis spectra of the solid films)[37] and greater photovoltaic performance, but also greater stiffness and brittleness.[4] This paper explores the range in side-chain length between n = 6 and n = 8 (**Figure 2.2**) within which we postulated the existence of a "sweet spot" that maximizes mechanical resilience and photovoltaic performance. In particular, we compared the tensile moduli, structure as deduced by ultraviolet-visible (UV-vis) spectroscopy and atomic force microscopy (AFM), and photovoltaic properties (when blended with $PC_{61}BM$) of the six polymeric samples shown in **Figure 2.1**.

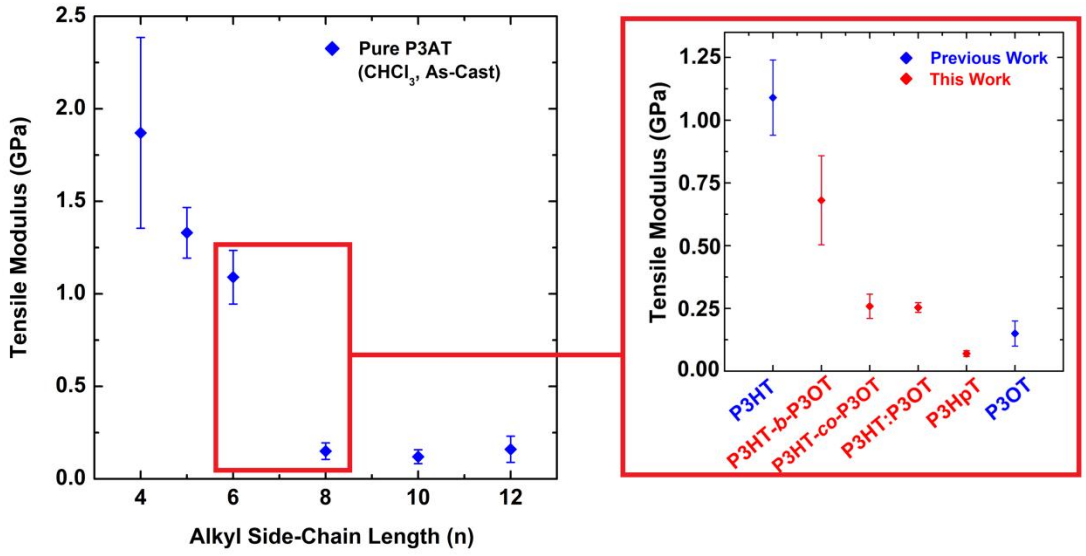

Figure 2.2. Plot of tensile modulus vs. alkyl side-chain length. Tensile moduli of the pure polymer thin films spin-coated from chloroform were measured via buckling methodology. Materials examined for the first time are indicated in red. The "sweet spot" between n = 6–8 is highlighted.

2.2 Experimental design

2.2.1 Selection of materials

P3HT, P3OT, and P3HpT. We chose P3HT because it is the most studied conjugated polymer for organic solar cells.[13,26] The photovoltaic performance of P3HT:$PC_{61}BM$ was used as the benchmark for the performance of all other tested organic photovoltaic devices. P3OT was selected for its low tensile modulus,[1] which is a necessary characteristic for polymers that are to be used in stretchable and flexible electronics. P3HpT was selected because the number of carbons in its alkyl side-chain (seven) is the average of the number of carbons in the alkyl side-chains of P3HT and P3OT. Our initial hypothesis was that the properties of P3HpT would be intermediate between those of P3HT and P3OT.[6]

Block and random copolymers. We also synthesized block and random copolymers having both hexyl and octyl side chains. Jenekhe and coworkers have measured differences in photovoltaic properties between physical blends of P3BT and P3OT and the covalently bonded block and random copolymers.[38,39] The authors found that the copolymers outperformed not only the physical blend, but also the homopolymers.[38,39] We expected that comparison of the properties of a physical blend, and block and random copolymers of P3HT and P3OT would provide insights into the relationship between molecular structure, morphology, and mechanical properties.

2.2.2 Mechanical characterization

Buckling-based metrology. We measured two parameters—the tensile modulus and the crack on-set strain—that permitted comparison of the elasticity and ductility of

each thin film. The tensile moduli were measured using the mechanical buckling technique originally described by Stafford et al.[40] This method provides rapid quantitative measurements and is well suited for analyzing the mechanical properties for various thin-film systems including conjugated polymer films.[1,4,23,24] The technique relates the tensile modulus of the film to the quantitative description of the surface buckling pattern of the film under compressive strains on a relatively compliant substrate—as described originally by Hutchinson, Whitesides, and coworkers.[41,42] The advantages of using the buckling technique are twofold: (1) conventional mechanical testing devices typically lack the sensitivity to measure the forces involved in straining a thin film;[40] and (2) techniques with adequate sensitivity such as nanoindentation do not provide accurate measurement for polymeric materials with viscoelastic behavior.[43] Briefly, the conjugated polymers were spin-coated onto passivated glass slides, then transferred to poly(dimethylsiloxane) (PDMS) substrates each bearing small pre-strain. After transfer, the PDMS substrates were relaxed; this action created a compressive strain that forced the conjugated polymer film to adopt sinusoidal buckles. The buckling wavelength, λ_b, and the thickness of the film, d_f, can be related to the tensile moduli of the film and the substrate, E_f and E_s, and the Poisson ratios of the two materials, v_f and v_s by the following equation:

$$E_f = 3E_s\left(\frac{1-v_f^2}{1-v_s^2}\right)\left(\frac{\lambda_b}{2\pi d_f}\right)^3 \qquad (1)$$

We measured the tensile modulus of the substrate, E_s (using a commercial pull tester), the buckling wavelength, λ_b (by optical microscopy), and the film thickness, d_f (by stylus profilometry). The slope of a plot of λ_b vs. d_f for three different film thicknesses was

inserted into Equation 1. The Poisson's ratios were taken as 0.5 and 0.35 for PDMS and the conjugated polymers films.[1,23] The experimental method is described in detail elsewhere.[1]

Ductility. Crack on-set strains have been shown to provide qualitative measure of the ductility of the thin polymer films,[1,3,4] with the caveat that poor adhesion of the P3AT to PDMS for long alkyl side chains ($n > 8$) leads to increased apparent brittleness.[1] The propensity of the conjugated polymer films to form cracks when stretched on a compliant substrate was measured by transferring the film to the PDMS substrate bearing no pre-strain, which was then stretched uniformly using a computer-controlled actuator. Optical micrographs of each film subjected to the strain of 1% to 80%, with a step size of 1%, were examined for the first sign of crack formation.

2.2.3 Theoretical determination of tensile modulus

We attempted to compare the tensile moduli obtained experimentally to those calculated by a semi-empirical theory that takes into account the chemical structure and thermal properties of the polymers. This approach was originally described by Seitz,[44] applied to conjugated polymers by Tahk et al,[23] and then modified to account for differential glass transition temperatures between polymers.[1] The model successfully predicts the tensile moduli of pure polythiophenes and, in conjunction with composite theory, blends of conjugated polymers with fullerene derivatives.[1,23] However, the simple theory does not account for the sequence of monomers within copolymers, and predicts, for example, the same tensile modulus for both block and random copolymers. A more

sophisticated approach is necessary to describe these copolymers and is being pursued by us in a separate project.

2.2.4 Fabrication of devices

We compared the photovoltaic properties of the various conjugated polymers using $PC_{61}BM$ as the electron acceptor. All conjugated polymer samples—P3HT, P3HpT, P3OT, physical blend (P3HT:P3OT), block copolymer (P3HT-*b*-P3OT), and random copolymer (P3HT-*co*-P3OT)—were mixed with $PC_{61}BM$ in a 1:1 ratio. We deposited a layer of PEDOT:PSS containing 7% DMSO and 0.1% Zonyl fluorosurfactant as the transparent anode.[45] For the top contact, we used a liquid metal cathode, eutectic gallium-indium (EGaIn), extruded manually from a syringe. The use of EGaIn (work function 4.1–4.2 eV) has been reported in the literature to give similar results to those of devices comprising evaporated aluminum.[46–48] We chose EGaIn because it facilitated rapid characterization of our devices and because of our overarching interest in stretchable materials and devices, in which EGaIn is a ubiquitous stretchable conductor.[49]

2.2.5 Weakly interacting H-aggregate model

Order in films of semiconducting polymers is associated with both greater electronic performance and increased stiffness.[3] The extent of order, as determined by UV-vis spectroscopy, has been correlated to increased tensile moduli in P3HT:PCBM films.[4] Spano et al. and others have shown that aggregates of P3HT in solid films can be considered as weakly interacting H-aggregates, due to cofacial π-π stacking and weak excitonic coupling.[4,37,50–53] We used this model to compare trends in conjugation length

from the UV-vis absorption spectra of the polymers, in an attempt to correlate these values with the mechanical stiffness and device performance. The model works as follows. Upon absorption of a photon, an electron is excited from the ground electronic state to an excited electronic state. In H-aggregates, these electronic excitations are coupled with nuclear vibrations.[37] This coupling can be understood by a semi-classical picture, in which the nuclei of the polymer aggregates can be thought of as existing in potential wells with quantized vibrational levels, analogous to an electron trapped in a potential well.[54] At lower vibrational levels, the potential wells can be approximated as harmonic oscillators; in this approximation, the vibrational energy levels are equally spaced.[37,54] In conjugated molecules, such as P3ATs, the vibrational levels arise from the symmetric stretching and ring breathing of the C = C bonds.[4,37,51,53] When an electron is excited, the position of the nuclear potential well in the excited state is shifted from the ground state and the electron and vibrational modes are therefore coupled.[37]

In the aggregated state (i.e., crystallites in solid films), these coupled electron-vibrational (vibronic) transitions determine the adsorption of weakly interactive H-aggregates and can be modeled as Gaussian fits by:[4,37,50,51,53]

$$A(E) \propto \sum_{m=0} \left(\frac{S^m}{m!}\right) \times \left(1 - \frac{We^{-S}}{2E_\mathrm{p}} \sum_{n \neq m} \frac{S^n}{n!\,(n-m)}\right)^2 \times exp\left(\frac{-\left(E - E_{00} - mE_\mathrm{p} - \frac{1}{2}WS^m e^{-S}\right)^2}{2\sigma^2}\right) \quad (\mathbf{2})$$

In the above equation, A is the absorption by an aggregate as a function of the photon energy (E). E_{00} is the energy of the 0→0 vibronic transition, which is allowed assuming some disorder in the aggregates.[37] S is the Huang-Rhys factor, which quantifies the nuclear potential well shift upon vibronic transition from the ground state to the excited state.[37] It is calculated from absorption and emission spectra, and is set to 1 for

P3ATs.[37,51] E_p is the intermolecular vibration energy, which (in the case where $S = 1$) is the difference in energy between the vibrational levels in the excited state. It is set to 0.179 eV as determined by Raman spectroscopy.[55] W is the free exciton bandwidth, which is related to the nearest neighbor interchain excitonic coupling. Upon coupling, a dispersion of the energies occurs, the width of which is equal to W (which is four times the nearest neighbor coupling).[37] W is also inversely related to conjugation length; a lower W indicates better ordering of the aggregates.[50] The terms m and n are the ground- and excited state vibrational levels and σ is the Gaussian linewidth.

2.3. Results and discussion

2.3.1 Characterization of the polymers

After synthesizing P3HT-*b*-P3OT and P3HT-*co*-P3OT, we examined the ^{1}H NMR spectra to estimate the ratios of 3HT and 3OT in the polymers. Because the signals arising from the terminal methyl groups of the hexyl and octyl side-chains were partially overlapped, we estimated the ratio of 3HT and 3OT monomers was the same as the molar ratios of the starting materials, approximately 1:1. The percent regioregularity for each sample was as follows: P3HT, 88%; P3HT-*b*-P3OT, 90%; P3HT-*co*-P3OT, 89%; P3HpT, 92%; P3OT, 82%. While the mechanical properties of most polymeric materials exhibit dependency on the molecular weight, this effect tends to saturate at a sufficiently high molecular weight.[56] Our laboratory has shown that the difference in tensile moduli between the commercial sample of P3HT (M_w = 29,000 g mol^{-1}, PDI = 2.0) and the sample synthesized in-house by the Grignard Metathesis polymerization[57] (M_w = 7500 g mol^{-1}, PDI = 1.2) was minimal: 1.09 ± 0.15 GPa for the commercial sample and 1.05 ±

0.35 GPa for the sample synthesized in-house.[2] Dauskardt and coworkers also reported the dependency of the mechanical properties on molecular weight, and found similar storage and loss moduli for samples with M_w ranging from 28,000 to 100,000 g mol^{-1} (samples with M_w < 28,000 g mol^{-1} were not tested).[58] These data suggest that in the elastic regime, M_w does not significantly affect the tensile moduli for the values of M_w of P3AT samples typically reported in the literature. We assumed covalent connectivity of the blocks in P3HT-*b*-P3OT by following the same synthetic protocol as used in several previous studies on P3AT block copolymers.[38,59–62]

2.3.2 Mechanical properties of pure polymer films

We began the characterization of the mechanical properties of each conjugated polymer by measuring the tensile modulus of the pure polymer film spin-coated from chloroform. In a previous report from our group, we measured decreasing moduli with increasing length of the alkyl side-chain in a series of P3ATs where A = butyl, hexyl, octyl, and dodecyl.[1] **Figure 2.2** and **Table 2.1** show the values obtained for the hybrid polymers on the same set of axes as those obtained in our previous study (we have since added pentyl and decyl to the plot for the purposes of this paper). The tensile moduli of the three individual polymer films containing both hexyl and octyl side-chains—the block and random copolymer and the physical blend—lie in between those of the P3HT and P3OT, as expected; however, the tensile modulus of block (680 ± 180 MPa) was determined to be almost three times those of random (260 ± 50 MPa) and physical blend (250 ± 20 MPa), which were nearly identical. For all three samples, the molar concentration of the 3HT and 3OT were approximately 1:1. We thus attributed the

differences in moduli to unequal microstructures of the three samples in the solid state rather than solely from the ratio of total hexyl and octyl side chains in the samples. Previous work on polymer-polymer blends that exhibit some extent of mutual solubility suggested that the tensile modulus of the blend is the synergistic modulus (weighted average) of the two homopolymers. For example, in the blend of poly(ether ether ketone) (PEEK) and poly(aryl ether sulfone) (PES),[63] and a blend of poly(ether imide) (PEI) and poly(trimethylene terephthalate) (PTT),[64] the authors demonstrated that the tensile moduli of each blend can be plotted against the molar concentration of one of the components to yield a linear relationship. Interestingly, we observed that the modulus of the block copolymer (P3HT-*b*-P3OT) was close to the synergistic modulus, while the moduli of the random copolymer and physical blend lied below (**Figure 2.3a**). To determine if the differences in moduli were attributable to variations in surface morphology, we examined thin films of these polymers by AFM; the results for these experiments are discussed in section 3.5.

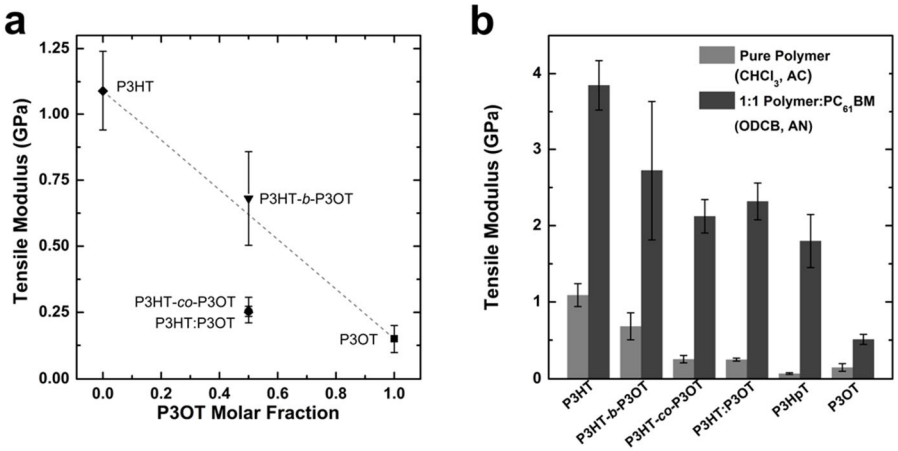

Figure 2.2. Tensile moduli of the polymers and polymer:fullerene blends in this work. **(**a) Tensile moduli of polymer films containing both hexyl and octyl side-chains along with the pure polymers. The dashed line shows the weighted average of the pure polymers. (b) Comparison between the pure polymer films spin-coated from chloroform (as-cast, AC) and the films comprising 1:1 polymer:$PC_{61}BM$ blends spin-coated from ODCB and thermally annealed at 100°C (AN).

Table 2.1. Tensile moduli of pure polymers spin-coated from $CHCl_3$ as-cast and their blends with $PC_{61}BM$ spin-coated from ODCB and thermally annealed at 100°C. *Values taken from ref. 1.

Polymer	Tensile Modulus (GPa)	
	Pure polymer ($CHCl_3$, As-Cast)	**1:1 Polymer:$PC_{61}BM$ (ODCB, Annealed)**
P3HT	1.09 ± 0.15 *	3.85 ± 0.32
P3HT-*b*-P3OT	0.68 ± 0.18	2.72 ± 0.91
P3HT-*co*-P3OT	0.26 ± 0.05	2.12 ± 0.22
P3HT:P3OT	0.25 ± 0.02	2.32 ± 0.24
P3HpT	0.07 ± 0.01	1.79 ± 0.35
P3OT	0.15 ± 0.05*	0.51 ± 0.07

Block copolymer. We attributed the higher value of tensile modulus of the block copolymer to the covalent bonds between the P3HT and P3OT segments that promote the formation of connected crystalline domains comprising both P3HT and P3OT. Jenekhe and coworkers observed two distinct interchain (lamellar) spacings by grazing incidence X-ray diffraction (GIXD) in a block copolymer of P3BT (n = 4) and P3OT of equal composition of monomers.[38] These two distinct signals corresponded to the lamellar spacings of the blocks of P3BT and P3OT.[38] We expected that P3HT-*b*-P3OT would behave similarly and form two distinct crystalline domains. Because the domains are covalently linked through the conjugated main chain, the more compliant P3OT phase is bound to the more rigid P3HT phase and thus the block copolymer is less able to accommodate strain than is the physical blend, P3HT:P3OT, discussed in the next paragraph.

Random copolymer. Unlike P3HT-*b*-P3OT, P3HT-*co*-P3OT, which has statistically incorporated monomers, is not likely to form two distinct crystalline domains. In films of a similar copolymer, P3BT-*co*-P3OT, Jenekhe and coworkers observed a single type of crystalline domain whose lamellar spacing correlated with the ratio of the monomers.[39] The standard model for packing within P3HT crystallites

assumes no interdigitation of side chains;[65] although interdigitation has been observed in the oligomer of 3HT with repeat units ≤ 20.[66] The randomness in packing of side chains in the interlamellar regions, along with decreased registration between the lamellae, could contribute to the tensile modulus that was lower for P3HT-*co*-P3OT than for P3HT-*b*-P3OT.

Physical blend. Our next task was to understand the mechanical behavior of the physical blend of P3HT and P3OT (P3HT:P3OT). A tensile modulus for P3HT:P3OT that was lower than the synergistic modulus would be consistent with a blend in which the phases were at least partially separated. In phase-separated blends, the more compliant P3OT phase may accommodate the strain, thus rendering the modulus of the blend closer to that of P3OT. This behavior is in contrast to that of P3HT-*b*-P3OT, in which the covalent connectivity of the domains resists deformation of the film. We note that co-crystallization has been observed in P3HT:P3OT blends by Nandi and coworkers by observation of a single lamellar spacing by X-ray diffraction.[67] The authors found, however, that the tendency to co-crystallize was extremely sensitive to differences in both the ratio of the components and regioregularity between the two isolated polymers.[67]

Poly(3-heptylthiophene). The P3ATs are a class of comb-like polymers[68] whose properties represent a compromise between the rigid main chain and the paraffinic side chains. For many systems, a monotonic decrease in T_g accompanies increasing side-chain length, n, up to a critical side-chain length, n_c. The trend exhibits a discontinuity at n_c, and for $n > n_c$, T_g changes little or even increases.[69] If one defines the critical alkyl side chain length in terms of the tensile modulus, then it appears that $n_c = 7$ for P3ATs, even though T_g continues to decrease up to at least $n = 12$.[70] The observed modulus of P3HpT

(70 ± 10 MPa) is within the same order of magnitude as that of P3OT and P3DDT (**Figure 2.2**).[1] Unlike the copolymers and the physical blend, the compliance of P3HpT cannot be a consequence of the interaction between monomers with different side chains. Our measurement of the modulus of poly(3-pentylthiophene) (P3PT, $n = 5$) (1.33 ± 0.14 GPa) and its placement on the line connecting P3BT and P3HT suggest that the conspicuously low modulus of P3HpT is also not a manifestation of the odd number of carbon atoms in the side chain. While the overall reduction in modulus with increasing n is expected on the basis of a corresponding reduction in T_g and the dilution of volume fraction of the main-chain with increasing length of the alkyl side-chains,[1] the sharp drop in modulus from $n = 6$ to $n = 7$ is nonetheless conspicuous. This drop in modulus is consistent with the fact that P3HpT is the P3AT with the shortest side chains whose T_g is extrapolated to be significantly below room temperature (T_g for P3HT has been measured in the range of 12–25 °C for P3HT and –14 °C for P3OT).[4,71] Our theoretical calculation of the tensile moduli using the molecular structure of the monomers[1,23,35,44] predicted a value for P3HpT (130 ± 20 MPa) that was close to the experimental value (70 ± 10 MPa). This simple model, however, was unable to simulate the moduli for the hybrid polymer samples. We believe that its failure arises from its inability to incorporate the interaction between different polymer chains within the films and the distribution of the monomers in the backbones (in both block and random copolymers).

Ductility. While the theoretical model failed to predict the tensile moduli of the copolymers and the physical blend, the trend in the apparent brittleness agrees well with the experimental values. Our group and others have found that the tensile modulus of P3AT correlates with brittleness when stretched on a compliant substrate.[1,3,4,24] We

measured the strain at which the first crack appeared on the surface of the film (crack on-set strain) of pure polymer films, spin-coated from chloroform without annealing (as-cast, AC). We observed that thin films of P3HT-*b*-P3OT crack at much lower applied strains (8%) than those of P3HT:P3OT and P3HT-*co*-P3OT, whose crack on-set strains are similar (30% and 32% respectively). In addition, P3HpT was observed to have a high crack on-set strain (58%), which was similar to those of P3OT and P3DDT.[1]

2.3.3 Mechanical properties of polymer:$PC_{61}BM$ composites

The presence of fillers has a strong influence on the mechanical properties of composite materials.[1,24] For bulk heterojunction solar cells, polymers are usually blended with fullerene derivatives ($PC_{61}BM$ or $PC_{71}BM$) at a ratio by weight of 1:1 to 1:4 (polymer:fullerene).[26,28] We measured the moduli of polymer:$PC_{61}BM$ films in a 1:1 ratio, which were spin-coated from ODCB and thermally annealed. All samples were annealed at the same temperature (100 °C) for consistency and to decouple the effect of temperature on the mechanical and electronic properties. Various studies have demonstrated that the addition of fullerenes to conjugated polymers produces composites that are stiffer and more brittle than are the pure polymers.[1–3,23,24] We have also previously shown that the moduli of 2:1 blends of P3AT:$PC_{61}BM$ (including P3BT, P3HT, P3OT, and P3DDT) are 2–3 times that of pure P3ATs.[1] The exact factor by which the blend is stiffer than the pure polymer, however, depends strongly on the identity of the polymer[24] and the processing conditions (e.g., as in fast-dried and slow-dried films).[4] A previous report showed that the increase in modulus of a P3HT:$PC_{61}BM$ film over that of the pure polymer was a factor of approximately five, whereas the increase in modulus

of DPPT-TT:$PC_{61}BM$ over the pure polymer was only 40 percent.[24] This behavior suggests that interaction between the polymer and the $PC_{61}BM$ additive depends heavily on the morphologies of the blend, including miscibility of the polymer and the fullerene,[72] intercalation of the fullerene molecules between the side chain of the polymer,[73] and possible formation of bimolecular crystallites.[74] Each of these effects would strongly influence the mechanical properties of the blended films, and we are investigating these effects separately. **Figure 2.3b** and **Table 2.1** show the values of the tensile moduli of polymer blends with $PC_{61}BM$. The P3AT:$PC_{61}BM$ composites are observed to have higher tensile moduli than the pure polymers for all cases. The value of P3HT:$PC_{61}BM$ reported here is similar to those reported previously in literature.[23,24]

2.3.4 Photovoltaic properties

We fabricated photovoltaic devices by mixing the polymers in a 1:1 ratio with $PC_{61}BM$. PEDOT:PSS was used as the transparent anode and eutectic gallium-indium (EGaIn) as the cathode.[46] **Figure 2.4a** shows the current density vs. voltage (*J–V*) plots for the devices based on P3AT homopolymers. The P3HT:$PC_{61}BM$ (*PCE* = 2.04 ± 0.27, *N* = 8) and P3OT:$PC_{61}BM$ (*PCE* = 0.67 ± 0.06, *N* = 7) devices performed as expected relative to each other and the results agree with previously published results.[8] The P3OT:$PC_{61}BM$ devices performed poorly due to the low short-circuit current (J_{sc}), 2.71 ± 0.32 mA cm^{-2}, and fill factor (*FF*), 43.7 ± 1.0%. Surprisingly, the performance of P3HpT:$PC_{61}BM$ (*PCE* = 2.16 ± 0.17, *N* = 8) did not fall between these values. Compared to P3HT:$PC_{61}BM$, these devices had a similar J_{sc} (6.95 ± 0.91 for P3HT:$PC_{61}BM$ vs. 6.27

± 0.48 mA cm^{-2} for P3HpT:$PC_{61}BM$), open circuit voltage (V_{oc}) (568 ± 9 vs. 598 ± 5 mV), and *FF* (51.7 ± 1.9 vs. 57.5 ± 1.8 %).

The *J-V* plots for the blended and copolymer devices are shown in **Figure 2.4b**. Among these polymers, the physical blend P3HT:P3OT:$PC_{61}BM$ (*PCE* = 1.24 ± 0.21, *N* = 7) performed the poorest, while P3HT-*b*-P3OT:$PC_{61}BM$ (*PCE* = 1.56 ± 0.25, *N* = 8) and P3HT-*co*-P3OT:$PC_{61}BM$ (*PCE* = 1.50 ± 0.19, *N* = 7) performed similarly. The poor performance by the physical blend devices is likely due to its much lower J_{sc} (3.67 ± 0.56 mA cm^{-2}) compared to P3HT-*b*-P3OT:$PC_{61}BM$ (5.80 ± 0.58 mA cm^{-2}) and P3HT-*co*-P3OT:$PC_{61}BM$ (5.19 ± 0.76 mA cm^{-2}). The reduced J_{sc} in the physical blend devices is attributed to the incorporation of P3OT phases, which have a low J_{sc} as shown in the homopolymers devices. The photovoltaic properties for all devices tested are summarized in **Table 2.2**.

Table 2.2. Summary of the averaged J_{sc} (short-circuit current), V_{oc} (open-circuit voltage), *FF* (fill factor), and *PCE* (power conversion efficiency) for the solar cells fabricated in this work ($N \geq 7$). The solar device architecture was PEDOT:PSS/Polymer/$PC_{61}BM$/EGaIn. The active layer was spin-coated from a solution of 1:1 Polymer:$PC_{61}BM$ in ODCB (40 mg mL^{-1}). To ensure the preparation of solar devices was consistent with the preparation of samples for mechanical testing, all devices were annealed at 100 °C in an inert atmosphere.

Polymer	J_{sc} (mA cm^{-2})	V_{oc} (mV)	*FF* (%)	*PCE* (%)
P3HT	6.95 ± 0.91	568 ± 9	51.7 ± 1.9	2.04 ± 0.27
P3HpT	6.27 ± 0.48	598 ± 5	57.5 ± 1.8	2.16 ± 0.17
P3OT	2.71 ± 0.32	570 ± 14	43.7 ± 1.0	0.67 ± 0.06
P3HT:P3OT	3.67 ± 0.56	592 ± 11	57.0 ± 1.6	1.24 ± 0.21
P3HT-*b*-P3OT	5.19 ± 0.76	607 ± 5	49.4 ± 0.5	1.56 ± 0.25
P3HT-*co*-P3OT	5.80 ± 0.58	549 ± 9	47.0 ± 1.6	1.50 ± 0.19

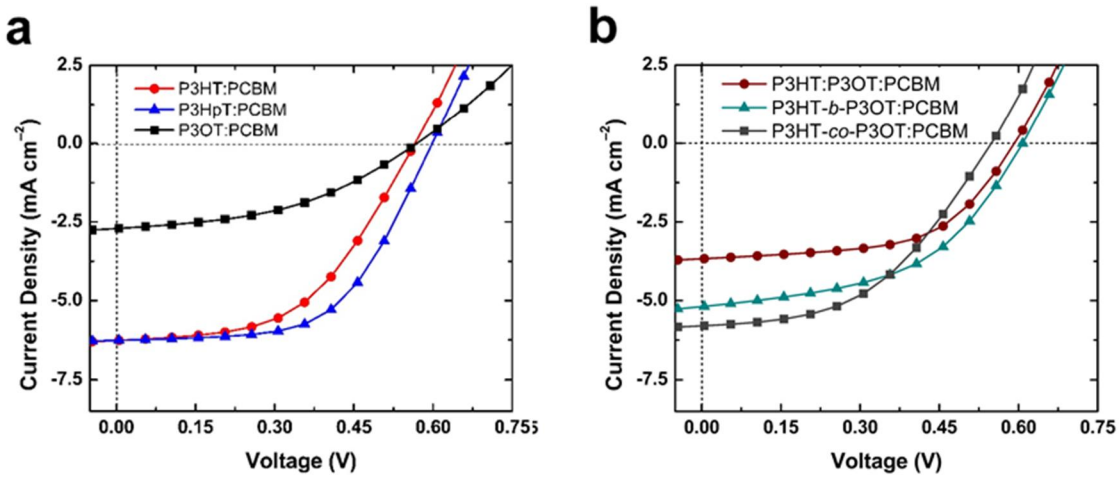

Figure 2.4. *J-V* curves of average devices ($N \geq 7$) with an active layer of 1:1 blend of polymer and $PC_{61}BM$. The architecture of the devices was PEDOT:PSS/polymer:$PC_{61}BM$/EGaIn.

2.3.5 Microstructural characterization of the polymer films

AFM analysis. To determine if the mechanical and photovoltaic properties were due to differences in the morphologies of the films, films of the pure polymers were characterized by atomic force microscopy (AFM). We characterized both as-cast films and films annealed at 100 °C. **Figure 2.5** shows the phase images obtained by AFM for these films. Fibril structures were observed in all as-cast films except for P3OT. Upon annealing, there was an increase in the phase contrast, which is indicative of an increase in order,[75] for all of the polymers except for P3HT-*b*-P3OT and P3HT-*co*-P3OT. The increase in order demonstrated by pure polymers and the physical blend was expected, but the apparent lack of further ordering in the P3HT-*b*-P3OT and P3HT-*co*-P3OT films was surprising. The covalent connectivity of the copolymers might suppress a change in microstructure that is too small to be visible by AFM. For a finer-grained analysis of the evolution in microstructure with annealing, we turned to UV-vis spectrophotometry.

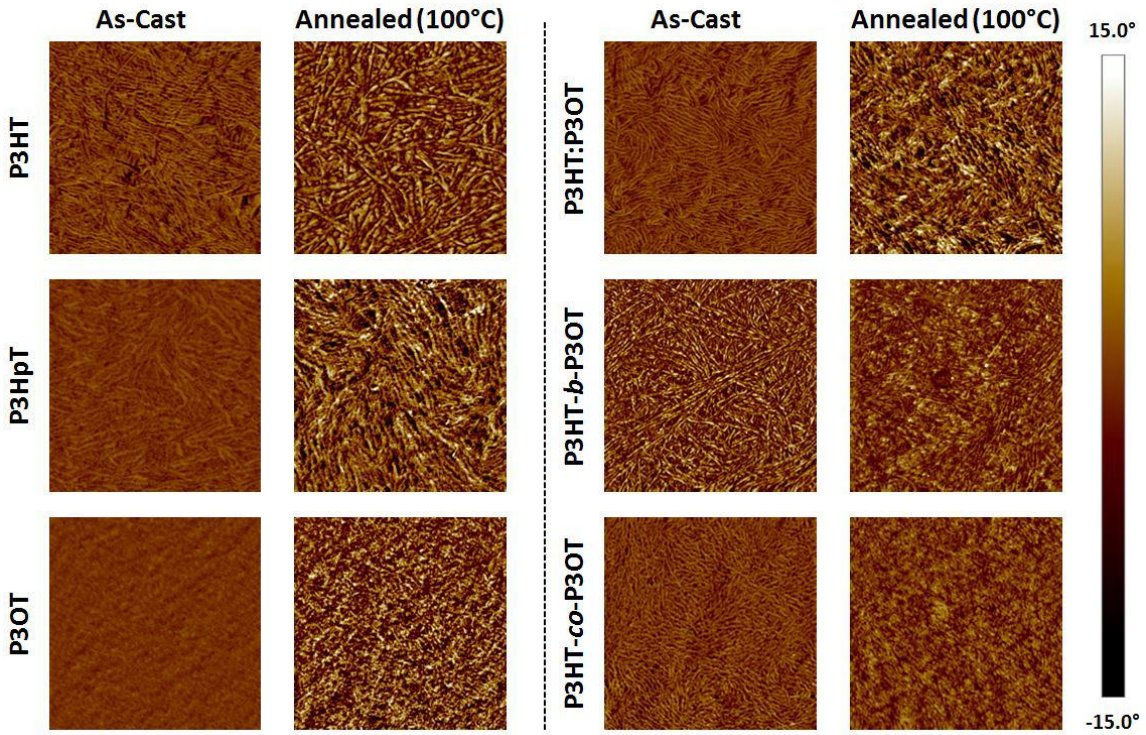

Figure 2.5. Phase images of pure polymers spin-coated from ODCB both as-cast and annealed. The dimensions are 1.5 μm x 1.5 μm.

UV-vis spectrophotometry. To extract information about the relative conjugation lengths of the pure polymers, we characterized them by UV-vis spectrophotometry. The polymers were spin-coated onto glass out of $CHCl_3$ and the absorption of the films was measured over the range 1.46–4.13 eV (λ = 850–300 nm). The UV-vis spectra of the homopolymers are shown in **Figures 2.6a** and **2.6b** and those of the polymer blend and copolymers are shown in **Figures 2.6c** and **2.6d**. The polymers represented in **Figures 2.6a** and **2.6c** were unannealed, while those represented in **Figures 2.6b** and **2.6d** are after annealing at 100 °C in an inert atmosphere. Two observations can be made from visual inspection of these absorption spectra. First, all of the curves for the annealed polymer films have better defined shoulders than their unannealed counterparts. The increase in definition of the shoulders indicates an increase

in order in the polymer films upon annealing.[4,37,50–53] Second, after annealing, P3HT and P3HpT have very similar absorption spectra, which implies similar electronic structures and order in the solid film. The absorption spectrum of P3OT suggests less ordering. The annealed P3HT-*b*-P3OT and P3HT:P3OT samples also have very similar absorption spectra which are consistent with similarly ordered crystallites in the films. Jenehke and coworkers have previously shown that block copolymers of P3BT and P3OT form distinct domains of each polymer.[76] From our analysis, we believe that our samples of P3HT-*b*-P3OT and P3HT:P3OT likely form distinct crystallites of P3HT and P3OT, as these materials have UV-vis spectra that essentially overlap with the superposition of the pure P3HT and P3OT films.

To explore further the effects of annealing on the polymer films, we utilized the weakly interacting H-aggregate model. The absorption spectrum of P3HT, and by extension other P3ATs, can be envisioned as a superposition of the absorption by polymer crystallites and the absorption by the regions of amorphous polymer. The absorption by crystallites dominates the lower energy region, while the absorption at higher energies occurs predominantly by the amorphous polymer.[4] The weakly interacting H-aggregate model was used to deconvolute the absorption spectra and determine the absorption by the polymer aggregates. From this model, we attempted to correlate the conjugation length (from the exciton bandwidth) to mechanical stiffness and device performance. With the Huang-Rhys factor, *S*, set to 1, the exciton bandwidth, *W*, can be calculated from the approximated expression:[50]

$$\frac{A_{0-0}}{A_{0-1}} \approx \left(\frac{1 - 0.24W/E_p}{1 + 0.073W/E_p}\right)^2 \qquad (\mathbf{3})$$

where A_{0-0} and A_{0-1} are the absorption intensities of photons with the energies of the 0→0 and 0→1 vibronic transitions, respectively. Qualitatively, a decrease in the ratio of A_{0-0} to A_{0-1} is related to an increase in local order.[4,37,50] More specifically, W is inversely related to conjugation length and order; a lower W is indicative of a longer conjugation length and better order.[50]

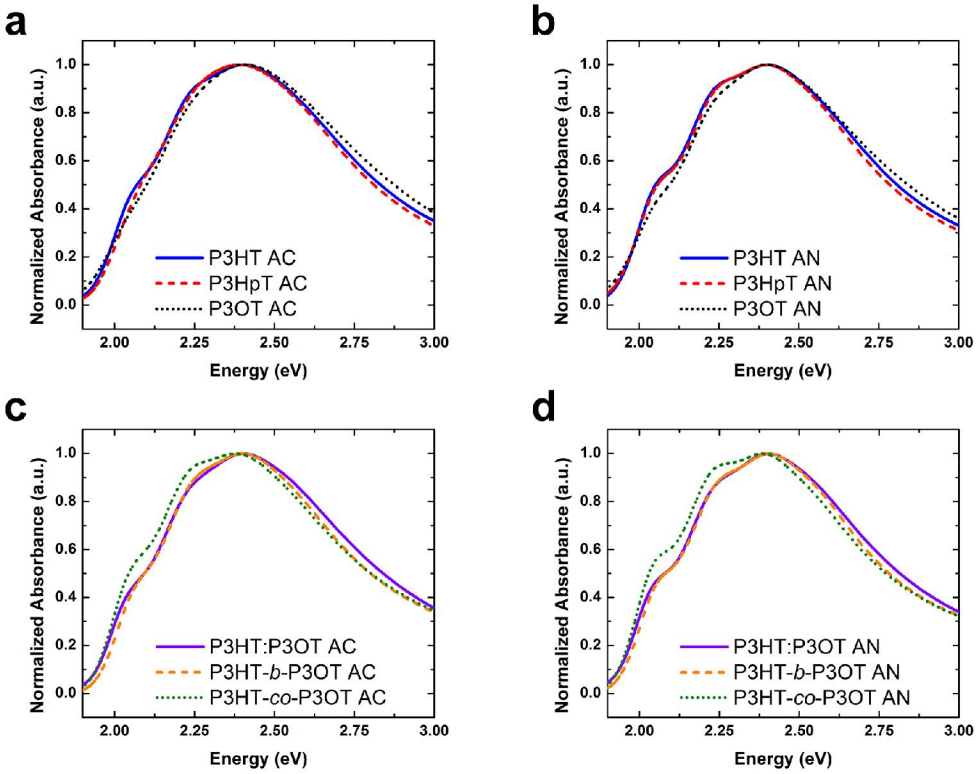

Figure 2.6. Absorption of polymer thin films cast from $CHCl_3$. (a) Homopolymers as-cast (AC). (b) Homopolymers annealed at 100 °C in an inert atmosphere (AN). (c) Blend and copolymers as-cast (AC). (d) Blend and copolymers annealed at 100 °C in an inert atmosphere (AN).

The energy of the 0→0 vibronic transition, E_{00}, was found by calculating the second derivative of the absorption curves using a Matlab program. The same procedure was repeated to find the energy of the 0→1 vibronic transition. The absorption at these energies was then used to calculate the exciton bandwidth, W from Equation 3. The

Gaussian linewidth, σ, and the scaling factor for the calculated absorption were then found by a least squares fit to the experimental absorption in the region of 1.93 to 2.25 eV.[4,53,77] This region was selected because the absorption is dominated by the polymer aggregates. Above 2.30 eV, the amorphous polymer dominates absorption.[51,77] The results are summarized in **Table 2.3**.

Table 2.3. Summary of the weakly interacting H-aggregate model parameters for the polymers in this work. All materials were cast from $CHCl_3$ and then annealed at 100 °C in an inert atmosphere.

Polymer	W (eV)	$1/W$ (eV^{-1})	σ (eV)	E_{00} (eV)	λ_{E00} (nm)
P3HT	0.160	6.250	0.079	2.043	607
P3HpT	0.158	6.335	0.081	2.050	605
P3OT	0.189	5.278	0.091	2.039	608
P3HT:P3OT	0.174	5.762	0.079	2.036	609
P3HT-*b*-P3OT	0.169	5.922	0.079	2.050	605
P3HT-*co*-P3OT	0.145	6.889	0.077	2.039	608

Among the homopolymers cast from chloroform after annealing, we found that the inverse of W, and thus conjugation length, of P3HT is similar to P3HpT and greater than P3OT. These values agree with our observations of the materials in our photovoltaic measurements and suggest that a contributing factor for poor device performance in P3OT is a shorter conjugation length than P3HT (and P3HpT). The conjugation length also appears to fit the trend (but not as strongly) of the tensile moduli of the materials. O'Connor and coworkers first noted the correlation of order derived from UV-vis data with tensile moduli.[4]

2.3.6 Correlations between tensile modulus and photovoltaic performance

We began our investigation motivated by our observations and those of others that mechanical compliance and electronic performance of organic semiconductors were

apparently in competition. Our analysis of four conjugated polymer samples with characteristics that represented different methods of hybridizing P3HT (stiff but good electronic properties) and P3OT (compliant but poor electronic properties) revealed P3HpT as the material that best combined both mechanical compliance and photovoltaic performance. In particular, the similarities of the photovoltaic properties and the order as measured by UV-vis spectroscopy and the H-aggregate model are largely manifestations of the crystalline regions in a polymer film, which were of similar extent in both P3HT and P3HpT. The mechanical properties for a material operating above its T_g, however, are largely manifestations of the amorphous regions of a polymer. The relatively long side chains of P3HpT and P3OT tend to suppress T_g well below room temperature, and provide increased elasticity and ductility compared to P3HT. The effect of blending $PC_{61}BM$ into polymers to form bulk heterojunctions is to increase the modulus of the polymer:fullerene composite relative to that of the pure polymer. Because the fullerenes exist in fullerene-rich and mixed phases (they do not intercalate into the crystalline phases of P3ATs), the increase in modulus is most likely dependent on the solubility of the fullerene in the amorphous regions of the polymer, which in turn depends at minimum on the length of the alkyl side chain. While the field has recently achieved an impressive model of the morphology of the bulk heterojunction,[78–80] additional work will be required to develop a composite theory that predicts accurately the mechanical properties of these types of blends. **Figure 2.7** presents our best evidence that combining mechanical compliance and electronic performance in the same material is possible in principle. That is, P3HpT lies in the extreme corner of the quadrant that combines favorable mechanical and electronic properties, as manifested in good photovoltaic

properties in blends with fullerenes. While the P3HpT:$PC_{61}BM$ blend is considerably stiffer than is the pure polymer, $PC_{61}BM$ is not the only acceptor that can be used in organic solar cells; it is likely that blending P3ATs with other acceptors will produce composites with mechanical properties that are far different from polymer:fullerene blends.

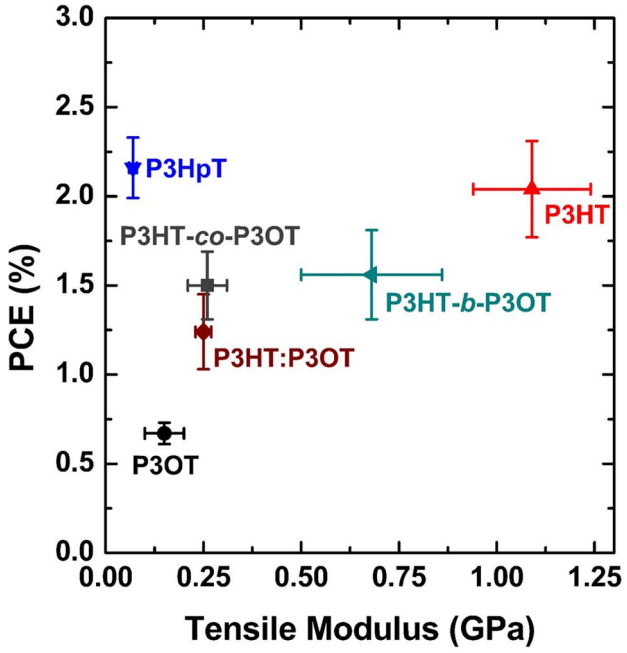

Figure 2.7. Plot of tensile moduli of the pure polymers vs. power conversion efficiency of the polymers in a 1:1 blend with $PC_{61}BM$. The position of P3HpT well above and to the left of the line connecting P3HT and P3OT suggest that in principle it is possible to co-engineer mechanical and photovoltaic properties in a single material.

2.4. Conclusion

This paper described our efforts to synthesize or discover a conjugated polymer that exhibited high values of mechanical compliance and electronic performance manifested in good photovoltaic properties using P3ATs as the model organic semiconductor. We discovered a very large effect of the alkyl side chain (between six and eight carbon atoms) in determining the mechanical and electronic properties. In

particular, we found that polythiophene with side chains containing seven carbon atoms, P3HpT, exhibited the optimal combination of mechanical compliance and photovoltaic efficiency. Examination of the mechanical and photovoltaic properties of the block and random copolymers and a physical blend of P3HT and P3OT revealed that the block copolymer exhibited the synergistic (average) modulus, while the random copolymer and physical blend did not.

Our findings may provide insights toward the design and synthesis of organic semiconductors that combine state-of-the-art electronic properties with extreme softness. It also highlights the critical role played by small changes (from six to seven carbon atoms in the alkyl side chain) in determining the bulk and electronic properties of these materials. Our work on copolymers exposed the shortcoming in a common semi-empirical approach to predicting the moduli of semiconducting polymers in its inability to differentiate the spatial distribution of unlike monomers (block vs. random copolymers with identical mole fractions of the components). Understanding of the role of chemical structure on the mechanical properties of organic semiconductors could lead the way toward truly multifunctional materials with tunable properties.

2.5. Experimental methods

2.5.1 Materials

Poly(3-pentylthiophene), Poly(3-heptylthiophene), and Poly(3-decylthiophene) were purchased from Rieke Metals, Inc. and used as received. Poly(3-hexylthiophene) and poly(3-octylthiophene) were purchased from Sigma-Aldrich and used as received. 3-Hexylthiophene and 3-octylthiophene were purchased from TCI and used as received.

Dichlorobistriphenylphosphinopropane nickel(II) was purchased from Strem. [6,6]-phenyl C_{61} butyric acid methyl ester ($PC_{61}BM$) was obtained from Sigma-Aldrich with >99% purity. PDMS, Sylgard 184 (Dow Corning), was prepared according to the manufacturer's instructions at a ratio of 10:1 (base:crosslinker) and cured at room temperature for 36 to 48 h before it was used for mechanical testing. (Tridecafluoro-1,1,2,2-tetrahydrooctyl)-1-trichlorosilane (FOTS) was obtained from Gelest. PEDOT:PSS (Clevios PH1000) was purchased from Heraeus. DMSO was purchased from BDH with purity of 99.9% and Zonyl (FS-300) fluorosurfactant were purchased from Sigma-Aldrich. All reagents were obtained from commercial suppliers and used without purification. Chloroform ($CHCl_3$), ortho-dichlorobenzene (ODCB), acetone, isopropyl alcohol (IPA), methanol, hexanes, and tetrahydrofuran (THF) were obtained from Sigma-Aldrich and used as received.

2.5.2 Synthesis of block and random copolymers

P3HT-*b*-P3OT. Poly(3-octylthiophene)-block-poly(3-hexylthiophene) (P3OT-*b*-P3HT, "block"). In the first round-bottom flask (flask A), a solution of 2,5-dibromo-3-octylthiophene (2.00 g, 5.65 mmol) was prepared in THF (60 mL) at ambient temperature. To this solution was added isopropyl magnesium chloride (4.5 mL of a 1.3 M solution in THF, 5.65 mmol). A suspension of $Ni(dppp)Cl_2$ (61 mg, 0.113 mmol, in 10 mL THF) was added by syringe in one portion. The polymerization proceeded to produce a dark red solution that fluoresced red-orange when illuminated with a long-wave ultraviolet lamp. This reaction was allowed to proceed for 10 min. Meanwhile, in a separate round-bottom flask (flask B), a solution of 2,5-dibromo-3-hexylthiophene (1.84

g, 5.65 mmol) was prepared in THF (60 mL). This solution was treated with isopropyl magnesium chloride (4.5 mL of a 1.3 M solution in THF, 5.65 mmol). After the 10 min reaction time in flask A, the contents of flask B were added to flask A by syringe. The combined solution was allowed to stir for 3 h. The reaction mixture was quenched by pouring into 400 mL of methanol. The quenched mixture was poured into centrifuge tubes, spun at 2.5 krpm, and decanted. The pellets were combined, placed on filter paper, and inserted into a Soxhlet extractor. The material was washed with methanol and hexanes, and extracted with chloroform. The chloroform fraction was concentrated in vacuo to give 562 mg (16% yield) of a red solid. ^{1}H NMR (300 MHz, $CDCl_3$): δ (ppm) = 7 (s, 1H), 2.92-2.45 (br, 2H), 1.82-1.63 (br, 2H), 1.54-1.23 (br ovlp, 8H), 0.94 (t ovlp, approx. 1.5H), 0.91 (t ovlp, approx. 1.5H).

P3HT-*co*-P3OT. Poly(3-octylthiophene)-co-poly(3-hexylthiophene) (P3OT-*co*-P3HT, "random"). In a round-bottom flask, a solution of 2,5-dibromo-3-octylthiophene (2.00 g, 5.65 mmol) and 2,5-dibromo-3-hexylthiophene (1.84 g, 5.65 mmol) was prepared in THF (120 mL) at ambient temperature. To this solution was added isopropyl magnesium chloride (9.0 mL of a 1.3 M solution in THF, 11.3 mmol). A suspension of Ni(dppp)Cl_2 (122 mg, 0.113 mmol, in 10 mL THF) was added by syringe in one portion. The reaction was allowed to stir for 3 h, then quenched and purified in the manner described for the block copolymer. The chloroform fraction was concentrated in vacuo to give 693 mg (18% yield) of a red solid. ^{1}H NMR (300 MHz, $CDCl_3$): δ (ppm) = 7 (s, 1H), 2.92-2.45 (br, 2H), 1.82-1.63 (br, 2H), 1.54-1.23 (br ovlp, 8H), 0.94 (t ovlp, approx. 1.5H), 0.91 (t ovlp, approx. 1.5H).

2.5.3 Preparation of substrates

Glass slides used as substrates for solar devices were cut into 1-in squares with a diamond-tipped scribe. They were then subsequently cleaned with Alconox solution (2 mg mL^{-1}), deionized water, acetone, and then isopropyl alcohol (IPA) in an ultrasonic bath for 10 min each and then rinsed and dried with compressed air. Next, the glass was plasma treated at ~30 W for 3 min at a base pressure of 200 mtorr ambient air to remove residual organic material and activate the surface.

Glass slides used as substrates for thin films for UV/vis spectrophotometry measurements were cut into 1-in squares with a diamond-tipped scribe. The slides were then rinsed with water and ultrasonicated in IPA for 20 min. The slides were then rinsed with IPA and dried by compressed air. Next the glass was plasma treated as described above. Blanks used to subtract the absorption of the glass were cleaned in the same manner.

Silicon substrates used for AFM measurements were cut into 1-cm^2 pieces. To remove debris from the surfaces, the silicon substrates were ultrasonicated in acetone for 10 min, followed by IPA for 10 min and subsequently rinsed with IPA and then dried with compressed air. The wafers were then plasma treated as described above.

2.5.4 Preparation of polymer solutions

Solutions of P3HT, P3HpT, P3OT, and hybrid materials of P3HT and P3OT (physical blend, random copolymer, and block copolymer) in $CHCl_3$ (15 mg ml^{-1}) were prepared for the buckling technique and UV-vis. Solutions of the polymers in ODCB (20 mg ml^{-1}) were prepared for AFM, and 1:1 polymer:$PC_{61}BM$ solutions in ODCB (40 mg

ml^{-1}) were prepared for solar cells. All solutions were allowed to stir overnight and filtered with a 1-μm glass microfiber (GMF) syringe filter immediately before being spin-coated onto glass or silicon substrates.

2.5.5 Fabrication of solar cells

We deposited a layer of PEDOT:PSS from an aqueous solution containing 92.9 wt% Clevios PH 1000 (~0.9-1.2 wt% PEDOT:PSS), 7.0 wt% DMSO, and 0.1 wt% Zonyl fluorosurfactant as the transparent anode. The solution was filtered with a 1-μm glass microfiber syringe filter and then spin-coated at a speed of 500 rpm (250 rpm s^{-1} ramp) for 60 s, followed by 2000 rpm (750 rpm s^{-1} ramp) for 60 s. The samples were subsequently dried at 150 °C for 30 minutes. The photoactive layer was then spin-coated onto the electrode layer at a speed of 500 rpm (250 rpm s^{-1} ramp) for 240 s, followed by 2000 rpm (750 rpm s^{-1} ramp) for 60 s. A thin strip of the PEDOT:PSS electrode was exposed by wiping away some of the photoactive layer with chloroform so that electrical contact could be made. The samples were then immediately placed in a nitrogen-filled glovebox and annealed at 100 °C for 30 min. The substrates were then allowed to cool slowly to room temperature. EGaIn (extruded by hand from a syringe) was used as the top contact. The photovoltaic properties were measured in a nitrogen-filled glovebox using a solar simulator with a 100 mW cm^{-2} flux that approximated the solar spectrum under AM 1.5G conditions (ABET Technologies 11016-U up-facing unit calibrated with a reference cell with a KG5 filter). The current density versus voltage was measured for both dark and under illumination using a Keithley 2400 SourceMeter.

2.5.6 Characterization of materials

The absorbance of the materials was measured using a PerkinElmer Lambda 1050 UV-vis-NIR spectrophotometer. The wavelength range measured was 850–300 nm with a step size of 1 nm. The polymer solutions were spin-coated onto the glass slides at a spin speed of 500 rpm (250 rpm s^{-1} ramp) for 240 s followed by 2000 rpm (750 rpm s^{-1} ramp) for 60 s. For each solution, two films were prepared. The first film was left as-cast and the second film was immediately placed in a nitrogen-filled glove box and annealed at 100 °C for 30 min under a Pyrex petri dish covered in aluminum foil. After 30 min, the samples were allowed to slowly cool back down to room temperature.

Atomic Force Microscopy (AFM) micrographs were taken using a Veeco Scanning Probe Microscope in tapping mode. Data was analyzed with NanoScope Analysis v1.40 software (Bruker Corp.). The samples were prepared in the same manner as the samples for UV-vis, except the substrates used were Si pieces.

All compounds were characterized by ^{1}H NMR (300 MHz, Varian) using $CDCl_3$ as the solvent. The residual chloroform peak at 7.26 ppm was used to calibrate the chemical shifts.

Acknowledgements

This work was supported by the Air Force Office of Scientific Research (AFOSR) Young Investigator Program, grant number FA9550–13–1–0156. Additional support was provided by the National Science Foundation Graduate Research Fellowship under Grant No. DGE-1144086, awarded to S.S., by Initiative for Maximizing Student Development awarded to D.R., and by laboratory startup funds from the University of California, San

Diego. The authors thank Prof. Brendan O'Connor, Prof. Frank Spano, and Prof. Paul Smith for helpful discussions.

Chapter 2, in full, is a reprint of the material as it appears in *Macromolecules*, 2014, 47, 1981. American Chemical Society, 2014. Suchol Savagatrup,[†] Adam D. Printz,[†] Daniel Rodriquez, and Darren J. Lipomi. ([†] Equal contribution). The dissertation author was the primary investigator and author of this paper.

References

(1) Savagatrup, S.; Makaram, A. S.; Burke, D. J.; Lipomi, D. J. Mechanical Properties of Conjugated Polymers and Polymer-Fullerene Composites as a Function of Molecular Structure. *Adv. Funct. Mater.* **2014**, *24*, 1169–1181.

(2) O'Connor, T. F.; Zaretski, A. V.; Shiravi, B. A.; Savagatrup, S.; Printz, A. D.; Diaz, M. I.; Lipomi, D. J. Stretching and Conformal Bonding of Organic Solar Cells to Hemispherical Surfaces. *Energy Environ. Sci.* **2014**, *7*, 370–378.

(3) O'Connor, B.; Chan, E. P.; Chan, C.; Conrad, B. R.; Richter, L. J.; Kline, R. J.; Heeney, M.; McCulloch, I.; Soles, C. L.; DeLongchamp, D. M. Correlations between Mechanical and Electrical Properties of Polythiophenes. *ACS Nano* **2010**, *4*, 7538–7544.

(4) Awartani, O.; Lemanski, B. I.; Ro, H. W.; Richter, L. J.; DeLongchamp, D. M.; O'Connor, B. T. Correlating Stiffness, Ductility, and Morphology of Polymer:Fullerene Films for Solar Cell Applications. *Adv. Energy Mater.* **2013**, *3*, 399–406.

(5) Babel, A.; Jenekhe, S. A. Alkyl Chain Length Dependence of the Field-Effect Carrier Mobility in Regioregular poly(3-Alkylthiophene)s. *Synth. Met.* **2005**, *148*, 169–173.

(6) Salammal, S.; Mikayelyan, E.; Grigorian, S.; Pietsch, U.; Koenen, N.; Scherf, U.; Brinkmann, M.; Kayunkid, N. Impact of Thermal Annealing on the Semicrystalline Nanomorphology of Spin-Coated Thin Films of Regioregular Poly (3-Alkylthiophene) S as Observed by High-Resolution Transmission Electron Microscopy and Grazing Incidence X-Ray Diffraction. *Macromolecules* **2012**, *45*, 5575–5585.

(7) Friedel, B.; McNeill, C.; Greenham, N. Influence of Alkyl Side-Chain Length on the Performance of Poly (3-alkylthiophene)/Polyfluorene All-Polymer Solar Cells. *Chem. Mater.* **2010**, *22*, 3389–3398.

(8) Nguyen, L. H.; Hoppe, H.; Erb, T.; Günes, S.; Gobsch, G.; Sariciftci, N. S. Effects of Annealing on the Nanomorphology and Performance of Poly(alkylthiophene):Fullerene Bulk-Heterojunction Solar Cells. *Adv. Funct. Mater.* **2007**, *17*, 1071–1078.

(9) Dupont, S. R.; Voroshazi, E.; Heremans, P.; Dauskardt, R. H. Adhesion Properties of Inverted Polymer Solarcells: Processing and Film Structure Parameters. *Org. Electron.* **2013**, *14*, 1262–1270.

(10) Sokolov, A. N.; Cao, Y.; Johnson, O. B.; Bao, Z. Mechanistic Considerations of Bending-Strain Effects within Organic Semiconductors on Polymer Dielectrics. *Adv. Funct. Mater.* **2012**, *22*, 175–183.

(11) Ghezzi, D.; Antognazza, M. R.; Maccarone, R.; Bellani, S.; Lanzarini, E.; Martino, N.; Mete, M.; Perile, G.; Bisti, S.; Lanzani, G.; Benfenati, F. A Polymer Optoelectronic Interface Restores Light Sensitivity in Blind Rat Retinas. *Nat. Photonics* **2013**, *7*, 400–406.

(12) Ilievski, F.; Mazzeo, A. Soft Robotics for Chemists. *Angew. Chem. Int. Ed.* **2011**, *50*, 1890–1895.

(13) Brinkmann, M. Structure and Morphology Control in Thin Films of Regioregular poly(3-Hexylthiophene). *J. Polym. Sci. Part B Polym. Phys.* **2011**, *49*, 1218–1233.

(14) Mei, J.; Bao, Z. Side Chain Engineering in Solution-Processable Conjugated Polymers. *Chem. Mater.* **2014**, *26*, 604–615.

(15) Krebs, F.; Gevorgyan, S.; Alstrup, J. A Roll-to-Roll Process to Flexible Polymer Solar Cells: Model Studies, Manufacture and Operational Stability Studies. *J. Mater. Chem.* **2009**, *19*, 5442.

(16) Kaltenbrunner, M.; White, M. S.; Głowacki, E. D.; Sekitani, T.; Someya, T.; Sariciftci, N. S.; Bauer, S. Ultrathin and Lightweight Organic Solar Cells with High Flexibility. *Nat. Commun.* **2012**, *3*, 770.

(17) Rogers, J. A.; Someya, T.; Huang, Y. Materials and Mechanics for Stretchable Electronics. **2010**, *327*, 1603–1607.

(18) Kaltenbrunner, M.; Sekitani, T.; Reeder, J.; Yokota, T.; Kuribara, K.; Tokuhara, T.; Drack, M.; Schwödiauer, R.; Graz, I.; Bauer-Gogonea, S.; Bauer, S.; Someya,

T. An Ultra-Lightweight Design for Imperceptible Plastic Electronics. *Nature* **2013**, *499*, 458–463.

(19) Krebs, F.; Tromholt, T.; Jørgensen, M. Upscaling of Polymer Solar Cell Fabrication Using Full Roll-to-Roll Processing. *Nanoscale* **2010**, *2*, 873–886.

(20) Lipomi, D. J.; Bao, Z. Stretchable, Elastic Materials and Devices for Solar Energy Conversion. *Energy Environ. Sci.* **2011**, *4*, 3314–3328.

(21) Martinez, R. V; Branch, J. L.; Fish, C. R.; Jin, L.; Shepherd, R. F.; Nunes, R. M. D.; Suo, Z.; Whitesides, G. M. Robotic Tentacles with Three-Dimensional Mobility Based on Flexible Elastomers. *Adv. Mater.* **2013**, *25*, 205–212.

(22) Suo, Z.; Ma, E.; Gleskova, H.; Wagner, S. Mechanics of Rollable and Foldable Film-on-Foil Electronics. *Appl. Phys. Lett.* **1999**, *74*, 1177.

(23) Tahk, D.; Lee, H. H.; Khang, D.-Y. Elastic Moduli of Organic Electronic Materials by the Buckling Method. *Macromolecules* **2009**, *42*, 7079–7083.

(24) Lipomi, D. J.; Chong, H.; Vosgueritchian, M.; Mei, J.; Bao, Z. Toward Mechanically Robust and Intrinsically Stretchable Organic Solar Cells: Evolution of Photovoltaic Properties with Tensile Strain. *Sol. Energy Mater. Sol. Cells* **2012**, *107*, 355–365.

(25) Chen, Z.; Lee, M. J.; Shahid Ashraf, R.; Gu, Y.; Albert-Seifried, S.; Meedom Nielsen, M.; Schroeder, B.; Anthopoulos, T. D.; Heeney, M.; McCulloch, I.; Sirringhaus, H. High-Performance Ambipolar Diketopyrrolopyrrole-thieno[3,2-B]thiophene Copolymer Field-Effect Transistors with Balanced Hole and Electron Mobilities. *Adv. Mater.* **2012**, *24*, 647–652.

(26) Dou, L.; You, J.; Hong, Z.; Xu, Z.; Li, G.; Street, R. A.; Yang, Y. 25Th Anniversary Article: A Decade of Organic/Polymeric Photovoltaic Research. *Adv. Mater.* **2013**, *25*, 6642–6671.

(27) McCulloch, I.; Heeney, M.; Bailey, C.; Genevicius, K.; Macdonald, I.; Shkunov, M.; Sparrowe, D.; Tierney, S.; Wagner, R.; Zhang, W.; Chabinyc, M. L.; Kline, R. J.; McGehee, M. D.; Toney, M. F. Liquid-Crystalline Semiconducting Polymers with High Charge-Carrier Mobility. *Nat. Mater.* **2006**, *5*, 328–333.

(28) Li, G.; Zhu, R.; Yang, Y. Polymer Solar Cells. *Nat. Photonics* **2012**, *6*, 153–161.

(29) Sommer-Larsen, P.; Jørgensen, M.; Søndergaard, R. R.; Hösel, M.; Krebs, F. C. Fast Inline Roll-to-Roll Printing for Indium-Tin-Oxide-Free Polymer Solar Cells Using Automatic Registration. *Energy Technol.* **2013**, *1*, 102–107.

(30) Facchetti, A. Π-Conjugated Polymers for Organic Electronics and Photovoltaic Cell Applications †. *Chem. Mater.* **2011**, *23*, 733–758.

(31) Liao, S.-H.; Li, Y.-L.; Jen, T.-H.; Cheng, Y.-S.; Chen, S.-A. Multiple Functionalities of Polyfluorene Grafted with Metal Ion-Intercalated Crown Ether as an Electron Transport Layer for Bulk-Heterojunction Polymer Solar Cells: Optical Interference, Hole Blocking, Interfacial Dipole, and Electron Conduction. *J. Am. Chem. Soc.* **2012**, *134*, 14271–14274.

(32) Osedach, T. P.; Andrew, T. L.; Bulović, V. Effect of Synthetic Accessibility on the Commercial Viability of Organic Photovoltaics. *Energy Environ. Sci.* **2013**, *6*, 711–718.

(33) Anctil, A.; Babbitt, C. W.; Raffaelle, R. P.; Landi, B. J. Cumulative Energy Demand for Small Molecule and Polymer Photovoltaics. *Prog. Photovolt Res. Appl.* **2013**, *21*, 1541–1554.

(34) Scherf, U.; Gutacker, A.; Koenen, N. All-Conjugated Block Copolymers. *Acc. Chem. Res.* **2008**, *41*, 1086–1097.

(35) Printz, A. D.; Savagatrup, S.; Burke, D. J.; Purdy, T. N.; Lipomi, D. J. Increased Elasticity of a Low-Bandgap Conjugated Copolymer by Random Segmentation for Mechanically Robust Solar Cells. *RSC Adv.* **2014**, *4*, 13635–13643.

(36) Pearson, A. J.; Wang, T.; Dunbar, A. D. F.; Yi, H.; Watters, D. C.; Coles, D. M.; Staniec, P. A.; Iraqi, A.; Jones, R. A. L.; Lidzey, D. G. Morphology Development in Amorphous Polymer:Fullerene Photovoltaic Blend Films During Solution Casting. *Adv. Funct. Mater.* **2014**, *24*, 659–667.

(37) Spano, F. C. Modeling Disorder in Polymer Aggregates: The Optical Spectroscopy of Regioregular poly(3-Hexylthiophene) Thin Films. *J. Chem. Phys.* **2005**, *122*, 234701.

(38) Ren, G.; Wu, P.-T.; Jenekhe, S. a. Enhanced Performance of Bulk Heterojunction Solar Cells Using Block Copoly(3-Alkylthiophene)s. *Chem. Mater.* **2010**, *22*, 2020–2026.

(39) Wu, P.-T.; Ren, G.; Jenekhe, S. a. Crystalline Random Conjugated Copolymers with Multiple Side Chains: Tunable Intermolecular Interactions and Enhanced Charge Transport and Photovoltaic Properties. *Macromolecules* **2010**, *43*, 3306–3313.

(40) Stafford, C. M.; Harrison, C.; Beers, K. L.; Karim, A.; Amis, E. J.; VanLandingham, M. R.; Kim, H.-C.; Volksen, W.; Miller, R. D.; Simonyi, E. E. A

Buckling-Based Metrology for Measuring the Elastic Moduli of Polymeric Thin Films. *Nat. Mater.* **2004**, *3*, 545–550.

(41) Bowden, N.; Brittain, S.; Evans, A. G.; Hutchinson, J. W.; Whitesides, G. M. Spontaneous Formation of Ordered Structures in Thin Films of Metals Supported on an Elastomeric Polymer. *Nature* **1998**, *393*, 146–149.

(42) Bowden, N.; Huck, W. T. S.; Paul, K. E.; Whitesides, G. M. The Controlled Formation of Ordered, Sinusoidal Structures by Plasma Oxidation of an Elastomeric Polymer. *Appl. Phys. Lett.* **1999**, *75*, 2557–2559.

(43) VanLandingham, M. R.; Villarrubia, J. S.; Guthrie, W. F.; Meyers, G. F. Nanoindentation of Polymers: An Overview. *Macromol. Symp.* **2001**, *167*, 15–43.

(44) Seitz, J. The Estimation of Mechanical Properties of Polymers from Molecular Structure. *J. Appl. Polym. Sci.* **1993**, *49*, 1331–1351.

(45) Vosgueritchian, M.; Lipomi, D. J.; Bao, Z. Highly Conductive and Transparent PEDOT:PSS Films with a Fluorosurfactant for Stretchable and Flexible Transparent Electrodes. *Adv. Funct. Mater.* **2012**, *22*, 421–428.

(46) Pasquier, A. Du; Miller, S.; Chhowalla, M. On the Use of Ga–In Eutectic and Halogen Light Source for Testing P3HT–PCBM Organic Solar Cells. *Sol. Energy Mater. Sol. Cells* **2006**, *90*, 1828–1839.

(47) Chiechi, R. C.; Weiss, E. A.; Dickey, M. D.; Whitesides, G. M. Eutectic Gallium-Indium (EGaIn): A Moldable Liquid Metal for Electrical Characterization of Self-Assembled Monolayers. *Angew. Chem. Int. Ed. Engl.* **2008**, *47*, 142–144.

(48) Dickey, M. D.; Chiechi, R. C.; Larsen, R. J.; Weiss, E. A.; Weitz, D. A.; Whitesides, G. M. Eutectic Gallium-Indium (EGaIn): A Liquid Metal Alloy for the Formation of Stable Structures in Microchannels at Room Temperature. *Adv. Funct. Mater.* **2008**, *18*, 1097–1104.

(49) Palleau, E.; Reece, S.; Desai, S. C.; Smith, M. E.; Dickey, M. D. Self-Healing Stretchable Wires for Reconfigurable Circuit Wiring and 3D Microfluidics. *Adv. Mater.* **2013**, *25*, 1589–1592.

(50) Clark, J.; Chang, J.-F.; Spano, F. C.; Friend, R. H.; Silva, C. Determining Exciton Bandwidth and Film Microstructure in Polythiophene Films Using Linear Absorption Spectroscopy. *Appl. Phys. Lett.* **2009**, *94*, 163306.

(51) Clark, J.; Silva, C.; Friend, R.; Spano, F. Role of Intermolecular Coupling in the Photophysics of Disordered Organic Semiconductors: Aggregate Emission in Regioregular Polythiophene. *Phys. Rev. Lett.* **2007**, *98*, 206406.

(52) Spano, F. C.; Clark, J.; Silva, C.; Friend, R. H. Determining Exciton Coherence from the Photoluminescence Spectral Line Shape in poly(3-Hexylthiophene) Thin Films. *J. Chem. Phys.* **2009**, *130*, 074904.

(53) Turner, S. T.; Pingel, P.; Steyrleuthner, R.; Crossland, E. J. W.; Ludwigs, S.; Neher, D. Quantitative Analysis of Bulk Heterojunction Films Using Linear Absorption Spectroscopy and Solar Cell Performance. *Adv. Funct. Mater.* **2011**, *21*, 4640–4652.

(54) Turro, N. J. *Modern Molecular Photochemistry*; 1st ed.; University Science Books: Sausalito, CA, 1991.

(55) Louarn, G.; Trznadel, M. Raman Spectroscopic Studies of Regioregular Poly (3-Alkylthiophenes). *J. Phys. Chem.* **1996**, *3654*, 12532–12539.

(56) Nielsen, L. E.; Landel, R. F. *Mechanical Properties of Polymers and Composites*; CRC Press; Rev and Expanded edition, 1993.

(57) McCullough, R. D. The Chemistry of Conducting Polythiophenes. *Adv. Mater.* **1998**, *10*, 93–116.

(58) Bruner, C.; Dauskardt, R. Role of Molecular Weight on the Mechanical Device Properties of Organic Polymer Solar Cells. *Macromolecules* **2014**, *47*, 1117–1121.

(59) Verswyvel, M.; Monnaie, F.; Koeckelberghs, G. AB Block Copoly(3-Alkylthiophenes): Synthesis and Chiroptical Behavior. *Macromolecules* **2011**, *44*, 9489–9498.

(60) Ge, J.; He, M.; Qiu, F.; Yang, Y. Synthesis, Cocrystallization, and Microphase Separation of All-Conjugated Diblock Copoly(3-Alkylthiophene)s. *Macromolecules* **2010**, *43*, 6422–6428.

(61) Ge, J.; He, M.; Yang, X.; Ye, Z.; Liu, X.; Qiu, F. Microphase Separation-Promoted Crystallization in All-Conjugated poly(3-Alkylthiophene) Diblock Copolymers with High Crystallinity and Carrier Mobility. *J. Mater. Chem.* **2012**, *22*, 19213–19221.

(62) He, M.; Zhao, L.; Wang, J.; Han, W.; Yang, Y.; Qiu, F.; Lin, Z. Self-Assembly of All-Conjugated Poly(3-Alkylthiophene) Diblock Copolymer Nanostructures from Mixed Selective Solvents. *ACS Nano* **2010**, *4*, 3241–3247.

(63) Nandan, B.; Kandpal, L. D.; Mathur, G. N. Poly(ether Ether ketone)/Poly(aryl Ether Sulfone) Blends: Relationships between Morphology and Mechanical Properties. *J. Appl. Polym. Sci.* **2003**, *90*, 2887–2905.

(64) Ramiro, J.; Equiazabal, J. I.; Nazabal, J. Synergistic Mechanical Behaviour and Improved Processability of Poly(ether Imide) by Blending with Poly(trimethylene Terephthalate). *Polym. Advan. Technol.* **2003**, *14*, 129–136.

(65) Chen, T.; Wu, X.; Rieke, R. Regiocontrolled Synthesis of Poly (3-Alkylthiophenes) Mediated by Rieke Zinc: Their Characterization and Solid-State Properties. *J. Am. Chem. Soc.* **1995**, *117*, 233–244.

(66) Koch, F. P. V.; Heeney, M.; Smith, P. Thermal and Structural Characteristics of Oligo (3-Hexylthiophene) S (3HT) N, N= 4–36. *J. Am. Chem. Soc.* **2013**, *135*, 13699–13709.

(67) Pal, S.; Nandi, A. K. Cocrystallization Behavior of Poly(3-Alkylthiophenes): Influence of Alkyl Chain Length and Head to Tail Regioregularity. *Macromolecules* **2003**, *36*, 8426–8432.

(68) Plate, N. A.; Shibaev, V. P. Comblike Polymers. Structure and Properties. *J. Polym. Sci. Macromol. Rev.* **1974**, *8*, 117–253.

(69) Reimschuessel, H. K. On the Glass Transition Temperature of Comblike Polymers: Effects of Side Chain Length and Backbone Chain Structure. *J. Polym. Sci. Polym. Chem. Ed.* **1979**, *17*, 2447–2457.

(70) Chen, S.; Ni, J.-M. Structure/Properties of Conjugated Conductive Polymers. 1. Neutral Poly(3-Alkyl Thiophene)s. *Macromolecules* **1992**, *25*, 6081–6089.

(71) Kim, J. Y.; Frisbie, C. D. Correlation of Phase Behavior and Charge Transport in Conjugated Polymer/Fullerene Blends. *J. Phys. Chem. C* **2008**, *112*, 17726–17736.

(72) Treat, N.; Mates, T.; Hawker, C. Temperature Dependence of the Diffusion Coefficient of PCBM in Poly (3-Hexylthiophene). *Macromolecules* **2013**, *46*, 1002–1007.

(73) Koppe, M.; Scharber, M.; Brabec, C.; Duffy, W.; Heeney, M.; McCulloch, I. Polyterthiophenes as Donors for Polymer Solar Cells. *Adv. Funct. Mater.* **2007**, *17*, 1371–1376.

(74) Kline, R. J.; McGehee, M. D.; Kadnikova, E. N.; Liu, J.; Frechet, J. M. J.; Toney, M. F. Dependence of Regioregular Poly (3-Hexylthiophene) Film Morphology and Field-Effect Mobility on Molecular Weight. *Macromolecules* **2005**, *38*, 3312–3319.

(75) Brinkmann, M.; Wittmann, J.-C. Orientation of Regioregular Poly(3-Hexylthiophene) by Directional Solidification: A Simple Method to Reveal the

Semicrystalline Structure of a Conjugated Polymer. *Adv. Mater.* **2006**, *18*, 860–863.

(76) Wu, P.-T.; Xin, H.; Kim, F. S.; Ren, G.; Jenekhe, S. A. Regioregular Poly(3-Pentylthiophene): Synthesis, Self-Assembly of Nanowires, High-Mobility Field-Effect Transistors, and Efficient Photovoltaic Cells. *Macromolecules* **2009**, *42*, 8817–8826.

(77) Pingel, P.; Zen, A. Temperature Resolved Local and Macroscopic Charge Carrier Transport in Thin P3HT Layers. *Adv. Funct. Mater.* **2010**, *20*, 2286–2295.

(78) Roehling, J. D.; Batenburg, K. J.; Swain, F. B.; Moulé, A. J.; Arslan, I. Three-Dimensional Concentration Mapping of Organic Blends. *Adv. Funct. Mater.* **2013**, *23*, 2115–2122.

(79) Liu, F.; Gu, Y.; Shen, X.; Ferdous, S.; Wang, H.-W.; Russell, T. P. Characterization of the Morphology of Solution-Processed Bulk Heterojunction Organic Photovoltaics. *Prog. Polym. Sci.* **2013**, *38*, 1990–2052.

(80) Brady, M. A.; Su, G. M.; Chabinyc, M. L. Recent Progress in the Morphology of Bulk Heterojunction Photovoltaics. *Soft Matter* **2011**, *7*, 11065–11077.

Chapter 3

Viability of stretchable poly(3-heptylthiophene) (P3HpT) for organic solar cells and field-effect transistors

Suchol Savagatrup,[†a] Adam D. Printz,[†a] Haosheng Wu,[b] Kirtana M. Rajan,[a] Eric J. Sawyer,[a] Aliaksandr V. Zaretski,[a] Christopher J. Bettinger,[b] and Darren J. Lipomi[a]

([†] Equal contribution)

[a] *Department of NanoEngineering, University of California, San Diego, 9500 Gilman Drive Mail Code 0448, La Jolla, CA 92093-0448.*

[b] *Department of Materials Science and Engineering, Carnegie Mellon University, 5000 Forbes Hall, Pittsburgh, PA, 15213-3890.*

Abstract

Mechanical compliance is a critical attribute for organic semiconductors in flexible, stretchable, mechanically robust, and biologically integrated electronics. This paper substantially develops the observation that a small change in the length of the alkyl side chain of regioregular poly(3-alkylthiophene)s has a dramatic effect on the interplay between their mechanical and charge-transport properties. Specifically, the thermal, mechanical, and charge-transport properties of poly(3-heptylthiophene) (P3HpT, n = 7), which we found to be an unusual example of a stretchable semiconducting thermoplastic, are described in comparison to those of poly(3-hexylthiophene) (P3HT, n = 6) and poly(3-octylthiophene) (P3OT, n = 8). Neat P3HpT was found to have mechanical properties similar to that of P3OT, and when mixed in 1:1 blends with the fullerene [6,6]-phenyl C_{61} butyric acid methyl ester (PCBM), exhibited electronic properties comparable to P3HT. However, the charge-carrier mobility of neat P3HpT is substantially inferior to that of P3HT; the good performance of P3HpT-based solar cells is the result of improved mobility in P3HpT:PCBM blends compared to the neat material. While P3HpT may be a favorable alternative to P3HT in ultra-flexible, stretchable, and mechanically robust organic solar cells, P3HpT would only make a good field-effect transistor in situations in which mechanical compliance was more important than high mobility.

3.1 Introduction

Given the vast literature devoted to the regioregular poly(3-alkylthiophenes) (P3ATs), it may seem that every aspect of the chemical, physical, and optoelectronic properties of this class of materials have been characterized exhaustively. This paper

shows that a small change in the length of the alkyl side chain—in the range of $6 \leq n \leq 8$—nevertheless has profound effects on these properties, in particular the flexibility, stretchability, and resistance to mechanical failure of devices. The mechanical properties of organic semiconductors are highly variable and sensitive to small molecular and microstructural changes.[1–4] Moreover, there is substantial evidence that suggests that good charge-transport and mechanical compliance are mutually exclusive properties.[5,6] We recently reported the tensile moduli of a series of P3AT homopolymers and copolymers and their power conversion efficiencies (*PCEs*) when combined in 1:1 blends with [6,6]-phenyl C_{61} butyric acid methyl ester (PCBM) in organic solar cells (OSCs).[2] We found that the tensile moduli of the thin films (E_f) exhibited a drop-off of more than one order of magnitude when the length of the side chain was increased from six carbon atoms—as in poly(3-hexylthiophene) (P3HT, E_f = 1.0 GPa) the workhorse of organic electronics—to seven carbon atoms, as in poly(3-heptylthiophene) (P3HpT, E_f = 0.07 GPa).[2] Spectroscopic evidence using the weakly interacting H-aggregate model showed similarities in the level of order between P3HT and P3HpT, and both materials exhibited similar photovoltaic performance. The good performance of P3HpT, especially in the context of OSCs, suggested to us that P3HpT could be useful in applications that demand mechanical flexibility, stretchability, and robustness (that is, some applications of organic semiconductors that currently use P3HT). The purpose of this paper is to develop substantially our previous finding by characterizing the thermal, mechanical, photovoltaic, and charge-transport properties of P3HpT in comparison to P3HT and poly(3-octylthiophene) (P3OT) for pure films (*i.e.*, for thin-film transistors) and when blended with PCBM (*i.e.*, for solar cells, **Figure 3.1a**). Our measurements point to

seemingly minor changes in the chemical structure of polymers that can have dramatic effects on their physical properties. We found that P3HpT is in fact an unusual example of a stretchable semiconducting thermoplastic. While we believe P3HpT is an excellent candidate to replace P3HT in OSCs, its high mobility in this context seems to be the result of blending with fullerenes. In pure form, as required for organic thin-film transistors, the material is more elastic and ductile than P3HT, but the charge-carrier mobility of P3HpT is inferior to that of P3HT.

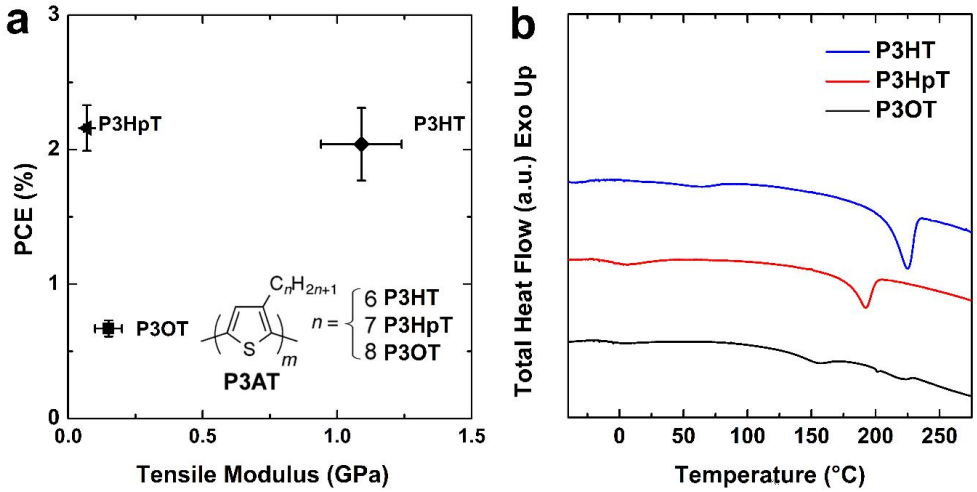

Figure 3.1. Mechanical, electronic, and thermal properties of the P3ATs in this work. (a) Plot of power conversion efficiency of the P3ATs in a 1:1 blend with $PC_{61}BM$ vs. tensile moduli of the pure polymers. The position of P3HpT well above and to the left of the line connecting P3HT and P3OT suggests the possibility of co-optimization of photovoltaic and mechanical properties (data reproduced from ref. 2) (b) DSC thermograms of representative P3HT, P3HpT, and P3OT samples at a heating rate of 10 °C min^{-1}. The chemical structures are inset in the figure. T_g values of 11 to 13 °C were determined for P3HT, –5 to –4 °C for P3HpT, and –10 to –8 °C for P3OT. T_m values were observed at 225, 192, and 155 °C for P3HT, P3HpT, and P3OT respectively.

3.2 Results and discussion

3.2.1 Characterization of the polymers

P3HT, P3HpT, and P3OT were examined for regioregularity and purity using ^1H NMR spectra. The percent regioregularity for each sample was as follows: P3HT, 88%;

P3HpT, 92%; and P3OT, 82%. We observed no additional peaks beside those expected (**Figure A.1,** Supporting Information). From size-exclusion chromatography, we determined that the molecular weights of the polymers are as follows: P3HT, M_n = 44 kDa, PDI = 2.0; P3HpT, M_n = 35 kDa, PDI = 1.5; and P3OT, M_n = 34 kDa, PDI = 2.5.

3.2.2 Thermal properties

The intuitive rationale for the increase in elasticity and ductility measured as a function of increasing length of the side chain P3AT (a comb-like polymer) is a reduction in the density of load-bearing carbon-carbon bonds along the main chain per cross sectional area.[1,7] The glass transition temperature (T_g) for comb-like polymers also decreases with increasing length of the side chain until a critical value, after which T_g remains roughly constant or even increases.[8] Long side chains installed for solubility on otherwise rigid backbone structures thus have deleterious consequences for polymers intended for structural applications.[9] For flexible and stretchable organic devices, however, high compliance (low tensile modulus) is desirable. Values of T_g in the literature occupy a wide range of values for P3HT, but it seems that the consensus value is equal to or slightly less than room temperature (*i.e.*, 15–25 °C, though our experience is that research laboratories are often kept at temperatures significantly below 25 °C).[5] The value for P3OT is unequivocally below room temperature,[10] and we have used the ductility of P3OT:PCBM composites at ambient temperature to stretch, conform, and bond whole OSCs to hemispherical surfaces without generating cracks or wrinkles.[11]

We used differential scanning calorimetry (DSC, **Figure 3.1b**) to measure the T_g and melting temperature (T_m) of P3HpT (red curve) and compared it to those of P3HT

(blue curve) and P3OT (black curve). From the analysis of the total heat flow for the heating of the pure polymer samples, we found values of T_g between 11 and 13 °C for P3HT, –5 and –4 °C for P3HpT, and –10 and –8 °C for P3OT. These data are consistent with decreasing T_g with increasing length of the side chain, and that T_g is substantially below room temperature for P3HpT and P3OT. The melting temperatures, T_m, also decreased with increasing length of the side chain, which agreed with previously reported results.[12] We note that the values of T_g found in literature can vary significantly due to the different heating rates employed and the thermal history of the sample. The relationship of T_g for P3HpT and P3OT to ambient temperature suggests that these materials can be treated as stretchable semiconducting thermoplastics. Our experience with OSCs based on either P3HpT or P3OT, however, suggest that the two polymers have significantly different semiconducting performance.

The addition of fullerene to P3HT has previously been reported to produce a greater T_g in the blend compared to that of the neat polymer.[13] We reasoned that this increase in T_g would occur in all P3ATs, and that the good photovoltaic performance of P3HpT:PCBM might be produced concomitantly with anti-plasticization of P3HpT by PCBM. To determine if the T_g of the P3ATs increased significantly with the addition of PCBM, we analysed the total heat flow for the P3AT:PCBM samples. We found the T_g of P3HT:PCBM increased to the range between 37 and 40 °C, which agrees with previously reported results,[14] and the T_g of P3OT:PCBM increased to the range between –5 and 0 °C. Interestingly, the T_g of P3HpT:PCBM increased to the range between 33 and 35 °C, which is close to that of P3HT:PCBM. The similarity in T_g between P3HT:PCBM and P3HpT:PCBM is consistent with their similar photovoltaic properties.[2]

3.2.3 Band structure

Increasing the length of the side chain in P3ATs has a very small effect on the bandgap, however, with a side chain longer than n = 6, the absolute positions of the frontier molecular orbitals decrease in energy (become more negative relative to the vacuum level).[15] To verify this trend previously identified in the literature for P3ATs with an even number of carbon atoms in the side chains,[15] we measured the positions of the HOMOs for the three P3ATs by cyclic voltammetry. The onset of oxidation for P3HT, P3HpT, and P3OT can be seen in **Figure 3.2a**, which reveals a linear dependence on ionization potential with the length of the side chain. To determine the LUMO, we added the optical band gap, $E_{g,opt}$, and 0.3 eV to the HOMO. The 0.3 eV is added because it is the typical difference between the optical and electrochemical band gaps, previously attributed to the exciton binding energy.[16] The absorption spectra of the solid films, shown in **Figure 3.2b**, reveal similar onsets of absorption, 1.92–1.94 eV (639–646 nm). The spectra also show better order in P3HT and P3HpT compared to P3OT. The optical and electrochemical properties of the P3ATs are summarized in **Table 3.1**. We initially hypothesized that similar order when n = 6 or 7 would produce similar charge-carrier mobilities, though the effect of unequal T_g between P3HT and P3HpT could also have an effect.

Table 3.1. Optical and electrochemical properties of the P3ATs.

Polymer	E_{ox} (V)	HOMO [a] (eV)	$E_{g,opt}$ (eV)	LUMO [b] (eV)
P3HT	0.54	–5.25	1.94	–3.01
P3HpT	0.68	–5.39	1.92	–3.17
P3OT	0.75	–5.46	1.92	–3.24

[a] HOMO = –e(E_{ox} + 4.71) (eV) [b] LUMO = $E_{g,opt}$ + 0.3 + HOMO (eV)

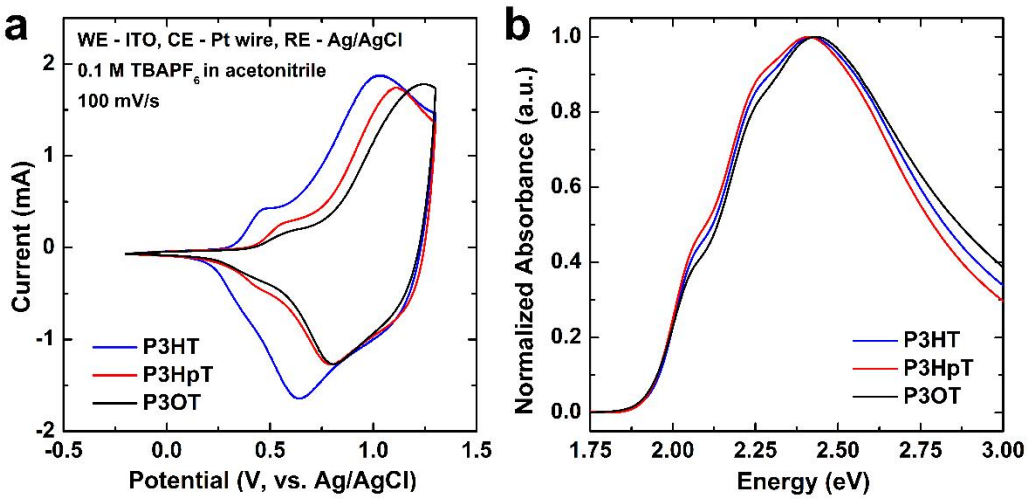

Figure 3.2. Determination of the HOMO and LUMO for P3HT, P3HpT, and P3OT. (a) Cyclic voltammetry oxidation curves measured at a scan rate of 100 mV/s. (b) Absorption spectra of the polymer thin films on ITO and annealed at 100 °C for 30 min.

3.2.4 Charge transport properties

The good charge-transport properties of P3ATs are generally attributed to the semicrystalline morphology in which well ordered aggregates (observed spectroscopically or by X-ray diffraction) have been correlated with high hole mobilities in organic thin-film transistors (OTFTs) and good efficiencies in OSCs.[5,17] To compare directly the field-effect hole mobility, μ_h, for P3HT, P3HpT, and P3OT, we fabricated bottom-gate, bottom-contact thin-film transistors with the dimensions of 500 µm (width) and 10 µm (length). **Figures 3.3a, 3.3b,** and **3.3c** show the output plots and **Figure 3.3d** shows the transfer plots for P3HT, P3HpT, and P3OT. The field effect mobilities, μ_h, were extracted from the slopes of the linear fits in the saturation regime on the plots of $(-I_{DS})^{1/2}$ vs. V_{GS} (**Figure 3.3d**), and the threshold voltages, V_T, were extracted from the interception of the linear fits and the x-axis using the following equation,[18,19]

$$\sqrt{I_{\mathrm{DS}}} = \sqrt{\mu_{\mathrm{h}} C_{\mathrm{d}} \frac{W}{2L}} (V_{\mathrm{GS}} - V_{\mathrm{T}}) \qquad (1)$$

where $C_{\mathrm{d}} = 1.38 \times 10^{-8}$ F cm^{-2}, W = 500 µm, and L = 10 µm. The mobilities, threshold voltage, and on-off ratios extracted from the current-voltage characteristics for the three materials are listed in **Table 3.2**.

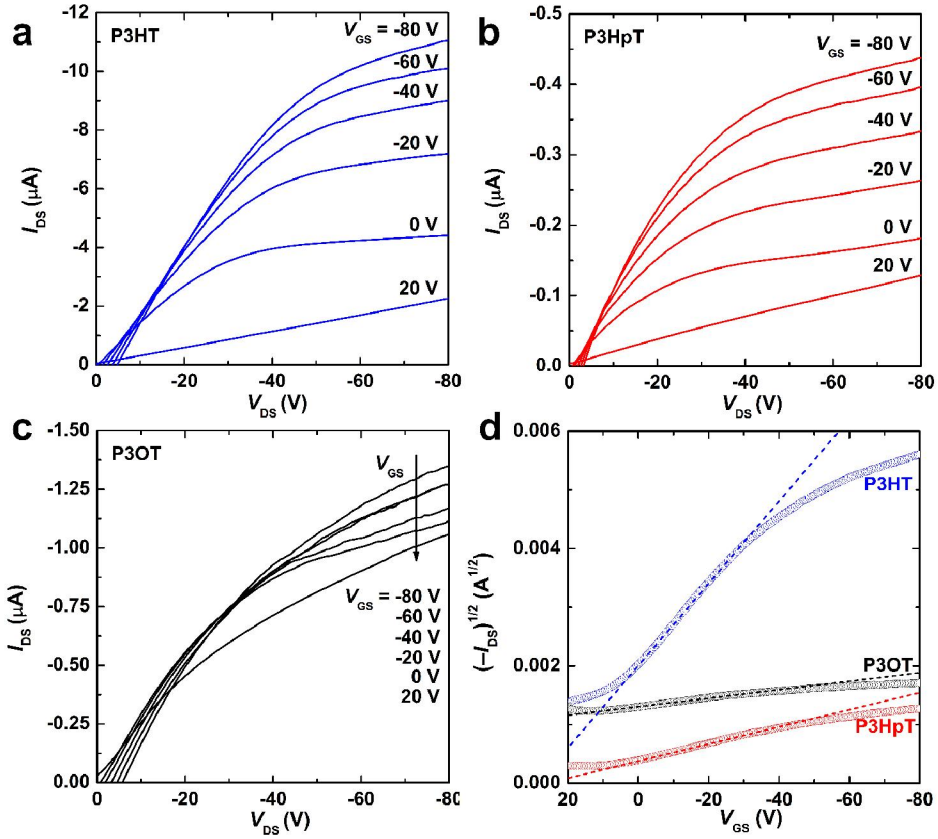

Figure 3.3. Electrical characteristics of P3AT organic thin films transistors (OTFTs): current-voltage output characteristics of a 10 µm (length) by 500 µm (width) channel for (a) P3HT, (b) P3HpT, and (c) P3OT. (d) Transfer characteristics $(-I_{DS})^{1/2}$ vs. V_{GS} at V_{DS} = –80V with respect to alkyl side chain length. Dashed lines represent the linear fit in the saturation regime.

As expected, P3HT exhibited the greatest mobility, 0.01 cm^2 V^{-1} s^{-1}, while P3OT exhibited the lowest, 0.0001 cm^2 V^{-1} s^{-1}. The mobility of P3HpT was intermediate, 0.0006 cm^2 V^{-1} s^{-1}, but closer to that of P3OT than to that of P3HT. Although P3HT, P3HpT, and P3OT have different HOMO values (Table 1), the injection barriers at

Au/P3AT interfaces are sufficiently small (work function of Au $\Phi_M \approx 5.1 \sim 5.3$ eV)[20,21] and should only result in minimal differences amoung three differenct P3AT samples in contact resistance values, which are largely dominated by the polymer nanomorphologies at the Au/channel contact edges in bottom-contact OTFT configuration.[22] The disparity in hole mobilities could be a manifestation of the thermal properties, where the amorphous domains are less mobile for P3HT than they are for P3HpT or P3OT. The relative rigidity of the amorphous domains of P3HT could be conducive to greater charge mobility than P3HpT, despite the similarity in aggregation apparent in the UV-vis spectra of the solid films (**Figure 3.2b**).

Table 3.2. Average mobility values obtained from the transfer curve of the P3HT, P3HpT, and P3OT OTFTs.

Materials	Mobility, μ_h ($\times 10^{-3}$) (cm^2 / V s)	Threshold Voltage, V_T (V)	On-off ratio[†]
P3HT	11 ± 1.8	34.5 ± 3.63	13.8 ± 3.00
P3HpT	0.55 ± 0.082	36.4 ± 4.25	10.2 ± 2.44
P3OT	0.14 ± 0.032	180 ± 32.0	1.68 ± 0.21
P3HT:PCBM	10 ± 3.3	12.8 ± 5.63	375 ± 231
P3HpT:PCBM	4.0 ± 1.0	23.5 ± 4.47	165 ± 86.8
P3OT:PCBM	1.2 ± 0.66	45.0 ± 18.1	48.8 ± 33.2

[†] On-off ratios were calculated through I (v_{gs} = –80 V) / I (v_{gs} = +20 V)

The low hole mobility of P3HpT should be deleterious to photovoltaic performance, yet we found that P3HpT:PCBM devices performed as well as P3HT:PCBM devices.[16] It has been reported by others that blending MDMO-PPV with PCBM can improve the hole mobility of the polymer by orders of magnitude.[23,24] The exact mechanism that produces the improvement in mobility is unknown, but it has been speculated that the presence of the fullerene improves ordering in the polymer.[25] We therefore tested this hypothesis for the three P3AT:PCBM composites. The hole mobility of P3HT, 0.01 cm^2 V^{-1} s^{-1}, remained similar to that of the neat polymer, however, the

mobilities of P3HpT and P3OT increased by an order of magnitude to 0.004 $cm^2\ V^{-1}\ s^{-1}$ and 0.001 $cm^2\ V^{-1}\ s^{-1}$, respectively. Such a large increase in μ_h for P3HpT and P3OT with the addition of fullerene correlates with the increase in T_g. These results support the hypothesis that immobilization of polymer chains with the incorporation of an anti-plasticizer may increase the mobility and thus the photovoltaic performance.

3.2.5 Combined mechanical and photovoltaic properties

Given that the charge-transport properties of P3HpT compare favourably to those of P3HT, we believed that P3HpT might be useful as a stretchable and mechanically robust semiconductor for flexible solar cells and wearable devices. **Figure 3.4a** compares the representative *J-V* curves of the three P3AT:PCBM devices and the figures of merit are summarized in **Table 3.3**. P3HT:PCBM and P3HpT:PCBM exhibited similar power conversion efficiencies, while P3OT:PCBM performed considerably poorer.

Table 3.3. Characteristics of P3HpT:PCBM films as a function of weight percentage of PCBM. All films were spin-coated from ODCB and thermally annealed at 100 °C.

Wt% PCBM[a]	***PCE*** [b] **(%)**	E_f [c] **(GPa)**	***CoS*** [d] **(%)**	***W*** [e] **(eV)**	**Agg. Fraction**[f]
0%	–	0.19 ± 0.05	54 ± 2	0.181	0.547
10%	0.014 ± 0.002	0.33 ± 0.07	40 ± 2	0.165	0.552
16.7%	0.12 ± 0.01	0.82 ± 0.28	26 ± 2	0.168	0.555
25%	0.59 ± 0.03	1.01 ± 0.22	16 ± 2	0.169	0.550
33.3%	1.24 ± 0.09	1.75 ± 0.35	12 ± 2	0.169	0.547
40%	1.58 ± 0.06	1.84 ± 0.28	6 ± 1	0.172	0.518
50%	2.16 ± 0.17	1.92 ± 0.22	4 ± 1	0.179	0.464

[a]The weight percentage of PCBM in the solution prepared in ODCB. [b]The architecture of the OSC devices was PEDOT:PSS/P3HpT:PCBM/EGain. The thickness of the active layer for each sample was ~150 nm. The power conversion efficiencies were averages of $N \geq 8$ devices. [c]Tensile modulus of each sample was determined by the buckling-based methodology. [d]Crack-onset strain was determined by transferring the film of each sample (~150 nm) onto an unstrained PDMS substrate and incrementally increasing the induced strain. Optical micrographs were taken to observe the formation of cracks. [e]The exciton bandwidth, *W*, which is inversely correlated to aggregate order, and [f]the Aggregate Fraction were calculated from a least-squares fit of the weakly interacting H-aggregate model to the absorption spectra.

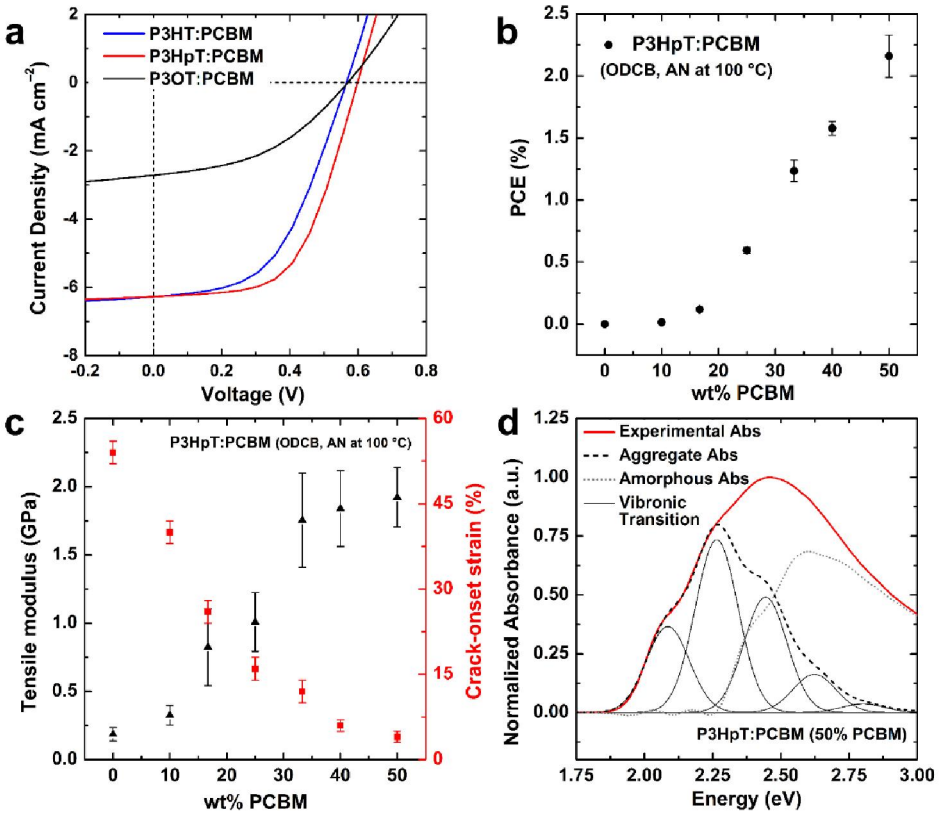

Figure 3.4. Optoelectronic and mechanical properties of P3AT:fullerene blends. (a) *J-V* curves of average devices ($N \geq 7$) with an active layer of 1:1 blend of P3AT and $PC_{61}BM$. The architecture of the devices was PEDOT:PSS/P3AT:PCBM/EGaIn. The data were reproduced from ref. [2]. (b) Power conversion efficiency of average devices ($N \geq 7$) comprising P3HpT and PCBM as a function of weight fraction of PCBM. (c) Values of tensile modulus and crack-onset strain of P3HpT:PCBM as a function of weight fraction of PCBM. All films were fabricated by spin-coating from solutions of ODCB and thermally annealed at 100 °C. (d) Example of deconvolution of the absorption spectra into vibronic transitions of ordered P3HpT and amorphous absorption using the weakly interacting H-aggregate model.

The necessity to add fullerenes (*e.g.*, PCBM) to conjugated polymers to make a bulk heterojunction has the unwanted effect of increasing the stiffness and brittleness of the composite film.[1,2,26] We hypothesized that there may be a concentration of PCBM that maximized both compliance and power conversion efficiency (*PCE*) of solar cells with the architecture glass/PEDOT:PSS/P3HpT:PCBM/eutectic gallium-indium (EGaIn). **Figure 3.4b** plots the *PCE* of P3HpT:PCBM blend as a function of the weight fraction of PCBM in the blend. The tensile modulus (E_f, left vertical axis) and the crack-onset strain (*CoS*, right vertical axis) as a function of PCBM concentration are plotted in **Figure 3.4c**.

We observed that the three quantities were highly correlated. This apparent trade-off between stiffness and electronic performance has been observed before in polythiophenes exhibiting different levels of crystalline order, specifically P3HT:PCBM blends with different order in the polymer phase produced by different rates of drying during solution casting,[5] and in the conductive polyelectrolyte complex PEDOT:PSS, when spin-coated from inks containing different concentrations of dimethylsulfoxide (DMSO).[27]

We also examined the effect of PCBM concentration on the extent of ordering in the polymer component, as measured by UV-vis spectroscopy and analysed by the weakly interacting H-aggregate model (**Figure 3.4d**). The UV-vis spectra can be deconvoluted into contributions from the aggregated material (the lower-energy shoulders in the spectra) and from the amorphous material. The percent aggregate has been correlated to increased stiffness and crack-onset strain in P3HT:PCBM blends.[5] Interestingly, small concentrations of PCBM appear to have an ordering effect on the polymer, however this effect disappears with larger loading of PCBM. Both the *W* value, which is inversely related to the aggregate order, and the aggregate fraction suggests that a decrease in ordering begins with a loading of PCBM above 33.3%. At lower loadings, the PCBM is likely to be dispersed in the amorphous domains of the polymer;[28] at higher loadings, larger PCBM-rich domains form that serve as electron-conducting regions required for efficient solar cells, but are also hard inclusions in the film that stiffen and embrittle the film and are deleterious to polymer ordering. Of note, these results suggest that the increase in hole mobility we measured in 1:1 P3AT:PCBM blends is not due to increased polymer ordering, and thus, further studies are required to fully understand the mechanism responsible.

We note that molecular weight affects the mechanical properties of the P3ATs in ways that have not yet been fully characterized. For example, Dauskardt and coworkers found that cohesive fracture energy of P3HT increases with molecular weight (M_w) in a range of 28 to 100 kDa,[29] while the entanglement molecular weight has been estimated to be 10–20 kDa for P3HT.[28] Koch et al. observed that monodisperse samples of P3HT with exceptionally low degrees of polymerization (dp = 12) can exhibit structures in which the side chains intercalate that have been described qualitatively as brittle.[30] We have previously found that the tensile modulus was similar within experimental error for P3HT with M_n between 7 and 44 kDa.[2,11] We thus did not attribute differences in mechanical properties to differences in the molecular weight (M_n) of the samples used in this study (P3HT 44 kDa, P3HpT 35 kDa, P3OT 34 kDa).

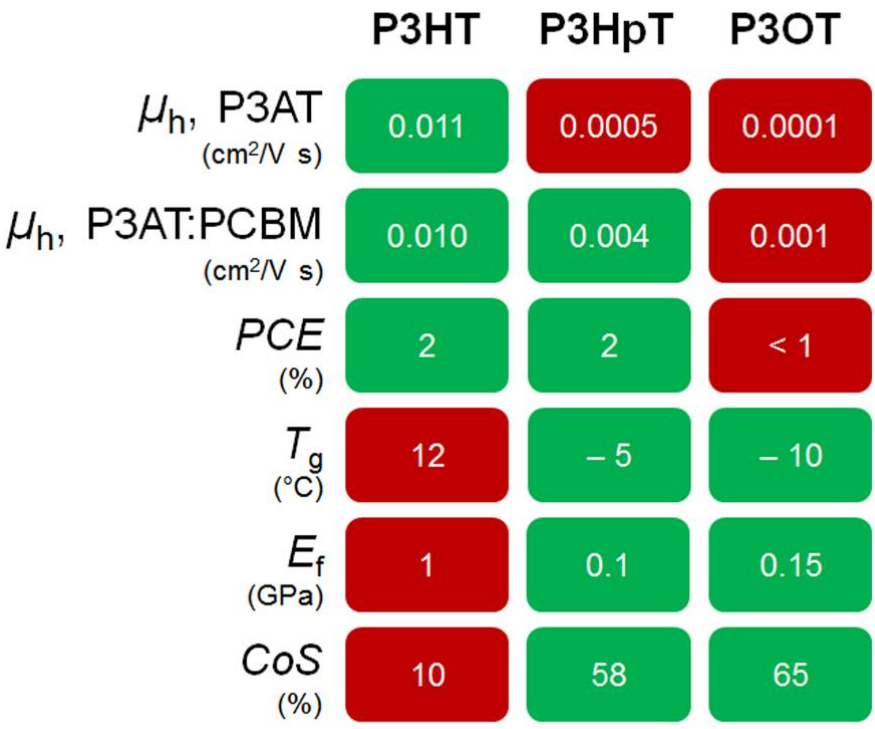

Figure 3.5. A summary of the electronic and mechanical properties of the polymers and polymer:fullerene blends studied in this work. Favourable properties are highlighted in green, while unfavourable properties are highlighted in red.

A summary of the electronic and mechanical properties of P3HT, P3HpT, and P3OT is presented in **Figure 3.5**. While P3HT has a favourable μ_h and *PCE*, it exhibits poor compliance and ductility. P3OT, on the other hand, has high compliance and ductility, but poor μ_h and *PCE*. In contrast, P3HpT is a chimera; in neat films, it has a similar compliance and ductility to P3OT, and when blended with fullerene, its electronic performance becomes closer to or equal to that of P3HT. While P3HpT is stiffened by PCBM, the blend is still less stiff than P3HT:PCBM by a factor of approximately two: E_f = 1.46 ± 0.16 GPa for P3HpT:PCBM compared to 2.75 ± 0.59 GPa for P3HT:PCBM.[31]

3.3 Conclusion

Poly(3-heptylthiophene) is an interesting example of a stretchable semiconducting thermoplastic. While P3OT could also be described as an STE, the semiconducting performance of P3HpT is better, especially when blended with PCBM. The mechanical compliance of P3HpT arises from the fact that its glass transition is the first in the series of P3ATs that is well below ambient temperature. When compared to P3HT and P3OT, the *PCE* of an organic solar cell with an active layer comprising P3HpT:PCBM is comparable to that of P3HT:PCBM, while the hole mobility of P3HpT is poor—closer to P3OT than P3HT—it is increased by nearly an order of magnitude with the addition of PCBM. P3HpT is thus attractive as a potential replacement for P3HT in flexible, stretchable, wearable, and mechanically robust solar cells, though it would not make an especially good transistor. More generally, the behaviour observed in these relatively simple conjugated polymer systems should provide insight into designing highly elastic

and high performing organic electronic devices in outdoor, portable, and wearable applications that require mechanical robustness

Acknowledgments

This work was supported by the Air Force Office of Scientific Research (AFOSR) Young Investigator Program, Grant Number FA9550-13-1-0156. Additional support was provided by the National Science Foundation Graduate Research Fellowship, awarded to both S.S. and A.Z., and by laboratory startup funds from the University of California, San Diego. The authors thank Prof. Joseph Wang and Amay Bandodkar for helpful discussions and use of their equipment to perform cyclic voltammetry experiments.

Chapter 3, in full, is a reprint of the material as it appears in *Synthetic Metals*, 2015, 203, 208. Elsevier B.V., 2015. Suchol Savagatrup,[†] Adam D. Printz,[†] Haosheng Wu, Kirtana Rajan, Eric J. Sawyer, Aliaksandr V. Zaretski, Christopher J. Bettinger, and Darren J. Lipomi, Darren J. ([†] Equal contribution). The dissertation author was the primary investigator and author of this paper.

References

(1) Savagatrup, S.; Makaram, A. S.; Burke, D. J.; Lipomi, D. J. Mechanical Properties of Conjugated Polymers and Polymer-Fullerene Composites as a Function of Molecular Structure. *Adv. Funct. Mater.* **2014**, *24*, 1169–1181.

(2) Savagatrup, S.; Printz, A. D.; Rodriquez, D.; Lipomi, D. J. Best of Both Worlds: Conjugated Polymers Exhibiting Good Photovoltaic Behavior and High Tensile Elasticity. *Macromolecules* **2014**, *47*, 1981–1992.

(3) Printz, A. D.; Savagatrup, S.; Burke, D. J.; Purdy, T. N.; Lipomi, D. J. Increased Elasticity of a Low-Bandgap Conjugated Copolymer by Random Segmentation for Mechanically Robust Solar Cells. *RSC Adv.* **2014**, *4*, 13635–13643.

(4) Tahk, D.; Lee, H. H.; Khang, D.-Y. Elastic Moduli of Organic Electronic Materials by the Buckling Method. *Macromolecules* **2009**, *42*, 7079–7083.

(5) Awartani, O.; Lemanski, B. I.; Ro, H. W.; Richter, L. J.; DeLongchamp, D. M.; O'Connor, B. T. Correlating Stiffness, Ductility, and Morphology of Polymer:Fullerene Films for Solar Cell Applications. *Adv. Energy Mater.* **2013**, *3*, 399–406.

(6) O'Connor, B.; Chan, E. P.; Chan, C.; Conrad, B. R.; Richter, L. J.; Kline, R. J.; Heeney, M.; McCulloch, I.; Soles, C. L.; DeLongchamp, D. M. Correlations between Mechanical and Electrical Properties of Polythiophenes. *ACS Nano* **2010**, *4*, 7538–7544.

(7) Moulton, J.; Smith, P. Electrical and Mechanical Properties of Oriented Poly (3-Alkylthiophenes): 2. Effect of Side-Chain Length. *Polymer (Guildf).* **1992**, *33*, 2340–2347.

(8) Reimschuessel, H. K.; Chemical, A. On the Glass Transition Temperature of Comblike Polymers : Effects of Side Chain Length and Backbone Chain Structure. **1979**, *17*, 2447–2457.

(9) Postema, A. R.; Liou, K.; Wudl, F.; Smith, P. Highly Oriented, Low-Modulus Materials from Liquid Crystalline Polymers: The Ultimate Penalty for Solubilizing Alkyl Side Chains. *Macromolecules* **1990**, *23*, 1842–1845.

(10) Kim, J. Y.; Frisbie, C. D. Correlation of Phase Behavior and Charge Transport in Conjugated Polymer/Fullerene Blends. *J. Phys. Chem. C* **2008**, *112*, 17726–17736.

(11) O'Connor, T. F.; Zaretski, A. V.; Shiravi, B. A.; Savagatrup, S.; Printz, A. D.; Diaz, M. I.; Lipomi, D. J. Stretching and Conformal Bonding of Organic Solar Cells to Hemispherical Surfaces. *Energy Environ. Sci.* **2014**, *7*, 370–378.

(12) Salammal, S.; Mikayelyan, E.; Grigorian, S.; Pietsch, U.; Koenen, N.; Scherf, U.; Brinkmann, M.; Kayunkid, N. Impact of Thermal Annealing on the Semicrystalline Nanomorphology of Spin-Coated Thin Films of Regioregular Poly (3-Alkylthiophene) S as Observed by High-Resolution Transmission Electron Microscopy and Grazing Incidence X-Ray Diffraction. *Macromolecules* **2012**, *45*, 5575–5585.

(13) Zhao, J.; Swinnen, A.; Van Assche, G.; Manca, J.; Vanderzande, D.; Van Mele, B. Phase Diagram of P3HT/PCBM Blends and Its Implication for the Stability of Morphology. *J. Phys. Chem. B* **2009**, *113*, 1587–1591.

(14) Bruner, C.; Novoa, F.; Dupont, S.; Dauskardt, R. Decohesion Kinetics in Polymer Organic Solar Cells. *ACS Appl. Mater. Interfaces* **2014**, *6*, 21474–21483.

(15) Friedel, B.; McNeill, C.; Greenham, N. Influence of Alkyl Side-Chain Length on the Performance of Poly (3-alkylthiophene)/Polyfluorene All-Polymer Solar Cells. *Chem. Mater.* **2010**, *22*, 3389–3398.

(16) Heeney, M.; Zhang, W.; Crouch, D. J.; Chabinyc, M. L.; Gordeyev, S.; Hamilton, R.; Higgins, S. J.; McCulloch, I.; Skabara, P. J.; Sparrowe, D.; Tierney, S. Regioregular Poly(3-hexyl)selenophene: A Low Band Gap Organic Hole Transporting Polymer. *Chem. Commun. (Camb).* **2007**, 5061–5063.

(17) Pingel, P.; Zen, A.; Abellón, R. D.; Grozema, F. C.; Siebbeles, L. D. A.; Neher, D. Temperature-Resolved Local and Macroscopic Charge Carrier Transport in Thin P3HT Layers. *Adv. Funct. Mater.* **2010**, *20*, 2286–2295.

(18) Giri, G.; Verploegen, E.; Mannsfeld, S. C. B.; Atahan-Evrenk, S.; Kim, D. H.; Lee, S. Y.; Becerril, H. A.; Aspuru-Guzik, A.; Toney, M. F.; Bao, Z. Tuning Charge Transport in Solution-Sheared Organic Semiconductors Using Lattice Strain. *Nature* **2011**, *480*, 504–508.

(19) Bettinger, C. J.; Bao, Z. Organic Thin-Film Transistors Fabricated on Resorbable Biomaterial Substrates. *Adv. Mater.* **2010**, *22*, 651–655.

(20) Singh, K. A.; Young, T.; McCullough, R. D.; Kowaiewski, T.; Porter, L. M. Planarization of Polymeric Field-Effect Transistors: Improvement of Nanomorphology and Enhancement of Electrical Performance. *Adv. Funct. Mater.* **2010**, *20*, 2216–2221.

(21) Sachtler, W. M. H.; Dorgelo, G. J. H.; Holscher, A. A. The Work Function of Gold. *Surf. Sci.* **1966**, *5*, 221–229.

(22) Park, Y.; Kim, D.; Jang, Y.; Cho, J.; Hwang, M. Effect of Side Chain Length on Molecular Ordering and Field-Effect Mobility in Poly (3-Alkylthiophene) Transistors. *Org. Electron.* **2006**, *7*, 514–520.

(23) Choulis, S. a.; Nelson, J.; Kim, Y.; Poplavskyy, D.; Kreouzis, T.; Durrant, J. R.; Bradley, D. D. C. Investigation of Transport Properties in Polymer/fullerene Blends Using Time-of-Flight Photocurrent Measurements. *Appl. Phys. Lett.* **2003**, *83*, 3812–3814.

(24) Melzer, C.; Koop, E. J.; Mihailetchi, V. D.; Blom, P. W. M. Hole Transport in Poly(phenylene vinylene)/Methanofullerene Bulk-Heterojunction Solar Cells. *Adv. Funct. Mater.* **2004**, *14*, 865–870.

(25) Beaujuge, P. M.; Fréchet, J. M. J. Molecular Design and Ordering Effects in Π-Functional Materials for Transistor and Solar Cell Applications. *J. Am. Chem. Soc.* **2011**, *133*, 20009–20029.

(26) Lipomi, D. J.; Chong, H.; Vosgueritchian, M.; Mei, J.; Bao, Z. Toward Mechanically Robust and Intrinsically Stretchable Organic Solar Cells: Evolution of Photovoltaic Properties with Tensile Strain. *Sol. Energy Mater. Sol. Cells* **2012**, *107*, 355–365.

(27) Savagatrup, S.; Chan, E.; Renteria-Garcia, S. M.; Printz, A. D.; Zaretski, A. V.; O'Connor, T. F.; Rodriquez, D.; Valle, E.; Lipomi, D. J. Plasticization of PEDOT:PSS by Common Additives for Mechanically Robust Organic Solar Cells and Wearable Sensors. *Adv. Funct. Mater.* **2015**, *25*, 427–436.

(28) Treat, N. D.; Chabinyc, M. L. Phase Separation in Bulk Heterojunctions of Semiconducting Polymers and Fullerenes for Photovoltaics. *Annu. Rev. Phys. Chem.* **2014**, *65*, 59–81.

(29) Bruner, C.; Dauskardt, R. Role of Molecular Weight on the Mechanical Device Properties of Organic Polymer Solar Cells. *Macromolecules* **2014**, *47*, 1117–1121.

(30) Koch, F. P. V.; Heeney, M.; Smith, P. Thermal and Structural Characteristics of Oligo (3-Hexylthiophene) S (3HT) N, N= 4–36. *J. Am. Chem. Soc.* **2013**, *135*, 13699–13709.

(31) Printz, A. D.; Savagatrup, S.; Rodriquez, D.; Lipomi, D. J. Role of Molecular Mixing on the Stiffness of Polymer:fullerene Bulk Heterojunction Films. *Sol. Energy Mater. Sol. Cells* **2015**, *134*, 64–72.

Chapter 4

Increased elasticity of a low-bandgap conjugated copolymer by random segmentation for mechanically robust solar cells

Adam D. Printz,[†] Suchol Savagatrup,[†] Daniel J. Burke, Trevor N. Purdy, and Darren J. Lipomi

([†] Equal contribution)

Department of NanoEngineering, University of California, San Diego

9500 Gilman Drive, Mail Code 0448, La Jolla, CA 92093-0448

Abstract

Despite the necessity of organic electronic materials to undergo large deformations in flexible, ultra-thin, and stretchable applications, many high-performance organic semiconductors are mechanically fragile. This paper describes an approach to increase the elasticity of low-bandgap conjugated polymers by statistical incorporation of unlike monomers. The material under study is PDPP2FT, an alternating copolymer. Synthesized by the Stille polymerization, it comprises an *N*-alkylated diketopyrrolopyrrole (DPP) unit flanked by two furan rings (2F) alternating with thiophene (T). In the modified ("segmented") polymer, PDPP2FT-seg-2T, the DPP is exchanged for a tail-to-tail coupled unit of two 3-hexylthiophene rings (bithiophene, 2T) in an average of one of approximately five repeat units. ^{1}H NMR spectroscopy, ultraviolet-visible spectroscopy, and gel-permeation chromatography confirm the presence and covalent incorporation of the 2T units within the conjugated backbone of the segmented polymer. The tensile modulus of the segmented polymer, 0.93 ± 0.16 GPa, is lower than that of the homopolymer, 2.17 ± 0.35 GPa. When blended with $PC_{61}BM$, the segmented material produces devices with power conversion efficiencies of 2.82 ± 0.28%, which is similar to that of PDPP2FT, 2.52 ± 0.34%. These results suggest that it is possible to increase the mechanical resiliency of semiconducting polymers for solar cells without having a deleterious effect on the photovoltaic properties.

4.1 Introduction

Mechanical compliance of organic electronic devices is typically regarded as a solved—or never extant—problem, and thus the mechanical properties of modern (*i.e.*,

low-bandgap, high mobility, and high photovoltaic efficiency) conjugated polymers are generally unreported.[1] Typical thicknesses of active materials (~100 nm) and substrates (~100 μm and recently ~1 μm) can accommodate small bending radii without imposing significant tensile deformations to the active materials.[2] Reports of ultra-flexible devices have enabled "imperceptible" electronics and skin-like devices on thin plastic foils and demonstrations of ultrathin organic solar cells with the highest power-to-mass ratio of any photovoltaic technology.[3] Implementation of this technology for large-area applications and full exploitation of the benefit provided by thinness[2] (including possible reductions in balance of systems costs) requires that the active materials accommodate at least modest tensile strains reversibly. Mechanical robustness is prerequisite for thinness because small environmental forces will produce large strains on ultra-thin substrates.[4,5] The mechanical properties of organic semiconductors, however, exhibit a range of tensile moduli and propensity to fracture.[1,6–8] Establishing not only the structural parameters that control the mechanical properties but simple methods to tune the elasticity without adversely affecting the electronic properties would be a significant benefit to the field of organic electronics.[9] The establishment of such knowledge might enable truly "rubber" semiconductors, which could have a range of applications in devices for energy and biomedicine.[10–12]

Our laboratory has studied the mechanical properties of regioregular poly(3-alkylthiophene) (P3AT) as a function of the length of the alkyl solubilizing group.[1] Our observations led us to conclude that this structural element had a drastic effect on both the mechanical and photovoltaic properties.[1] In particular, we concluded that the length of the side chain was inversely correlated with photovoltaic efficiency for

P3AT:$PC_{61}BM$, from A = hexyl to A = dodecyl, but that the length of the side chain was directly correlated with compliance.[1] The tensile modulus of P3HT was nearly an order of magnitude greater (1.09 GPa) than that of P3OT (0.15 GPa), but the photovoltaic efficiency of P3HT-based devices was noted by us and others to be significantly greater than that of P3OT-based devices.[13] There is a notion that electronic and mechanical properties tend to be in competition (if one places value on elasticity and ductility). Notably, Awartani et al. have shown that increasing order in the pure P3HT phases in P3HT:$PC_{61}BM$ blends with decreasing rate of evaporation of solvent during spin coating produces efficient—but stiff and brittle—photovoltaic active layers.[6]

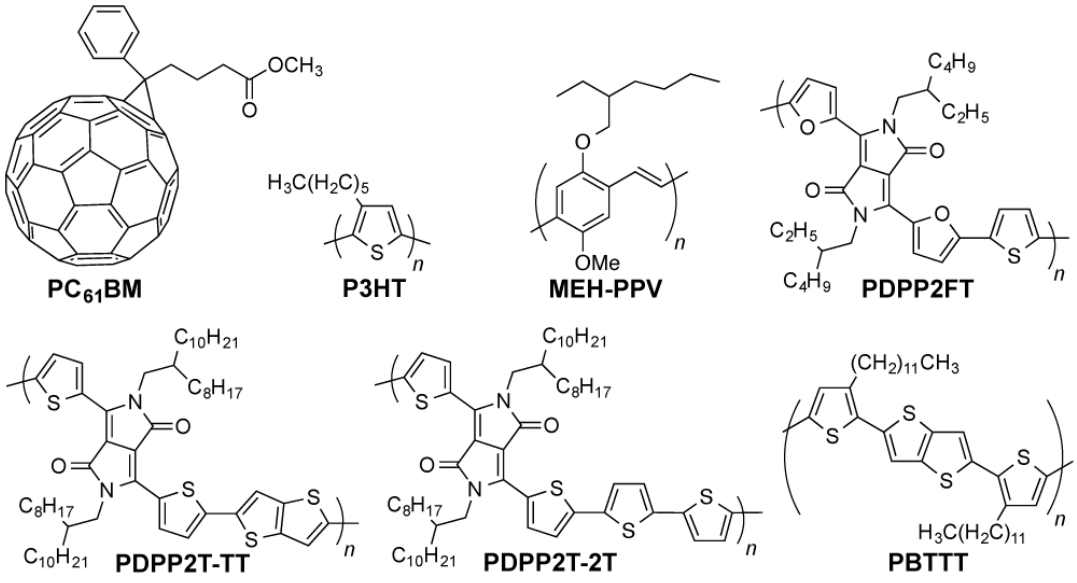

Figure 4.1. Chemical structures of materials discussed in the text.

While the regioregular P3ATs represent an important class of materials for fundamental studies of mechanical properties, it seems likely that a low-bandgap, donor-acceptor copolymer will emerge as the preferred "p-type" material,[14] with a fullerene or another polymer as the "n-type" material, provided both materials can be manufactured at scale with low cost and with low environmental impact.[15] To this end, a previous report

measured the tensile moduli of PDPP2T-TT and PDPP2T-2T and attributed the slightly lower tensile modulus of PDPP2T-2T (0.74 GPa) to that of PDPP2T-TT (0.99 GPa) to the relative stiffness[7] of the fused thienothiophene (TT) unit to that of the separated bithiophene (2T) unit (**Figure 4.1**).[16] These values of modulus, however, are very close, and it does not seem that replacement of fused rings for isolated rings will be the most effective strategy to provide improvements in mechanical properties. Within classes of similar materials, the mechanical compliance is inversely correlated to the crystallinity.[7] This effect has been noted in both P3ATs with different side chain lengths[1] and P3ATs compared to highly crystalline annealed films of PBTTT.[7,17] While it has previously been believed that high crystallinity was necessary for high charge transport, PDPP2T-TT exhibits balanced electron and hole mobilities for field-effect transistors that are among the highest of any material yet reported,[18,19] but it is significantly less crystalline than are annealed films of PBTTT.[20] Indeed, while the power conversion efficiencies (*PCE*s) of blends of MEH-PPV and MDMO-PPV[21] with $PC_{61}BM$ are no longer state-of-the-art, the efficiencies are not drastically lower than that of the typical P3HT:$PC_{61}BM$ cell[22] (~2 times lower), even though P3HT is semicrystalline and MEH-PPV and MDMO-PPV are amorphous.[23] PCDTBT is another example of a predominantly amorphous polymer[24] that has achieved values of *PCE* in blends with $PC_{71}BM$ greater than typical values for P3HT:$PC_{61}BM$.[25,26] Thus an effective strategy to combine mechanical compliance and photovoltaic efficiency might include the use of a conjugated polymer with good transport along the molecular axis but with a disrupted ability to form large crystallites in the solid state[27] which may stiffen the film.[7]

Block copolymers prepared by controlled living radical polymerization offer opportunities to combine advantageous properties of their component blocks,[28] but the method is not amenable to the preparation of low-bandgap conjugated polymers. Recently, segmented, or "blocky" copolymers have been prepared by metal mediated olefin polymerization[29] and also by polycondensation reactions.[30] This work has demonstrated that segmented polymers can separate into domains rich in their component segments; segmentation thus provides a route to tailor the properties in a way that is analogous to block copolymerization, specifically for improved mechanical properties and processing behavior. All-conjugated block copolymers, such as analogues of regioregular polythiophenes, are generally synthesized by chain-growth mechanism. Alternating copolymerization, which is necessary to produce low-bandgap materials, follows step-growth kinetics and is not easily adapted to the production of block copolymers.[31] Ku et al., however, recently demonstrated a hybrid strategy in which a low-bandgap copolymer was appended to a polythiophene segment bearing a reactive chain end.[32] Our goal was thus to apply the strategy of segmented polymerization to a wholly low-bandgap conjugated polymer.

We focused our efforts on PDPP2FT and derivatives thereof. PDPP2FT, first reported by Woo et al., is a furan-containing donor-acceptor copolymer that is promising for photovoltaic applications.[33] It is synthesized by a metal-mediated polycondensation reaction of two monomers: the DPP unit flanked by two furan rings terminated in bromides and a unit of distannylated thiophene.[33] Superior solubility of polymers containing the furan moiety permits the use of ethylhexyl solubilizing groups whereas an analogous material in which the furans are substituted with thiophenes requires the much

longer octyldodecyl side chains to afford useful solubility.[33] Solar cells based on PDPP2FT:$PC_{71}BM$ blends spin-coated from chlorobenzene with a chloronapthalene additive exhibited photovoltaic efficiencies of 5.0%.[33] Using PDPP2FT as a starting point, we tested a simple method for increasing the elasticity of the material through random segmentation—that is, random incorporation of an alkylated conjugated units throughout the backbone (**Figure 4.2**). We believed this approach would have two effects: (1) disruption of the regular order in the main chain of the polymer and (2) alteration of the distribution of side chains. We predicted that both effects could lower the tensile modulus without significantly affecting the photovoltaic response of these materials in blends with fullerenes.

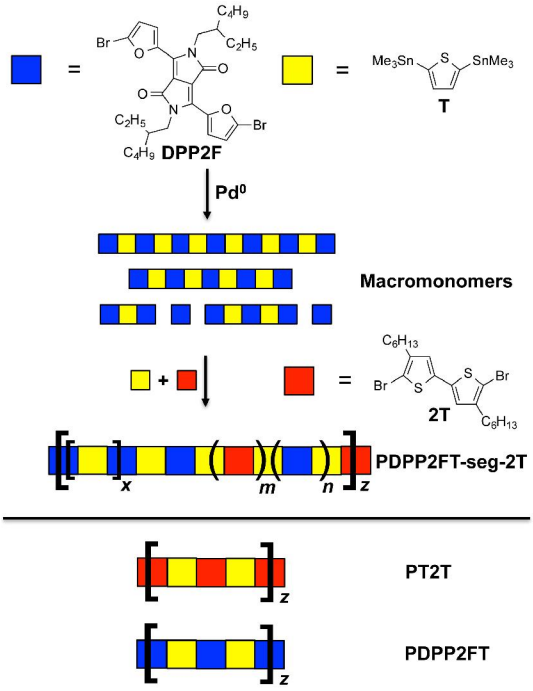

Figure 4.2. Summary of the synthetic strategy used to generate segmented copolymers. Two monomers, the dibromide (DPP2F) and the distannane (T), are reacted in the presence of Pd^0. Shortly after initialization of the reaction (when "macromonomers" began to form), additional T and dibrominated bithiophene (2T) were added to the reaction mixture to form the segmented polymer, PDPP2FT-seg-2T. Separately, the homopolymers PT2T and PDPP2FT were also prepared.

4.2 Experimental Section

4.2.1 Materials

A soluble fullerene derivative, [6,6]-phenyl C_{61} butyric acid methyl ester ($PC_{61}BM$) was obtained from Sigma-Aldrich with >99% purity. PDMS, Sylgard 184 (Dow Corning), was prepared according to the manufacturer's instructions at a ratio of 10:1 (base:crosslinker) and cured at room temperature for 36 to 48 hours before it was used for mechanical testing. (Tridecafluoro-1,1,2,2-tetrahydrooctyl)-1-trichlorosilane (FOTS) was obtained from Gelest. PEDOT:PSS (Clevios PH1000) was purchased from Heraeus. DMSO was purchased from BDH with purity of 99.9% and Zonyl (FS-300) fluorosurfactant was purchased from Sigma-Aldrich.

4.2.2 General

All reagents were obtained from commercial suppliers and used without purification. Chloroform ($CHCl_3$), ortho-dichlorobenzene (ODCB), dimethylformamide (DMF) and tetrahydrofuran (THF) were obtained from Sigma-Aldrich. All compounds were characterized by ^1H NMR and ^{13}C NMR (300 MHz, Varian) using $CDCl_3$ as the solvent. The residual chloroform peak at 7.26 ppm was used to calibrate the chemical shifts for ^1H NMR. Gel-permeation chromatography (GPC) was performed in chloroform ($CHCl_3$) on a Waters 2690 Separation Module equipped with a Waters 2414 Refractive Index Detector and a Waters 2996 Photodiode Array Detector. Molecular weights were calculated relative to linear PS standards. Atomic force microscope (AFM) images were obtained with a Veeco Scanning Probe Microscope in tapping mode. AFM data was analyzed with NanoScope Analysis v1.40 software (Bruker Corp.). Ultraviolet-visible

(UV-vis) spectra were obtained of the polymers in chroloform and in the solid state, as-cast from 4:1 $CHCl_3$:ODCB (by volume, 5 mg ml^{-1}) using a Perkin Elmer Lambda 1050 UV-vis-NIR spectrophotometer. We synthesized the two known polymers, PDPP2FT[33] and PT2T (formerly called C_6-TT),[34,35] according to previously established procedures.

4.2.3 Synthesis of PDPP2FT-seg-2T

We synthesized this material using a method related to that of PDPP2FT, except that after allowing the **DPP2F** and **T** (**Figure 4.2**) to react for a short time, we added brominated bithiophene monomer (**2T**) and additional stannylated thiophene (**T**), as follows. In a 12-mL reaction tube, **DPP2F** (234 mg, 0.360 mmol), 2,5-bis(trimethylstannyl)-thiophene (**T**, 147 mg, 0.360 mmol), $Pd_2(dba)_3$ (2 mol %) and P(o-tol)$_3$ (8 mol %) were dissolved in 4 mL chlorobenzene and degassed by bubbling argon through the mixture for 20 min. In a separate identical reaction tube, 2,5-bis(trimethylstannyl)-thiophene (**T**, 49 mg, 0.120 mmol) and brominated bithiophene (**2T**, 59 mg, 0.120 mmol) were dissolved in 2 mL chlorobenzene and degassed in the same manner. The first reaction tube was heated in an oil bath to 110 °C for 15 min, and a color change was observed from red monomer to green/blue oligomeric species. The first tube was removed from the oil bath and allowed to cool, and then the contents of the second reaction tube were added by cannula. The reaction was again heated to 110 °C for 6 h and then was allowed to cool to room temperature and was diluted with chloroform to reduce viscosity, and was precipitated into cold methanol. The solid was collected on filter paper, which was loaded into a Soxhlet and extracted with methanol and hexanes before the segmented polymer was collected by extraction with

chloroform. Concentration under reduced pressure yielded 235 mg of a dark solid. GPC analysis provided values of M_w = 55 kDa and PDI = 2.5. ^{1}H NMR (300 MHz, $CDCl_3$): δ (ppm) = 8.70-8.30 (br, 2H), 7.22-6.33 (br, 4H), 4.65-3.3 (br, 4H), 2.88-2.38 (br, 0.91H inferred, signal due to randomly incorporated **2T**), 2.03-1.76 (br, 2H), 1.74-1.63 (br ovlp, 0.91H inferred), 1.60-1.06 (br, 16H), 1.04-0.70 (br ovlp, 13.36H inferred).

4.2.4 Mechanical characterization

We measured the tensile modulus of each material using the mechanical buckling technique originally described by Stafford et al.[36] This method has been used in various thin film systems including conjugated polymer films for heterojunction OPV devices.[1,6,8,16] In brief, the films were spin-coated on passivated glass slides and transferred to poly(dimethylsiloxane) (PDMS) substrates bearing a small pre-strain. After transfer, the PDMS substrates were relaxed and the conjugated polymer film adopted sinusoidal buckles. The buckling wavelength, λ_b, is related to the thickness of the film, d_f, the tensile moduli of the film and the substrate, E_f and E_s, and the Poisson's ratios of the two materials, v_f and v_s by the following equation:

$$E_f = 3E_s\left(\frac{1-v_f^2}{1-v_s^2}\right)\left(\frac{\lambda_b}{2\pi d_f}\right)^3 \qquad (1)$$

We measured the tensile modulus of the substrate, E_s (using a commercial pull tester), the buckling wavelength, λ_b (by optical microscopy), and the film thickness, d_f (by stylus profilometry). The slope of a plot of λ_b vs. d_f for three different film thicknesses was inserted into Equation 1. The Poisson's ratios were taken as 0.5 and 0.35 for PDMS and

the conjugated polymers films, which agree well with the previously reported values and our theoretical predictions.[1,8]

We also computed the values for the tensile moduli of the conjugated polymer using a theoretical model originally described by Seitz,[37] applied to conjugated polymers by Tahk,[8] and further refined by our group to account for differential glass transition temperature between various conjugated polymers.[1] The model incorporated the knowledge of the chemical structure of the polymer—*i.e.* molecular weight, van der Waals volume, the length and the number of rotational bonds in the monomer—and the glass transition temperature (T_g).

4.2.5 Fabrication and testing of photovoltaic devices

The conjugated polymer:fullerene bulk heterojunction (BHJ) films were spin-coated onto glass slides pre-coated with a PEDOT:PSS films. Prior to spin-coating the PEDOT:PSS, the glass slides were cleaned with Alconox solution (2 mg mL^{-1}), deionized water, acetone, and then isopropyl alcohol (IPA) in an ultrasonic bath for 10 min each, followed by a plasma treatment at ~30 W for 3 min at a base pressure of 200 mTorr in ambient air. The PEDOT:PSS layer was deposited from an aqueous solution containing 93 wt% Clevios PH 1000 (~0.9–1.2 wt% PEDOT:PSS), 6.9 wt% DMSO, and 0.1 wt% Zonyl.[38] The solution was filtered with a 1-μm glass microfiber (GMF) syringe filter and then spin coated at a speed of 500 rpm (100 rpm s^{-1} ramp) for 60 s, followed by 2000 rpm (750 rpm s^{-1} ramp) for 60 s, which produced in a layer 200 nm thick. The samples were subsequently dried at 150 °C for 30 min before the deposition of the polymer:fullerene BHJ films. The BHJ films were deposited from solutions of 1:2 by weight polymer and

$PC_{61}BM$ in 4:1 $CHCl_3$:ODCB (2.5 mg mL^{-1}), which were stirred overnight and filtered with 0.20 μm poly(tetrafluoroethylene) (PTFE) syringe filters. The solutions were then spin coated onto the electrode layer at a speed of 300 rpm (100 rpm s^{-1} ramp) for 240 s, followed by 2000 rpm (750 rpm s^{-1} ramp) for 60 s. For each device, a thin strip of the PEDOT:PSS electrode was exposed by wiping away some of the polymer:$PC_{61}BM$ film with chloroform so that electrical contact could be made. To minimize exposure to ambient air by transferring devices into and out of an evaporator in a different building, EGaIn (extruded by hand from a syringe) was used as the top contact.[39] The photovoltaic properties were measured in a nitrogen-filled glovebox using a solar simulator with a 100 mW cm^{-2} flux that approximated the solar spectrum under AM 1.5G conditions (ABET Technologies 11016-U up-facing unit calibrated with a reference cell with a KG5 filter). The current density versus voltage was measured for both dark and under illumination using a Keithley 2400 SourceMeter.

4.3 Results and Discussion

4.3.1 ^1H NMR

Our first task was to verify the incorporation of the 2T units in the PDPP2FT-seg-2T polymer. **Figure 4.3** compares the ^1H NMR spectra for PDPP2FT, PDPP2FT-seg-2T and PT2T; the inset highlights the signal from 3.0 to 1.5 ppm. Because the PDPP2FT and PDPP2FT-seg-2T are compositionally similar, differences in spectra were expected to be quite minor. The spectrum for PDPP2FT-seg-2T is largely similar to that of PDPP2FT, except that PDPP2FT-seg-2T exhibited a signal at 2.88-2.38 ppm and a partially overlapping signal at 1.74-1.63 ppm, which we attribute to the methylene protons located

α and β to the aromatic rings of the bithiophene unit as shown in the inset of **Figure 4.3**. From integration of the signals, we estimated that there was one 2T unit incorporated per 4.4 DPP2F units in the segmented polymer. While the ^{1}H NMR experiments provided evidence for 2T units in our samples, further investigation was necessary to conclude that they were covalently incorporated into the main polymer chain. ^{13}C NMR spectra of the polymer samples are shown in **Figure B.1** but were inconclusive owing to a low signal to noise ratio for PDPP2FT and PDPP2FT-seg-2T, which we attribute to a low effective concentration of magnetically distinct carbon atoms even at the limit of solubility (*ca*. 50 mg mL^{-1}) and with data collection times of 9 h.

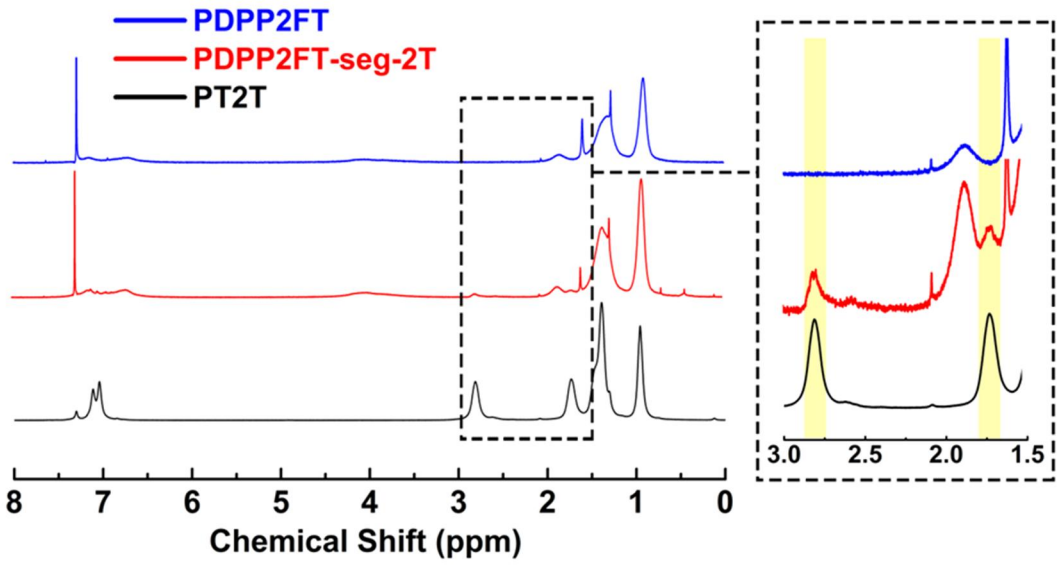

Figure 4.3. ^{1}H NMR spectra of PDPP2FT, PDPP2FT-seg-2T, and PT2T. Peaks associated with the bithiophene are highlighted in the inset at δ = 2.88-2.38 ppm and 1.74-1.63 ppm.

4.3.2 UV-Visible absorption

We compared the ultraviolet-visible absorption spectra of the three materials. **Figure 4.4** shows the absorption spectrum. The band gaps were determined from the

onset of absorption for thin films of the pure polymers (**Figure 4.4a**). PT2T exhibited an onset of optical absorption at around 660 nm (band gap = 1.88 eV), with a maximum absorption around 540 nm, while the pure PDPP2FT exhibited an onset of optical absorption at around 930 nm (band gap = 1.33 eV), with a maximum at 800 nm. PDPP2FT-seg-2T, which contains segments of PDPP2FT interspersed by statistical incorporation of monomers (PDPP2FT-seg-2T) exhibits features similar to PDPP2FT. However, the peaks in PDPP2FT-seg-2T are broader and less defined, which could suggest decreased order than what is observed in the homopolymer, PDPP2FT. The details of the vibronic structure have been used to correlate the extent of π-stacked, ordered structures (H-aggregates) in P3HT:$PC_{61}BM$ blends to their tensile moduli and ductility, with samples that exhibited significant H-aggregates also exhibited increased stiffness and ductility.[6] Further work would be required to correlate order as measured spectroscopically to mechanical properties for this class of low-bandgap materials.

To determine if the ^{1}H NMR and the above UV-vis results were due to PT2T contamination in the PDPP2FT-seg-2T sample as opposed to covalently bound segments, we performed two additional UV-vis experiments. We first measured the extinction coefficients of the pure polymers from their absorption in $CHCl_3$ (1×10^{-5} M) and used these values to calculate the absorption spectra of physical blends of PDPP2FT:PT2T (**Figure 4.4b**). Because the samples were dilute and did not form aggregates, our calculated absorptions were superpositions of the pure polymers in various ratios. We calculated the minimum ratio of PDPP2FT:PT2T before a noticeable onset of absorption in the PT2T absorbing region to be approximately 100:1. The normalized absorption spectra of the pure polymers and the calculated 100:1 physical blend absorption spectra,

as well as the ratio of DPP2F:2T in PDPP2FT-seg-2T (4.4:1) are plotted in **Figure B.2**. We then determined the absorption of a thin film of a 100:1 physical blend of PDPP2FT:PT2T (**Figure B.3**). The absorption spectrum of the physical blend was approximately that of the pure PDPP2FT, with more well defined peaks than those of PDPP2FT-seg-2T.

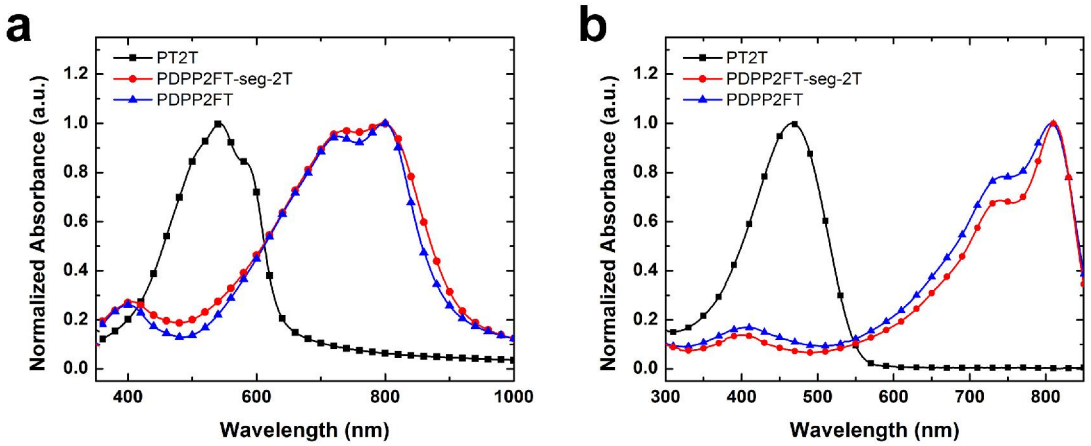

Figure 4.4. Absorption spectra of the three polymers synthesized in this work. (a) Thin films of the pure polymers spin cast from 4:1 $CHCl_3$:ODCB and (b) the pure polymers in $CHCl_3$ at a concentration of 1×10^{-5} M.

4.3.3 Gel-permeation chromatography

From the ^{1}H NMR spectra, we demonstrated that both PDPP2FT and 2T units are present in the product. The next essential step was to confirm the purity—*i.e.*, the absence of homopolymers—within the segmented product. Gel permeation chromatography provided evidence of covalent connectivity of the bithiophene units within the segmented polymer. **Figure 4.5** shows the GPC traces (intensity vs. retention time) and contour plots (wavelength vs. retention time) of all three conjugated polymer samples. For PDPP2FT (**Figure 4.5a**), the main absorbance peak occurred at 550-800 nm from 10 to 14 min with a much smaller peak at 350-450 nm. Minor tailing was observed in the GPC traces; these

tails probably correspond to lower molecular weight polymers. A relatively polydisperse sample was expected from a step-growth mechanism. The GPC trace for the segmented polymer (PDPP2FT-seg-2T) also showed similar tailing and a broad shoulder. This shoulder may originate from either lower molecular weight segmented polymer or from the presence of residual homopolymers. We addressed this concern using the contour plot based on a photodiode UV detector as described by Hawker and coworkers for an all-conjugated block copolymer.[32] The contour plot for the segmented polymer (PDPP2FT-seg-2T, **Figure 4.5b**) shows two absorbance peaks at 350-550 and 550-800 nm centered on a single retention time of 11-14 min. The plot for PT2T (**Figure 4.5c**) also suggests the absence of major impurities; it shows a dominant absorbance peak from 350-500 nm at 13 min. This analysis strongly suggests that the product in PDPP2FT-seg-2T contains no contamination of either homopolymers and the low molecular weight tail contains both PDPP2FT and 2T segments. If homopolymers contamination were to occur, two distinct absorption regions with different retention times would be observed. The closeness in retention time of PDPP2FT and PDPP2FT-seg-2T suggests a minimal difference in molecular weights; thus we neglect the effects of molecular weight on the mechanical properties and photovoltaic properties of the two materials (**Table 4.1**).

Table 4.1. Molecular weights and PDIs for the conjugated polymer samples as determined by GPC versus polystyrene standards.

Polymer	M_n (g mol^{-1})	M_w (g mol^{-1})	PDI
PDPP2FT	26 400	69 600	2.64
PDPP2FT-seg-2T	22 300	55 300	2.47
PT2T	14 800	19 400	1.31

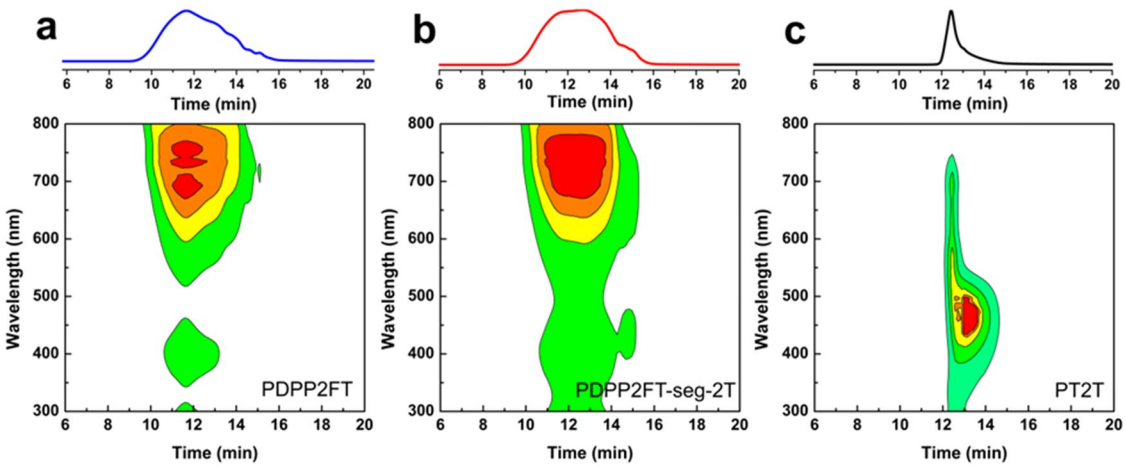

Figure 4.5. GPC traces and contour plots for (a) PDPP2FT, (b) PDPP2FT-seg-2T, and (c) PT2T based on a UV detector.

4.3.4 Tensile moduli of conjugated polymer thin films

We determined the tensile moduli of the pure polymer thin films spin-coated from chloroform. For each film, the buckling wavelengths were plotted as a function of the film thickness. The slopes of the linear fits were then substituted into Equation 1 to obtain the tensile moduli of the thin films. The tensile modulus of PT2T, whose structure is closely related to P3HT,[35] was determined to be 1.11 ± 0.19 GPa. This value agrees well with the values of P3HT reported previously by our group[1] and literature values[8,16] obtained using the same method. The obtained value for PDPP2FT, 2.17 ± 0.35 GPa, was twice that of PT2T. This value was greater than that previous reported for PDPP2T-TT (0.99 GPa),[16] though we note that PDPP2T-TT contains octyldodecyl side chains and PDPP2FT contains ethylhexyl side chains. Long alkyl side chains tend to reduce the tensile modulus and increase the ductility of a conjugated polymer significantly.[1]

We then measured the tensile modulus of the segmented polymer, PDPP2FT-seg-2T. The incorporation of the 2T units, as determined from ^{1}H NMR spectra, produced a

significantly reduced stiffness (modulus = 0.93 ± 0.16 GPa) compared to PDPP2FT. The reduction in modulus by segmentation is possibly attributable to three effects. The first effect is that random incorporation tends to disrupt the ability of a conjugated polymer to form crystallites, and highly crystalline films tend to be stiffer than amorphous ones with similar chemical structures.[7] The second effect is that in the segmented sample, approximately one of every five DPP2F units is substituted for a 2T unit. Substitution of fused rings for isolated rings have been correlated to decreased stiffness of the film in both polythiophene[7] and DPP-based systems.[16] The third effect is that statistical incorporation of alkylated bithiophene units significantly altered the distribution of side chains compared to that of the homopolymer. While predicting the effect of this change in the distribution of side chains on the mechanical properties would be difficult to accomplish, small changes in the lengths of the side-chains have significant effects on the thermal, electrical, and mechanical properties of P3ATs.[1,40] As a control experiment, we also measured the tensile modulus of the 100:1 physical blend between PDPP2FT and PT2T (**Figure B.4** and **Table B.1**). We found that, within experimental error, the physical blend had a comparable tensile modulus to PDPP2FT.

Our theoretical calculations of the tensile moduli that uses the molecular structure of the monomer as well as the T_g of the polymer[1,8,37] agreed extremely well with experimental values for the homopolymers, PT2T and PDPP2FT. The calculated values were 1.13 ± 0.14 (PT2T) and 2.47 ± 0.30 (PDPP2FT), using the T_g values of 14 °C and 50 °C. This simple theoretical model, however, failed to predict the reduction in modulus of PDPP2FT-seg-2T relative to that of the homopolymer, PDPP2FT. We attribute its

failure primarily to its inability to incorporate the effects of randomness in the polymer chain.

4.3.5 Photovoltaic characteristics

To determine the applicability of these materials in organic solar cells, we fabricated devices by mixing the polymers in a 1:2 ratio with $PC_{61}BM$. We used PEDOT:PSS as the transparent anode and eutectic gallium-indium (EGaIn) as the cathode.[39] **Figure 4.6** shows the current density vs. voltage (*J–V*) plots for representative devices. (**Figure B.5** and **Table B.2** include devices fabricated with a 100:1 PDPP2FT:PT2T physical blend, which performed similarly to, but slightly poorer than the PDPP2FT devices). The poor behavior we observed for the PT2T sample is consistent with similarly poor performance reported by Koppe et al.,[35] who attributed the inefficiency of PT2T:$PC_{61}BM$ compared to P3HT:$PC_{61}BM$ (despite favorable offsets of the frontier molecular orbitals) to intercalation of $PC_{61}BM$ within the large gap between side chains in PT2T and suppression of the ability of the polymer to crystallize.[35] The power conversion efficiency (*PCE*) of PDPP2FT:$PC_{61}BM$ (*PCE* = 2.52 ± 0.34%, *N* = 7) and PDPP2FT-seg-2T:$PC_{61}BM$ (*PCE* = 2.82 ± 0.28%, *N* = 6), however, were similar. The data for all devices tested are summarized in **Table 4.2**. The short circuit current (J_{sc}), open circuit voltage (V_{oc}), fill factor (*FF*), series resistance (R_{series}), and *PCE* are all very similar for PDPP2FT and PDPP2FT-seg-2T. The similarity in figures of merit suggests that the charge-transport properties are preserved despite the incorporation of 2T units. Interestingly, even though the incorporation of the 2T units increased the

mechanical compliance of PDPP2FT-seg-2T, it did not appear to have a deleterious effect on the photovoltaic properties.

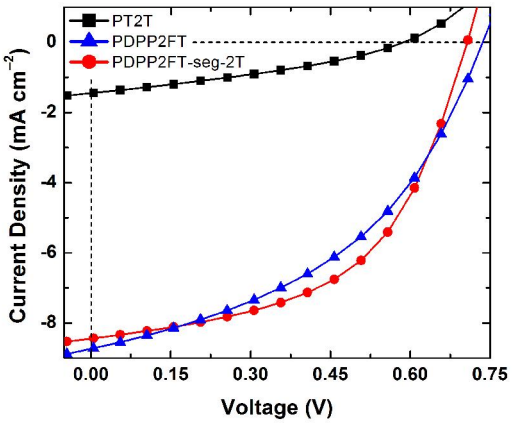

Figure 4.6. Photovoltaic characteristics of representative samples of polymer-fullerene blends. All active layers comprised 1:2 polymer:$PC_{61}BM$.

Table 4.2. Summary of the figures of merit for the solar cells fabricated in this work.

Polymer	***n***	J_{sc} **[mA cm^{-2}]**	V_{oc} **[mV]**	***FF*** **[%]**	η_e **[%]**
PT2T	3	1.5 ± 0.1	579 ± 21	32.9 ± 1.1	0.28 ± 0.01
PDPP2FT-seg-2T	6	8.4 ± 0.5	699 ± 23	48.2 ± 3.3	2.82 ± 0.28
PDPP2FT	7	8.3 ± 0.5	715 ± 25	42.5 ± 3.6	2.52 ± 0.34

4.3.6 Atomic force microscopy

To determine if the difference in tensile modulus between the PDPP2FT and the PDPP2FT-seg-2T could be attributed to a significant change in the morphology of the films, we examined spin-coated films by AFM. Previous studies have suggested that roughness observable by AFM correlates with crystalline order, as determined by grazing-incidence X-ray diffraction, in conjugated polymer films annealed below T_m.[41] A similar effect was noted in a series of P3ATs from A = butyl to A = dodecyl, where the shortest alkyl chains had the greatest roughness (presumably due to greater crystallinity) and stiffness.[1] **Figure 4.7** shows AFM micrographs of the heights of the PDPP2FT and

the PDPP2FT-seg-2T films. We observed that PDPP2FT had a root mean square (rms) roughness of 1.13 ± 0.09 nm and PDPP2FT-seg-2T had an rms roughness of 1.25 ± 0.08 nm. The similarity of these values suggests that the correlation between roughness (as a manifestation of crystallinity) and tensile modulus—as observed in other systems—is not general.

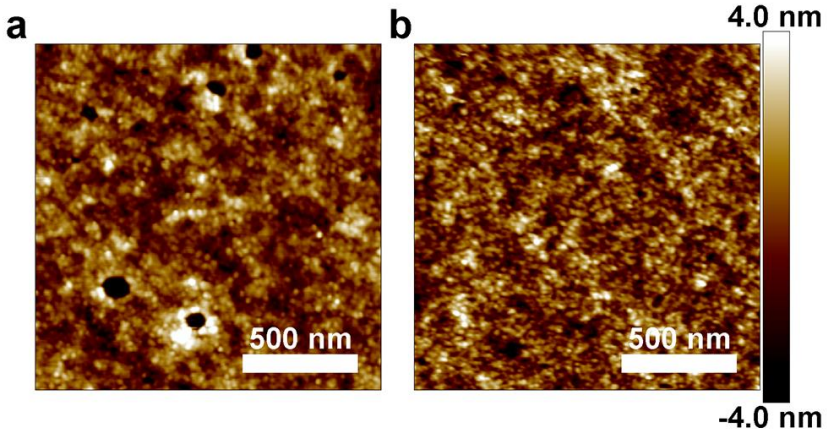

Figure 4.7. Height images from atomic force micrographs of unannealed polymer thin films. (a) PDPP2FT and (b) PDPP2FT-seg-2T.

4.3.7 Competition between photovoltaic performance and stiffness

Within groups of structurally related conjugated polymers, charge transport and photovoltaic efficiency are regarded as antithetical to mechanical compliance.{Merging Citations} Along with the tensile moduli of the pure polymers, we measured the moduli of the 1:2 polymer:$PC_{61}BM$ blends spin-coated from 4:1 chloroform:ODCB. **Figure 4.8a** compares the tensile moduli of the pure polymer films and the blended films. For all three polymers, we observed increased in the tensile moduli with the addition of $PC_{61}BM$. Various studies have reported the same trend in system comprising conjugated polymer and fullerene composites.[1,7,8,13,16] In **Figure 4.8b**, we plotted the power conversion efficiencies (*PCE*) of the polymer:$PC_{61}BM$ BHJ films as a function of tensile modulus.

For materials in which these figures of merit are strongly correlated, such as in P3HT:$PC_{61}BM$ exhibiting increasing order, the data points would sit (very roughly) on a diagonal extending from low tensile modulus and low *PCE* to high values of both parameters. Interestingly, the sample PDPP2FT-seg-2T:$PC_{61}BM$ shows a similar *PCE* to that of PDPP2FT:$PC_{61}BM$, but the PDPP2FT-seg-2T is a factor of two more elastic than PDPP2FT. While polymer:$PC_{61}BM$ blends are always measured to be stiffer than the pure polymers, the factor by which the tensile modulus of the blend is greater than that of the pure polymer tends to be similar within similar classes of materials.[1,16] The segmented copolymer, PDPP2FT-seg-2T appears to exhibit photovoltaic properties resembling PDPP2FT, but mechanical properties resembling those of PT2T. It is possible that the "random" segments interspersed between PDPP2FT segments have a softening effect on the material. The all-conjugated nature of the "random" segments may provide advantages over block copolymers in which the plasticizing block is insulating.[42]

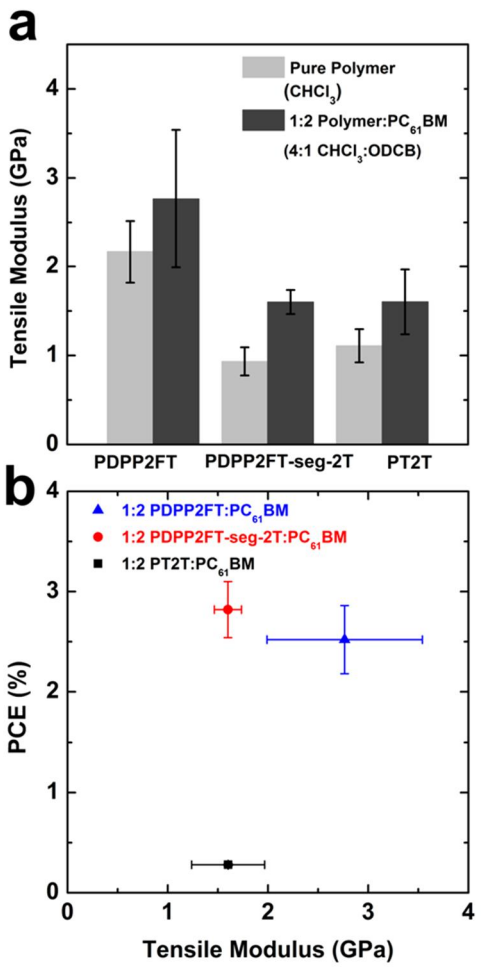

Figure 4.8. Mechanical and electronic properties of the polymer and polymer:fullerene blends in this work. (a) Comparison between the tensile moduli of pure polymer films spin-coated from chloroform and the films comprising 1:2 polymer:$PC_{61}BM$ blends spin-coated from 4:1 chloroform:ODCB. (b) Plot of power conversion efficiency of the polymers in a 1:2 blend with $PC_{61}BM$ spin-coated from 4:1 chloroform:ODCB. The architecture of the devices was PEDOT:PSS/polymer:$PC_{61}BM$/EGaIn. The vertical error bars for 1:2 PT2T:$PC_{61}BM$ sample overlap with the marker.

4.4 Conclusion

We have demonstrated that segmentation could be an effective strategy to increase the mechanical compliance of low-bandgap conjugated polymers without deleteriously affecting their optoelectronic properties. The method does not add significant complexity to the synthetic protocol—a third monomer is simply added to the

reaction mixture after a predetermined length of time. The polymerization strategy described here suggests the possibility of fully segmented polymer comprising "macromonomers" of polymers with different band structures. Such materials could be analogous to block copolymers except that block copolymers are synthesized by living, chain-growth processes. In contrast, polymers in which both components are synthesized by step-growth processes (*i.e.*, the Stille polymerization) are not amenable to the synthesis of block copolymers. Segmented polymerization may therefore be a route to synthesizing single-component organic semiconductors with tailored thermal and mechanical properties (*i.e.*, semiconducting thermoplastic elastomers). Our analysis also exposed deficiencies in the ways in which standard semi-empirical theories predict mechanical properties in semicrystalline polymers. Future work will attempt to incorporate the effects of randomness in the polymer backbones as well as address the behavior of these softened polymers in real-world conditions.

Acknowledgements

This work was supported by the Air Force Office of Scientific Research (AFOSR) Young Investigator Program, grant number FA9550-13-1-0156. Additional support was provided by the NSF Graduate Research Fellowship under grant number DGE-1144086, awarded to S. S., and by laboratory startup funds from the University of California, San Diego.

Chapter 4, in full, is a reprint of the material as it appears in *RSC Advances*, 2014, 4, 13635. The Royal Society of Chemistry, 2014. Adam D. Printz,[†] Suchol Savagatrup,[†]

Daniel J. Burke, Trevor N. Purdy, and Darren J. Lipomi. († Equal contribution). The dissertation author was the primary investigator and author of this paper.

References

(1) Savagatrup, S.; Makaram, A. S.; Burke, D. J.; Lipomi, D. J. Mechanical Properties of Conjugated Polymers and Polymer-Fullerene Composites as a Function of Molecular Structure. *Adv. Funct. Mater.* **2014**, *24*, 1169–1181.

(2) Kaltenbrunner, M.; White, M. S.; Głowacki, E. D.; Sekitani, T.; Someya, T.; Sariciftci, N. S.; Bauer, S. Ultrathin and Lightweight Organic Solar Cells with High Flexibility. *Nat. Commun.* **2012**, *3*, 770.

(3) Kaltenbrunner, M.; Sekitani, T.; Reeder, J.; Yokota, T.; Kuribara, K.; Tokuhara, T.; Drack, M.; Schwödiauer, R.; Graz, I.; Bauer-Gogonea, S.; Bauer, S.; Someya, T. An Ultra-Lightweight Design for Imperceptible Plastic Electronics. *Nature* **2013**, *499*, 458–463.

(4) Dupont, S. R.; Oliver, M.; Krebs, F. C.; Dauskardt, R. H. Interlayer Adhesion in Roll-to-Roll Processed Flexible Inverted Polymer Solar Cells. *Sol. Energy Mater. Sol. Cells* **2012**, *97*, 171–175.

(5) Brand, V.; Bruner, C.; Dauskardt, R. H. Cohesion and Device Reliability in Organic Bulk Heterojunction Photovoltaic Cells. *Sol. Energy Mater. Sol. Cells* **2012**, *99*, 182–189.

(6) Awartani, O.; Lemanski, B. I.; Ro, H. W.; Richter, L. J.; DeLongchamp, D. M.; O'Connor, B. T. Correlating Stiffness, Ductility, and Morphology of Polymer:Fullerene Films for Solar Cell Applications. *Adv. Energy Mater.* **2013**, *3*, 399–406.

(7) O'Connor, B.; Chan, E. P.; Chan, C.; Conrad, B. R.; Richter, L. J.; Kline, R. J.; Heeney, M.; McCulloch, I.; Soles, C. L.; DeLongchamp, D. M. Correlations between Mechanical and Electrical Properties of Polythiophenes. *ACS Nano* **2010**, *4*, 7538–7544.

(8) Tahk, D.; Lee, H. H.; Khang, D.-Y. Elastic Moduli of Organic Electronic Materials by the Buckling Method. *Macromolecules* **2009**, *42*, 7079–7083.

(9) Lipomi, D. J.; Bao, Z. Stretchable, Elastic Materials and Devices for Solar Energy Conversion. *Energy Environ. Sci.* **2011**, *4*, 3314–3328.

(10) Sekitani, T.; Someya, T. Stretchable Organic Integrated Circuits for Large-Area Electronic Skin Surfaces. *Mrs Bull.* **2012**, *37*, 236–245.

(11) Rogers, J. A.; Someya, T.; Huang, Y. Materials and Mechanics for Stretchable Electronics. **2010**, *327*, 1603–1607.

(12) Kim, D.-H.; Lu, N.; Ma, R.; Kim, Y.-S.; Kim, R.-H.; Wang, S.; Wu, J.; Won, S. M.; Tao, H.; Islam, A.; Yu, K. J.; Kim, T.; Chowdhury, R.; Ying, M.; Xu, L.; Li, M.; Chung, H.-J.; Keum, H.; McCormick, M.; Liu, P.; Zhang, Y.-W.; Omenetto, F. G.; Huang, Y.; Coleman, T.; Rogers, J. A. Epidermal Electronics. *Science* **2011**, *333*, 838–843.

(13) O'Connor, T. F.; Zaretski, A. V.; Shiravi, B. A.; Savagatrup, S.; Printz, A. D.; Diaz, M. I.; Lipomi, D. J. Stretching and Conformal Bonding of Organic Solar Cells to Hemispherical Surfaces. *Energy Environ. Sci.* **2014**, *7*, 370–378.

(14) Dou, L.; You, J.; Hong, Z.; Xu, Z.; Li, G.; Street, R. A.; Yang, Y. 25Th Anniversary Article: A Decade of Organic/Polymeric Photovoltaic Research. *Adv. Mater.* **2013**, *25*, 6642–6671.

(15) Burke, D. J.; Lipomi, D. J. Green Chemistry for Organic Solar Cells. *Energy Environ. Sci.* **2013**, *6*, 2053–2066.

(16) Lipomi, D. J.; Chong, H.; Vosgueritchian, M.; Mei, J.; Bao, Z. Toward Mechanically Robust and Intrinsically Stretchable Organic Solar Cells: Evolution of Photovoltaic Properties with Tensile Strain. *Sol. Energy Mater. Sol. Cells* **2012**, *107*, 355–365.

(17) McCulloch, I.; Heeney, M.; Bailey, C.; Genevicius, K.; Macdonald, I.; Shkunov, M.; Sparrowe, D.; Tierney, S.; Wagner, R.; Zhang, W.; Chabinyc, M. L.; Kline, R. J.; McGehee, M. D.; Toney, M. F. Liquid-Crystalline Semiconducting Polymers with High Charge-Carrier Mobility. *Nat. Mater.* **2006**, *5*, 328–333.

(18) Chen, Z.; Lee, M. J.; Shahid Ashraf, R.; Gu, Y.; Albert-Seifried, S.; Meedom Nielsen, M.; Schroeder, B.; Anthopoulos, T. D.; Heeney, M.; McCulloch, I.; Sirringhaus, H. High-Performance Ambipolar Diketopyrrolopyrrole-thieno[3,2-B]thiophene Copolymer Field-Effect Transistors with Balanced Hole and Electron Mobilities. *Adv. Mater.* **2012**, *24*, 647–652.

(19) Bronstein, H.; Chen, Z.; Ashraf, R. S.; Zhang, W.; Du, J.; Durrant, J. R.; Tuladhar, P. S.; Song, K.; Watkins, S. E.; Geerts, Y.; Wienk, M. M.; Janssen, R. A.; Anthopoulos, T.; Sirringhaus, H.; Heeney, M.; McCulloch, I. Thieno[3,2-B]thiophene-Diketopyrrolopyrrole-Containing Polymers for High-Performance Organic Field-Effect Transistors and Organic Photovoltaic Devices. *J. Am. Chem. Soc.* **2011**, *133*, 3272–3275.

(20) Zhang, X.; Richter, L. J.; Delongchamp, D. M.; Kline, R. J.; Hammond, M. R.; McCulloch, I.; Heeney, M.; Ashraf, R. S.; Smith, J. N.; Anthopoulos, T. D.; Schroeder, B.; Geerts, Y. H.; Fischer, D. A.; Toney, M. F. Molecular Packing of High-Mobility Diketo Pyrrolo-Pyrrole Polymer Semiconductors with Branched Alkyl Side Chains. *J. Am. Chem. Soc.* **2011**, *133*, 15073–15084.

(21) Shaheen, S. E.; Brabec, C. J.; Sariciftci, N. S.; Padinger, F.; Fromherz, T.; Hummelen, J. C. 2.5% Efficient Organic Plastic Solar Cells. *Appl. Phys. Lett.* **2001**, *78*, 841–843.

(22) Jørgensen, M.; Carlé, J. E.; Søndergaard, R. R.; Lauritzen, M.; Dagnæs-Hansen, N. A.; Byskov, S. L.; Andersen, T. R.; Larsen-Olsen, T. T.; Böttiger, A. P. L.; Andreasen, B.; Fu, L.; Zuo, L.; Liu, Y.; Bundgaard, E.; Zhen, X.; Chen, H.; Krebs, F. C. The State of Organic Solar cells—A Meta Analysis. *Sol. Energy Mater. Sol. Cells* **2013**, *119*, 84–93.

(23) Qin, T.; Troisi, A. Relation between Structure and Electronic Properties of Amorphous MEH-PPV Polymers. *J. Am. Chem. Soc.* **2013**, *135*, 11247–11256.

(24) Pearson, A. J.; Wang, T.; Dunbar, A. D. F.; Yi, H.; Watters, D. C.; Coles, D. M.; Staniec, P. A.; Iraqi, A.; Jones, R. A. L.; Lidzey, D. G. Morphology Development in Amorphous Polymer:Fullerene Photovoltaic Blend Films During Solution Casting. *Adv. Funct. Mater.* **2014**, *24*, 659–667.

(25) Seo, J. H.; Gutacker, A.; Sun, Y.; Wu, H.; Huang, F.; Cao, Y.; Scherf, U.; Heeger, A. J.; Bazan, G. C. Improved High-Efficiency Organic Solar Cells via Incorporation of a Conjugated Polyelectrolyte Interlayer. *J. Am. Chem. Soc.* **2011**, *133*, 8416–8419.

(26) Osedach, T. P.; Andrew, T. L.; Bulović, V. Effect of Synthetic Accessibility on the Commercial Viability of Organic Photovoltaics. *Energy Environ. Sci.* **2013**, *6*, 711–718.

(27) Rivnay, J.; Toney, M. F.; Zheng, Y.; Kauvar, I. V.; Chen, Z.; Wagner, V.; Facchetti, A.; Salleo, A. Unconventional Face-on Texture and Exceptional in-Plane Order of a High Mobility N-Type Polymer. *Adv. Mater.* **2010**, *22*, 4359–4363.

(28) Hawker, C. J.; Russell, T. P. Block Copolymer Lithography: Merging "Bottom-Up" with "Top-Down" Processes. *MRS Bull.* **2005**, *30*, 952–966.

(29) Arriola, D. J.; Carnahan, E. M.; Hustad, P. D.; Kuhlman, R. L.; Wenzel, T. T. Catalytic Production of. *Science (80-.).* **2006**, *312*, 714–719.

(30) Zhang, M.; Moore, R. B.; Long, T. E. Melt Transesterification and Characterization of Segmented Block Copolyesters Containing 2,2,4,4-Tetramethyl-1,3-Cyclobutanediol. *J. Polym. Sci. Part A Polym. Chem.* **2012**, *50*, 3710–3718.

(31) Scherf, U.; Gutacker, A.; Koenen, N. All-Conjugated Block Copolymers. *Acc. Chem. Res.* **2008**, *41*, 1086–1097.

(32) Ku, S.-Y.; Brady, M. a; Treat, N. D.; Cochran, J. E.; Robb, M. J.; Kramer, E. J.; Chabinyc, M. L.; Hawker, C. J. A Modular Strategy for Fully Conjugated Donor-Acceptor Block Copolymers. *J. Am. Chem. Soc.* **2012**, *134*, 16040–16046.

(33) Woo, C. H.; Beaujuge, P. M.; Holcombe, T. W.; Lee, O. P.; Fréchet, J. M. J. Incorporation of Furan into Low Band-Gap Polymers for Efficient Solar Cells. *J. Am. Chem. Soc.* **2010**, *132*, 15547–15549.

(34) Tierney, S.; Heeney, M.; McCulloch, I. Microwave-Assisted Synthesis of Polythiophenes via the Stille Coupling. *Synth. Met.* **2005**, *148*, 195–198.

(35) Koppe, M.; Scharber, M.; Brabec, C.; Duffy, W.; Heeney, M.; McCulloch, I. Polyterthiophenes as Donors for Polymer Solar Cells. *Adv. Funct. Mater.* **2007**, *17*, 1371–1376.

(36) Stafford, C. M.; Harrison, C.; Beers, K. L.; Karim, A.; Amis, E. J.; VanLandingham, M. R.; Kim, H.-C.; Volksen, W.; Miller, R. D.; Simonyi, E. E. A Buckling-Based Metrology for Measuring the Elastic Moduli of Polymeric Thin Films. *Nat. Mater.* **2004**, *3*, 545–550.

(37) Seitz, J. T. The Estimation of Mechanical Properties of Polymers from Molecular Structure. *J. Appl. Polym. Sci.* **1993**, *49*, 1331–1351.

(38) Vosgueritchian, M.; Lipomi, D. J.; Bao, Z. Highly Conductive and Transparent PEDOT:PSS Films with a Fluorosurfactant for Stretchable and Flexible Transparent Electrodes. *Adv. Funct. Mater.* **2012**, *22*, 421–428.

(39) Pasquier, A. Du; Miller, S.; Chhowalla, M. On the Use of Ga–In Eutectic and Halogen Light Source for Testing P3HT–PCBM Organic Solar Cells. *Sol. Energy Mater. Sol. Cells* **2006**, *90*, 1828–1839.

(40) Babel, A.; Jenekhe, S. A. Alkyl Chain Length Dependence of the Field-Effect Carrier Mobility in Regioregular poly(3-Alkylthiophene)s. *Synth. Met.* **2005**, *148*, 169–173.

(41) Verploegen, E.; Mondal, R.; Bettinger, C. J.; Sok, S.; Toney, M. F.; Bao, Z. Effects of Thermal Annealing Upon the Morphology of Polymer-Fullerene Blends. *Adv. Funct. Mater.* **2010**, *20*, 3519–3529.

(42) Müller, C.; Goffri, S.; Breiby, D. W.; Andreasen, J. W.; Chanzy, H. D.; Janssen, R. a J.; Nielsen, M. M.; Radano, C. P.; Sirringhaus, H.; Smith, P.; Stingelin-Stutzmann, N. Tough, Semiconducting Polyethylene-poly(3-Hexylthiophene) Diblock Copolymers. *Adv. Funct. Mater.* **2007**, *17*, 2674–2679.

Chapter 5

Role of molecular mixing on the stiffness of polymer:fullerene bulk heterojunction films

Adam D. Printz, Suchol Savagatrup, Daniel Rodriquez, and Darren J. Lipomi

Department of NanoEngineering, University of California, San Diego

9500 Gilman Drive, Mail Code 0448, La Jolla, CA 92093-0448

Abstract

Bulk heterojunction films, which typically comprise a polymer donor and fullerene acceptor, are considerably stiffer than films of the neat polymer alone. The increase in stiffness upon blending is dependent on the miscibility of the polymer and the fullerene, and potentially on the details of molecular mixing, in particular, intercalation of the fullerene molecules between the polymer side chains. This paper describes the effects of molecular mixing on the tensile modulus of polythiophenes in 1:1 blends with [6,6]-phenyl C_{61} butyric acid methyl ester ($PC_{61}BM$). A series of four polymers and their blends with $PC_{61}BM$ are tested using mechanical, spectroscopic, and photovoltaic device-based measurements to determine if it is possible to predict trends in the tensile modulus based on the extent of molecular mixing. The four polymers are poly-2,2′:5′,2″-(3,3″-dihexyl-terthiophene) (PT2T), which forms an amorphous, molecularly mixed composite, poly(2,5-bis(3-tetradecylthiophen-2-yl)thieno[3,2-b]thiophene) (PBTTT), which forms a well ordered blend with bimolecular crystallization, and regioregular poly(3-hexylthiophene) (P3HT) and poly(3-heptylthiophene) (P3HpT), which form a ternary blend with an amorphous mixed phase. The tensile moduli are measured by the buckling technique and correlations are found between the modulus of the polymer and the blends. Although spectroscopic and photovoltaic device-based measurements of P3HT:$PC_{61}BM$ and PT2T:$PC_{61}BM$, along with literature precedent, suggest completely different extents of molecular mixing, they were found to have similar moduli (2.75 ± 0.59 GPa and 2.61 ± 0.39 GPa, after annealing). A strong correlation between the moduli of the blended films and the moduli of the neat polymer films suggest that the stiffness of the blend is

determined to a large extent by that of the polymer, and is unexpectedly insensitive to the details of molecular mixing, at least for the materials investigated.

5.1 Introduction

The pursuit of low-cost, flexible and stretchable organic electronics requires an understanding of the ways in which state-of-the-art electronic properties can coexist with mechanical resilience. Bulk heterojunction (BHJ) photovoltaic devices, which have a photoactive layer comprising donor and acceptor phases mixed on the molecular scale or nanoscale, are the most commonly studied organic photovoltaic (OPV) devices because of their high efficiency and easy processability.[1–4] The extent of molecular mixing (or the size of the phases) in BHJs influences the molecular packing and interfacial interactions, which in turn, greatly affects exciton dissociation, recombination, and charge transport.[5,6] While the relationship between molecular mixing and electronic properties has been studied extensively, the effect of the extent of mixing on the mechanical properties and stability against fracture is not well known. Improving the mechanical resilience of active materials and interfaces will improve the yield of working devices in roll-to-roll manufacturing, and the lifetime in outdoor, portable, and wearable applications.[7–9]

The goal of our experiments was to understand the influence of molecular mixing on the stiffness—i.e., tensile modulus—of BHJ films. In particular, we measured the tensile moduli of four different blends of polymers with main-chains comprising thiophene rings and the methanofullerene [6,6]-phenyl C_{61} butyric acid methyl ester ($PC_{61}BM$) (**Figure 5.1**), whose behaviors in a blend are known in the literature to span a range from an amorphous, molecularly mixed composite (PT2T:$PC_{61}BM$),[10,11] a well ordered blend with

bimolecular crystallization (PBTTT:$PC_{61}BM$),[12,13] and two ternary blends with pure or enriched phases separated by mixed phases (P3HT:$PC_{61}BM$[14,15] and P3HpT:$PC_{61}BM$[16,17]). The ternary blends are differentiated primarily by the relationship of the glass transition temperature (T_g) of the neat polymer to ambient temperature: T_g for P3HT is close to room temperature[18,19] and is generally reported as stiff (tensile modulus ~1 GPa),[20,21] while T_g is below room temperature for P3HpT[16] and is highly elastic (tensile modulus ≤ 0.1 GPa).[16] While all polymer:fullerene blends reported so far have greater elastic moduli than do the neat polymers,[9,11,16,20–22] the factor by which the blend is stiffer than the neat polymer varies over a wide range (**Figure 5.1**). Our goal was to understand the role of molecular mixing by combining our mechanical measurements with knowledge of the well studied microstructures of these four systems. Understanding the effects of molecular mixing on the compliance of BHJs will provide the insight necessary for the selection of materials with mechanical properties appropriate to the application and to mitigate mechanical forms of degradation.

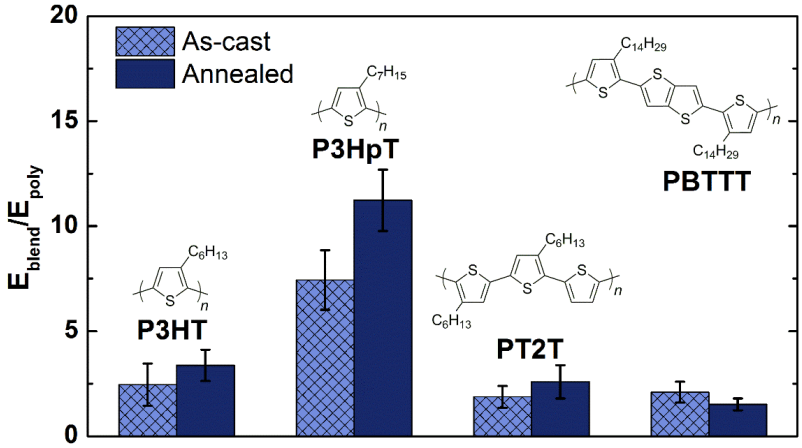

Figure 5.1. The ratios of the tensile moduli of as-cast/annealed 1:1 polymer:fullerene blends to as-cast/annealed neat polymers and the chemical structures of the conjugated polymers examined in this work: regioregular poly(3-hexylthiophene) (P3HT), regioregular poly(3-heptylthiophene) (P3HpT), poly-2,2′:5′,2″-(3,3″-dihexyl-terthiophene) (PT2T), and poly(2,5-bis(3-tetradecylthiophen-2-yl)thieno[3,2-b]thiophene) (PBTTT).

5.2 Background

The first organic solar cells (OSCs) had a planar heterojunction between a layer of pure donor and a layer of pure acceptor in direct contact.[23,24] This architecture exhibited relatively low efficiencies because of the limited interfacial area between the donor and the acceptor.[25] The discovery of the bulk heterojunction (BHJ)—an intimately mixed blend of donor and acceptor, which are frequently a conjugated polymer and a soluble fullerene derivative—led to devices exhibiting much higher efficiencies.[1–4,26,27] The advent of BHJs generated significant interest in understanding the extent of molecular mixing to elucidate the relationship between microstructure and electronic performance.[5,14,28] Of equal interest, in terms of the yield of functional devices and their stability in outdoor and portable environments, are the ways in which the morphology of the bulk heterojunction influence the mechanical properties of the composite film.[7–9,29,30] The mechanical aspects of the stability of organic electronic devices have, until recently, received relatively little attention.

The most extensively studied bulk heterojunction blend is P3HT:$PC_{61}BM$[9,14,20–22,31–37] The current model for this system comprises a ternary blend of a pure polymer phase, a pure (or enriched) fullerene phase, and an amorphous mixed phase of polymer and fullerene.[38] These ternary blends form because $PC_{61}BM$ exhibits high solubility in amorphous P3HT, and is excluded from the pure polymer phase, which is well ordered.[33,39] For efficient charge transport, pure phases of both polymer and fullerene are required so that, once separated, charges can travel to the electrodes.[14] Without these percolated networks, losses due to recombination reduce the efficiency. In P3HT:$PC_{61}BM$, the segregated polymer and fullerene phases are believed to account for most of the charge

transport in BHJ devices; the presence of the mixed phase is regarded as deleterious to the efficiency due to the disruption of contiguous pathways for charge transport to the electrodes.[14] Like P3HT, P3HpT—a polythiophene with a side-chain longer than P3HT by one methylene unit ($n = 7$)—is also believed to form ternary blends with $PC_{61}BM$.[17] P3HpT is of particular interest because it has previously been shown to simultaneously display excellent compliance and good photovoltaic characteristics.[16]

Very little is known about what, if any, specific molecular interactions are responsible for the solubility of PCBM in amorphous P3HT. On the other hand, some conjugated polymers, which exhibit lower densities of side chains than do P3HT, contain notches along the polymer chain into which fullerenes can sit.[10,13] This outcome—intercalation—either prevents crystallization or produces bimolecular crystallites; the morphology depends on the dimensions of the fullerene compared to the dimensions of the free volume between side chains. For example, the poly(terthiophene) PT2T is similar to P3HT except that every third thiophene in PT2T is without a side chain (and also that the coupling between 3-alkylthiophene rings is tail-to-tail in PT2T and head-to-tail in P3HT, **Figure 5.1**). In neat form, the side chains of PT2T interdigitate, and a highly ordered film is obtained.[10] In bulk heterojunction films, due to the notch between side chains, PT2T is hypothesized to allow intercalation of fullerene along the main chain;[10] intercalation forces the formation of a largely amorphous molecularly mixed phase. Intercalation of the $PC_{61}BM$ likely inhibits cofacial π-stacking as well as lamellar stacking, and this disruption in order produces lowered efficiencies of devices.[10,11] This hypothesis is supported by the much lower power conversion efficiency (*PCE*) demonstrated in PT2T:$PC_{61}BM$ devices when compared to those of P3HT:$PC_{61}BM$, even though the relative positions of the

frontier molecular orbitals of PT2T to $PC_{61}BM$ suggest that this system might be more efficient than P3HT:$PC_{61}BM$.[10]

Cates Miller et al. studied the intercalation of fullerenes between the alkyl solubilizing groups of PBTTT and found that the fullerene solubilizing groups were critical in determining if intercalation occurred.[13,40] Monofunctionalized fullerenes, such as $PC_{61}BM$ and $PC_{71}BM$, readily intercalated between the side chains of PBTTT, while some multifunctionalized fullerenes, such as bis-$PC_{61}BM$ and bis-$PC_{71}BM$, did not intercalate between the side chains due to steric hindrance.[13] The absence of intercalation of multifunctionalized fullerenes was not a generalizable rule, though. Because of its less bulky solubilizing groups, indene-C_{60} bisadduct (ICBA) was found to intercalate.[40] (It should be noted that photovoltaic devices made with ICBA underperformed those made with $PC_{61}BM$ because the ICBA preferentially aligned with its side groups parallel to the polymer backbone, which prevented efficient charge transport between fullerenes.)[40] In the cases where the fullerene intercalated—such as with $PC_{61}BM$ and $PC_{71}BM$—an excess of fullerene was required to make efficient devices. At a ratio of 1:1 PBTTT:fullerene, the fullerene was completely consumed by intercalation; the absence of pure fullerene domains prevented the formation of a percolated network to transport electrons to the cathode. The efficiency of PBTTT:$PC_{71}BM$ devices was optimized at a ratio of 1:4.[5,41,42] That is, an excess of fullerene was necessary to form a percolated network of pure (or enriched) phases. While a large volume fraction of fullerene improved electronic performance, it also had a deleterious effect on the mechanical properties. Dauskardt, McGehee, and coworkers studied the effect of intercalation on the cohesion of poly(3,3’’’-didocecyl quaterthiophene) (PQT-12) and PBTTT and found that high ratios of fullerenes (1:4)

produced BHJ films with decreased cohesive energy compared to 1:1 blends.[8] A lower cohesive energy was also found in 1:1 blends with fullerene that did not intercalate (bis-$PC_{71}BM$) when compared to blends with fullerene that did intercalate ($PC_{71}BM$).[8] The lower cohesion was attributed to the weak van der Waals interactions in the fullerene-enriched phases; weakened intermolecular forces facilitated decohesion of the active layer.[8]

5.3 Experimental Design

5.3.1 Selection of materials

To isolate the effects of molecular mixing on the mechanical properties of polymer:fullerene blends from the effects of different mechanical properties inherent with different fullerenes, we used a single fullerene, $PC_{61}BM$, in our experiments. $PC_{61}BM$ was selected because it is ubiquitous in literature and has previously been studied in blends with all of the polymers of this work.[11,16,40,43] We chose four different conjugated polymers for this work on the basis of the nature of the molecular mixing with fullerenes and the overall morphology of the bulk heterojunction. To summarize, P3HT and P3HpT are believed to form ternary blends comprising crystalline polymer phases, $PC_{61}BM$-enriched phases, and mixed phases. The principal difference in properties of the two polymer films is that the tensile modulus of P3HpT is about an order of magnitude lower than that of P3HT at ambient temperature.[16] PBTTT and PT2T have lower side chain densities than do the P3ATs, and thus permit intercalation of fullerenes. In the case of PBTTT, intercalation produces bimolecular crystallites.[5,42] In the case of PT2T, intercalation produces an amorphous, molecularly mixed blend.[10,11]

5.3.2 Mechanical characterization

The tensile moduli of the neat polymer and 1:1 polymer:fullerene thin films were measured using the mechanical buckling technique originally described by Stafford et al.[44] Under compressive strain on a relatively compliant substrate, a thin film forms a sinusoidal wrinkled or buckled pattern. The wavelength of the buckled pattern is then related to the tensile modulus. The distinct advantage of using the buckling technique is that it eliminates the difficulty of preparing and handling free-standing films ≤100 nm that would be required for conventional mechanical testing. The tensile modulus of the neat fullerene was difficult to measure by the buckling technique using a single layer of fullerene due to its brittleness. We instead determined the modulus using the bilayer buckling technique,[45] which utilizes a second, more compliant layer with a modulus determined independently using the conventional single-layer buckling method (PEDOT:PSS), layered with the more brittle material of unknown modulus (in this case, $PC_{61}BM$).

The deviation from the rule of mixtures (or the volume fraction average) tensile modulus was calculated utilizing the simplex method first used by Kleiner to describe polymer composites.[46] This method allowed a qualitative description of the relative strength of interactions between the polymers and the $PC_{61}BM$.

5.3.3 UV–vis spectroscopy

To describe qualitatively the relative order within the thin films, we measured the absorption spectra of the polymers and polymer:fullerene blends, and compared the vibronic peaks associated with absorption of the aggregated (e.g., ordered) phases. We have previously applied the weakly interacting H-aggregate model to P3ATs and found

that the aggregated phases of both P3HT and P3HpT have essentially identical degrees of extent and intra-aggregate order in neat polymer films.[16] Here, we did not use the H-aggregate model, but simply compared the differences in vibronic and maximum absorption peaks between thin films of neat polymer and polymer:fullerene blends before and after annealing.

5.3.4 Photovoltaic devices

We compared the photovoltaic properties of the polymers in 1:1 blends with $PC_{61}BM$ as the electron acceptor. The ratio of 1:1 was selected to isolate the effects of molecular mixing and to limit the formation of pure fullerene phases. In the case of high molecular mixing, there is expected to be limited fullerene percolation pathways and a reduction in electron transport, as manifested in a low power conversion efficiency.[40] The transparent anode was spin-coated from a solution of PEDOT:PSS with 7% DMSO and 0.1% Zonyl fluorosurfactant (now called Capstone by Dupont).[47–49] The top contact was a liquid metal cathode, eutectic gallium-indium (EGaIn), which was extruded from a syringe. We selected EGaIn because it has been shown to produce similar results as Al top contacts,[50] allowed for rapid characterization of devices, and by nature of being a liquid metal, is stretchable.[51]

5.4 Results and discussion

5.4.1 Mechanical properties of the neat polymers

The tensile moduli of the neat polymers were determined using the buckling method on thin films spin-coated from chloroform (**Figure 5.2**). The tensile moduli of films

of P3HT were found to be similar both as-cast (AC, 0.80 ± 0.12 GPa) and after annealing at 125 °C for 30 min (AN, 0.82 ± 0.05 GPa). P3HpT exhibited moduli that are about an order of magnitude lower than those of P3HT (0.082 ± 0.001 GPa as-cast and 0.130 ± 0.001 GPa after annealing at 100 °C for 30 min). We previously attributed the lower modulus of P3HpT to its side-chain length of seven carbon atoms to be the critical side-chain length for polythiophenes, that is, the critical side-chain length is the length at which T_g no longer drops monotonically with increasing side-chain length; $n = 7$ is also the shortest side-chain length for which T_g is well below room temperature.[16] Because PT2T is very similar structurally to P3HT, it is not surprising that the two materials had nearly identical tensile moduli as-cast (1.07 ± 0.23 GPa) and after annealing at the same conditions (1.01 ± 0.27 GPa). The higher stiffness of PBTTT (2.90 ± 0.30 GPa) has been attributed to interdigitation of the side chains in the crystalline phase, and the fused thienothiophene moieties between the separated bithiophene units along the backbone.

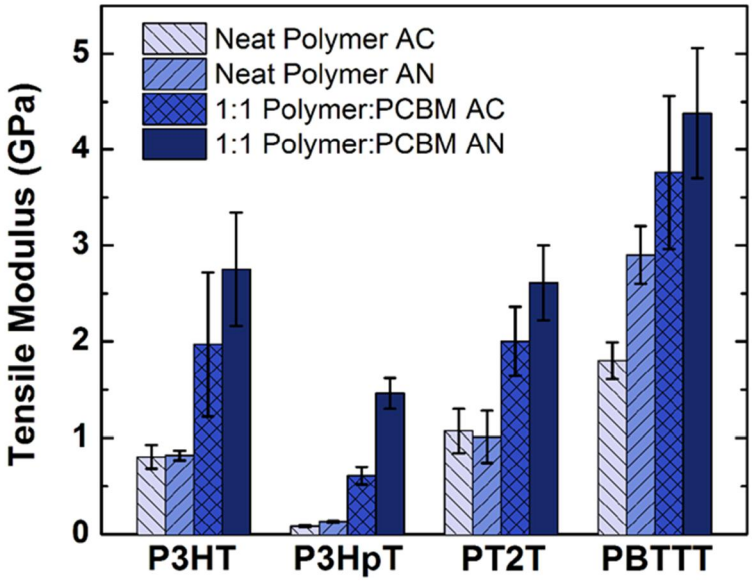

Figure 5.2. Summary of the tensile moduli of both as-cast (AC) and annealed (AN) films. All were cast from $CHCl_3$. P3HpT was annealed at 100 °C, P3HT and PT2T were annealed at 125 °C, and PBTTT was annealed at 180 °C.

5.4.2 Mechanical properties of the polymer:fullerene blends

Organic photovoltaic devices (OPVs) are frequently fabricated with active layers comprising a conjugated polymer acting as an electron donor and a fullerene acting as the electron acceptor. Devices reported in literature often have polymer:fullerene blends with concentrations between 1:1 to 1:4. Because we were motivated to determine the effects of molecular mixing on compliance, we decided to measure the tensile moduli of 1:1 polymer:fullerene blends (**Figure 5.2a**). The ratio of 1:1 limits the formation of pure fullerene phases, which we were concerned would dominate the mechanical properties of the blend. P3HpT:$PC_{61}BM$ (0.61 ± 0.09 GPa AC, 1.46 ± 0.16 GPa AN) had the lowest moduli of all of the blends. The fullerene blends with P3HT (1.97 ± 0.75 GPa AC, 2.75 ± 0.59 GPa AN) and PT2T (2.00 ± 0.36 GPa AC, 2.61 ± 0.39 GPa AN) exhibited similar tensile moduli. This similarity is somewhat surprising considering the extent of molecular mixing is expected to be different for P3HT, which does not allow fullerene intercalation, and PT2T, which does allow fullerene intercalation, and is in effect "all mixed." PBTTT, which also allows fullerene intercalation, was found to have the highest tensile modulus both as-cast (3.76 ± 0.80 GPa) and after annealing (4.38 ± 0.68 GPa). This stiffness can be attributed to the intercalation of the fullerenes and the subsequent reduction in free volume.

To compare how much stiffer films become upon addition of fullerene, we calculated the ratio of the tensile modulus of the polymer:fullerene blend to that of the neat polymer, E_{blend}/E_{poly} (**Figure 5.1**). The factor by which the modulus of the P3HpT:$PC_{61}BM$ blend was greater than that of the neat polymer was the highest of all four systems tested (7.44 ± 1.4 as-cast, 11.2 ± 1.5 after annealing). We attribute this high value to the anti-plasticizing effect of $PC_{61}BM$ on the amorphous domains of P3HpT. Since P3HT (2.45 ±

1.01 as-cast, 3.37 ± 0.75 after annealing), PT2T (1.87 ± 0.52 as-cast, 2.58 ± 0.79 after annealing), and PBTTT (2.09 ± 0.50 as-cast, 1.51 ± 0.28 after annealing), are already in the glassy state at room temperature, the effect on the mechanical properties of the amorphous domains may have been masked.

Kleiner et al. showed that for a blend of two compatible glassy materials, the modulus can be described by a simplex equation in terms of the tensile moduli and volume fractions of the materials as well as an interaction energy between the materials.[46] The simplex equation describes the deviation of the blend modulus from the expected value based on the rule of mixtures, which is simply the average of the properties of the materials within the composite, weighted by volume fraction.[9] While P3HT, PT2T, and PBTTT are all glassy at room temperature, P3HpT is not.[16] However, it has been shown by others that the T_g of P3ATs increases with the addition of PCBM.[16,19] This increase in the T_g suggests that the simplex model is appropriate in describing the tensile modulus of P3HpT:$PC_{61}BM$ blends.

Awartani et al. used the following simplex equation to describe the interaction energy between P3HT and $PC_{61}BM$: [9]

$$E_{12} = E_1\phi_1 + E_2\phi_2 + \beta_{12}\phi_1\phi_2 \qquad (\mathbf{1})$$

Here, E_{12} is the modulus of the blend film, E_1 and E_2 are the moduli of the neat polymer and neat fullerene films, respectively, and ϕ_1 and ϕ_2 are the volume fractions of the polymer and fullerene. The volume fractions were calculated from reported densities of 1.1 g cm^{-3} for the thiophenes[52] and 1.6 g cm^{-3} for $PC_{61}BM$.[52] The interaction term, β_{12}, describes the deviation from the rule of mixtures. A positive interaction term may be attributed to an increase in crystallinity of the components when compared to the neat films, or a change

in molecular packing resulting in a negative volume of mixing. A negative interaction term suggests opposite scenarios. The modulus of $PC_{61}BM$ was 15.18 ± 4.39 GPa as measured by the bilayer buckling method. This value is consistent with values of other small molecule semiconductors, such as pentacene, for which Tahk et al. obtained a modulus of 15 GPa by the buckling method.[20] We have also found that the moduli of $PC_{61}BM$ is highly dependent on purity (i.e., the extent to which $PC_{71}BM$ is removed from the mixture).[53] While the uncertainty in the modulus of neat $PC_{61}BM$ was high, it did not change our analysis because the sensitivity of the interaction term to the modulus of the $PC_{61}BM$ is linear for all materials discussed here. This linear sensitivity means that even if we used the modulus of the fullerene measured by others (e.g., 3.06 GPa[9] or 6.2 GPa[34]), it would affect all of the interaction terms identically; that is the values obtained for β_{12} would have the same qualitative ranking.

The tensile moduli of the polymers, fullerene, and polymer:fullerene blends, along with their moduli predicted on the basis of the rule of mixtures and the simplex equation are plotted in **Figure 5.3**. After annealing, all of the polymer:fullerene blends had a negative interaction term. The lowest interaction term was observed in P3HpT (–19.9 ± 8.3 GPa). The interaction terms for P3HT (–16.2 ± 8.7 GPa) and PT2T (–17.3 ± 8.5 GPa) are relatively similar, while the interaction term for PBTTT is slightly higher (–14.6 ± 8.9 GPa). The higher interaction term of PBTTT is attributed to the negative volume of mixing due to intercalation.

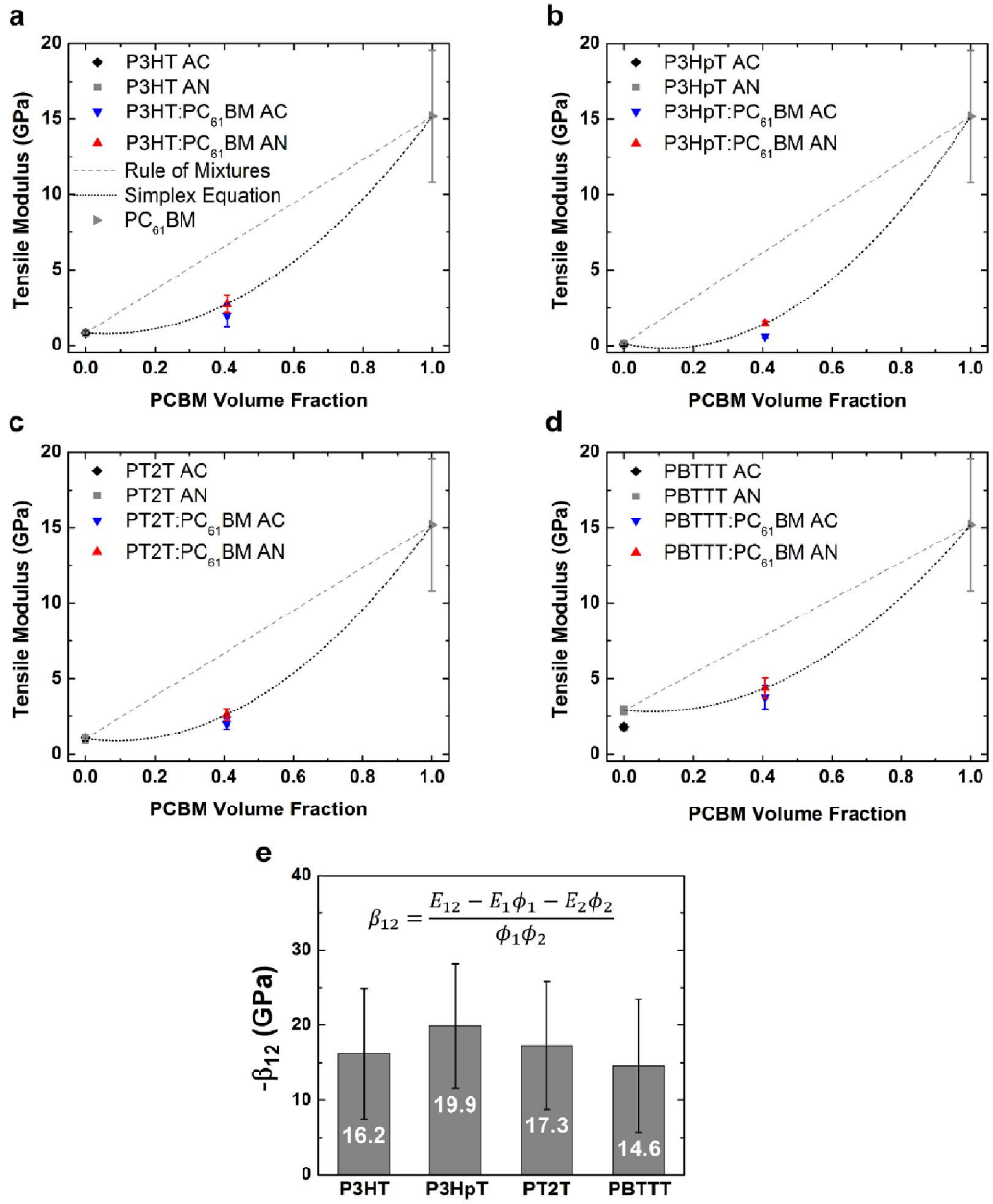

Figure 5.3. The tensile moduli of the polymer:fullerene blends studied here deviate from the rule of mixtures. The volume fractions were calculated for the films and the interaction term, β_{12}, was determined from eq 1; the moduli for the neat polymer films as well as the fullerene blends are plotted here. Additionally, the rule of mixtures and the simplex equation moduli are plotted for all volume fractions of $PC_{61}BM$ for blends with (a) P3HT, (b) P3HpT, (c) PT2T, and (d) PBTTT. The negative of the calculated values of the interaction term, as well as the equation for calculating them, are shown in (e). The large error bars in (e) are a consequence of the error obtained when measuring the modulus of $PC_{61}BM$ by the bilayer bucking method; the uncertainty is in the absolute value, as opposed to in the qualitative ranking of the magnitude of the interaction term.

5.4.3 Photovoltaic properties

The interaction term indicates a deviation from the rule of mixtures, but does not provide any insight as to the origin of the deviation. For example, blending could change the crystallization behavior of the pure phases. Bulk heterojunction OPVs need percolated networks of both donor and acceptor rich regions to separate charge and transport it to the electrodes. Intimate mixing of the polymer donor and fullerene acceptor can have deleterious effects on the creation of percolated networks for charge transport. To determine if these percolated networks were disrupted by extensive molecular mixing, photovoltaic devices were fabricated by mixing the polymers in a 1:1 ratio with $PC_{61}BM$ (**Figure 5.4**). **Table 5.1** shows the figures of merit for the devices fabricated for this work. The power conversion efficiencies (*PCE*) of the devices comprising active layers of P3HT:$PC_{61}BM$ and P3HpT:$PC_{61}BM$ were 2.04 ± 0.27% and 2.16 ± 0.17%, respectively, as previously reported.[16] The *PCE*s of PT2T:$PC_{61}BM$ (0.15 ± 0.01%) and PBTTT:$PC_{61}BM$ (0.10 ± 0.01%) devices were much lower. These low *PCE*s were attributed to a greater extent of molecular mixing than in P3HT and P3HpT; the high extent of molecular mixing prevents the formation of contiguous fullerene domains necessary for efficient charge transport to the cathode.

Table 5.1. Summary of the averaged figures of merit for the solar cells fabricated in this work ($N \geq 3$). The solar device architecture was PEDOT:PSS/Polymer/$PC_{61}BM$/EGaIn. The active layer was spin-coated from a solution of 1:1 Polymer:$PC_{61}BM$ in ODCB. All devices were annealed at temperatures as described in the text in an inert atmosphere. †Previously reported data from ref. 16.

Polymer	J_{sc} **(mA cm^{-2})**	V_{oc} **(mV)**	***FF*** **(%)**	***PCE*** **(%)**
P3HT†	6.95 ± 0.91	568 ± 9	51.7 ± 1.9	2.04 ± 0.27
P3HpT†	6.27 ± 0.48	598 ± 5	57.5 ± 1.8	2.16 ± 0.17
PT2T	0.92 ± 0.07	511 ± 28	31.7 ± 0.9	0.15 ± 0.01
PBTTT	0.60 ± 0.03	460 ± 20	35.1 ± 1.4	0.10 ± 0.01

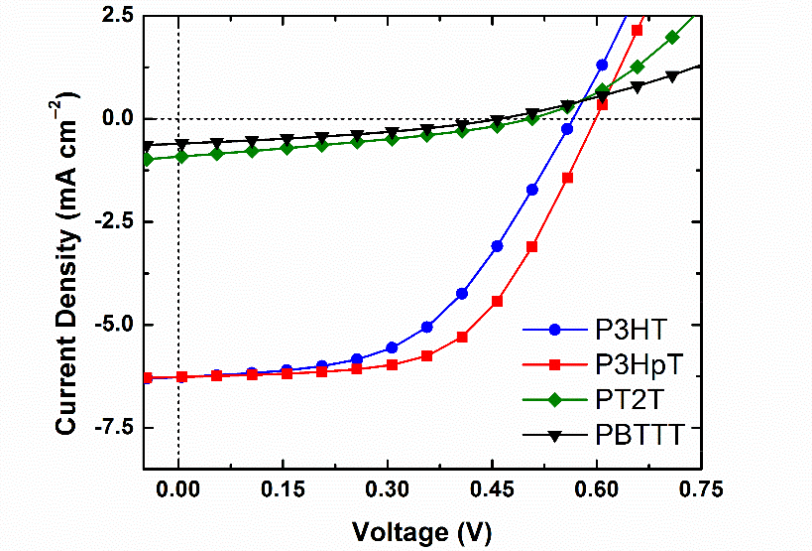

Figure 5.4. *J-V* curves of the 1:1 polymer:fullerene blends spin-cast from ODCB. P3HpT:$PC_{61}BM$[a] devices were annealed at 100 °C for 30 min, P3HT:$PC_{61}BM$[a] and PT2T:$PC_{61}BM$ devices were annealed at 125 °C for 30 min, and PBTTT:$PC_{61}BM$ devices were annealed at 180 °C for 10 min. [a] Previously reported data from ref. 16.

5.4.4 UV-vis absorption of the neat polymers and polymer:fullerene blends

The performance of OPV devices is heavily dependent on processing conditions;[9] therefore, OPV performance alone cannot describe the extent of molecular mixing in polymer:fullerene blends. To further examine the influence of the addition of $PC_{61}BM$ on the order within the polymer phases, we measured the absorption spectra of thin films of the neat polymers and polymer:fullerene blends. Aggregated phases are evident (through vibronic transition peaks) in the absorption spectra of neat P3HT and P3HpT (**Figures 5.5a and 5.5b**). When blended with the fullerene $PC_{61}BM$, these phases still exist, but the blue-shift in the maximum absorption peaks and the decrease in magnitude of the vibronic peaks at 550 and 605 nm for P3HT and P3HpT suggests that the conjugation length (which is a measure of aggregate quality) of the polymer decreases.

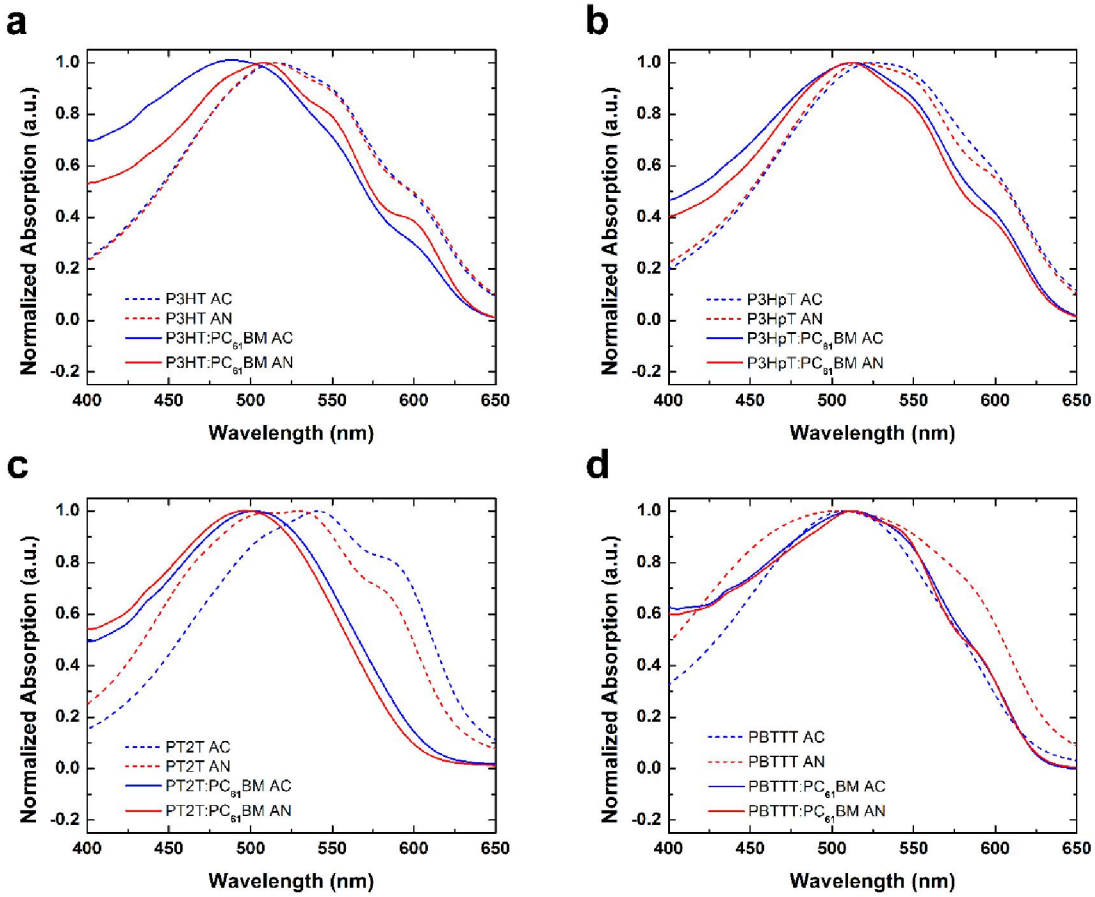

Figure 5.5. Absorption spectra of neat polymers and polymer:fullerene blends both as-cast (AC) and annealed (AN). (a) P3HT and 1:1 P3HT:$PC_{61}BM$; annealing was at 125 °C for 30 min. (b) P3HpT and 1:1 P3HpT:$PC_{61}BM$; annealing was at 100 °C for 30 min. (c) PT2T and 1:1 PT2T:$PC_{61}BM$; annealing was at 125 °C for 30 min. (d) PBTTT and 1:1 PBTTT:$PC_{61}BM$; annealing was at 180 °C for 10 min. All films were spin-coated from $CHCl_3$.

The absorption spectrum of neat PT2T (**Figure 5.5c**), like P3HT, has observable vibronic transition peaks associated with the ordered phases. With the addition of $PC_{61}BM$, these vibronic peaks disappear and the absorption spectrum becomes broad and featureless, which is indicative of an amorphous polymer. The shift from ordered to amorphous polymer with the addition of $PC_{61}BM$ is attributable to the fullerene intercalating between the side chains of PT2T and preventing crystalline lamellae from forming. Interestingly, PBTTT, which is another polymer that has been shown to allow fullerene intercalation,

exhibits a qualitative change in order, but not a complete loss thereof (as determined by the absorption spectrum) with the addition of $PC_{61}BM$ (**Figure 5.5d**). We attribute the difference in order between the two polymers that allow fullerene intercalation, PT2T and PBTTT, to the length of the side chains. The side chains of PT2T are six carbon atoms long, while those of PBTTT are fourteen carbon atoms long. When the fullerene intercalates between the side chains of PT2T, the interactions between side chains are inhibited; the inhibition of side chain interactions disrupts the formation of stacks of lamellae, and thus crystallites, in PT2T. Conversely, the longer side chains in PBTTT reach past the intercalated fullerene and the van der Waals interactions between strands of PBTTT allow stacks of lamellae to form. This interpretation is consistent with the conclusions of McGehee and coworkers upon grazing-incidence X-ray diffraction studies of intercalated and non-intercalated blends.[5,40,54]

5.4.5 Correlation between moduli of neat polymers and polymer:fullerene blends

Though the moduli of the polymer:fullerene blends deviates from the expected value based on the rule of mixtures, examination of **Figure 5.2** suggested that the moduli of the blends were correlated to the moduli of the neat polymers. Interestingly, the samples demonstrated a linear correlation ($R^2 = 0.97$ for as-cast, $R^2 = 0.95$ for annealed, **Figure 5.6**). There is a decrease in slope of the linear fit from the as-cast films (**Figure 5.6a**) to the annealed films (**Figure 5.6b**). We attribute this observation—i.e., an apparent decreased dependence of the modulus of the blend on the modulus of the neat polymer upon thermal annealing—principally to two factors: (1) the large increase in modulus of P3HpT:$PC_{61}BM$ compared to P3HpT upon thermal annealing (which reflects substantial

enrichment of the fullerene phases and increased order in the polymer phases, possibly due to the increased fluidity of P3HpT chains compared to P3HT) and (2) the fact that PBTTT:$PC_{61}BM$ films exhibit similar levels of order in both the as-cast and annealed films (as seen in **Figure 5.5d**, which suggests a strong driving force for intercalation for these materials that is operative before thermal annealing). While it is possible that the linear correlation between the moduli of the polymer:fullerene blends and the moduli of the neat polymer of the materials studied here was coincidental, it at least warrants further investigation, and at most suggests a design rule for flexible OPV devices: the stiffness of the polymer substantially determines the stiffness of the blend. This conclusion seems intuitive, but perhaps not in light of the very different microstructures of the blended films.

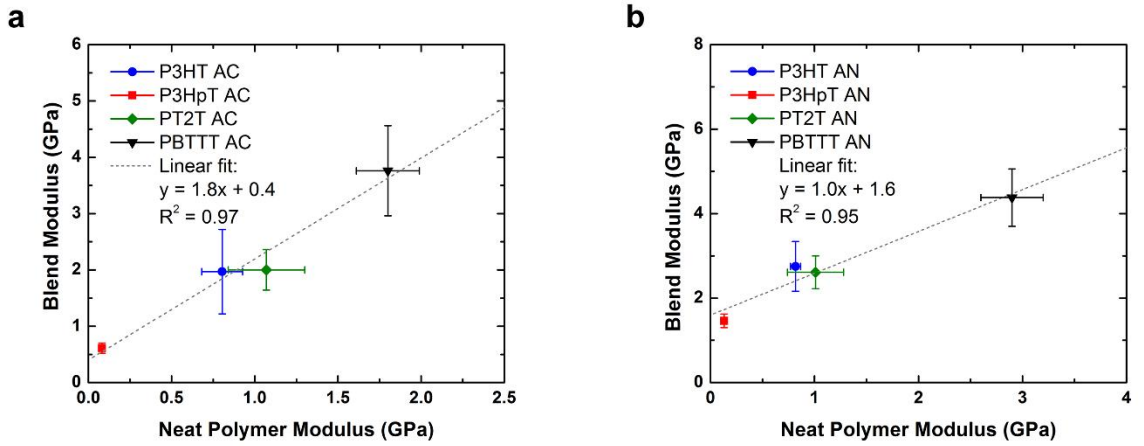

Figure 5.6. Tensile moduli of the 1:1 polymer:fullerene blends vs. moduli of the neat polymers for both (a) as-cast and (b) annealed films.

5.5 Conclusion

This paper examined the effects of the extent of molecular mixing on the tensile modulus of polymer:fullerene blends. Unexpectedly, our analysis suggests that there is no direct correlation between the extent of molecular mixing and the tensile modulus or differential tensile modulus of polymer:fullerene blends. This observation is highlighted

by the nearly identical tensile moduli of the structurally similar PT2T, which allows intercalation of $PC_{61}BM$, and P3HT, which prohibits intercalation. We also found a roughly linear correlation between the tensile moduli of the polymer:fullerene blends to those of the neat polymers studied in this work. This correlation suggests that the molecular interactions that determine the tensile modulus of neat polymer films are dominant in determining the tensile modulus of polymer:fullerene blends.

Our findings suggest that for some polymers, the details of molecular mixing, while important to the electronic properties, apparently do not have an equally large effect on the stiffness of bulk heterojunction films. Although the extent of molecular mixing is evidently not a strong predictor for mechanical compliance for the materials tested in this work, the linear correlation between the tensile moduli of the neat polymer films and the polymer:fullerene blends suggests that flexibility and mechanical resilience can be tuned at the level of the polymer; while all polymer:fullerene blends reported so far have greater moduli than do the neat polymers, low-modulus polymers produce comparatively low-modulus blends. A greater understanding of the ways in which molecular mixing and phase separation dictate the mechanical properties of photoactive blends is of critical importance for the rational design of functional devices and for their stability in outdoor and portable environments.

5.6 Experimental methods

5.6.1 Materials

Poly(3-hexylthiophene) (P3HT, M_w = 29 000 g mol^{-1}, PDI = 2.0) and [6,6]-phenyl C_{61} butyric acid methyl ester ($PC_{61}BM$) were purchased from Sigma-Aldrich and used as

received. Poly(3-heptylthiohene) (P3HpT, M_w = 30 100 g mol^{-1}, PDI = 1.49) was purchased from Rieke Metals, Inc. PBTTT was purchased from Solarmer Materials, Inc. and used as received. Poly-2,2′:5′,2″-(3,3″-dihexyl-terthiophene) (PT2T, M_w = 19 400 g mol^{-1}, PDI = 1.31) was synthesized using previously established procedures.[10,55] Poly(dimethylsiloxane) (PDMS), Sylgard 184 (Dow Corning), was prepared according to the manufacturer's instructions at a ratio of 10:1 (base:crosslinker) and cured at room temperature for 36 to 48 h before it was used for mechanical testing. (Tridecafluoro-1,1,2,2-tetrahydrooctyl)-1-trichlorosilane (FOTS) was obtained from Gelest. Chloroform ($CHCl_3$), ortho-dichlorobenzene (ODCB), acetone, and isopropyl alcohol (IPA) were obtained from Sigma-Aldrich and used as received.

5.6.2 Preparation of substrates

Glass slides used as substrates for UV-vis spectrophotometry measurements were cut into 2.5 cm × 2.5 cm squares with a diamond-tipped scribe. They were then subsequently cleaned with Alconox solution (2 mg mL^{-1}), deionized water, acetone, and then isopropyl alcohol (IPA) in an ultrasonic bath for 10 min each and then rinsed and dried with compressed air. Next, the glass was plasma treated at ~30 W for 3 min at a base pressure of 200 mtorr ambient air to remove residual organic material and activate the surface.

Glass slides used as substrates for thin films for to be transferred to PDMS for buckle testing were prepared in the same manner as above, and then subsequently placed in a vacuum desiccator with a glass vial containing ~100 µL of FOTS and put under house vacuum for a minimum of 3 h to passivate the surface.

5.6.3 Preparation of polymer solutions

Solutions of P3HT, P3HpT, PT2T, and PBTTT in $CHCl_3$ (7.5 mg ml^{-1}) and 1:1 polymer:$PC_{61}BM$ (15.0 mg ml^{-1}) were prepared for the buckling technique and UV-vis. Solutions of 1:1 P3HT:$PC_{61}BM$ and P3HpT:$PC_{61}BM$ (40 mg ml^{-1}), 1:1 PBTTT:$PC_{61}BM$ (15 mg ml^{-1}), and 1:1 PT2T:$PC_{61}BM$ (10 mg ml^{-1}) in ODCB were prepared for fabricating photovoltaic devices. All solutions were allowed to stir overnight (PBTTT and PBTTT:$PC_{61}BM$ solutions were heated to 90 °C) and filtered with a 1-μm glass microfiber (GMF) syringe filter immediately before being spin-coated onto glass substrates.

5.6.4 Characterization of materials

The tensile moduli of the materials were measured with the buckling method as described elsewhere.[21] Briefly, the elastomer PDMS was chosen as the substrate for all tests. The PDMS was prepared as described above and then cut into rectangular strips (l = 8 cm, w = 1 cm, h = 0.3 cm) before being stretched 4% using a computer-controlled linear actuator. While still under strain, FOTS treated glass slides (5 cm × 2.5 cm) were clipped onto the back of each strip using binder clips. To transfer the polymer or polymer:fullerene films to PDMS, the films were first spin-coated onto FOTS treated glass slides (2.5 cm × 2.5 cm) and then scored to facilitate transfer. The films were then placed against the PDMS, and after applying minimal pressure to achieve a conformal seal, the PDMS and glass slide with film were separated in one fast motion, leaving behind the film on the PDMS. After transfer, the PDMS substrates were relaxed; this action created a compressive strain that forced the conjugated polymer film to adopt sinusoidal buckles. The buckling wavelength, λ_b, and the thickness of the film, d_f, can be related to the tensile moduli of the film and the

substrate, E_f and E_s, and the Poisson ratios of the two materials, v_f and v_s by the following equation:

$$E_f = 3E_s\left(\frac{1-v_f^2}{1-v_s^2}\right)\left(\frac{\lambda_b}{2\pi d_f}\right)^3 \quad (\mathbf{2})$$

We measured the tensile modulus of the substrate, E_s (using a commercial pull tester), the buckling wavelength, λ_b (by optical microscopy), and the film thickness, d_f (by stylus profilometry). The slope of a plot of λ_b vs d_f for three different film thicknesses was inserted into eq 2. The Poisson's ratios were taken as 0.5 and 0.35 for PDMS and the conjugated polymers films. The experimental method is described in detail elsewhere.

Determination of the tensile modulus of $PC_{61}BM$ was difficult using the method described above because of its propensity to crack upon transfer to the PDMS substrate. To measure this modulus, we instead used a bilayer buckling method. The bilayer buckling method entails measuring the tensile modulus of a bilayer film—one compliant layer with a known modulus layered with the more brittle material of unknown modulus. The effective modulus of the bilayer film is expressed with the following equation:

$$E_{\text{eff}} = \frac{1+m^2n^4+2mn(2n^2+3n+2)}{(1+n)^3(1+mn)}E_1 \text{ where } m=\frac{E_2}{E_1},\ n=\frac{h_2}{h_1} \quad (\mathbf{3})$$

Where E_1 and E_2 are the moduli of the two films and h_1 and h_2 are the thicknesses of the two films. To calculate the modulus for $PC_{61}BM$, we mathematically solved the above equation using PEDOT:PSS as the layer with the known modulus.

5.6.5 Fabrication of solar cells

We deposited a layer of PEDOT:PSS from an aqueous solution containing 92.9 wt % Clevios PH 1000 (~0.9−1.2 wt % PEDOT:PSS), 7.0 wt% DMSO, and 0.1 wt% Zonyl fluorosurfactant as the transparent anode. The solution was filtered with a 1-μm glass microfiber syringe filter and then spin-coated at a speed of 500 rpm (250 rpm s^{-1} ramp) for 60 s, followed by 2000 rpm (750 rpm s^{-1} ramp) for 60 s. The samples were subsequently dried at 150 °C for 30 min. The photoactive layer was then spin-coated onto the electrode layer at a speed of 500 rpm (250 rpm s^{-1} ramp) for 240 s, followed by 2000 rpm (750 rpm s^{-1} ramp) for 60 s for the P3HT:PC_{61}BM and P3HpT:PC_{61}BM devices, and at a speed of 300 rpm (250 rpm s^{-1} ramp) for 240 s, followed by 2000 rpm (750 rpm s^{-1} ramp) for 60 s for all other devices. A thin strip of the PEDOT:PSS electrode was exposed by wiping away some of the photoactive layer with chloroform so that electrical contact could be made. The samples were then immediately placed in a nitrogen-filled glovebox. The P3HpT:PC_{61}BM samples were annealed at 100 °C for 30 min. The P3HT:PC_{61}BM and PT2T:PC_{61}BM samples were annealed at 125 °C for 30 min, while the PBTTT:PC_{61}BM samples were annealed at 180 °C for 10 min. All substrates were then allowed to cool slowly to room temperature. EGaIn (extruded by hand from a syringe) was used as the top contact. The photovoltaic properties were measured in a nitrogen-filled glovebox using a solar simulator with a 100 mW cm^{-2} flux that approximated the solar spectrum under AM 1.5G conditions (ABET Technologies 11016-U up-facing unit calibrated with a reference cell with a KG5 filter). The current density versus voltage was measured for both dark and under illumination using a Keithley 2400 SourceMeter.

5.6.6 UV–vis spectroscopy

The absorbance of the materials was measured using a PerkinElmer Lambda 1050 UV-vis-NIR spectrophotometer. The wavelength range measured was 850–300 nm with a step size of 1 nm. The polymer solutions were spin-coated onto the glass slides at a spin speed of 500 rpm (250 rpm s^{-1} ramp) for 240 s followed by 2000 rpm (750 rpm s^{-1} ramp) for 60 s. For each solution, two films were prepared. The first film was left as-cast and the second film was heated at 100 °C for 30 min for P3HpT, 125 °C for 30 min for P3HT and PT2T, and 180 °C for 10 min for PBTTT. After heating, all samples were allowed to cool for at least 30 min under a Pyrex petri dish covered in aluminum foil. All fullerene blends were prepared in the same manner as the neat polymer films.

Acknowledgements

This work was supported by the Air Force Office of Scientific Research (AFOSR) Young Investigator Program, Grant Number FA9550-13-1-0156. Additional support was provided by the National Science Foundation Graduate Research Fellowship under Grant No. DGE-1144086, awarded to S.S., by the Initiative for Maximizing Student Development awarded to D.R., and by laboratory startup funds from the University of California, San Diego.

Chapter 5, in full, is a reprint of the material as it appears in *Solar Energy Materials & Solar Cells*, 2015, 134, 62. Elsevier B.V., 2015. Adam D. Printz, Suchol Savagatrup, Daniel Rodriquez, and Darren J. Lipomi. The dissertation author was the primary investigator and author of this paper.

References

(1) Yu, G.; Gao, J.; Hummelen, J. C.; Wudl, F.; Heeger, A. J. Polymer Photovoltaic Cells: Enhanced Efficiencies via a Network of Internal Donor-Acceptor Heterojunctions. *Science* **1995**, *270*, 1789–1791.

(2) Dennler, G.; Scharber, M. C.; Brabec, C. J. Polymer-Fullerene Bulk-Heterojunction Solar Cells. *Adv. Mater.* **2009**, *21*, 1323–1338.

(3) Tamayo, A. B.; Dang, X.-D.; Walker, B.; Seo, J.; Kent, T.; Nguyen, T.-Q. A Low Band Gap, Solution Processable Oligothiophene with a Dialkylated Diketopyrrolopyrrole Chromophore for Use in Bulk Heterojunction Solar Cells. *Appl. Phys. Lett.* **2009**, *94*, 103301.

(4) Beaujuge, P. M.; Fréchet, J. M. J. Molecular Design and Ordering Effects in Π-Functional Materials for Transistor and Solar Cell Applications. *J. Am. Chem. Soc.* **2011**, *133*, 20009–20029.

(5) Mayer, A. C.; Toney, M. F.; Scully, S. R.; Rivnay, J.; Brabec, C. J.; Scharber, M.; Koppe, M.; Heeney, M.; McCulloch, I.; McGehee, M. D. Bimolecular Crystals of Fullerenes in Conjugated Polymers and the Implications of Molecular Mixing for Solar Cells. *Adv. Funct. Mater.* **2009**, *19*, 1173–1179.

(6) Dang, M. T.; Hirsch, L.; Wantz, G.; Wuest, J. D. Controlling the Morphology and Performance of Bulk Heterojunctions in Solar Cells . Lessons Learned from the Benchmark System. *Chem. Rev.* **2013**, *113*, 3734–3765.

(7) Lipomi, D. J.; Bao, Z. Stretchable, Elastic Materials and Devices for Solar Energy Conversion. *Energy Environ. Sci.* **2011**, *4*, 3314–3328.

(8) Bruner, C.; Miller, N. C.; McGehee, M. D.; Dauskardt, R. H. Molecular Intercalation and Cohesion of Organic Bulk Heterojunction Photovoltaic Devices. *Adv. Funct. Mater.* **2013**, *23*, 2863–2871.

(9) Awartani, O.; Lemanski, B. I.; Ro, H. W.; Richter, L. J.; DeLongchamp, D. M.; O'Connor, B. T. Correlating Stiffness, Ductility, and Morphology of Polymer:Fullerene Films for Solar Cell Applications. *Adv. Energy Mater.* **2013**, *3*, 399–406.

(10) Koppe, M.; Scharber, M.; Brabec, C.; Duffy, W.; Heeney, M.; McCulloch, I. Polyterthiophenes as Donors for Polymer Solar Cells. *Adv. Funct. Mater.* **2007**, *17*, 1371–1376.

(11) Printz, A. D.; Savagatrup, S.; Burke, D. J.; Purdy, T. N.; Lipomi, D. J. Increased Elasticity of a Low-Bandgap Conjugated Copolymer by Random Segmentation for Mechanically Robust Solar Cells. *RSC Adv.* **2014**, *4*, 13635–13643.

(12) Mcculloch, I.; Heeney, M.; Bailey, C.; Genevicius, K.; Macdonald, I.; Shkunov, M.; Sparrowe, D.; Tierney, S.; Wagner, R.; Zhang, W.; Chabinyc, M. L.; Kline, R. J.; McGehee, M. D.; Toney, M. F. Liquid-Crystalline Semiconducting Polymers with High Charge-Carriermobility. *Nat. Mater.* **2006**, *5*, 328–333.

(13) Miller, N. C.; Cho, E.; Gysel, R.; Risko, C.; Coropceanu, V.; Miller, C. E.; Sweetnam, S.; Sellinger, A.; Heeney, M.; McCulloch, I.; Brédas, J.; Toney, M. F.; McGehee, M. D. Factors Governing Intercalation of Fullerenes and Other Small Molecules Between the Side Chains of Semiconducting Polymers Used in Solar Cells. *Adv. Energy Mater.* **2012**, *2*, 1208–1217.

(14) Noriega, R.; Rivnay, J.; Vandewal, K.; Koch, F. P. V; Stingelin, N.; Smith, P.; Toney, M. F.; Salleo, A. A General Relationship between Disorder, Aggregation and Charge Transport in Conjugated Polymers. *Nat. Mater.* **2013**, *12*, 1038–1044.

(15) Brady, M. A.; Su, G. M.; Chabinyc, M. L. Recent Progress in the Morphology of Bulk Heterojunction Photovoltaics. *Soft Matter* **2011**, *7*, 11065–11077.

(16) Savagatrup, S.; Printz, A. D.; Rodriquez, D.; Lipomi, D. J. Best of Both Worlds: Conjugated Polymers Exhibiting Good Photovoltaic Behavior and High Tensile Elasticity. *Macromolecules* **2014**, *47*, 1981–1992.

(17) Salammal, S.; Mikayelyan, E.; Grigorian, S.; Pietsch, U.; Koenen, N.; Scherf, U.; Brinkmann, M.; Kayunkid, N. Impact of Thermal Annealing on the Semicrystalline Nanomorphology of Spin-Coated Thin Films of Regioregular Poly (3-Alkylthiophene) S as Observed by High-Resolution Transmission Electron Microscopy and Grazing Incidence X-Ray Diffraction. *Macromolecules* **2012**, *45*, 5575–5585.

(18) Kim, J. Y.; Frisbie, C. D. Correlation of Phase Behavior and Charge Transport in Conjugated Polymer/Fullerene Blends. *J. Phys. Chem. C* **2008**, *112*, 17726–17736.

(19) Zhao, J.; Swinnen, A.; Van Assche, G.; Manca, J.; Vanderzande, D.; Van Mele, B. Phase Diagram of P3HT/PCBM Blends and Its Implication for the Stability of Morphology. *J. Phys. Chem. B* **2009**, *113*, 1587–1591.

(20) Tahk, D.; Lee, H. H.; Khang, D.-Y. Elastic Moduli of Organic Electronic Materials by the Buckling Method. *Macromolecules* **2009**, *42*, 7079–7083.

(21) Savagatrup, S.; Makaram, A. S.; Burke, D. J.; Lipomi, D. J. Mechanical Properties of Conjugated Polymers and Polymer-Fullerene Composites as a Function of Molecular Structure. *Adv. Funct. Mater.* **2014**, *24*, 1169–1181.

(22) Savagatrup, S.; Printz, A. D.; O'Connor, T. F.; Zaretski, A. V.; Lipomi, D. J. Molecularly Stretchable Electronics. *Chem. Mater.* **2014**, *26*, 3028–3041.

(23) Tang, C. W. Two-Layer Organic Photovoltaic Cell. *Appl. Phys. Lett.* **1986**, *48*, 183–185.

(24) Sariciftci, N. S.; Braun, D.; Zhang, C.; Srdanov, V. I.; Heeger, A. J.; Stucky, G.; Wudl, F. Semiconducting Polymer-Buckminsterfullerene Heterojunctions: Diodes, Photodiodes, and Photovoltaic Cells. *Appl. Phys. Lett.* **1993**, *62*, 585–587.

(25) Gu, S.; Neugebauer, H.; Sariciftci, N. S.; Günes, S. Conjugated Polymer-Based Organic Solar Cells. *Chem. Rev.* **2007**, *107*, 1324–1338.

(26) Zhao, G.; He, Y.; Li, Y. 6.5% Efficiency of Polymer Solar Cells Based on poly(3-Hexylthiophene) and Indene-C(60) Bisadduct by Device Optimization. *Adv. Mater.* **2010**, *22*, 4355–4358.

(27) Walker, B.; Kim, C.; Nguyen, T.-Q. Small Molecule Solution-Processed Bulk Heterojunction Solar Cells †. *Chem. Mater.* **2011**, *23*, 470–482.

(28) Treat, N. D.; Chabinyc, M. L. Phase Separation in Bulk Heterojunctions of Semiconducting Polymers and Fullerenes for Photovoltaics. *Annu. Rev. Phys. Chem.* **2014**, *65*, 59–81.

(29) Hösel, M.; Søndergaard, R. R.; Jørgensen, M.; Krebs, F. C. Failure Modes and Fast Repair Procedures in High Voltage Organic Solar Cell Installations. *Adv. Energy Mater.* **2014**, *4*, 1301625.

(30) Krebs, F. C.; Nielsen, T. D.; Fyenbo, J.; Wadstrøm, M.; Pedersen, M. S. Manufacture, Integration and Demonstration of Polymer Solar Cells in a Lamp for the "Lighting Africa" Initiative. *Energy Environ. Sci.* **2010**, *3*, 512–525.

(31) Chen, D.; Nakahara, A.; Wei, D.; Nordlund, D.; Russell, T. P. P3HT/PCBM Bulk Heterojunction Organic Photovoltaics: Correlating Efficiency and Morphology. *Nano Lett.* **2011**, *11*, 561–567.

(32) Van Bavel, S.; Sourty, E.; de With, G.; Frolic, K.; Loos, J. Relation between Photoactive Layer Thickness, 3D Morphology, and Device Performance in P3HT/PCBM Bulk-Heterojunction Solar Cells. *Macromolecules* **2009**, *42*, 7396–7403.

(33) Treat, N. D.; Brady, M. A.; Smith, G.; Toney, M. F.; Kramer, E. J.; Hawker, C. J.; Chabinyc, M. L. Interdiffusion of PCBM and P3HT Reveals Miscibility in a Photovoltaically Active Blend. *Adv. Energy Mater.* **2011**, *1*, 82–89.

(34) Khang, D.-Y.; Rogers, J. A.; Lee, H. H. Mechanical Buckling: Mechanics, Metrology, and Stretchable Electronics. *Adv. Funct. Mater.* **2009**, *19*, 1526–1536.

(35) O'Connor, B.; Chan, E. P.; Chan, C.; Conrad, B. R.; Richter, L. J.; Kline, R. J.; Heeney, M.; McCulloch, I.; Soles, C. L.; DeLongchamp, D. M. Correlations between Mechanical and Electrical Properties of Polythiophenes. *ACS Nano* **2010**, *4*, 7538–7544.

(36) O'Connor, T. F.; Zaretski, A. V.; Shiravi, B. A.; Savagatrup, S.; Printz, A. D.; Diaz, M. I.; Lipomi, D. J. Stretching and Conformal Bonding of Organic Solar Cells to Hemispherical Surfaces. *Energy Environ. Sci.* **2014**, *7*, 370–378.

(37) Lipomi, D. J.; Chong, H.; Vosgueritchian, M.; Mei, J.; Bao, Z. Toward Mechanically Robust and Intrinsically Stretchable Organic Solar Cells: Evolution of Photovoltaic Properties with Tensile Strain. *Sol. Energy Mater. Sol. Cells* **2012**, *107*, 355–365.

(38) Roehling, J. D.; Batenburg, K. J.; Swain, F. B.; Moulé, A. J.; Arslan, I. Three-Dimensional Concentration Mapping of Organic Blends. *Adv. Funct. Mater.* **2013**, *23*, 2115–2122.

(39) Treat, N. D.; Varotto, A.; Takacs, C. J.; Batara, N.; Al-Hashimi, M.; Heeney, M. J.; Heeger, A. J.; Wudl, F.; Hawker, C. J.; Chabinyc, M. L. Polymer-Fullerene Miscibility: A Metric for Screening New Materials for High-Performance Organic Solar Cells. *J. Am. Chem. Soc.* **2012**, *134*, 15869–15879.

(40) Miller, N. C.; Sweetnam, S.; Hoke, E. T.; Gysel, R.; Miller, C. E.; Bartelt, J. A.; Xie, X.; Toney, M. F.; McGehee, M. D. Molecular Packing and Solar Cell Performance in Blends of Polymers with a Bisadduct Fullerene. *Nano Lett.* **2012**, *12*, 1566–1570.

(41) Cates, N. C.; Gysel, R.; Beiley, Z.; Miller, C. E.; Toney, M. F.; Heeney, M.; McCulloch, I.; McGehee, M. D. Tuning the Properties of Polymer Bulk Heterojunction Solar Cells by Adjusting Fullerene Size to Control Intercalation. *Nano Lett.* **2009**, *9*, 4153–4157.

(42) Miller, N. C.; Gysel, R.; Miller, C. E.; Verploegen, E.; Beiley, Z.; Heeney, M.; McCulloch, I.; Bao, Z.; Toney, M. F.; McGehee, M. D. The Phase Behavior of a Polymer-Fullerene Bulk Heterojunction System That Contains Bimolecular Crystals. *J. Polym. Sci. Part B Polym. Phys.* **2011**, *49*, 499–503.

(43) Vanlaeke, P.; Swinnen, a.; Haeldermans, I.; Vanhoyland, G.; Aernouts, T.; Cheyns, D.; Deibel, C.; D'Haen, J.; Heremans, P.; Poortmans, J.; Manca, J. V. P3HT/PCBM

Bulk Heterojunction Solar Cells: Relation between Morphology and Electro-Optical Characteristics. *Sol. Energy Mater. Sol. Cells* **2006**, *90*, 2150–2158.

(44) Stafford, C. M.; Harrison, C.; Beers, K. L.; Karim, A.; Amis, E. J.; VanLandingham, M. R.; Kim, H.-C.; Volksen, W.; Miller, R. D.; Simonyi, E. E. A Buckling-Based Metrology for Measuring the Elastic Moduli of Polymeric Thin Films. *Nat. Mater.* **2004**, *3*, 545–550.

(45) Stafford, C. M.; Guo, S.; Harrison, C.; Chiang, M. Y. M. Combinatorial and High-Throughput Measurements of the Modulus of Thin Polymer Films. *Rev. Sci. Instrum.* **2005**, *76*, 062207.

(46) Kleiner, L. W.; Karasz, F. E.; Macknight, W. J. Compatible Glassy Polyblends Based Upon Poly(2,6-Dimet Hyl-I ,4-Phenylene Oxide): **1979**, *19*, 5–10.

(47) Vosgueritchian, M.; Lipomi, D. J.; Bao, Z. Highly Conductive and Transparent PEDOT:PSS Films with a Fluorosurfactant for Stretchable and Flexible Transparent Electrodes. *Adv. Funct. Mater.* **2012**, *22*, 421–428.

(48) Chiechi, R. C.; Weiss, E. A.; Dickey, M. D.; Whitesides, G. M. Eutectic Gallium-Indium (EGaIn): A Moldable Liquid Metal for Electrical Characterization of Self-Assembled Monolayers. *Angew. Chem. Int. Ed. Engl.* **2008**, *47*, 142–144.

(49) Dickey, M. D.; Chiechi, R. C.; Larsen, R. J.; Weiss, E. A.; Weitz, D. A.; Whitesides, G. M. Eutectic Gallium-Indium (EGaIn): A Liquid Metal Alloy for the Formation of Stable Structures in Microchannels at Room Temperature. *Adv. Funct. Mater.* **2008**, *18*, 1097–1104.

(50) Pasquier, A. Du; Miller, S.; Chhowalla, M. On the Use of Ga–In Eutectic and Halogen Light Source for Testing P3HT–PCBM Organic Solar Cells. *Sol. Energy Mater. Sol. Cells* **2006**, *90*, 1828–1839.

(51) Palleau, E.; Reece, S.; Desai, S. C.; Smith, M. E.; Dickey, M. D. Self-Healing Stretchable Wires for Reconfigurable Circuit Wiring and 3D Microfluidics. *Adv. Mater.* **2013**, *25*, 1589–1592.

(52) Ro, H. W.; Akgun, B.; O'Connor, B. T.; Hammond, M.; Kline, R. J.; Snyder, C. R.; Satija, S. K.; Ayzner, A. L.; Toney, M. F.; Soles, C. L.; DeLongchamp, D. M. Poly(3-Hexylthiophene) and [6,6]-Phenyl-C61-Butyric Acid Methyl Ester Mixing in Organic Solar Cells. *Macromolecules* **2012**, *45*, 6587–6599.

(53) Savagatrup, S.; Rodriquez, D.; Printz, A. D.; Sieval, A. B.; Hummelen, J. C.; Lipomi, D. J. [70]PCBM and Incompletely Separated Grades of Methanofullerenes Produce Bulk Heterojunctions with Increased Robustness for Ultra-Flexible and Stretchable Electronics. *Chem. Mater.* **2015**, *27*, 3902–3911.

(54) Miller, N. C.; Cho, E.; Junk, M. J. N.; Gysel, R.; Risko, C.; Kim, D.; Sweetnam, S.; Miller, C. E.; Richter, L. J.; Kline, R. J.; Heeny, M.; McCulloch, I.; Amassian, A.; Acevedo-Feliz, D.; Knox, C.; Hansen, M. R.; Dudenko, D.; Chmelka, B. F.; Toney, M. F.; Brédas, J.; McGehee, M. D. Use of X-Ray Diffraction, Molecular Simulations, and Spectroscopy to Determine the Molecular Packing in a Polymer-Fullerene Bimolecular Crystal. *Adv. Mater.* **2012**, *24*, 6071–6079.

(55) Tierney, S.; Heeney, M.; McCulloch, I. Microwave-Assisted Synthesis of Polythiophenes via the Stille Coupling. *Synth. Met.* **2005**, *148*, 195–198.

Chapter 6

Yield point of semiconducting polymer films on stretchable substrates determined by onset of buckling

Adam D. Printz, Aliaksandr V. Zaretski, Suchol Savagatrup, Andrew S.-C. Chiang, and Darren J. Lipomi

Department of NanoEngineering, University of California, San Diego, 9500 Gilman Drive, Mail Code 0448, La Jolla, Ca, 92093-0448

Abstract

Mechanical buckling of thin films on elastomeric substrates is often used to determine the mechanical properties of polymers whose scarcity precludes obtaining a stress-strain curve. While the modulus and crack-onset strain can readily be obtained by such film-on-elastomer systems, information critical to the development of flexible, stretchable, and mechanically robust electronics—i.e., the range of strains over which the material exhibits elastic behavior—cannot be measured easily. This paper describes a new technique called laser determination of yield point (LADYP), in which a polymer film on an elastic substrate is subjected to cycles of tensile strain that incrementally increase in steps of 1% (i.e., 0% $\rightarrow$ 1% $\rightarrow$ 0% $\rightarrow$ 2% $\rightarrow$ 0% $\rightarrow$ 3% $\rightarrow$ 0% etc.). The formation of buckles manifests as a diffraction pattern obtained using a laser, and represents the onset of plastic deformation, or the yield point of the polymer. In the series of conjugated polymers poly(3-alkylthiophene), where the alkyl chain is pentyl, hexyl, heptyl, octyl, and dodecyl, the yield point is found to increase with increasing length of the side chain (from approximately 5% to 15% over this range when holding the thickness between ~200 and 300 nm). A skin-depth effect is observed in which films of <150 nm thickness exhibit substantially greater yield points, up to 40% for poly(3-dodecylthiophene). Along with the tensile modulus obtained by the conventional analysis of the buckling instability, knowledge of the yield point allows one to calculate the modulus of resilience. Combined with knowledge of the crack-onset strain, one can estimate the total energy absorbed by the film (i.e., the modulus of toughness).

6.1 Introduction

Thin film organic conductors and semiconductors are promising materials for the fabrication of robust devices capable of surviving the repetitive strains applied during use in portable, outdoor, and wearable or implantable applications.[1–6] In these applications, permanent (or plastic) deformation is often undesirable, except in the cases in which one-time bonding to non-planar surfaces is required.[7,8] Ideally, the materials used would remain in the elastic regime—below the yield point—at the strains expected to be reached during normal use. For bulk materials, the yield point can be obtained using a tensile test. However, the scarcity of materials such as conjugated polymers—of which only a few hundred milligrams may be obtained in a laboratory-scale synthesis—precludes obtaining these measurements using a tensile test. To conserve material, performing mechanical testing on thin films is ideal, however, there are difficulties associated with isolating and manipulating free-standing films of sub-micron thickness. We thus developed a new method based on the onset of buckling of a film on an elastomer, which we call laser determination of yield point (LADYP). LADYP measurements are performed by cyclically straining and relaxing a polymer film on an elastomeric substrate and then recording the strain at which a diffraction pattern appears when irradiated with a laser beam. When the yield point is reached, the thin film plastically deforms, and upon relaxation, the film is compressed and surface wrinkles are formed which then diffract the light.[9,10] While other buckling-based metrology techniques have compressed unstrained thin films and used laser diffraction (or micrographs) to measure their *tensile modulus*,[9–12] LADYP is the first technique that compresses plastically deformed films and uses laser diffraction to determine their *yield point*.

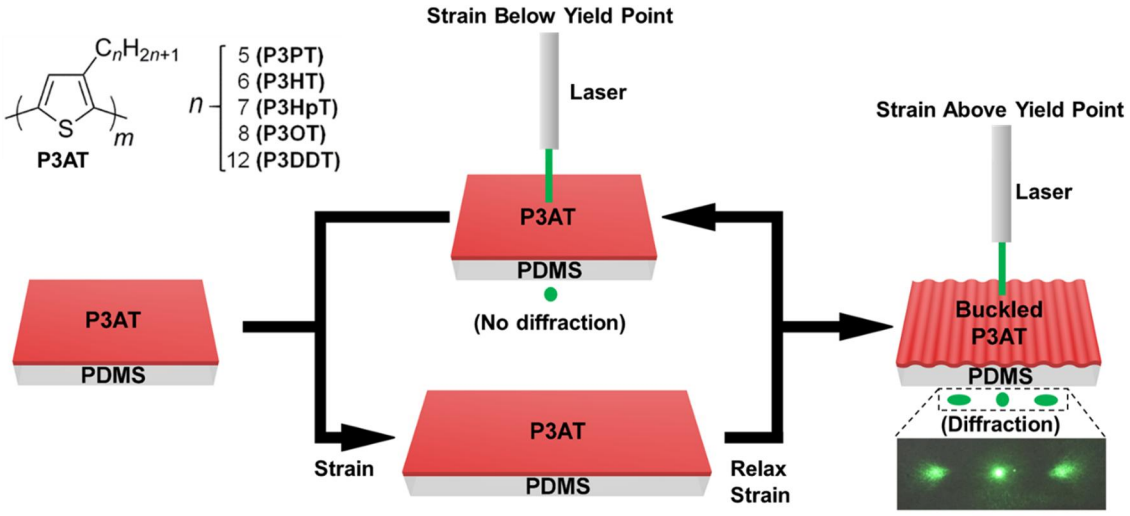

Figure 6.1. Schematic diagram of the procedure and the molecular structure of the polymers studied in this work. Each polymer thin film was transferred to PDMS and then stretched and relaxed with subsequently increasing strain with each cycle. At the point of relaxation, laser was transmitted through the film, and above the yield point, the film buckled and diffracted the laser. A photograph of the diffraction peaks is included in the inset.

We used this technique to explore the effects of the alkyl side-chain length, as well as the film thickness, on the yield point of poly(3-alkylthiophene)s (P3ATs) (**Figure 6.1**), which are excellent model polymers due to their relatively simple molecular structure comprising repeat units of thiophenes with alkyl side chains. We previously measured the tensile modulus—the inverse of mechanical compliance—and ductility of P3ATs—as manifested in their crack-onset strains—and found that these parameters are related to the alkyl side-chain length, with longer side-chains leading to more compliant and ductile films.[11,12] We expected that the yield point would follow a similar trend. In addition to the effect of alkyl side-chain length, we explored the effects of film thickness on the yield point. Others had previously shown that decreasing film thickness depresses the glass transition temperature of thin films,[13–16] and we hypothesized that this would lead to an increase in yield point in P3ATs, as has been shown for polystyrene and

poly(2-vinylpyridine) using a relatively complex method.[17,18] Our goal was thus to develop a simple procedure to measure the yield point using similar equipment—an actuator, a laser, and a microscope—to those already used routinely to measure tensile modulus and crack-onset strain.

6.2 Background

Mechanical properties are often assumed to be favorable in all organic conductors and semiconductors, and thus, the selection of materials for a given application is made on the basis of electronic performance.[7,19,20] For example, poly(3-hexylthiophene) (P3HT) is the most prevalent semiconducting polymer in the literature because of its good electronic performance,[21–27] yet it has a high tensile modulus (stiffness) and is brittle at common laboratory temperatures.[11,28] While the modulus is a critical parameter when designing a flexible or stretchable system with reduced interfacial stresses, it does not, however, predict the range over which a thin film exhibits elastic behavior. Most conjugated polymers crack in the regime of plastic deformation; it is therefore important to determine the yield point. For thin films, measurement of the yield point has not been straightforward[29,30] because of the difficulty of isolating and manipulating films with submicron thicknesses.[9,11,31–34] Kim and coworkers have developed specialized equipment to perform stress-strain measurements of films supported by liquid, but this is a potentially limited method due to the requirements that the liquid have high surface tension and low viscosity and that the thin film must be compatible with the liquid.[35,36]

Given the difficulty of manipulating free-standing films, mechanical properties are often determined indirectly using film-on-elastomer (FOE) systems. The most well

known method is the buckling-based metrology originally developed by Stafford and coworkers,[9,11,37] which exploits the buckling instability (surface wrinkling) that occurs when a relatively rigid film is compressed on a relatively soft elastomeric substrate (such as PDMS which, because of its high elasticity when not treated with oxygen plasma or UV-Ozone, will not contribute buckles of its own under small compressive strains). The buckling wavelength is related to the balance between the energy required to bend the rigid substrate and that required to deform the soft substrate and can be used to calculate the tensile modulus of the thin film.[10] The strain to fracture is generally measured indirectly by recording the strain at which the first crack appears in a film on a stretchable substrate.[38,39] However, the crack-onset strain is indirectly connected to ductility because it is also a function of adhesion of the film to the substrate: films that are well adhered to their substrates have high crack-onset strains.[11,40] To date, only the tensile modulus and crack-onset strain can be extracted easily from FOE systems, while previous methods for measuring the yield point are substantially more complex and limited to certain types of polymers.[17,18] Other properties relevant to mechanical reliability in flexible devices, such as adhesion and cohesive fracture energy, can also be obtained from thin films in other configurations.[29,30]

Figure 6.2 illustrates the information easily obtainable from FOE systems superimposed on a hypothetical stress-strain curve obtained from a conventional pull tester. While the tensile modulus obtained from the buckling-based metrology defines the initial slope of the curve, and the crack-onset strain defines its endpoint, the width of the elastic regime is not defined, and thus the range over which the polymer could be deformed without plastic deformation is not known. Moreover, without defining the

upper limit of strain at the yield point, the energies absorbed by the polymer in the elastic regime (i.e., the resilience) and the total energy absorbed at the point of fracture (i.e., the toughness) cannot be known. Knowledge of the yield point "calibrates" the curve: it permits calculation of the resilience and a rough estimate of the toughness. Beyond knowledge of the resilience and toughness, it is technologically relevant to define the amount of strain a thin film can undergo before plastically deforming. The required accommodation of strain can vary greatly depending on the intended use of a device, and understanding the material limits (e.g., elasticity) is necessary in the selection of appropriate materials for specific applications. For example, a device worn to measure a pulse will undergo much less strain (<1%) than a device worn on an elbow when it bends (>50%).[41] While a material that might have higher electronic performance, but a low yield point would be appropriate for the former application, a sacrifice of electronic performance might be required to ensure that the device can maintain predictable performance at high strains in the latter application.

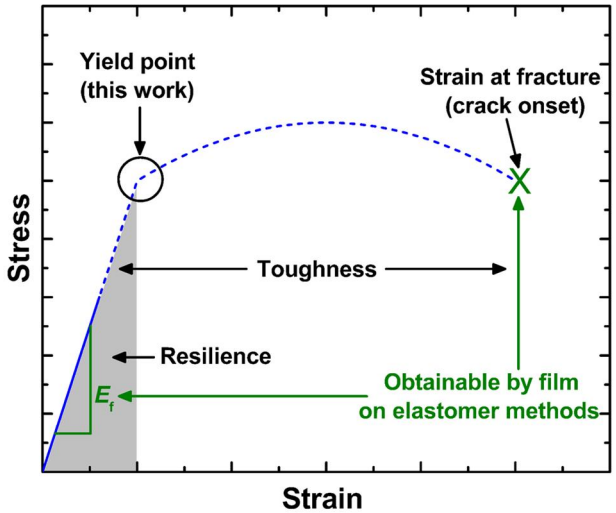

Figure 6.2. A hypothetical stress-strain curve for a bulk polymer. The elements in green—the tensile modulus and the strain at fracture—have been previously measured by film-on-elastomer systems. Measurement of the yield point is reported in this work. The area between the yield point and the strain at fracture is the plastic regime, which is still not measurable for thin films on elastomeric substrates.

6.3 Experimental methods

6.3.1 Materials

Poly(3-pentylthiophene) (P3PT, M_n = 13 kDa, PDI = 2.5), poly(3-heptylthiophene) (P3HpT, M_n = 35 kDa, PDI = 1.5), and poly(3-dodecylthiophene) (P3DDT, M_n = 21 kDa, PDI = 1.8) were purchased from Rieke Metals, Inc. and used as received. Poly(3-hexylthiophene) (P3HT, M_n = 44 kDa, PDI = 2.0) and poly(3-octylthiophene) (P3OT, M_n = 34 kDa, PDI = 2.5) were purchased from Sigma-Aldrich and used as received. (While the authors note this is a large range of M_n, a previous study by us showed that the difference in tensile modulus between P3HT with M_n = 6.25 kDa, PDI = 1.2 and M_n = 14.5 kDa, PDI = 2.0 was negligible.)[42] PDMS, Sylgard 184 (Dow Corning), was prepared according to the manufacturer's instructions at a ratio of 10:1 (base:crosslinker) and cured at 75 °C for 25 min before it was used for mechanical testing. (Tridecafluoro-1,1,2,2-tetrahydrooctyl)-1-trichlorosilane (FOTS) was obtained from Gelest. Chloroform, acetone, and isopropyl alcohol (IPA) were obtained from Sigma-Aldrich and used as received.

6.3.2 Preparation of substrates

Glass slides were cut into squares (2.5 cm × 2.5 cm) with a diamond-tipped scribe. They were then subsequently cleaned with Alconox solution (2 mg mL^{-1}), deionized water, acetone, and then isopropyl alcohol (IPA) in an ultrasonic bath for 10 min each and then rinsed and dried with compressed air. Next, the glass was plasma treated at ~30 W for 3 min at a base pressure of 200 mtorr ambient air to remove residual organic material and activate the surface. The slides were then placed in a vacuum

desiccator with a glass vial containing ~100 μL of FOTS and put under house vacuum for a minimum of 3 h to passivate the surface. The surface was then rinsed thoroughly with IPA to remove any excess FOTS and leave only a monolayer behind. The contact angle of water with the resulting surface was 109°.

6.3.3 Preparation of films

To compare the yield points of P3ATs based on alkyl side-chain length, solutions of P3PT, P3HT, P3HpT, P3OT, and P3DDT in chloroform (15 mg mL^{-1}) were prepared and allowed to stir overnight. The solutions of P3PT were heated to 50 °C for 10 min to promote dissolution before use. All solutions were then filtered with 1 μm glass microfiber (GMF) filter immediately before being spin-coated onto FOTS passivated glass using a Headway Research PWM32. We chose to spin-coat the films onto FOTS glass and transfer to PDMS. Spinning directly onto PDMS would require treatment with either oxygen plasma or UV-Ozone which would embrittle the substrate. The solutions were spun at 500 rpm (250 rpm s^{-1} ramp) for 120 s, followed by 2000 rpm (1000 rpm s^{-1} ramp) for 30 seconds, which produced films 200-300 nm thick.

To examine the effect of film thickness on the yield point, solutions with various concentrations of P3DDT in chloroform (7.5–15.0 mg mL^{-1}) were made and allowed to stir overnight. These solutions were filtered and spin-coated as specified above, resulting in film thicknesses of 130-250 nm. Films of P3DDT for analysis by UV-vis were spin-coated onto the FOTS passivated glass slides at a spin speed of 500 rpm (250 rpm s^{-1} ramp) for 120 s followed by 2000 rpm (1000 rpm s^{-1} ramp) for 30 s. All films were dried under vacuum for 15 min to remove residual solvent.

6.3.4 Laser Detection of Yield Point (LADYP)

PDMS was prepared as stated above and cut into rectangular strips (l = 8 cm, w = 1 cm, h = 0.4 cm). The polymer films were then transferred to the PDMS strips. Transferring the conjugated polymer films to the pre-strained PDMS substrate was performed by initially scoring the films along the edges with a razor and placing the films against the PDMS. After applying a minimum amount of pressure to create a conformal seal between the PDMS and the conjugated polymer film, the glass/PDMS was separated from the glass/conjugated polymer film in one fast motion.[43] Micrographs were taken of the films at 0% strain to ensure clean transfer to the PDMS (e.g., no delamination, no cracking). The films were then strained using a computer-controlled stage, which applied strains to samples using a linear actuator. The samples were cyclically strained and relaxed, again increasing the strain with each cycle (i.e., 0% $\rightarrow$ 1% $\rightarrow$ 0% $\rightarrow$ 2% $\rightarrow$ 0% $\rightarrow$ 3% $\rightarrow$ 0% etc.). At each point of relaxation, the sample was irradiated with a 5 mW, 532 nm laser beam; the laser beam was transmitted through the film onto a screen which was observed to detect diffraction. At the onset of diffraction, the strain was recorded, and micrographs were taken to look for visible buckles. After the onset of diffraction, micrographs were taken at each subsequent strain. When buckles were visible in the microscope, this strain was recorded, as was the strain where the diffraction peaks were persistent (i.e., lasted longer than 1 min).

6.3.5 UV-vis spectroscopy and analysis

The absorbance of the materials was measured using an Agilent 8453 UV-vis spectrophotometer. The wavelength range measured was 850–300 nm with a step size of

1 nm. The films were transferred to PDMS as stated above. Absorption spectra of the films on PDMS were initially taken at 0% strain. The films were then strained to 10, 15, and 20% and clipped onto FOTS passivated glass at each strain before their absorption was measured.

The extent of order, as determined by UV-vis spectroscopy, has been correlated to increased tensile moduli in P3AT films. Spano et al. and others have shown that aggregates of P3HT in solid films can be considered as weakly interacting H aggregates, due to cofacial π-π stacking and weak excitonic coupling.[32,44–47] We used this model to compare trends in aggregation and aggregate order from the UV-vis absorption spectra of the polymer thin films, in an attempt to correlate these values with the yield point.

In the aggregated state (i.e., crystallites and other aggregates in solid films), coupled electron-vibrational (vibronic) transitions determine the absorption of weakly interacting H aggregates and can be modeled as Gaussian fits by:

$$A(E) \propto \sum_{m=0} \left(\frac{S^m}{m!}\right) \times \left(1 - \frac{We^{-S}}{2E_p} \sum_{n \neq m} \frac{S^n}{n!\,(n-m)}\right)^2 \times exp\left(\frac{-\left(E - E_{00} - mE_p - \frac{1}{2}WS^m e^{-S}\right)^2}{2\sigma^2}\right) \quad (1)$$

In the above equation, A is the absorption by an aggregate as a function of the photon energy (E). E_{00} is the energy of the 0→0 vibronic transition, which is allowed assuming some disorder in the aggregates. S is the Huang-Rhys factor, which quantifies the nuclear potential well shift upon vibronic transition from the ground state to the excited state. It is calculated from absorption and emission spectra, and is set to 1 for P3ATs.[45] E_p is the intermolecular vibration energy, which (in the case where S = 1) is the difference in energy between the vibrational levels in the excited state. It is set to 0.179 eV as determined by Raman spectroscopy. W is the free exciton bandwidth, which is related to

the nearest neighbor interchain excitonic coupling. Upon coupling, a dispersion of the energies occurs, the width of which is equal to W (which is four times the nearest neighbor coupling). W is also inversely related to conjugation length; a lower W indicates better ordering of the aggregates. The terms m and n are the ground- and excited state vibrational levels and σ is the Gaussian linewidth.

The parameters E_{00}, W, σ, and a scaling factor were found by using Matlab to perform a least squares fit to the experimental absorption data in the region of 1.93 to 2.25 eV. This region was selected because the absorption is dominated by the polymer aggregates. Above 2.30 eV, the amorphous polymer dominates absorption.[48]

6.4 Results and discussion

We began by exploring the effect of side-chain length on the yield point of P3ATs (**Figure 6.3**). P3PT (n = 5), P3HT (n = 6), P3HpT (n = 7), P3OT (n = 8), and P3DDT (n = 12) were selected because they cover a wide range of side-chain lengths. P3AT films of similar thicknesses (~200–300 nm) were prepared to isolate the effect of the side-chain length. To confirm that the diffraction was correlated with the appearance of buckles in the thin films, we tracked three separate parameters: the strain at which diffraction of the laser first occurred, the strain at which diffraction lasted longer than 1 min, and the strain at which buckles were visible in the optical microscope. **Table 6.1** summarizes the LADYP data of the P3ATs. A correlation between increasing strain and increasing alkyl side-chain length was observed for all three parameters. This trend agrees with previously reported results of a dependence on the side-chain length of other mechanical properties (i.e., compliance and ductility) in P3ATs.[11,12] We also found that the initial diffraction

peaks lasted less than 1 min and occurred at lower strains than the visibility of buckles in the microscope. This observation suggested the onset of diffraction was not attributable to the yield point, but instead to the viscoelasticity of the PDMS.[43] There was a very strong agreement between the strains at which buckles were visible by microscope and the strains at which the LADYP diffraction peaks lasted longer than 1 min. When the diffraction lasted longer than 1 min, the buckles were in a more permanent state, meaning the film has been plastically deformed and the yield point had been passed. The increase in yield point for the P3ATs from n = 5 (P3PT) to n = 8 (P3OT) is attributed to the decreasing glass transition temperature with alkyl side-chain length, which results in greater chain mobility.[12,49] The observation that yield point decreases from n = 8 (P3OT) to n = 12 (P3DDT)—even though the glass transition temperatures of P3OT and P3DDT are similar—is parallel to our earlier observation that crack-onset strain decreases over this same interval.[11] For P3ATs, surface energy decreases with increasing length of the alkyl chain, and reduced adhesion for polymers with longer side chains localizes strain to thin areas and defects in regions of local delamination.[11] Cracks thus form sooner in poorly adhered films than in perfectly adhered films, in which strain in the film is equal to the strain in the substrate at every point.[11,40] The same effect might produce earlier plastic deformation in P3DDT than in P3OT, though we cannot rule out the possibility that P3ATs with long side chains (n > 8) actually have a shorter elastic regime intrinsically. Micrographs of representative films just below (left column) and above (right column) the yield point are in **Figure 6.4**. In the micrographs of the films strained below the yield point, no sign of film buckling is observed. However, when the yield

point is reached, the film is deformed and upon relaxation forms buckles out-of-plane, perpendicular to the direction of strain.

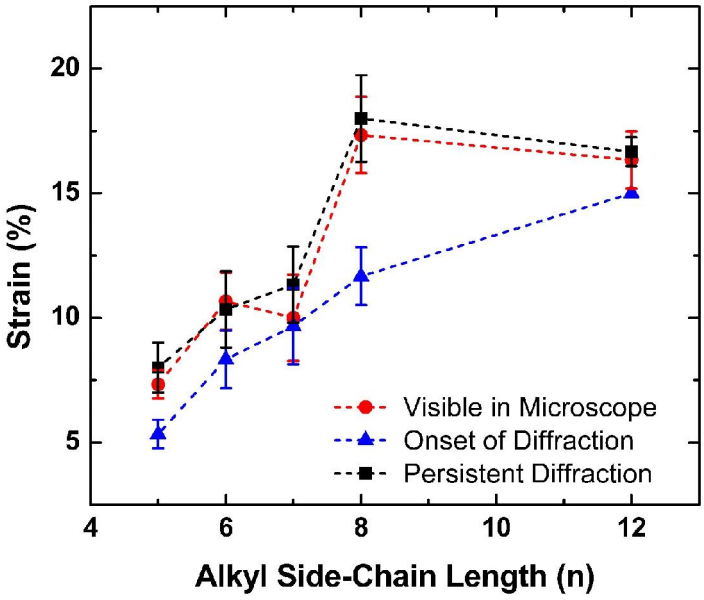

Figure 6.3. The yield point vs alkyl side-chain length for the P3ATs. All films were transferred to an elastic PDMS substrate and subsequently strained until the yield point—as determined by the appearance of buckles—was observed.

Table 6.1. Summary of the yield point vs alkyl side-chain length for the P3ATs as measured in FOE systems. The persistent diffraction agrees well with the visibility of buckles in the microscope.

Polymer	Buckles in Microscope Strain (%)	Onset of Diffraction Strain (%)	Persistent Diffraction Strain (%)
P3PT	7.3 ± 0.6	5.3 ± 0.6	8.0 ± 1.0
P3HT	10.6 ± 1.2	8.3 ± 1.2	10.3 ± 1.5
P3HpT	10.0 ± 1.7	9.7 ± 1.5	11.3 ± 1.5
P3OT	17.3 ± 1.5	11.7 ± 1.2	18.0 ± 1.7
P3DDT	16.3 ± 1.2	15.0 ± 0.0	16.7 ± 0.6

The effect of film thickness on the yield point of one of the P3ATs, P3DDT was also assessed using LADYP. The strain (in percent) is plotted against the film thickness in **Figure 6.5**. The yield point was stable above a thickness of 156 ± 10 nm to at least 251 ± 26 nm (17.7 ± 3.2% and 17.0 ± 1.0%, respectively, for the yield point determined by

laser diffraction peaks lasting longer than 1 min); however, below this thickness, there was a substantial increase in the yield point strain. At a thickness of 147 ± 6 nm, the yield point increased slightly to 19.7 ± 0.6%.

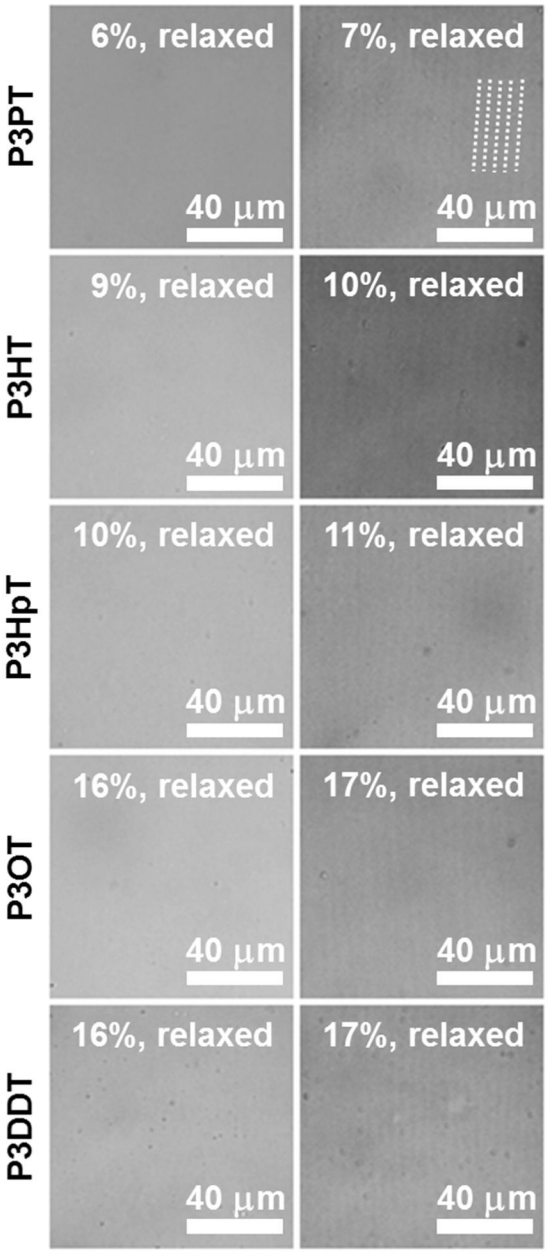

Figure 6.4. Micrographs of representative films of the P3ATs studied in this work. The micrographs in the column on the left are of films in the relaxed state which had been strained just below the yield point. The micrographs in the column on the right are of films in the relaxed state after they have been strained above the yield point. The dashed lines drawn in the P3PT micrograph in the right column are eye guides to highlight buckling of the film.

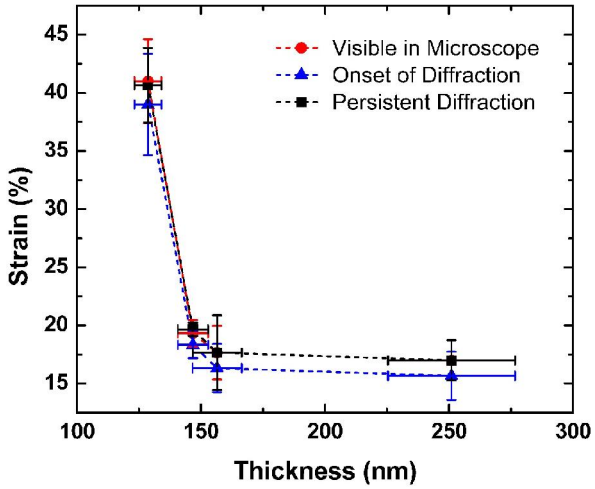

Figure 6.5. The yield point vs thickness for P3DDT. All films were prepared and evaluated as described above.

When the film thickness was further decreased to 129 ± 5 nm, a much more substantial increase in yield point was observed (40.7 ± 3.2%). The observation of a large increase in the yield point strain with decreasing thickness agrees with similar measurements of polystyrene.[17] These results suggest that in addition to alkyl side-chain length, the film thickness is a parameter that can—at least below the critical film thickness—be adjusted to tune film elasticity.[10,31,50]

To understand the evolution of the microstructure of the polymer around the yield point, we evaluated thin films of P3DDT under strain with the weakly interacting H-aggregate model developed by Spano and used by others.[12,44,45,47,51] We recorded the polarized absorption (both parallel and perpendicular to the direction of strain) of films of P3DDT unstrained, and at strains below, near, and above the yield point (10, 15, and 20%). The spectra were then evaluated with a MATLAB program which performed a least-squares fit of the weakly interacting H-aggregate model to the data. To isolate the effects of the strain and eliminate any film-to-film variations, the calculated parameters

were then normalized to the unstrained values (**Figure 6.6**). We found that the quantity of aggregates both perpendicular and parallel to the strain was essentially equal to each other up to about 10% strain. Above 10% strain, the quantity of aggregates perpendicular to the strain decreased as aggregates were pulled apart, while the quantity of aggregates parallel to the strain increased as chains were aligned and aggregated along the strained axis. Likewise, the aggregate quality—as indicated by the exciton bandwidth, *W*, the inverse of which is related to conjugation length of the polymer—both perpendicular and parallel to the strain were equivalent at 0% and 10% strain. Above 10% strain, the *W* value increased considerably perpendicular to strain. The *W* value parallel to strain decreased from 10% to 15% strain, suggesting an improvement in the ordering of the aggregates, before it increased from 15% to 20% strain. One possible explanation for this observation is that chains have begun slipping past each other to a less favorable configuration,[52] which agrees with our findings that the yield point of P3DDT is above 15% but below 20% strain.

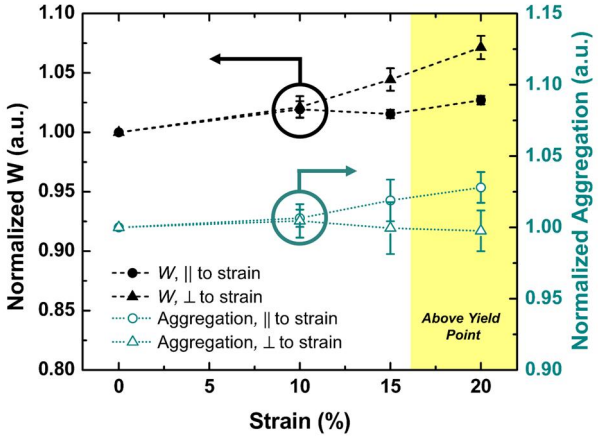

Figure 6.6. The evolution of weakly interacting H-aggregate model parameters with strain in P3DDT. The measurements were taken with polarized light both parallel and perpendicular to the direction of strain. *W* is the exciton bandwidth and is inversely related to conjugation length. The region above the yield point as determined by buckling onset is highlighted in yellow.

Finally, we utilized the yield point found by LADYP, the crack-onset determined by the same cyclic straining, and the tensile modulus previously reported by us for the P3ATs[11,12] to approximate (very roughly) their stress-strain curves (**Figure 6.7**), so that it would be possible to calculate the modulus of resilience and estimate the modulus of toughness. We made the assumption that the stress-strain curve can be approximated by the tensile modulus (i.e., a straight line) to the yield point and that above the yield point, the stress remains unchanged until crack-onset, which we consider the strain at fracture (though we point out that it is not yet possible to know the stress at fracture from FOE systems, and this uncertainty is why one can only estimate the total energy absorbed at this point—i.e., the toughness—very roughly). This highly simplified curve shape (i.e., the behavior from the yield point to the strain at fracture is approximated by a horizontal line) is nevertheless similar to the stress-strain curve previously reported for bulk P3HT.[36,53] We then used the curves to determine the moduli of resilience and to roughly estimate the modulus of toughness for the P3ATs. In the cases of P3PT and P3HT, the crack-onset strain was lower than the yield point strain, however, we attributed this to differences in the preparation of the substrates and inhomogeneities in thickness in the films (which localize strain and produce cracks).[11,12]

Because the goal of these calculations was to roughly estimate the resilience and toughness, we estimated the crack-onset to be equal to the yield point in these cases. The mechanical properties derived from a typical stress-strain curve are summarized in **Table 6.2**. We found that although the higher modulus materials (i.e., P3PT and P3HT) have a higher approximate modulus of resilience, the P3OT and P3DDT films had a much higher modulus of toughness due to their greater crack-onset strain. This approximation

suggests that—at least in the technologically relevant FOE systems—the films of P3OT and P3DDT can absorb a greater amount of energy before film failure due to cracking. The toughness of these films is important particularly in outdoor or wearable applications, where the resistance to fracture due to sudden unintended impact events (e.g., an object being accidentally dropped onto the device) is critical for continued real world device performance.

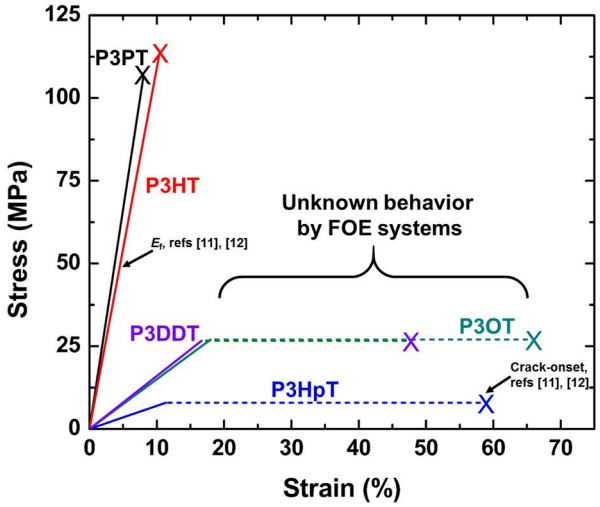

Figure 6.7. The approximated stress-strain curves for the P3ATs based on this work and that of refs. 11 and 12.

Table 6.2. Summary of the mechanical properties of the P3ATs as measured in FOE systems. Crack-onset and modulus measurements were performed with elastomer substrates cured at room temperature between 36 and 48 hours, while the yield point measurements were performed on substrates cured at 70 °C for 25 min. The error for the moduli of resilience and toughness were calculated as a propagation of error from the tensile modulus, yield point strain, and crack-onset strain measurements; the error does not include any contribution from the approximation of the curve shape.

Polymer	Tensile Modulus (GPa)	Yield Point Strain (%)	Crack-onset Strain (%)	Approximate Modulus of Resilience (MPa)	Approximate Modulus of Toughness (MPa)
P3PT	1.33 ± 0.14[12]	8.0 ± 1.0	6.3 ± 0.6	4.3 ± 0.9	4.3 ± 0.9
P3HT	1.09 ± 0.15[11]	10.3 ± 1.5	9.0 ± 1.2[11]	5.8 ± 1.5	5.8 ± 1.5
P3HpT	0.07 ± 0.01[12]	11.3 ± 1.5	58.0 ± 2.0[12]	0.4 ± 0.1	4.2 ± 0.8
P3OT	0.15 ± 0.05[11]	18.0 ± 1.7	65.0 ± 2.5[11]	2.4 ± 0.9	15.1 ± 4.6
P3DDT	0.16 ± 0.07[11]	16.7 ± 0.6	47.0 ± 3.1[11]	2.2 ± 1.0	10.3 ± 3.8

6.5 Conclusion

We described a new technique for measuring the yield point of polymer thin films supported on elastic substrates, LADYP, which provided insights on the effects of alkyl side-chain length and film thickness on this previously difficult to measure mechanical property. Experimental results indicated a correlation between alkyl side-chain length with yield point and a critical film thickness below which the yield point increases by up to a factor of three. These findings were then used to roughly estimate the modulus of resilience and modulus of toughness of FOE systems to inform the design of more robust materials and devices for portable, outdoor, and wearable applications. Further investigation of the effects of the amount of crystallinity or aggregation of the thin films, adhesion of the film to the substrate, rate-dependency of strain on the yield point, and substrate mechanical properties (e.g., tensile modulus and elastic limit) will be necessary to fully understand how devices will perform under real world stresses. Moreover, the method we described is highly practical, as the onset of buckling may not represent the yield point one would obtain in a typical tensile test. Deviations could arise from the highly anisotropic geometry of a thin film, microstructures that depend on depth, the adhesion with the substrate, and unequal chemical environments at the top and bottom surfaces of the film. Nevertheless, it is the properties of the film when integrated with a flexible or stretchable substrate—not those of a bulk sample—that will determine the extent to which a real device can be deformed.

Acknowledgements

This work was supported by the Air Force Office of Scientific Research (AFOSR) Young Investigator Program, grant number FA9550-13-1-0156. Additional support was provided by the National Science Foundation Graduate Research Fellowship, awarded to both S. Savagatrup and A.V. Zaretski, the UC LEADS fellowship and the STARS Summer Research Program, awarded to A. S.-C. Chiang, and by laboratory startup funds from the University of California, San Diego. The authors thank Prof. Frank Spano for helpful discussions.

Chapter 6, in full, is a reprint of the material as it appears in *ACS Applied Materials & Interfaces*, 2015, 7, 23257. American Chemical Society, 2015. Adam D. Printz, Aliaksandr V. Zaretski, Suchol Savagatrup, Andrew S.-C. Chiang, and Darren J. Lipomi. The dissertation author was the primary investigator and author of this paper.

References

(1) Lipomi, D. J.; Bao, Z. Stretchable, Elastic Materials and Devices for Solar Energy Conversion. *Energy Environ. Sci.* **2011**, *4*, 3314–3328.

(2) Bruner, C.; Miller, N. C.; McGehee, M. D.; Dauskardt, R. H. Molecular Intercalation and Cohesion of Organic Bulk Heterojunction Photovoltaic Devices. *Adv. Funct. Mater.* **2013**, *23*, 2863–2871.

(3) Krebs, F. C.; Nielsen, T. D.; Fyenbo, J.; Wadstrøm, M.; Pedersen, M. S. Manufacture, Integration and Demonstration of Polymer Solar Cells in a Lamp for the "Lighting Africa" Initiative. *Energy Environ. Sci.* **2010**, *3*, 512–525.

(4) O'Connor, T. F.; Rajan, K. M.; Printz, A. D.; Lipomi, D. J. Toward Organic Electronics with Properties Inspired by Biological Tissue. *J. Mater. Chem. B* **2015**, *2*, 4947–4952.

(5) Ghezzi, D.; Antognazza, M. R.; Maccarone, R.; Bellani, S.; Lanzarini, E.; Martino, N.; Mete, M.; Pertile, G.; Bisti, S.; Lanzani, G.; Benfenati, F. A Polymer

Optoelectronic Interface Restores Light Sensitivity in Blind Rat Retinas. *Nat. Photonics* **2013**, *7*, 400–406.

(6) Seyedin, M. Z.; Razal, J. M.; Innis, P. C.; Wallace, G. G. Strain-Responsive Polyurethane/PEDOT:PSS Elastomeric Composite Fibers with High Electrical Conductivity. *Adv. Funct. Mater.* **2014**, *24*, 2957–2966.

(7) Savagatrup, S.; Printz, A. D.; O'Connor, T. F.; Zaretski, A. V.; Rodriquez, D.; Sawyer, E. J.; Rajan, K. M.; Acosta, R. I.; Root, S. E.; Lipomi, D. J. Mechanical Degradation and Stability of Organic Solar Cells: Molecular and Microstructural Determinants. *Energy Environ. Sci.* **2015**, *8*, 55–80.

(8) Savagatrup, S.; Printz, A. D.; O'Connor, T. F.; Zaretski, A. V.; Lipomi, D. J. Molecularly Stretchable Electronics. *Chem. Mater.* **2014**, *26*, 3028–3041.

(9) Stafford, C. M.; Harrison, C.; Beers, K. L.; Karim, A.; Amis, E. J.; VanLandingham, M. R.; Kim, H.-C.; Volksen, W.; Miller, R. D.; Simonyi, E. E. A Buckling-Based Metrology for Measuring the Elastic Moduli of Polymeric Thin Films. *Nat. Mater.* **2004**, *3*, 545–550.

(10) Stafford, C. M.; Guo, S.; Harrison, C.; Chiang, M. Y. M. Combinatorial and High-Throughput Measurements of the Modulus of Thin Polymer Films. *Rev. Sci. Instrum.* **2005**, *76*, 062207.

(11) Savagatrup, S.; Makaram, A. S.; Burke, D. J.; Lipomi, D. J. Mechanical Properties of Conjugated Polymers and Polymer-Fullerene Composites as a Function of Molecular Structure. *Adv. Funct. Mater.* **2014**, *24*, 1169–1181.

(12) Savagatrup, S.; Printz, A. D.; Rodriquez, D.; Lipomi, D. J. Best of Both Worlds: Conjugated Polymers Exhibiting Good Photovoltaic Behavior and High Tensile Elasticity. *Macromolecules* **2014**, *47*, 1981–1992.

(13) Keddie, J. L.; Jones, R. L.; Cory, R. A. Size-Dependent Depression of the Glass Transition Temperature in Polymer Films. *Europhys. Lett.* **1994**, *27*, 59–64.

(14) Ellison, C. J.; Torkelson, J. M. The Distribution of Glass-Transition Temperatures in Nanoscopically Confined Glass Formers. *Nat. Mater.* **2003**, *2*, 695–700.

(15) Fakhraai, Z.; Forrest, J. A. Measuring the Surface Dynamics of Glassy Polymers. *Science* **2008**, *319*, 600–604.

(16) O'Connell, P. A.; McKenna, G. B. Rheological Measurements of the Thermoviscoelastic Response of Ultrathin Polymer Films. *Science* **2005**, *307*, 1760–1763.

(17) Gurmessa, B. J.; Croll, A. B. Onset of Plasticity in Thin Polystyrene Films. *Phys. Rev. Lett.* **2013**, *110*, 074301.

(18) Gurmessa, B.; Croll, A. B. Influence of Thin Film Confinement on Surface Plasticity in Polystyrene and Poly(2-Vinylpyridine) Homopolymer and Block Copolymer Films. *Macromolecules* **2015**, *48*, 5670–5676.

(19) Jørgensen, M.; Norrman, K.; Krebs, F. C. Stability/Degradation of Polymer Solar Cells. *Sol. Energy Mater. Sol. Cells* **2008**, *92*, 686–714.

(20) Jørgensen, M.; Norrman, K.; Gevorgyan, S. A.; Tromholt, T.; Andreasen, B.; Krebs, F. C. Stability of Polymer Solar Cells. *Adv. Mater.* **2012**, *24*, 580–612.

(21) Trznadel, M.; Pron, A.; Zagorska, M.; Chrzaszcz, R.; Pielichowski, J. Effect of Molecular Weight on Spectroscopic and Spectroelectrochemical Properties of Regioregular Poly(3-Hexylthiophene). *Macromolecules* **1998**, *31*, 5051–5058.

(22) Babel, A.; Jenekhe, S. A. Field-Effect Mobility of Charge Carriers in Blends of Regioregular Poly(3-Alkylthiophene)s. *J. Phys. Chem. B* **2003**, *107*, 1749–1754.

(23) Babel, A.; Jenekhe, S. A. Alkyl Chain Length Dependence of the Field-Effect Carrier Mobility in Regioregular Poly(3-Alkylthiophene)s. *Synth. Met.* **2005**, *148*, 169–173.

(24) Brinkmann, M. Structure and Morphology Control in Thin Films of Regioregular Poly(3-Hexylthiophene). *J. Polym. Sci. Part B Polym. Phys.* **2011**, *49*, 1218–1233.

(25) Ro, H. W.; Akgun, B.; O'Connor, B. T.; Hammond, M.; Kline, R. J.; Snyder, C. R.; Satija, S. K.; Ayzner, A. L.; Toney, M. F.; Soles, C. L.; DeLongchamp, D. M. Poly(3-Hexylthiophene) and [6,6]-Phenyl -C61-Butyric Acid Methyl Ester Mixing in Organic Solar Cells. *Macromolecules* **2012**, *45*, 6587–6599.

(26) Wang, C.; Rivnay, J.; Himmelberger, S.; Vakhshouri, K.; Toney, M. F.; Gomez, E. D.; Salleo, A. Ultrathin Body Poly(3-Hexylthiophene) Transistors with Improved Short-Channel Performance. *ACS Appl. Mater. Interfaces* **2013**, *5*, 2342–2346.

(27) Gargi, D.; Kline, R. J.; DeLongchamp, D. M.; Fischer, D. A.; Toney, M. F.; O'Connor, B. T. Charge Transport in Highly Face-On Poly(3-Hexylthiophene) Films. *J. Phys. Chem. C* **2013**, *117*, 17421–17428.

(28) Printz, A. D.; Savagatrup, S.; Rodriquez, D.; Lipomi, D. J. Role of Molecular Mixing on the Stiffness of Polymer:Fullerene Bulk Heterojunction Films. *Sol. Energy Mater. Sol. Cells* **2015**, *134*, 64–72.

(29) Dauskardt, R. H.; Lane, M.; Ma, Q.; Krishna, N. Adhesion and Debonding of Multi-Layer Thin Film Structures. *Eng. Fract. Mech.* **1998**, *61*, 141–162.

(30) Dupont, S. R.; Novoa, F.; Voroshazi, E.; Dauskardt, R. H. Decohesion Kinetics of PEDOT:PSS Conducting Polymer Films. *Adv. Funct. Mater.* **2013**, *24*, 1325–1332.

(31) Lee, J.-H.; Chung, J. Y.; Stafford, C. M. Effect of Confinement on Stiffness and Fracture of Thin Amorphous Polymer Films. *ACS Macro Lett.* **2012**, *1*, 122–126.

(32) Awartani, O.; Lemanski, B. I.; Ro, H. W.; Richter, L. J.; DeLongchamp, D. M.; O'Connor, B. T. Correlating Stiffness, Ductility, and Morphology of Polymer:Fullerene Films for Solar Cell Applications. *Adv. Energy Mater.* **2013**, *3*, 399–406.

(33) Savagatrup, S.; Chan, E.; Renteria-Garcia, S. M.; Printz, A. D.; Zaretski, A. V.; O'Connor, T. F.; Rodriquez, D.; Valle, E.; Lipomi, D. J. Plasticization of PEDOT:PSS by Common Additives for Mechanically Robust Organic Solar Cells and Wearable Sensors. *Adv. Funct. Mater.* **2015**, *25*, 427–436.

(34) Printz, A. D.; Savagatrup, S.; Burke, D. J.; Purdy, T. N.; Lipomi, D. J. Increased Elasticity of a Low-Bandgap Conjugated Copolymer by Random Segmentation for Mechanically Robust Solar Cells. *RSC Adv.* **2014**, 13635–13643.

(35) Kim, H. J.; Kim, J.; Ryu, J.; Kim, Y.; Kang, H.; Lee, W. B.; Kim, T.; Kim, B. J. Architectural Engineering of Rod–Coil Compatibilizers for Producing Mechanically and Thermally Stable Polymer Solar Cells. *ACS Nano* **2014**, *8*, 10461–10470.

(36) Kim, J.-S.; Kim, J.-H.; Lee, W.; Yu, H.; Kim, H. J.; Song, I.; Shin, M.; Oh, J. H.; Jeong, U.; Kim, T.-S.; Kim, B. J. Tuning Mechanical and Optoelectrical Properties of Poly(3-Hexylthiophene) through Systematic Regioregularity Control. *Macromolecules* **2015**, *48*, 4339–4346.

(37) Torres, J. M.; Stafford, C. M.; Vogt, B. D. Impact of Molecular Mass on the Elastic Modulus of Thin Polystyrene Films. *Polymer.* **2010**, *51*, 4211–4217.

(38) O'Connor, B.; Chan, E. P.; Chan, C.; Conrad, B. R.; Richter, L. J.; Kline, R. J.; Heeney, M.; McCulloch, I.; Soles, C. L.; DeLongchamp, D. M. Correlations between Mechanical and Electrical Properties of Polythiophenes. *ACS Nano* **2010**, *4*, 7538–7544.

(39) Lipomi, D. J.; Chong, H.; Vosgueritchian, M.; Mei, J.; Bao, Z. Toward Mechanically Robust and Intrinsically Stretchable Organic Solar Cells: Evolution of Photovoltaic Properties with Tensile Strain. *Sol. Energy Mater. Sol. Cells* **2012**, *107*, 355–365.

(40) Lu, N.; Wang, X.; Suo, Z.; Vlassak, J. Metal Films on Polymer Substrates Stretched beyond 50%. *Appl. Phys. Lett.* **2007**, *91*, 221909.

(41) Jeong, Y. R.; Park, H.; Jin, S. W.; Hong, S. Y.; Lee, S.-S.; Ha, J. S. Highly Stretchable and Sensitive Strain Sensors Using Fragmentized Graphene Foam. *Adv. Funct. Mater.* **2015**, *25*, 4228–4236.

(42) O'Connor, T. F.; Zaretski, A. V.; Shiravi, B. A.; Savagatrup, S.; Printz, A. D.; Diaz, M. I.; Lipomi, D. J. Stretching and Conformal Bonding of Organic Solar Cells to Hemispherical Surfaces. Energy Environ. Sci. 2014, 7, 370–378.

(43) Meitl, M. A.; Zhu, Z.-T.; Kumar, V.; Lee, K. J.; Feng, X.; Huang, Y. Y.; Adesida, I.; Nuzzo, R. G.; Rogers, J. A.; . Transfer Printing by Kinetic Control of Adhesion to an Elastomeric Stamp. *Nat. Mater.* **2005**, *5*, 33–38.

(44) Spano, F. C. Modeling Disorder in Polymer Aggregates: The Optical Spectroscopy of Regioregular Poly(3-Hexylthiophene) Thin Films. *J. Chem. Phys.* **2005**, *122*, 234701.

(45) Clark, J.; Chang, J.-F.; Spano, F. C.; Friend, R. H.; Silva, C. Determining Exciton Bandwidth and Film Microstructure in Polythiophene Films Using Linear Absorption Spectroscopy. *Appl. Phys. Lett.* **2009**, *94*, 163306.

(46) Spano, F. C.; Clark, J.; Silva, C.; Friend, R. H. Determining Exciton Coherence from the Photoluminescence Spectral Line Shape in poly(3-Hexylthiophene) Thin Films. *J. Chem. Phys.* **2009**, *130*, 074904.

(47) Turner, S. T.; Pingel, P.; Steyrleuthner, R.; Crossland, E. J. W.; Ludwigs, S.; Neher, D. Quantitative Analysis of Bulk Heterojunction Films Using Linear Absorption Spectroscopy and Solar Cell Performance. *Adv. Funct. Mater.* **2011**, *21*, 4640–4652.

(48) Pingel, P.; Zen, A.; Abellón, R. D.; Grozema, F. C.; Siebbeles, L. D. A.; Neher, D. Temperature-Resolved Local and Macroscopic Charge Carrier Transport in Thin P3HT Layers. *Adv. Funct. Mater.* **2010**, *20*, 2286–2295.

(49) Savagatrup, S.; Printz, A. D.; Wu, H.; Rajan, K. M.; Sawyer, E. J.; Zaretski, A. V.; Bettinger, C. J.; Lipomi, D. J. Viability of Stretchable Poly(3-Heptylthiophene) (P3HpT) for Organic Solar Cells and Field-Effect Transistors. Synth. Met. 2015, 203, 208–214.

(50) Stafford, C. M.; Vogt, B. D.; Harrison, C.; Julthongpiput, D.; Huang, R. Elastic Moduli of Ultrathin Amorphous Polymer Films. *Macromolecules* **2006**, *39*, 5095–5099.

(51) Savagatrup, S.; Rodriquez, D.; Printz, A. D.; Sieval, A. B.; Hummelen, J. C.; Lipomi, D. J. [70]PCBM and Incompletely Separated Grades of Methanofullerenes Produce Bulk Heterojunctions with Increased Robustness for Ultra-Flexible and Stretchable Electronics. *Chem. Mater.* **2015**, *27*, 3902–3911.

(52) Yamagata, H.; Pochas, C. M.; Spano, F. C. Designing J-and H-Aggregates through Wave Function Overlap Engineering: Applications to poly(3-Hexylthiophene). *J. Phys. Chem. B* **2012**, *116*, 14494–14503.

(53) Koch, F. P. V.; Rivnay, J.; Foster, S.; Müller, C.; Downing, J. M.; Buchaca-domingo, E.; Westacott, P.; Yu, L.; Yuan, M.; Baklar, M.; Fei, Z.; Luscombe, C.; McLachlan, M. A.; Heeney, M.; Rumbles, G.; Silva, C.; Salleo, A.; Nelson, J.; Smith, P.; Stingelin, N. The Impact of Molecular Weight on Microstructure and Charge Transport in Semicrystalline Polymer Semiconductors–Poly(3-Hexylthiophene), a Model Study. *Prog. Polym. Sci.* **2013**, *38*, 1978–1989.

Chapter 7

Fatigue in organic semiconductors: Spectroscopic evolution of microstructure due to cyclic loading in poly(3-heptylthiophene)

Adam D. Printz, Andrew S.-C. Chiang, Suchol Savagatrup, and Darren J. Lipomi

Department of NanoEngineering, University of California, San Diego, 9500 Gilman Drive, Mail Code 0448, La Jolla, Ca, 92093-0448

Abstract

Organic electronic materials have many characteristics that make them attractive for mechanically deformable—i.e., flexible and stretchable—applications. While deformation often degrades the performance of these devices, very little is known about the effects of cyclic loading—i.e., mechanical fatigue—on the microstructure and mechanical properties of the active materials. This paper examines the evolution of microstructure and stiffness of thin films of poly(3-heptylthiophene) (P3HpT) as the film undergoes cyclic straining using ultraviolet-visible (UV-vis) spectroscopy and the mechanical buckling technique. Thin films of P3HpT are cyclically stretched by 5, 10, or 25 percent (i.e., below, at, and above the yield point—the point at which the polymer plastically deforms with strain) up to 10000 cycles. UV-vis absorption spectroscopy is taken in intervals and the weakly interacting H-aggregate model is used to determine the aggregate quantity (from the vibronic progression) and quality (from the exciton bandwidth) in the films. Films cyclically strained at 5 and 10 percent (below and at the yield point) do not undergo significant reduction in the aggregated fraction of polymer chains, while films strained to 25% (above the yield point) undergo a reduction in aggregated fraction of over 10% by the 2000^{th} cycle. At 25% strain, a significant reduction in the buckling wavelength from 3.4 ± 0.4 μm to 2.4 ± 0.3 μm is observed within the first 100 strain cycles suggesting a significant reduction in the stiffness and resilience of the films. These results suggest that materials cyclically strained below their yield point will retain a microstructure that is their most electronically favorable, and that the mechanical properties of materials strained above their yield point will evolve significantly under repeated deformation. This information can be used to inform design

where accommodation of repetitive strain is required, such as outdoor, portable, and wearable devices.

7.1 Introduction

Organic electronic devices have several key advantages over their inorganic counterparts, including low cost,[1–3] manufacturability by roll-to-roll processes,[4–6] molecular customizability,[7,8] and their flexibility or stretchability—qualities that (though often assumed) are not always present.[9–11] These properties could enable devices in a new range of new applications including wearable[12–14] and implantable biosensors,[15,16] electronic skins,[17,18] and mechanically robust organic photovoltaics that can handle harsh outdoor environments.[11,19,20] Many of these applications require materials capable of handling repetitive strains. For example, in the "Lighting Africa" initiative, lamps powered by flexible OPVs were deployed to rural Africa; these lamps and flexible organic photovoltaic (OPV) devices were subjected to the repeated mechanical stresses of everyday use.[21] After only three weeks of testing, it was found that 40% of the devices suffered catastrophic mechanical failure, attributed to contact failure.[21] While it is expected that the failure due to contacts will be resolved, it highlights an area of the field that requires further understanding: how devices behave when repeatedly strained. It is thus important to understand how the microstructure of semiconducting layers of devices evolves under cyclic loading. Ideally, the semiconducting materials selected for a device will be able to accommodate the strain elastically so that no permanent deformation of the active components of the device occurs. However, under cyclic strain, even devices that accommodate the strain elastically might deform with continued cycling. Prior to

catastrophic failure of devices such as organic solar cells and thin-film transistors due to cracking, changes in the morphology could produce changes in the electronic structure of the material, which may be deleterious to the performance of devices.

Fatigue is a phenomenon in materials science whose effects are well known to be deleterious. In metals, strain hardening due to the accumulation of dislocations causes embrittlement and eventual structural failure. In conventional polymers, accommodation of cyclic strains dissipates heat that can produce chain scission and the rearrangement of microstructure that both have the effect of reducing the load-bearing capacity of a structure. In the context of semiconducting polymers, the effect of repetitive loading has not been explored but should almost certainly have an effect on the microstructure and thus the electronic structure. We thus explored the effect of the repetitive strain on the microstructure of thin films of the polymer poly(3-heptylthiophene) (P3HpT) (**Figure 1**). We measured the absorption of relaxed films after straining and used the weakly interacting H-aggregate model developed by Spano and others to evaluate the evolution of the fraction of polymer aggregates and the order within these aggregates, as manifested in the exciton bandwidth.[22–25] We expected that as the number of cycles of strain increased, the aggregation would decrease, which would be concomitant with a decrease in the amount of energy needed to deform the film (i.e., reduced modulus and resilience). We observed different behavior for films cycled below, at, and above the yield point of P3HpT (using a value of yield point previously measured by our group).[26]

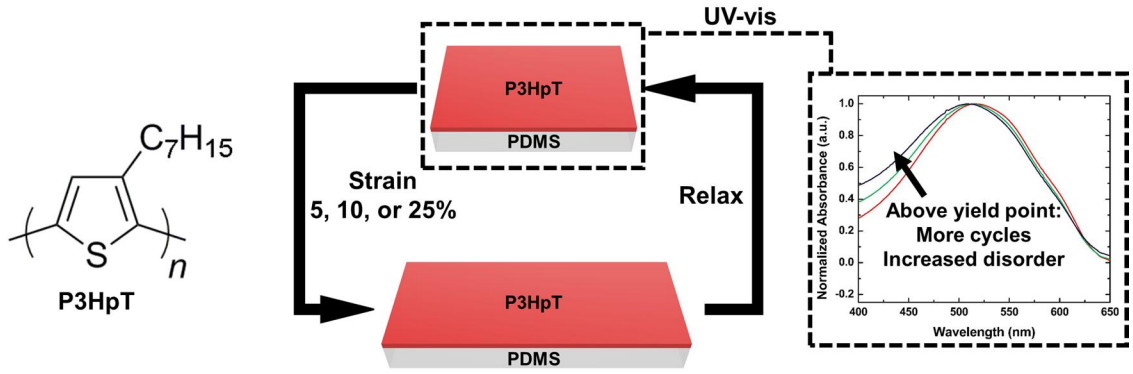

Figure 7.1. Thin films of poly(3-heptylthiophene) (P3HpT) were transferred to elastomeric substrates polydimethylsiloxane (PDMS) and strained cyclically 5%, 10%, or 25%. To evaluate the evolution of their microstructure, absorption spectra were taken periodically and the weakly interacting H-aggregate model was fit to the data.

7.2 Experimental Design

7.2.1 Selection of materials

Poly(3-heptylthiophene) was selected as the conjugated polymer to be analyzed because of its favorable electronic and mechanical properties.[27,28] We previously reported that, when mixed with [6,6]-phenyl-C61-butyric acid methyl ester ($PC_{61}BM$) in organic photovoltaic devices with all stretchable components, the power conversion efficiency (*PCE*) of devices made from P3HpT was 2.16 ± 0.17%, similar to that of P3HT devices (2.04 ± 0.27%).[27] In addition to good photovoltaic performance, P3HpT had a tensile modulus of 0.07 ± 0.01 GPa, which was an order of magnitude lower than P3HT (1.09 ± 0.15 GPa). Moreover, the crack-onset strain of the films on elastic substrates was significantly greater for P3HpT (58%) than for P3HT (10%).[27] Conveniently, all members of the family of poly(3-alkylthiophene)s (P3ATs) form thin films with aggregates that can be modeled by the weakly interacting H-aggregate model.[22,25] Polydimethylsiloxane (PDMS) was selected as the elastomeric substrate because it is transparent to visible light

and therefore allowed measurement of the absorption spectra of our films over the wavelengths of interest (300–850 nm).

7.2.2 Weakly interacting H-aggregate model

The stiffness of thin films of the poly(3-alkylthiophene) (P3AT), poly(3-hexylthiophene) (P3HT) has been correlated to the order present in the films.[25,29] In the aggregated state, the coupled electron-vibrational (vibronic) transitions determine the absorption of weakly interacting H-aggregates. Spano and others developed the weakly interacting H-aggregate model, which models the absorption by aggregated states in polymer films that form H-aggregates as Gaussian fits by:[22–25]

$$A(E) \propto \sum_{m=0} \left(\frac{S^m}{m!}\right) \times \left(1 - \frac{We^{-S}}{2E_{\mathrm{p}}} \sum_{n \neq m} \frac{S^n}{n!\,(n-m)}\right)^2 \times exp\left(\frac{-\left(E - E_{00} - mE_{\mathrm{p}} - \frac{1}{2}WS^m e^{-S}\right)^2}{2\sigma^2}\right) \quad (\mathbf{1})$$

where A is the absorption by an aggregate as a function of the photon energy (E). W is the free exciton bandwidth, which is related to the nearest neighbor interchain excitonic coupling. Upon coupling, a dispersion of the energies occurs, the width of which is equal to W (which is four times the nearest neighbor coupling).[30] E_{00} is the energy of the 0→0 vibronic transition, which is allowed assuming some disorder in the aggregates.[22] S is the Huang−Rhys factor, which is calculated from absorption and emission spectra, and is set to 1 for P3HTs.[22,23] E_{p} is the intermolecular vibration energy, which (in the case where S = 1) is set to 0.179 eV as determined by Raman spectroscopy.[31] The terms m and n are the ground- and excited- state vibrational levels, and σ is the Gaussian line width. The Gaussian line width, σ, E_{p}, W, and the scaling factor for the calculated absorption were found by a least-squares fit to the experimental absorption in the region of 550−620 nm

(2.25−2.00 eV).[24,25,32] This range was selected because in it the absorption is dominated by the polymer aggregates, while above 540 nm (2.30 eV), the amorphous polymer dominates absorption.[23,32]

7.2.3 Cyclic loading of P3HpT

To understand the evolution of the microstructure of thin films of P3HpT as they are strained cyclically, we measured the absorption spectra before straining, as well as after 1, 10, 20, 50, 100, 200, 500, 1000, 2000, 5000, and 10000 strain cycles while the films were in the relaxed state. Seven samples were strained simultaneously using a purpose-built apparatus (**Figure 7.2**). We then applied the weakly interacting H-aggregate model to these spectra to determine the quantity and quality of aggregation in the films. We also wanted to understand the effects on microstructure of cyclic straining below, at, and above the yield point. In P3HpT, the yield point was previously determined to be 11.3 ± 1.5%, so we chose to cyclically strain the films 5, 10, and 25%.[26] We anticipated the greatest changes in microstructure would occur above the yield point, while lower changes would occur near the yield point, and almost no change would occur below the yield point.

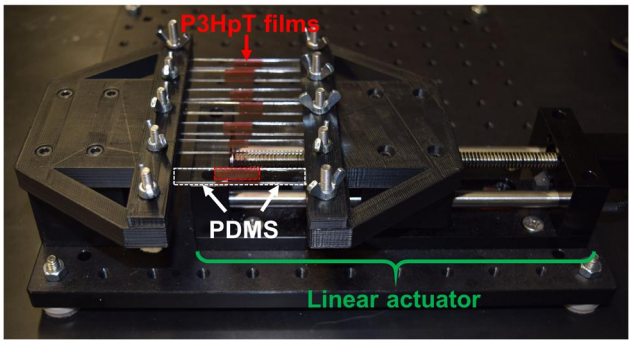

Figure 7.2. Photograph of the stretch apparatus stretching P3HpT thin films on PDMS substrates.

7.3 Results and discussion

The absorption spectra of P3HpT after increasing cycles of strain are shown in **Figure 7.3**. The strongly absorbing region by the aggregates in the films are between 550 and 620 nm, and shoulder features—i.e., vibronic transitions—were clearly observable in this region for all of the samples before strain had been applied. The ratio of the magnitude of the 0→0 (the shoulder at 605 nm) and 0→1 (the shoulder at 550 nm) vibronic transitions is associated with local ordering (specifically the conjugation length) in the aggregates.[22,23,25] While a large change in the vibronic peaks was not observable in the films cyclically strained 5% (**Figure 7.3a**), a reduction in the vibronic peaks was observable in films cyclically strained 10% (**Figure 7.3b**) and 25% (**Figure 7.3c**). The decrease in the vibronic peaks is indicative of a decrease in the quality (or ordering) of the aggregates. At wavelengths below 540 nm, the amorphous polymer is more strongly absorbing. In the films that have been cyclically strained 25%, there is a significant increase in the absorbance below 500 nm as the number of strain cycles increases. This increase in the absorption at lower wavelengths suggests that there is a decrease in the quantity of aggregates—or an increase in the quantity of disordered or amorphous regions—in the film. The increase in disorder is consistent with the possibility of plastic deformation in the film with repetitive strain.

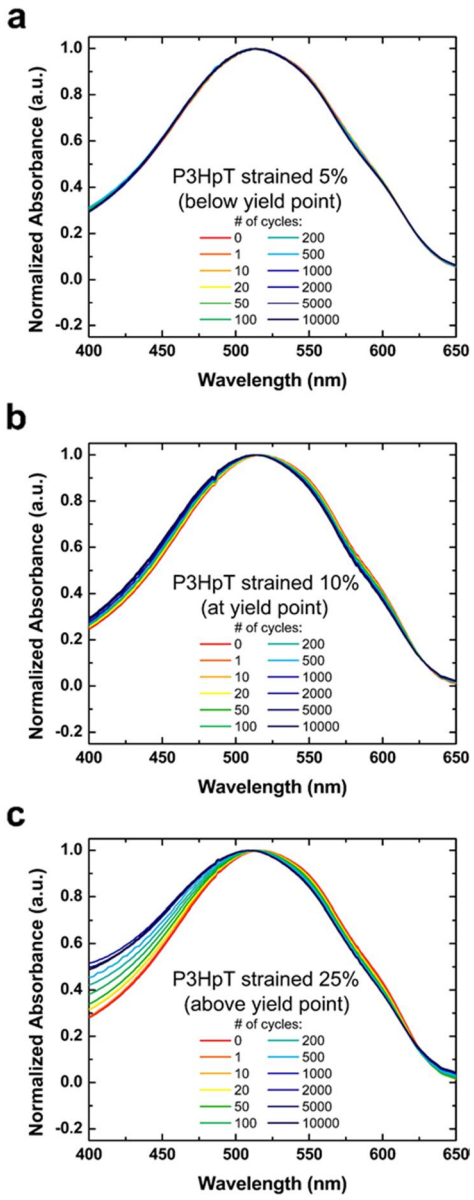

Figure 7.3. Absorption spectra of P3HpT thin films undergoing cyclic strain. (a) Thin films strained below the yield point of P3HpT (all curves essentially overlap). (b) Thin films strained near the yield point of P3HpT. (c) Thin films strained above the yield point of P3HpT.

Next, we probed the evolution of the microstructure by applying the weakly interacting H-aggregate model to the absorption spectra (**Figure 7.4**). The normalized fraction of aggregates is plotted against the number of strain cycles in **Figure 7.4a**. The

values were normalized to account for variations between samples. Additionally, to account for oxidative degradation, a control sample that was not cyclically strained was made and measured at the same time as those samples that were cyclically strained. The normalized parameters for the control were calculated and their deviation from unity was then subtracted from the data of the cyclically strained samples. A small decrease in aggregation was observed in the samples cyclically strained 5 and 10%, while a much greater decrease in aggregation was observed in samples cyclically strained 25%. It should be noted that while the normalized aggregation values for the samples strained 5% increase to above 1.0, it is likely an artifact due to subtracting out the deviation of the control from unity. In all cases, the disruption in aggregation that occurred appeared to slow down once the samples had undergone 2000 strain cycles. This observation suggests that most degradation due to microstructural evolution in conjugated polymers is likely to saturate—for P3HpT saturation occurs around 2000 cycles.

The exciton bandwidth, *W*, is inversely related to conjugation length and provides information about the local ordering (or quality) of the polymer aggregates. The normalized exciton bandwidth (with the control factored out) for 5, 10, and 25% strain plotted against the number of cycles is shown in **Figure 7.4b**. We observed that *W* in the samples strained 5% does not change significantly, indicating little change in the quality of aggregates and in the conjugation length). However, at 10% and 25% strain, the *W* values increased, indicating a decrease in the aggregate conjugation length. The decrease in the aggregate conjugation length at 25% is unsurprising and is consistent with the observation of decreased aggregation. However, the decrease in aggregate conjugation length of the samples cyclically strained at 10% is surprising because it is not coupled

with a decrease in aggregate quantity. One possible explanation for this observation is that there is a critical amount of local disorder that must occur in aggregates because they become completely disrupted.

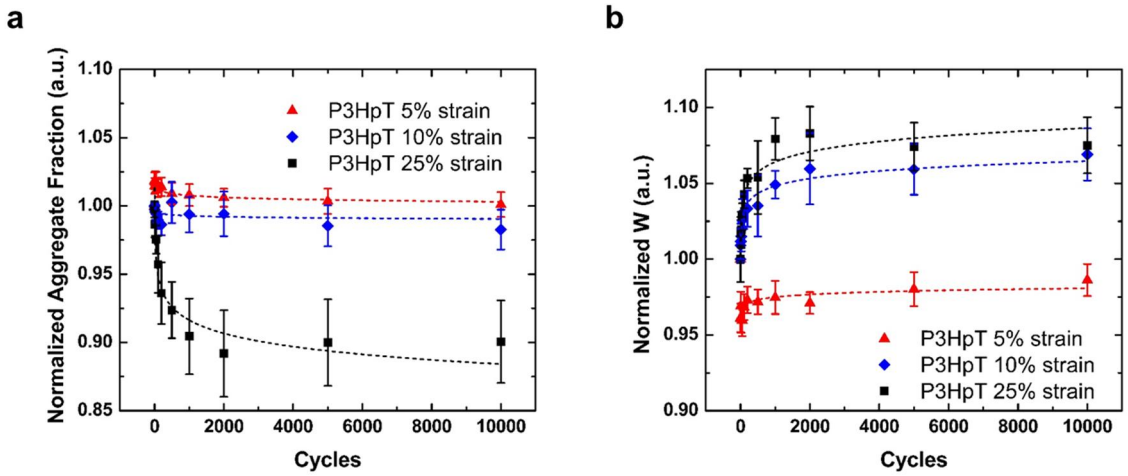

Figure 7.4. Weakly interacting H-aggregate model parameters for the cyclically strained films. (a) The fraction of aggregates in the films normalized to the amount of aggregation initially present. The aggregation was measured only between 400 and 650 nm, therefore the contribution to absorbance by the amorphous material is underestimated. (b) The exciton bandwidth, *W*, normalized to the initial values. *W* is inversely related to the average conjugation length of the polymer, and is therefore an indicator of aggregate order. The dotted lines represent exponential fits for the data from 1 cycle to 10000 cycles.

Micrographs of the P3HpT films after 0, 1, 10, and 10000 strain cycles are shown in **Figure 7.5**. The films strained at 5%—below the yield point—showed little evidence of plastic deformation (i.e., buckling of the film was barely detectable—i.e., low-amplitude—by optical microscopy above 10 cycles), although some delamination was evident at 5000 cycles. These observations are consistent with the absorption spectra and H-aggregate parameters, which suggest minimal microstructural evolution. When the cyclic strain was increased to 10%—near the previously reported yield point of P3HpT[26]—the films developed surface buckles by 10 cycles, although the buckles were again very faint in the micrograph. While the buckling did not become more evident with

increased cycling at 10% strain, delamination occurred in a few samples by 2000 cycles and in all by 5000 cycles. A much more dramatic effect occurred for the films cyclically strained 25%, which was above the yield point of P3HpT.[26] Buckling of the film was observed after the first cycle, and the buckles became more pronounced (i.e., higher amplitude) by 10 cycles. By 5000 cycles, significant delamination was observed. The significant buckling and delamination at 25% strain was consistent with the plastic deformation (and associated decrease in aggregate quantity and quality) suggested by the absorption spectra and H-aggregate parameters for these samples. We believe the micrographs, absorption spectra, and H-aggregate results point to an important design parameter for devices expected to undergo cyclic straining, the material yield point. The cyclic straining of the samples at or below the material yield point were much less disruptive to the film aggregation than that the samples strained above the yield point (although the W of the samples at the yield point increased considerably), suggesting that in applications where repetitious strain is required, selection of materials which have a yield point higher than the anticipated strain are likely to undergo only minor changes in microstructure.

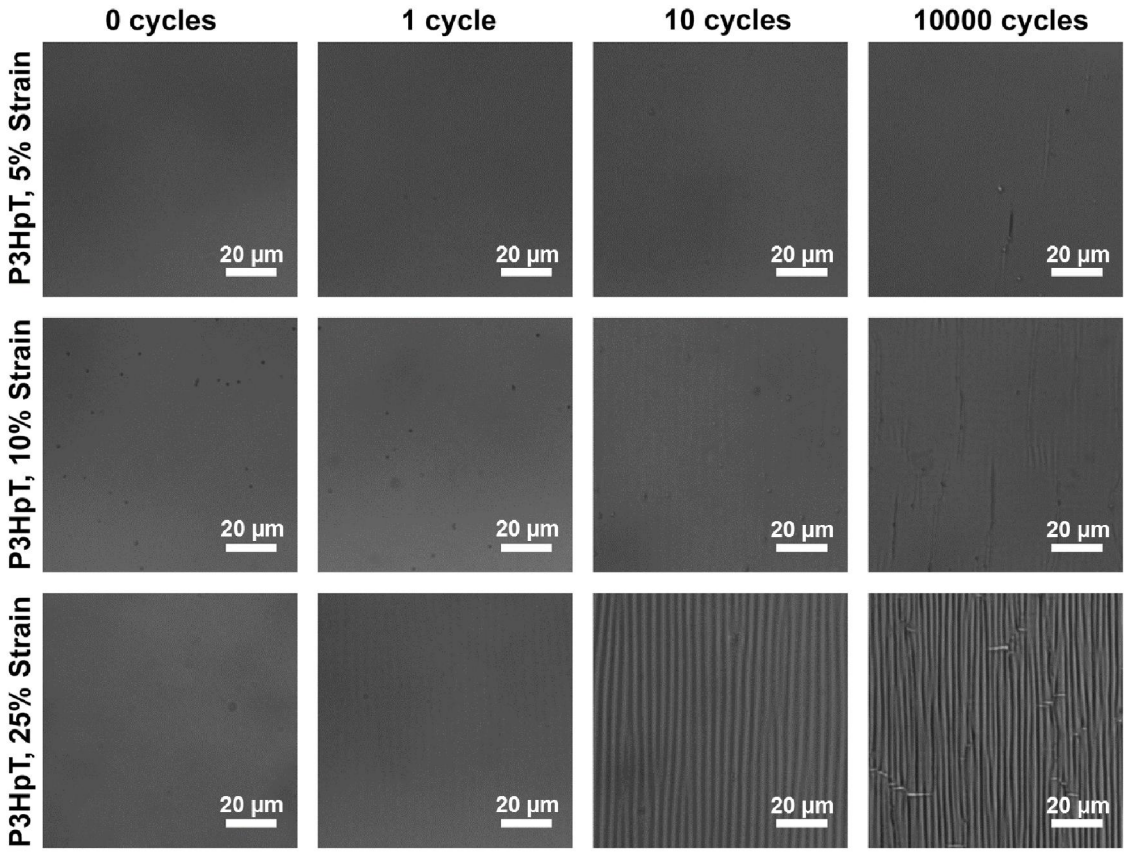

Figure 7.5. Micrographs of the cyclically strained P3HpT films. Barely detectable—i.e., very low amplitude—buckling occurred in the films strained below the yield point (although delamination occurred after many cycles). At strain near the yield point, buckling occurred by 10 cycles, and at strain above the yield point, buckling occurred on the first cycle. Delamination occurred in all samples by 10000 cycles.

To determine if the evolution of microstructure was correlated with a change in mechanical properties, we measured the buckling wavelength of the films cyclically strained 25% after various cycles (**Figure 7.6**). (The samples strained 25% were selected because they featured the most prominent buckling.) Under ideal conditions—i.e., small compressive strains, ≤5%, and a purely elastic film—the buckling wavelength is correlated to the tensile modulus because it is dependent on an energy balance between deforming the underlying soft substrate and bending the relatively rigid film.[33] Using this effect, Stafford et al. developed a buckling-based metrology to determine the tensile

modulus of thin films.[34] The tensile modulus is correlated with the buckling wavelength, meaning stiffer films have a longer buckling wavelength, and more compliant films have a shorter buckling wavelength.[34–36] We found that the buckling wavelength was the highest after the first strain cycle (3.4 ± 0.4 μm) and it dropped considerably to 2.8 ± 0.5 μm by the 10th cycle. By the 100th strain cycle, the buckling wavelength was 2.4 ± 0.3 μm and remained relatively constant with an increasing number of cycles. This data agreed with previous literature—and the UV-vis analysis in this study—that reported a decrease in stiffness (i.e., decrease in tensile modulus) with decreasing fraction of aggregated polymer chains and order,[25,29] and suggests that the films became more compliant as they were cyclically strained (at least for the first few hundred strain cycles).

We were unable to quantify the precise reduction in modulus due to cycling and indicated by the decrease in buckling wavelength for two reasons. (1) The buckling methodology of Stafford et al. is valid only for small compressive strains (i.e., less than about 5%).[34] In our experiments, a total strain of 25% of a material with a yield point of about 10% would elongate the material plastically by 15%, and thus produce a compressive strain of 15%—too large for analysis by the buckling methodology—when the film and substrate was returned to equilibrium. (2) Analysis by the method of Stafford et al. would require that no plastic deformation occurs after the first cycle of strain, which cannot be granted automatically, especially in light of the microstructural evolution indicated by UV-vis spectroscopy. (However, given that the modulus decreases with the third power of buckling wavelength, it is probably safe to assume a reduction in modulus by at least a factor of 2-3 for the films after 10000 cycles of 25% strain.) An illustration of the microstructural evolution of P3HpT strained cyclically above its yield point is

shown in **Figure 7.7**. The quantity and quality of the aggregates in the as-cast films are disrupted after repetitive strain. This decrease in aggregate quality and quantity results in a film with a much lower tensile modulus.

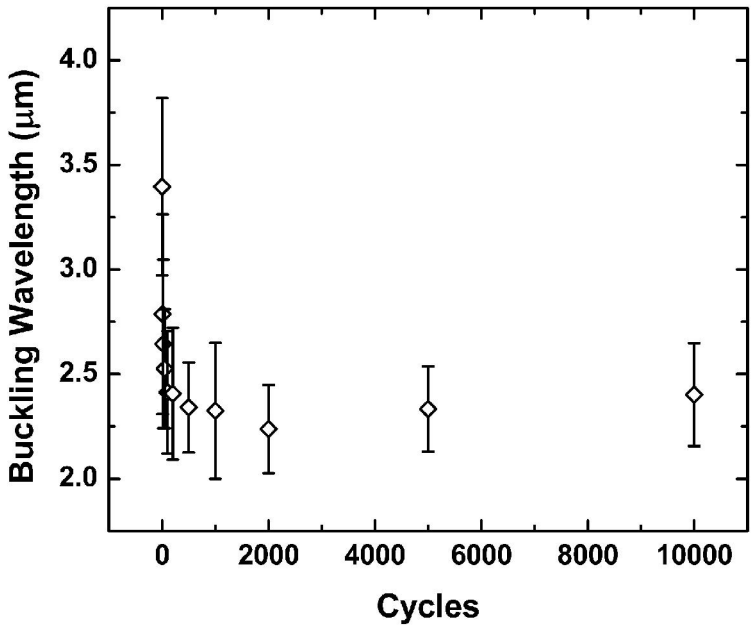

Figure 7.6. The buckling wavelength versus number of cycles for P3HpT samples cyclically strained 25%. The decrease in buckling wavelength is indicative of a lower tensile modulus.

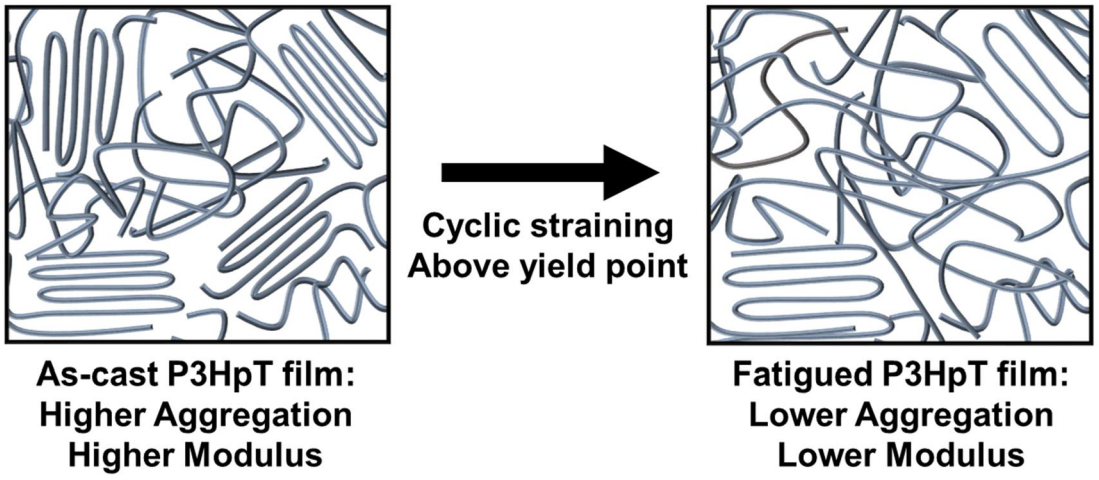

Figure 7.7. An illustration demonstrating the disruption of aggregation in thin films of P3HpT cyclically strained above its yield point.

7.4 Conclusion

This paper described the evolution of microstructure in P3HpT with increasing cycles of strain below, at, and above the thin film yield point using the weakly interacting H-aggregate model. Experimental evidence showed that disruption of aggregation is negligible when films are cycled at strains below or near the material yield point (although the quality of the aggregates decreased with cycling at the yield point). However, when the films are cycled at strains above the yield point, significant disruption of aggregates occurs. We also observed that the majority of microstructural evolution at a single strain occurs within the first 2000 strain cycles, meaning that the degradation of electronic performance due to microstructural degradation will likely saturate. Importantly, we found that—in the samples strained above the yield point—the buckling wavelength decreased as the number of strain cycles increased, suggesting a material that became less stiff as it was cyclically strained. Our findings thus highlight the yield point as an important figure of merit for devices used in applications where repetitive strain is expected, as in applications requiring repetitive strain such as outdoor, portable, and wearable devices.

7.5 Experimental methods

7.5.1 Materials

Poly(3-heptylthiophene) (P3HpT, M_n = 35 kDa, PDI = 1.5) was purchased from Rieke Metals, Inc. and used as received. PDMS, Sylgard 184 (Dow Corning), was prepared according to the manufacturer's instructions at a ratio of 10:1 (base:crosslinker) and cured at 75 °C for 25 min before it was used for mechanical testing. (Tridecafluoro-

1,1,2,2-tetrahydrooctyl)-1-trichlorosilane (FOTS) was obtained from Gelest. Chloroform, acetone, and isopropyl alcohol (IPA) were obtained from Sigma-Aldrich and used as received.

7.5.2 Preparation of samples for testing

Glass slides were cut into squares (2.5 cm × 2.5 cm) with a diamond-tipped scribe. They were then subsequently cleaned with Alconox solution (2 mg mL^{-1}), deionized water, acetone, and then isopropyl alcohol (IPA) in an ultrasonic bath for 10 min each and then rinsed and dried with compressed air. Next, the glass was plasma treated at ~30 W for 3 min at a base pressure of 200 mtorr ambient air to remove residual organic material and activate the surface. The slides were then placed in a vacuum desiccator with a glass vial containing ~100 μL of FOTS and put under house vacuum for a minimum of 3 h to passivate the surface. The surface was then rinsed thoroughly with IPA to remove any excess FOTS and leave only a monolayer behind.

A solution of P3HpT in chloroform (7.5 mg mL^{-1}) were prepared and allowed to stir overnight. It was then filtered with 1 μm glass microfiber (GMF) filter immediately before being spin-coated onto FOTS passivated glass. The solution was spun at 300 rpm (250 rpm s^{-1} ramp) for 120 s, followed by 2000 rpm (1000 rpm s^{-1} ramp) for 30 seconds. The films were dried under vacuum for 15 min to remove residual solvent and then transferred to PDMS after it had been oven cured.

7.5.3 Cyclic straining of samples

The thin film on elastomer samples (n = 7 for each strain) were mounted to a computer controlled linear actuator (before securing them, care was taken so that there was no sagging of the films). The samples were then strained and relaxed cyclically at either 5, 10, or 25%, up to 10000 cycles, with the absorption spectra measured before any strain cycles and after 1, 10, 20, 50, 100, 200, 500, 1000, 2000, 5000, and 10000 cycles.

7.5.4 UV-vis absorption spectroscopy

The absorbance of the materials was measured using an Agilent 8453 UV-vis spectrophotometer. The wavelength range measured was 850–300 nm with a step size of 1 nm. The weakly interacting H-aggregate model was then used to perform a least squares fit to the absorption spectra between 550 and 620 nm (2.25 and 2.00 eV) using a Matlab program. The curves were initially normalized by setting the lowest point between 670 and 750 nm (1.85 and 1.65 eV) to zero[25] and then normalizing to the peak between 480 and 560 nm (2.58 and 2.21eV).

Acknowledgements

This work was supported by the Air Force Office of Scientific Research (AFOSR) Young Investigator Program, grant number FA9550-13-1-0156. Additional support was provided by the National Science Foundation Graduate Research Fellowship Program under Grant DGE-1144086 awarded to S.S., the UC LEADS fellowship and the STARS Summer Research Program awarded to A. S.-C. Chiang, and by laboratory startup funds from the University of California, San Diego.

Chapter 7, in part is currently being prepared for submission for publication of the material. Adam D. Printz, Andrew S.-C. Chiang, Suchol Savagatrup, and Darren J. Lipomi. The dissertation/thesis author was the primary investigator and author of this material.

References

(1) Po, R.; Carbonera, C.; Bernardi, A.; Tinti, F.; Camaioni, N. Polymer- and Carbon-Based Electrodes for Polymer Solar Cells: Toward Low-Cost, Continuous Fabrication over Large Area. *Sol. Energy Mater. Sol. Cells* **2012**, *100*, 97–114.

(2) Espinosa, N.; Hösel, M.; Angmo, D.; Krebs, F. C. Solar Cells with One-Day Energy Payback for the Factories of the Future. *Energy Environ. Sci.* **2012**, *5*, 5117–5132.

(3) Anctil, A.; Babbitt, C. W.; Raffaelle, R. P.; Landi, B. J. Cumulative Energy Demand for Small Molecule and Polymer Photovoltaics. *Prog. Photovolt Res. Appl.* **2013**, *21*, 1541–1554.

(4) Krebs, F. C. Fabrication and Processing of Polymer Solar Cells: A Review of Printing and Coating Techniques. *Sol. Energy Mater. Sol. Cells* **2009**, *93*, 394–412.

(5) Sommer-Larsen, P.; Jørgensen, M.; Søndergaard, R. R.; Hösel, M.; Krebs, F. C. Fast Inline Roll-to-Roll Printing for Indium-Tin-Oxide-Free Polymer Solar Cells Using Automatic Registration. *Energy Technol.* **2013**, *1*, 102–107.

(6) Krebs, F. C.; Espinosa, N.; Hösel, M.; Søndergaard, R. R.; Jørgensen, M. 25th Anniversary Article: Rise to Power - OPV-Based Solar Parks. *Adv. Mater.* **2014**, *26*, 29–39.

(7) Yiu, A. T.; Beaujuge, P. M.; Lee, O. P.; Woo, C. H.; Toney, M. F.; Fréchet, J. M. J. Side-Chain Tunability of Furan-Containing Low-Band-Gap Polymers Provides Control of Structural Order in Efficient Solar Cells. *J. Am. Chem. Soc.* **2012**, *134*, 2180–2185.

(8) Mei, J.; Bao, Z. Side Chain Engineering in Solution-Processable Conjugated Polymers. *Chem. Mater.* **2014**, *26*, 604–615.

(9) Brand, V.; Bruner, C.; Dauskardt, R. H. Cohesion and Device Reliability in Organic Bulk Heterojunction Photovoltaic Cells. *Sol. Energy Mater. Sol. Cells* **2012**, *99*, 182–189.

(10) Dupont, S. R.; Oliver, M.; Krebs, F. C.; Dauskardt, R. H. Interlayer Adhesion in Roll-to-Roll Processed Flexible Inverted Polymer Solar Cells. *Sol. Energy Mater. Sol. Cells* **2012**, *97*, 171–175.

(11) Lipomi, D. J.; Chong, H.; Vosgueritchian, M.; Mei, J.; Bao, Z. Toward Mechanically Robust and Intrinsically Stretchable Organic Solar Cells: Evolution of Photovoltaic Properties with Tensile Strain. *Sol. Energy Mater. Sol. Cells* **2012**, *107*, 355–365.

(12) Tee, B. C.-K.; Wang, C.; Allen, R.; Bao, Z. An Electrically and Mechanically Self-Healing Composite with Pressure- and Flexion-Sensitive Properties for Electronic Skin Applications. *Nat. Nanotechnol.* **2012**, *7*, 825–832.

(13) Kaltenbrunner, M.; Sekitani, T.; Reeder, J.; Yokota, T.; Kuribara, K.; Tokuhara, T.; Drack, M.; Schwödiauer, R.; Graz, I.; Bauer-Gogonea, S.; Bauer, S.; Someya, T. An Ultra-Lightweight Design for Imperceptible Plastic Electronics. *Nature* **2013**, *499*, 458–463.

(14) Savagatrup, S.; Chan, E.; Renteria-Garcia, S. M.; Printz, A. D.; Zaretski, A. V.; O'Connor, T. F.; Rodriquez, D.; Valle, E.; Lipomi, D. J. Plasticization of PEDOT:PSS by Common Additives for Mechanically Robust Organic Solar Cells and Wearable Sensors. *Adv. Funct. Mater.* **2015**, *25*, 427–436.

(15) Ghezzi, D.; Antognazza, M. R.; Maccarone, R.; Bellani, S.; Lanzarini, E.; Martino, N.; Mete, M.; Perile, G.; Bisti, S.; Lanzani, G.; Benfenati, F. A Polymer Optoelectronic Interface Restores Light Sensitivity in Blind Rat Retinas. *Nat. Photonics* **2013**, *7*, 400–406.

(16) Hammock, M. L.; Chortos, A.; Tee, B. C.-K.; Tok, J. B.-H.; Bao, Z. 25th Anniversary Article: The Evolution of Electronic Skin (E-Skin): A Brief History, Design Considerations, and Recent Progress. *Adv. Mater.* **2013**, *25*, 5997–6038.

(17) Mannsfeld, S. C. B.; Tee, B. C.-K.; Stoltenberg, R. M.; Chen, C. V. H.-H.; Barman, S.; Muir, B. V. O.; Sokolov, A. N.; Reese, C.; Bao, Z. Highly Sensitive Flexible Pressure Sensors with Microstructured Rubber Dielectric Layers. *Nat. Mater.* **2010**, *9*, 859–864.

(18) Lipomi, D. J.; Vosgueritchian, M.; Tee, B. C.-K.; Hellstrom, S. L.; Lee, J. a.; Fox, C. H.; Bao, Z. Skin-like Pressure and Strain Sensors Based on Transparent Elastic Films of Carbon Nanotubes. *Nat. Nanotechnol.* **2011**, *6*, 788–792.

(19) Jørgensen, M.; Norrman, K.; Krebs, F. C. Stability/degradation of Polymer Solar Cells. *Sol. Energy Mater. Sol. Cells* **2008**, *92*, 686–714.

(20) Jørgensen, M.; Norrman, K.; Gevorgyan, S. A.; Tromholt, T.; Andreasen, B.; Krebs, F. C. Stability of Polymer Solar Cells. *Adv. Mater.* **2012**, *24*, 580–612.

(21) Krebs, F. C.; Nielsen, T. D.; Fyenbo, J.; Wadstrøm, M.; Pedersen, M. S. Manufacture, Integration and Demonstration of Polymer Solar Cells in a Lamp for the "Lighting Africa" Initiative. *Energy Environ. Sci.* **2010**, *3*, 512–525.

(22) Spano, F. C. Modeling Disorder in Polymer Aggregates: The Optical Spectroscopy of Regioregular poly(3-Hexylthiophene) Thin Films. *J. Chem. Phys.* **2005**, *122*, 234701.

(23) Clark, J.; Chang, J.-F.; Spano, F. C.; Friend, R. H.; Silva, C. Determining Exciton Bandwidth and Film Microstructure in Polythiophene Films Using Linear Absorption Spectroscopy. *Appl. Phys. Lett.* **2009**, *94*, 163306.

(24) Turner, S. T.; Pingel, P.; Steyrleuthner, R.; Crossland, E. J. W.; Ludwigs, S.; Neher, D. Quantitative Analysis of Bulk Heterojunction Films Using Linear Absorption Spectroscopy and Solar Cell Performance. *Adv. Funct. Mater.* **2011**, *21*, 4640–4652.

(25) Awartani, O.; Lemanski, B. I.; Ro, H. W.; Richter, L. J.; DeLongchamp, D. M.; O'Connor, B. T. Correlating Stiffness, Ductility, and Morphology of Polymer:Fullerene Films for Solar Cell Applications. *Adv. Energy Mater.* **2013**, *3*, 399–406.

(26) Printz, A. D.; Zaretski, A. V.; Savagatrup, S.; Chiang, A. S.-C.; Lipomi, D. J. Yield Point of Semiconducting Polymer Films on Stretchable Substrates Determined by Onset of Buckling. *ACS Appl. Mater. Interfaces* **2015**, *7*, 23257–23264.

(27) Savagatrup, S.; Printz, A. D.; Rodriquez, D.; Lipomi, D. J. Best of Both Worlds: Conjugated Polymers Exhibiting Good Photovoltaic Behavior and High Tensile Elasticity. *Macromolecules* **2014**, *47*, 1981–1992.

(28) Savagatrup, S.; Printz, A. D.; Wu, H.; Rajan, K. M.; Sawyer, E. J.; Zaretski, A. V.; Bettinger, C. J.; Lipomi, D. J. Viability of Stretchable poly(3-Heptylthiophene) (P3HpT) for Organic Solar Cells and Field-Effect Transistors. *Synth. Met.* **2015**, *203*, 208–214.

(29) Kim, J.-S.; Kim, J.-H.; Lee, W.; Yu, H.; Kim, H. J.; Song, I.; Shin, M.; Oh, J. H.; Jeong, U.; Kim, T.-S.; Kim, B. J. Tuning Mechanical and Optoelectrical Properties

of Poly(3-Hexylthiophene) through Systematic Regioregularity Control. *Macromolecules* **2015**, *48*, 4339–4346.

(30) Spano, F. C. Absorption in Regio-Regular poly(3-Hexyl)thiophene Thin Films: Fermi Resonances, Interband Coupling and Disorder. *Chem. Phys.* **2006**, *325*, 22–35.

(31) Louarn, G.; Trznadel, M. Raman Spectroscopic Studies of Regioregular Poly (3-Alkylthiophenes). *J. Phys. Chem.* **1996**, *3654*, 12532–12539.

(32) Pingel, P.; Zen, A.; Abellón, R. D.; Grozema, F. C.; Siebbeles, L. D. A.; Neher, D. Temperature-Resolved Local and Macroscopic Charge Carrier Transport in Thin P3HT Layers. *Adv. Funct. Mater.* **2010**, *20*, 2286–2295.

(33) Bowden, N.; Brittain, S.; Evans, A. G.; Hutchinson, J. W.; Whitesides, G. M. Spontaneous Formation of Ordered Structures in Thin Films of Metals Supported on an Elastomeric Polymer. *Nature* **1998**, *393*, 146–149.

(34) Stafford, C. M.; Harrison, C.; Beers, K. L.; Karim, A.; Amis, E. J.; VanLandingham, M. R.; Kim, H.-C.; Volksen, W.; Miller, R. D.; Simonyi, E. E. A Buckling-Based Metrology for Measuring the Elastic Moduli of Polymeric Thin Films. *Nat. Mater.* **2004**, *3*, 545–550.

(35) Stafford, C. M.; Vogt, B. D.; Harrison, C.; Julthongpiput, D.; Huang, R. Elastic Moduli of Ultrathin Amorphous Polymer Films. *Macromolecules* **2006**, *39*, 5095–5099.

(36) Tahk, D.; Lee, H. H.; Khang, D.-Y. Elastic Moduli of Organic Electronic Materials by the Buckling Method. *Macromolecules* **2009**, *42*, 7079–7083.

Appendix A

Supporting Information for Chapter 3

Viability of stretchable poly(3-heptylthiophene) (P3HpT) for organic solar cells and field-effect transistors

Suchol Savagatrup,[†a] Adam D. Printz,[†a] Haosheng Wu,[b] Kirtana M. Rajan,[a] Eric J. Sawyer,[a] Aliaksandr V. Zaretski,[a] Christopher J. Bettinger,[b] and Darren J. Lipomi[a]

([†] Equal contribution)

[a] *Department of NanoEngineering, University of California, San Diego, 9500 Gilman Drive Mail Code 0448, La Jolla, CA 92093-0448.*

[b] *Department of Materials Science and Engineering, Carnegie Mellon University, 5000 Forbes Hall, Pittsburgh, PA, 15213-3890.*

A.1 Experimental methods

A.1.1 Materials

Poly(3-heptylthiophene) (P3HpT, M_n = 35 kDa, PDI = 1.5) was purchased from Rieke Metals, Inc. and used as received. Poly(3-hexylthiophene) (P3HT, M_n = 44 kDa, PDI = 2.0) and poly(3-octylthiophene) (P3OT, M_n = 34 kDa, PDI = 2.5) were purchased from Sigma-Aldrich and used as received. PDMS, Sylgard 184 (Dow Corning), was prepared according to the manufacturer's instructions at a ratio of 10:1 (base:crosslinker) and cured at room temperature for 36 to 48 h before it was used for mechanical testing. (Tridecafluoro-1,1,2,2-tetrahydrooctyl)-1-trichlorosilane (FOTS) was obtained from Gelest. PEDOT:PSS (Clevios PH1000) was purchased from Heraeus. DMSO was purchased from BDH with purity of 99.9% and Zonyl (FS-300) fluorosurfactant were purchased from Sigma-Aldrich. Chloroform ($CHCl_3$), ortho-dichlorobenzene (ODCB), acetone, isopropyl alcohol (IPA), and ITO-coated glass slides were obtained from Sigma-Aldrich and used as received.

A.1.2 Preparation of substrates

Glass slides used as substrates for solar cells were cut into squares (2.5 cm × 2.5 cm) with a diamond-tipped scribe. They were then subsequently cleaned with Alconox solution (2 mg mL^{-1}), deionized water, acetone, and then isopropyl alcohol (IPA) in an ultrasonic bath for 10 min each and then rinsed and dried with compressed air. Next, the glass was plasma treated at ~30 W for 3 min at a base pressure of 200 mtorr ambient air to remove residual organic material and activate the surface. ITO-coated slides for cyclic voltammetry and UV–vis spectrophotometry were cleaned in the same manner. Glass

slides used as substrates for thin films to be transferred to PDMS for mechanical testing by the buckling methodology were prepared in the same manner as above, and then subsequently placed in a vacuum desiccator with a glass vial containing ~100 μL of FOTS and put under house vacuum for a minimum of 3 h to passivate the surface.

A.1.3 Preparation of polymer solutions

Solutions of P3HT, P3HpT, and P3OT in $CHCl_3$ (15 mg mL^{-1}) were prepared for cyclic voltammetry and UV-vis. Solutions of the different ratios of P3HpT:$PC_{61}BM$ in ODCB (at a constant concentration of 40 mg mL^{-1}) were prepared for solar cells, crack-onset strain (*CoS*), and H-aggregate analysis. All solutions were allowed to stir overnight and filtered with a 1-μm glass microfiber (GMF) syringe filter immediately before being spin-coated onto glass or silicon substrates.

A.1.4 Thermal analysis

DSC was performed using a Perkin Elmer Diamond differential scanning calorimeter. Indium was used to calibrate the cell capacitance. Samples were prepared from drop-casting thin films of pure polymer and BHJ films onto aluminum pans. The mass of each sample was approximately 10 to 15 mg. Nitrogen was used as a purge gas with flow rate of 50 mL min^{-1}. The samples were held at –50 °C for 10 min and then ramped up to the upper limit of 300°C with the heating rate of 10°C min^{-1}. The samples were held at 30 °C for 1 min before cooling down to –50 °C at the same heating rate. The second heating curves were used for analysis.

A.1.5 Cyclic voltammetry (CV)

Cyclic voltammograms of P3HT, P3HpT and P3OT deposited onto ITO glass were measured relative to ferrocene at room temperature. The electrolyte used was a 0.1 M solution of $TBAPF_6$ in acetonitrile. The data was acquired using a μAutolab III potentiostat at scan rates of 10, 50 and 100 mV s^{-1} using an electrochemical cell consisting of the polymer acting as the working electrode, a platinum counter electrode, and an Ag/AgCl reference electrode.

A.1.6 UV-vis spectroscopy and analysis

The absorbance of the materials was measured using a PerkinElmer Lambda 1050 UV-vis-NIR spectrophotometer. The wavelength range measured was 850–300 nm with a step size of 1 nm. The polymer solutions were spin-coated onto the ITO-coated glass slides at a spin speed of 500 rpm (250 rpm s^{-1} ramp) for 240 s followed by 2000 rpm (750 rpm s^{-1} ramp) for 60 s. The films were immediately placed in a nitrogen-filled glove box and annealed at 100 °C for 30 min under a Pyrex petri dish covered in aluminum foil. After 30 min, the samples were allowed to cool slowly to room temperature.

Order in films of semiconducting polymers is associated with both greater electronic performance and increased stiffness. The extent of order, as determined by UV-vis spectroscopy, has been correlated to increased tensile moduli in P3HT:PCBM films. Spano et al. and others have shown that aggregates of P3HT in solid films can be considered as weakly interacting H aggregates, due to cofacial π-π stacking and weak excitonic coupling.[1–5] We used this model to compare trends in aggregation and

aggregate order from the UV-vis absorption spectra of the polymers, in an attempt to correlate these values with the mechanical stiffness.

In the aggregated state (i.e., crystallites and other aggregates in solid films), coupled electron-vibrational (vibronic) transitions determine the absorption of weakly interacting H aggregates and can be modeled as Gaussian fits by:

$$A(E) \propto \sum_{m=0} \left(\frac{S^m}{m!}\right) \times \left(1 - \frac{We^{-S}}{2E_{\mathrm{p}}} \sum_{n \neq m} \frac{S^n}{n!\,(n-m)}\right)^2 \times exp\left(\frac{-\left(E - E_{00} - mE_{\mathrm{p}} - \frac{1}{2}WS^m e^{-S}\right)^2}{2\,\sigma^{\,2}}\right) \quad (\mathbf{1})$$

In the above equation, A is the absorption by an aggregate as a function of the photon energy (E). E_{00} is the energy of the 0→0 vibronic transition, which is allowed assuming some disorder in the aggregates. S is the Huang-Rhys factor, which quantifies the nuclear potential well shift upon vibronic transition from the ground state to the excited state. It is calculated from absorption and emission spectra, and is set to 1 for P3ATs. E_{p} is the intermolecular vibration energy, which (in the case where S = 1) is the difference in energy between the vibrational levels in the excited state. It is set to 0.179 eV as determined by Raman spectroscopy. W is the free exciton bandwidth, which is related to the nearest neighbor interchain excitonic coupling. Upon coupling, a dispersion of the energies occurs, the width of which is equal to W (which is four times the nearest neighbor coupling). W is also inversely related to conjugation length; a lower W indicates better ordering of the aggregates. The terms m and n are the ground- and excited state vibrational levels and σ is the Gaussian linewidth.

The parameters E_{00}, W, σ, and a scaling factor were found by using Matlab to perform a least squares fit to the experimental absorption data in the region of 1.93 to

2.25 eV. This region was selected because the absorption is dominated by the polymer aggregates. Above 2.30 eV, the amorphous polymer dominates absorption.[6]

A.1.7 Buckling-based metrology

The tensile moduli of the materials with the buckling method as described elsewhere. Briefly, the elastomer PDMS was chosen as the substrate for all tests. The PDMS was prepared as described above and then cut into rectangular strips (l = 8 cm, w = 1 cm, h = 0.3 cm) before being stretched 4% using a computer-controlled linear actuator. While still under strain, FOTS treated glass slides (5 cm × 2.5 cm) were clipped onto the back of each strip using binder clips. To transfer the polymer or polymer:fullerene films to PDMS, the films were first spin-coated onto FOTS treated glass slides (2.5 cm × 2.5 cm) and then scored to facilitate transfer. The films were then placed against the PDMS, and after applying minimal pressure to achieve a conformal seal, the PDMS and glass slide with film were separated in one fast motion, leaving behind the film on the PDMS. After transfer, the PDMS substrates were relaxed; this action created a compressive strain that forced the conjugated polymer film to adopt sinusoidal buckles. The buckling wavelength, λ_b, and the thickness of the film, d_f, can be related to the tensile moduli of the film and the substrate, E_f and E_s, and the Poisson ratios of the two materials, v_f and v_s by the following equation:

$$E_f = 3E_s\left(\frac{1-\upsilon_f^2}{1-\upsilon_s^2}\right)\left(\frac{\lambda_b}{2\pi d_f}\right)^3 \qquad (2)$$

We measured the tensile modulus of the substrate, E_s (using a commercial pull tester), the buckling wavelength, λ_b (by optical microscopy), and the film thickness, d_f

(by stylus profilometry). The slope of a plot of λ_b vs. d_f for three different film thicknesses was inserted into eq S2. The Poisson's ratios were taken as 0.5 and 0.35 for PDMS and the conjugated polymers films. The experimental method is described in detail elsewhere.[7]

A.1.8 Fabrication of OTFT devices

The P3HT OTFTs were fabricated in a bottom gate, bottom contact configuration. Heavily n++ doped silicon wafers were used as the common gate with 250 nm of SiO_2 on top acting as the dielectric layer. The source/drain electrodes (2 nm Ti/20 nm Au) were photolithographically patterned on the SiO_2 surfaces with a channel length and width of L = 10 mm and W = 500 mm, respectively. The patterned substrates were cleaned with acetone, IPA, and DI water, and dried under an N_2 flow and placed in a UV-Ozone cleaner for 5 min. The substrates were then chemically modified by submerging in a 3 mM solution of octadecyltrichlorosilane (OTS) in trichloroethylene overnight. After the OTS modification, the substrates were cleaned with acetone, IPA, and DI water in an ultrasonic bath for 5 min each and dried under an N_2 flow.

In a N_2 filled glove box, solutions of P3HT (P3HT:PCBM), P3HPT (P3HpT:PCBM), and P3OT (P3OT:PCBM) in anhydrous chloroform at a concentration of 1 mg mL^{-1} (2 mg mL^{-1}) were completely dissolved on a hotplate at 37 °C. The solutions were cooled down to room temperature before being filtered through a 200 mm PTFE filter. The OTS modified substrates were placed in the center of a glass petri dish and 250 μL of chloroform was added to create a solvent saturated environment. Next, 10 mL of the polymer or polymer:fullerene solution was drop-cast to completely cover the

substrate surfaces (4 mm × 7 mm). After drop-casting the solution, the substrates were immediately covered by the petri dish. The solutions took about 15 min to dry and form a film. After the formation of the semiconducting layers, the devices were taken out of the glove box and kept in a high vacuum chamber (~10^{-6} Torr) for 16 h to completely remove the residual solvent in the films before testing. The devices were characterized in a probe station with continuous Ar flow on the device surfaces.

A.1.9 Fabrication of solar cells

We deposited a layer of PEDOT:PSS from an aqueous solution containing 92.9 wt% Clevios PH 1000 (~0.9-1.2 wt% PEDOT:PSS), 7.0 wt% DMSO, and 0.1 wt% Zonyl fluorosurfactant as the transparent anode. The solution was filtered with a 1-μm glass microfiber syringe filter and then spin-coated at a speed of 500 rpm (250 rpm s^{-1} ramp) for 60 s, followed by 2000 rpm (750 rpm s^{-1} ramp) for 60 s. The samples were subsequently dried at 150 °C for 30 minutes. The photoactive layer was then spin-coated onto the electrode layer at a speed of 500 rpm (250 rpm s^{-1} ramp) for 240 s, followed by 2000 rpm (750 rpm s^{-1} ramp) for 60 s. A thin strip of the PEDOT:PSS electrode was exposed by wiping away some of the photoactive layer with chloroform so that electrical contact could be made. The samples were then immediately placed in a nitrogen-filled glovebox and annealed at 100 °C for 30 min. The substrates were then allowed to cool slowly to room temperature. EGaIn (extruded by hand from a syringe) was used as the top contact. The photovoltaic properties were measured in a nitrogen-filled glovebox using a solar simulator with a 100 mW cm^{-2} flux that approximated the solar spectrum under AM 1.5G conditions (ABET Technologies 11016-U up-facing unit calibrated with

a reference cell with a KG5 filter). The current density versus voltage was measured for both dark and under illumination using a Keithley 2400 SourceMeter.

A.2 UV-vis absorption of P3HpT:PCBM with different PCBM loading

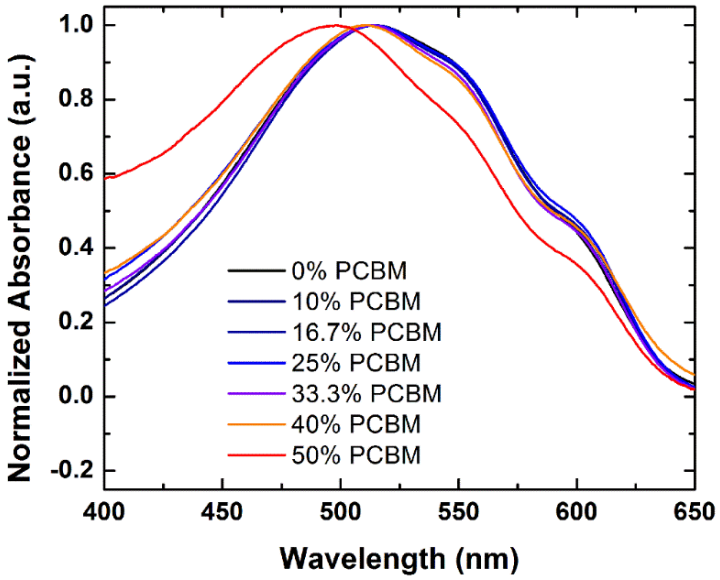

Figure A.1. Normalized UV-Vis spectra of blends of P3HpT:PCBM with different weight concentrations of PCBM after subtracting out the PCBM contribution. Most of the spectra overlap well, but there is a decrease in order above 33.3% PCBM loading, and a distinct blue shift in the absorption at 50% PCBM loading.

A.3 Differential scanning calorimetry (DSC) for P3AT:PCBMs

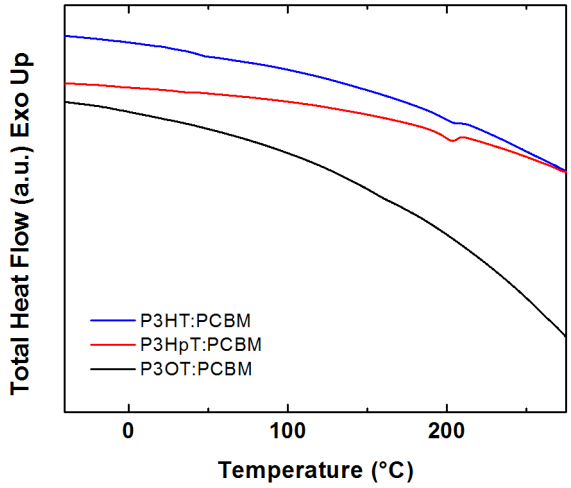

Figure A.2. DSC thermograms of P3AT:PCBMs. The T_g for P3HT:PCBM was detected between 37 and 40 °C. The T_g of P3HpT:PCBM was detected between 33 and 35 °C. The T_g for P3OT:PCBM increased slight from that of P3OT to the range between -5 and 0 °C.

A.4 Approximation of the onset of oxidation from cyclic voltammetry

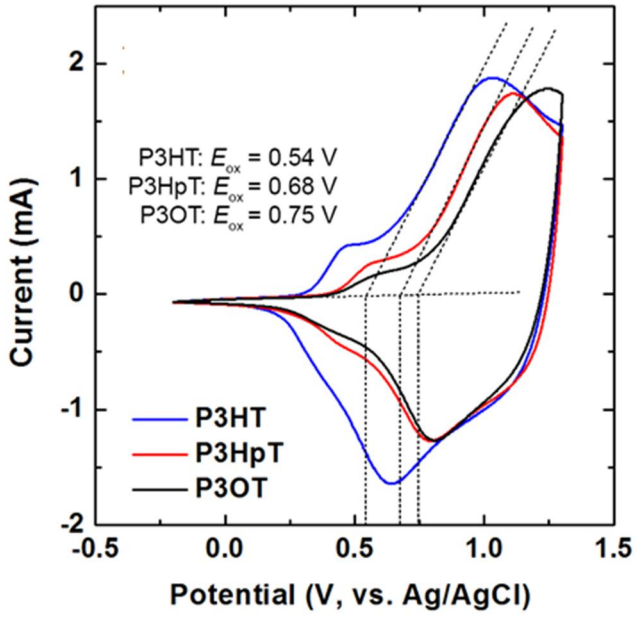

Figure A.3. The oxidation onsets of the P3ATs were determined by the intersection of the extrapolation of the slope of the oxidation curve and the baseline.

A.5 Charge transport properties of P3AT:PCBMs

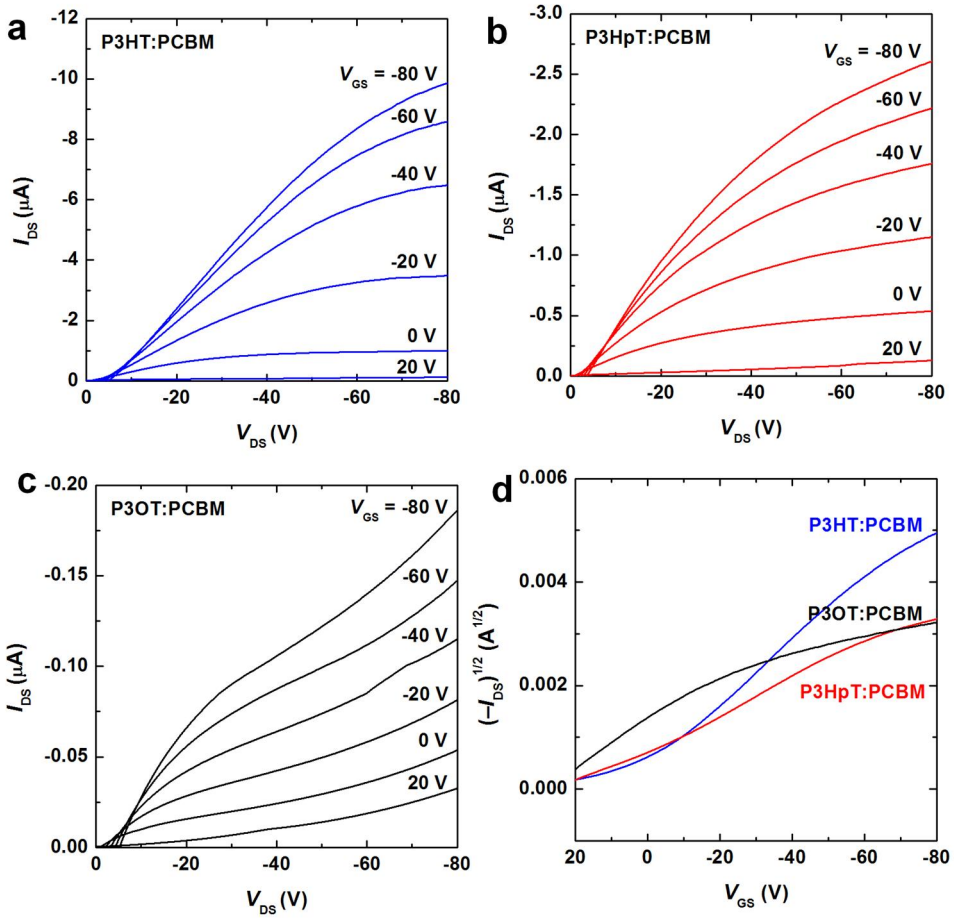

Figure A.4. Electrical characteristics of P3AT organic thin films transistors (OTFTs): current-voltage output characteristics of a 10 μm (length) by 500 μm (width) channel for (a) P3HT:PCBM, (b) P3HpT:PCBM, and (c) P3OT:PCBM. (d) Transfer characteristics $(-I_{DS})^{1/2}$ vs. V_{GS} at V_{DS} = –80 V with respect to alkyl side chain length.

References

(1) Spano, F. C. Modeling Disorder in Polymer Aggregates: The Optical Spectroscopy of Regioregular poly(3-Hexylthiophene) Thin Films. *J. Chem. Phys.* **2005**, *122*, 234701.

(2) Awartani, O.; Lemanski, B. I.; Ro, H. W.; Richter, L. J.; DeLongchamp, D. M.; O'Connor, B. T. Correlating Stiffness, Ductility, and Morphology of Polymer:Fullerene Films for Solar Cell Applications. *Adv. Energy Mater.* **2013**, *3*, 399–406.

(3) Clark, J.; Chang, J.-F.; Spano, F. C.; Friend, R. H.; Silva, C. Determining Exciton Bandwidth and Film Microstructure in Polythiophene Films Using Linear Absorption Spectroscopy. *Appl. Phys. Lett.* **2009**, *94*, 163306.

(4) Spano, F. C.; Clark, J.; Silva, C.; Friend, R. H. Determining Exciton Coherence from the Photoluminescence Spectral Line Shape in poly(3-Hexylthiophene) Thin Films. *J. Chem. Phys.* **2009**, *130*, 074904.

(5) Turner, S. T.; Pingel, P.; Steyrleuthner, R.; Crossland, E. J. W.; Ludwigs, S.; Neher, D. Quantitative Analysis of Bulk Heterojunction Films Using Linear Absorption Spectroscopy and Solar Cell Performance. *Adv. Funct. Mater.* **2011**, *21*, 4640–4652.

(6) Pingel, P.; Zen, A.; Abellón, R. D.; Grozema, F. C.; Siebbeles, L. D. A.; Neher, D. Temperature-Resolved Local and Macroscopic Charge Carrier Transport in Thin P3HT Layers. *Adv. Funct. Mater.* **2010**, *20*, 2286–2295.

(7) Savagatrup, S.; Makaram, A. S.; Burke, D. J.; Lipomi, D. J. Mechanical Properties of Conjugated Polymers and Polymer-Fullerene Composites as a Function of Molecular Structure. *Adv. Funct. Mater.* **2014**, *24*, 1169–1181.

Appendix B

Supporting Information for Chapter 4

Increased elasticity of a low-bandgap conjugated copolymer by random segmentation for mechanically robust solar cells

Adam D. Printz,[†] Suchol Savagatrup,[†] Daniel J. Burke, Trevor N. Purdy, and Darren J. Lipomi

([†] Equal contribution)

Department of NanoEngineering, University of California, San Diego, 9500 Gilman Drive Mail Code 0448, La Jolla, CA 92093-0448.

B.1 ^{13}C NMR

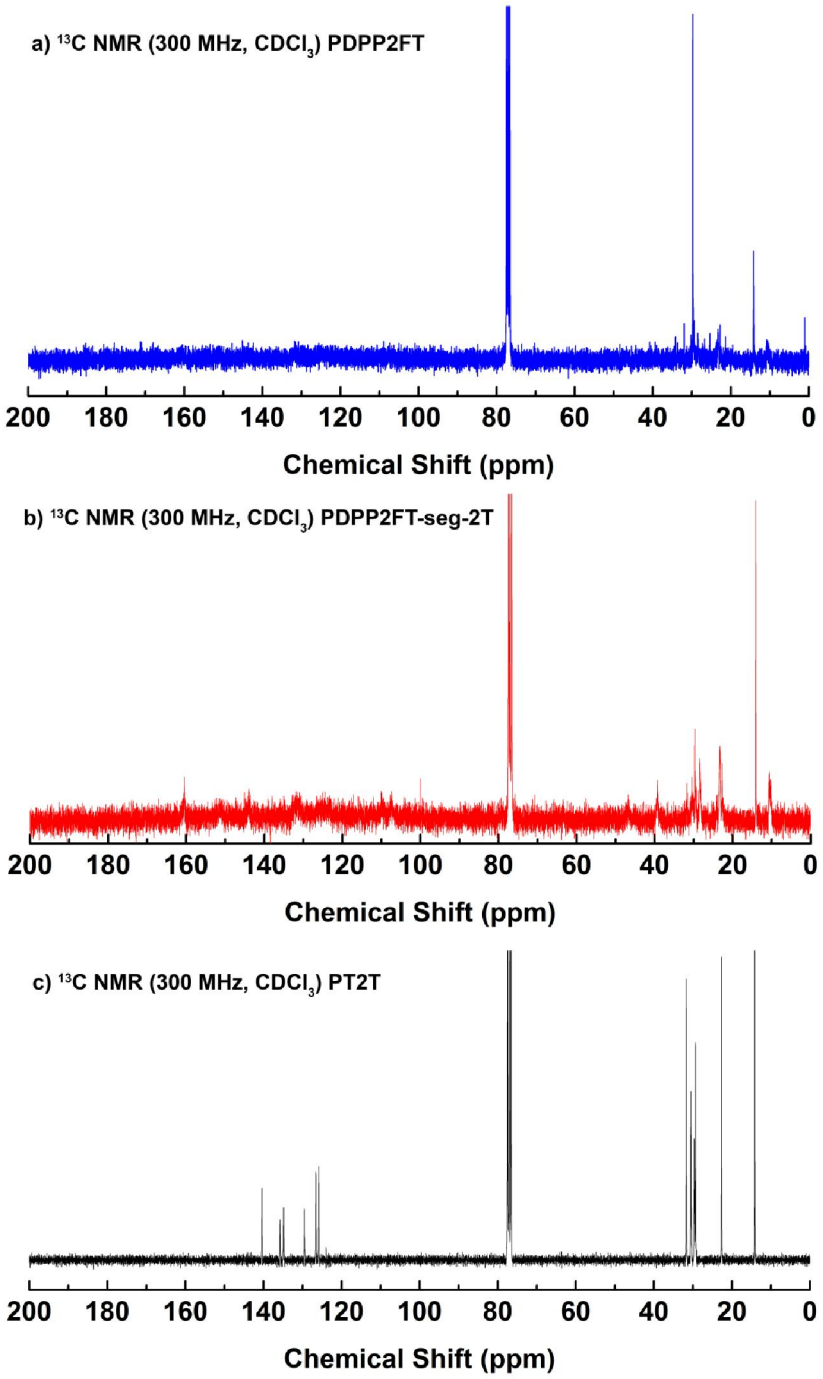

Figure B.1. ^{13}C NMR of (a) PDPP2FT, (b) PDPP2FT-seg-2T, and (c) PT2T.

B.2. UV-vis absorption of polymers (including 100:1 PDPP2FT:PT2T physical blend)

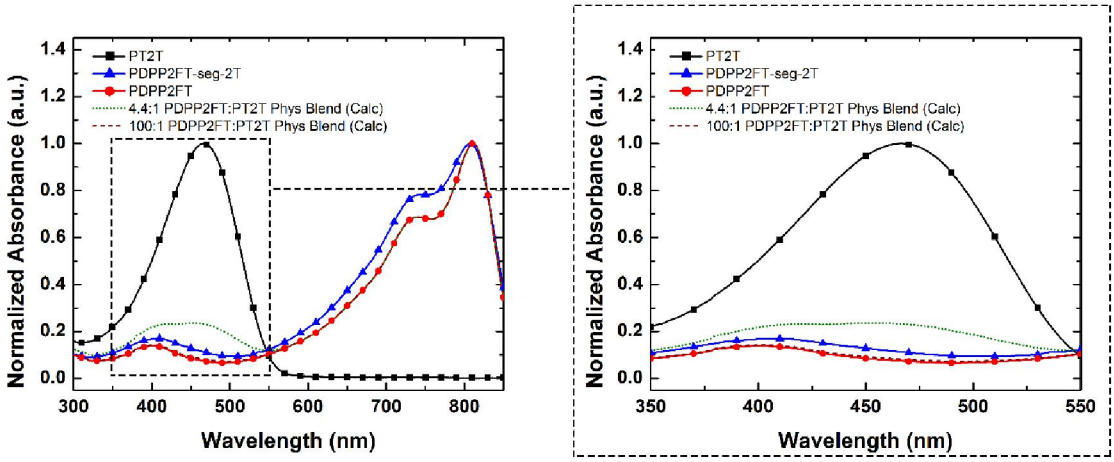

Figure B.2. Normalized absorption spectra of solutions of the pure polymers discussed in this paper. Measurements were made at a concentration of 1×10^{-5} M. Calculated absorption spectra of 4.4:1 and 100:1 physical blends of PDPP2FT:PT2T were superimposed onto the graph. The physical blend absorption spectra were calculated from the extinction coefficients of the pure polymers. The region from 350–550 nm is expanded to show the effect of PT2T contamination in PDPP2FT. The increase in absorption by a blend with a ratio of 100:1 PDPP2FT:PT2T over pure PDPP2FT is imperceptible in the absorbing region of PT2T. However, when the ratio of PDPP2FT:PT2T is decreased to 4.4:1 (the ratio in PDPP2FT-seg-2T as determined by NMR), there is a noticeable increase in absorption. The absence of this increased absorption in the PDPP2FT-seg-2T suggests that the segments are covalently bound and not simply a physical blend of the two components.

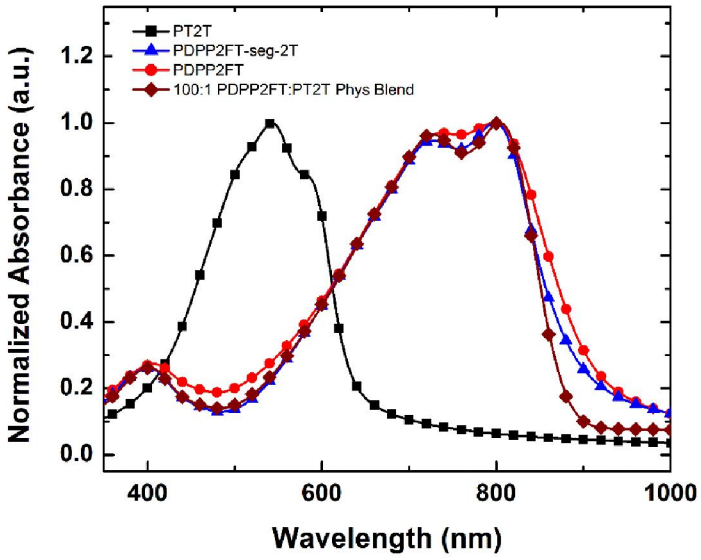

Figure B.3. Normalized absorption of thin films discussed in this paper with a 100:1 physical blend of PDPP2FT:PT2T superimposed on top. The physical blend matches the absorption of the pure PDPP2FT thin film well, which suggests that minor contamination of PT2T in PDPP2FT does not greatly affect the absorption in the solid state.

B.3. *PCE* vs. E_f of polymers (including 100:1 PDPP2FT:PT2T physical blend)

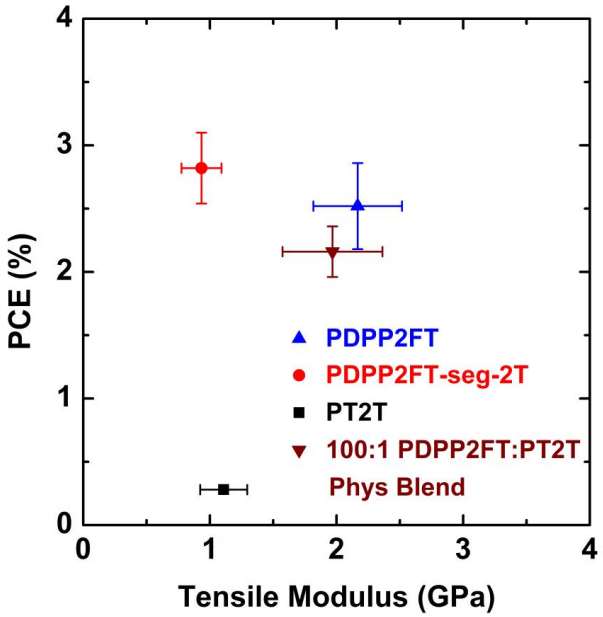

Figure B.4. Plot of the power conversion efficiency of 1:2 blends of the polymer:$PC_{61}BM$ as a function of the tensile modulus of the pure polymer. The PCE of the physical blend is 2.16 ± 0.2 % and the tensile modulus is 1.97 ± 0.39 GPa.

Table B.1. Tensile moduli of pure polymer films spin-coated from chloroform and 1:2 polymer:$PC_{61}BM$ films spin-coated from 4:1 $CHCl_3$:ODCB. The tensile modulus of the physical blend is within error of the pure PDPP2FT.

Polymer	Tensile Modulus (GPa)	
	Pure polymer ($CHCl_3$)	1:2 Polymer:$PC_{61}BM$ (4:1 $CHCl_3$:ODCB)
PDPP2FT	2.17 ± 0.35	2.76 ± 0.77
PDPP2FT-seg-2T	0.93 ± 0.16	1.60 ± 0.14
PT2T	1.11 ± 0.19	1.60 ± 0.36
100:1 PDPP2FT:PT2T physical blend	1.97 ± 0.39	—

B.4. Photovoltaic characteristics of 1:2 polymer:$PC_{61}BM$ devices (including 100:1 PDPP2FT:PT2T physical blend)

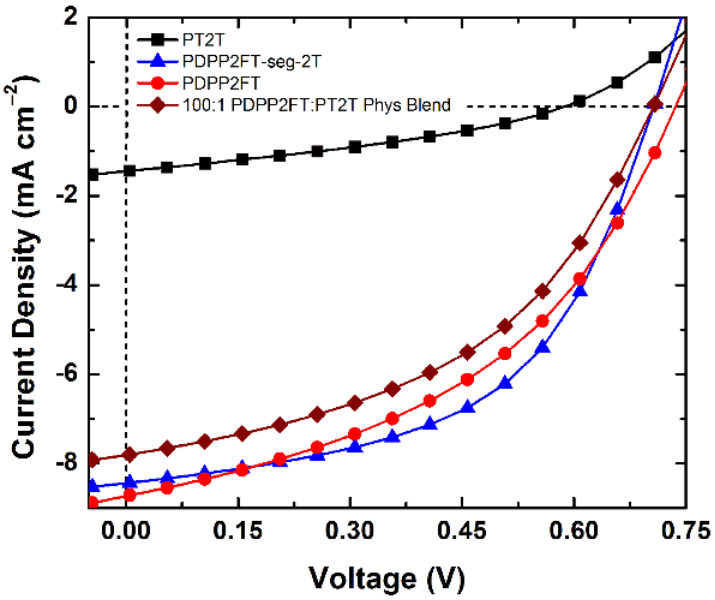

Figure B.5. Photovoltaic characteristics of representative samples of polymer-fullerene blends including a device fabricated with an active layer of 100:1 PDPP2FT:PT2T (and fullerene) physical blend. The *J-V* curve of the physical blend is most similar to the curve of pure PDPP2FT:$PC_{61}BM$.

Table B.2. Summary of the figures of merit for the solar cells fabricated in this work. The photoactive layers comprised a 1:2 polymer:$PC_{61}BM$ blend. In addition to the devices shown in **Table 4.2** of the manuscript, we have also included the figures of merit for solar cells fabricated with an active layer of 100:1 PDPP2FT:PT2T (and fullerene) physical blend. The J_{sc} and η_{ε} are lower than the PDPP2FT:$PC_{61}BM$, although the V_{oc} and *FF* are comparable.

Polymer	***n***	J_{sc} **[mA cm^{-2}]**	V_{oc} **[mV]**	***FF*** **[%]**	η_{ε} **[%]**
PT2T	3	1.5 ± 0.1	579 ± 21	32.9 ± 1.1	0.28 ± 0.01
PDPP2FT-seg-2T	6	8.4 ± 0.5	699 ± 23	48.2 ± 3.3	2.82 ± 0.28
PDPP2FT	7	8.3 ± 0.5	715 ± 25	42.5 ± 3.6	2.52 ± 0.34
100:1 PDPP2FT:PT2T Phys Blend	7	6.8 ± 0.5	710 ± 4	44.6 ± 1.5	2.16 ± 0.20

Appendix C

Photoresist-Free Patterning by Mechanical Abrasion of Water-Soluble Lift-Off Resists and Bare Substrates: Toward Green Fabrication of Transparent Electrodes

Adam D. Printz, Esther Chan, Celine Liong, René S. Martinez, and Darren J. Lipomi

Department of NanoEngineering, University of California, San Diego, 9500 Gilman Drive, Mail Code 0448, La Jolla, Ca, 92093-0448

Abstract

This paper describes the fabrication of transparent electrodes based on grids of copper microwires using a non-photolithographic process. The process—"abrasion lithography"—takes two forms. In the first implementation (Method I), a water-soluble commodity polymer film is abraded with a sharp tool, coated with a conductive film, and developed by immersion in water. Water dissolves the polymer film and lifts off the conductive film in the unabraded areas. In the second implementation (Method II), the substrate is abraded directly by scratching with a sharp tool (*i.e.*, no polymer film necessary). The abraded regions of the substrate are recessed and roughened. Following deposition of a conductive film, the lower profile and roughened topography in the abraded regions prevents mechanical exfoliation of the conductive film using adhesive tape, and thus the conductive film remains only where the substrate is scratched. As an application, conductive grids exhibit average sheet resistances of 17 Ω sq^{-1} and transparencies of 86% are fabricated and used as the anode in organic photovoltaic cells in concert with the conductive polymer, poly(3,4-ethylenedioxythiophene):poly(4-styrenesulfonate) (PEDOT:PSS). Compared to devices in which PEDOT:PSS alone serves as an anode, devices comprising grids of copper/nickel microwires and PEDOT:PSS exhibit lowered series resistance, which manifests in greater fill factor and power conversion efficiency. This simple method of forming micropatterns could find use in applications where cost and environmental impact should be minimized, especially as a potential replacement for the transparent electrode indium tin oxide (ITO) in thin-film electronics over large areas (i.e., solar cells) or as a method of rapid prototyping for laboratory-scale devices.

C.1 Introduction

Transparent electrodes are essential components of virtually all displays, touch screens, and thin-film photovoltaic devices. The global market for transparent electrodes is expected to grow from $2 billion in 2012[1] to at least $10 billion by 2016.[2] Thin-film solar installations, in particular, will likely expand the market for transparent electrodes even further in the near future. Indium tin oxide (ITO) comprises ninety percent of the global market. Indium, however, has an abundance in the Earth's crust of 0.05 ppm, and its cost has risen an order of magnitude over the past decade.[3] The imminent scarcity of indium has fueled an enormous amount of research on potential replacements for ITO for large-area and laboratory-scale optoelectronic devices. Prominent examples of next-generation materials include carbon nanotubes[4,5] and graphene,[6] silver nanowires,[7,8] and printed metallic grids produced by high-resolution photolithography or nanoimprint lithography.[9] Many of these materials suffer from high energies of production, use of proprietary materials, or natural abundances as low as that of indium (*e.g.*, silver). A transparent electrode can only comprise a fraction of the cost of a thin-film photovoltaic module, which, according to the analysis by Lewis and Nocera, may only be $10 m^{-2} in total to compete with fossil fuels for primary energy.[10] Any method of producing transparent electrodes for thin-film photovoltaic devices must be manufacturable on the scale of thousands of square kilometers for approximately the cost of paint.[11]

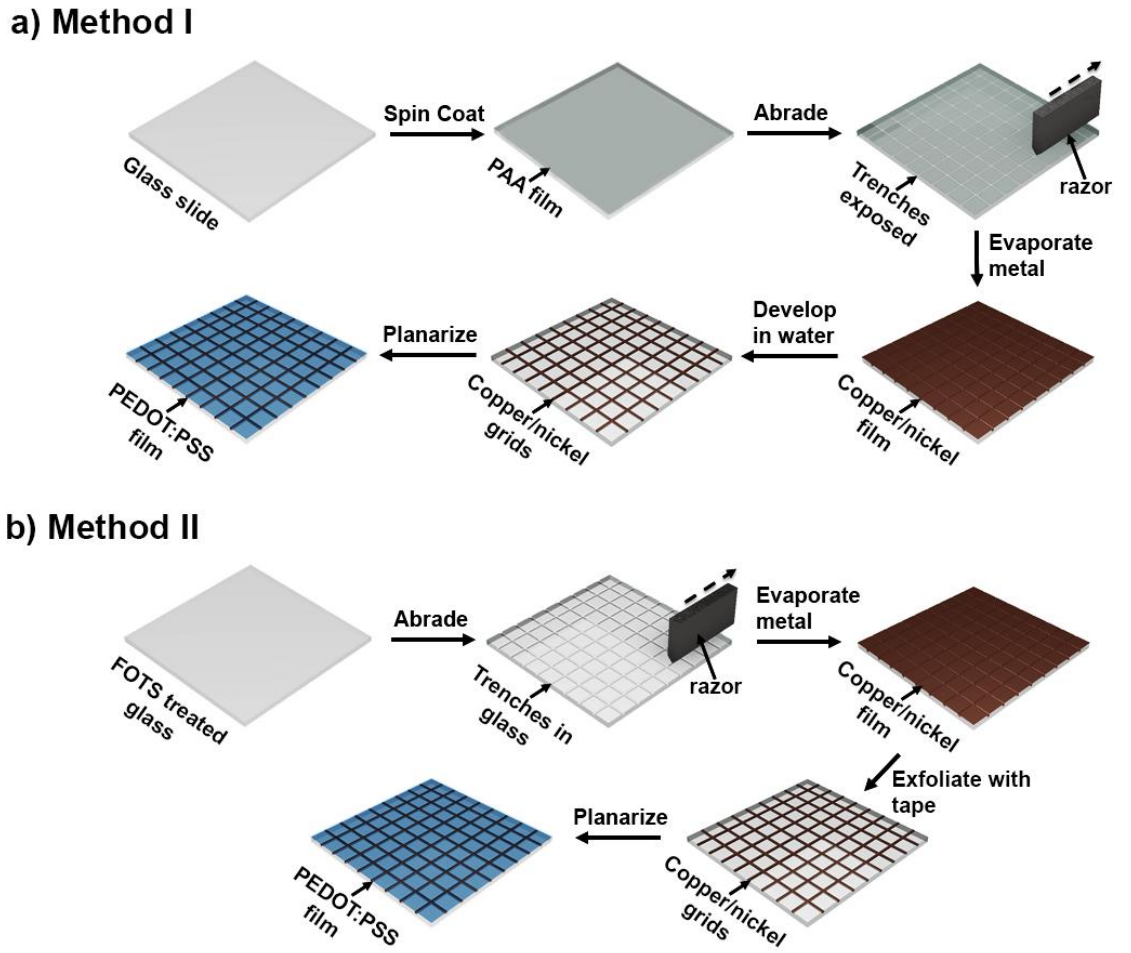

Figure C.1. Schematic diagrams summarizing the two implementations of abrasion lithography. (a) Method I uses mechanical abrasion with a sharp tool to pattern water-soluble thin films. (b) Method II produces patterns by direct abrasion of glass substrates.

Our goal was to generate functional micropatterns for transparent electrodes using an extremely simple method and the greenest, least expensive materials possible. We describe an approach to micropatterning at whose core is mechanical abrasion of surfaces followed by lift-off in the unabraded regions. We have nicknamed the process "abrasion lithography." Abrasion lithography can be used in one of two ways. In the first method (Method I, **Figure C.1a**), a sharp tool was used to scratch furrows in a water-soluble commodity polymer, which behaved as a lift-off resist. Following blanket deposition of a

thin conductive film, the substrate was immersed in water, the commodity polymer dissolved, and the conductive film remained on the surface only in the abraded regions. In the second method (Method II, **Figure C.1b**), the substrate was abraded directly, with no lift-off resist needed. Blanket deposition of a thin conductive film left material in the recessed furrows created by the abrasion. Lift-off of the unabraded areas with adhesive tape again created conductive patterns defined by the mechanical patterning.

C.2 Background

Transparent electrodes. Transparent electrodes fall roughly into two categories, those comprising contiguous films of conductive materials that are partially transmissive to optical wavelengths when sufficiently thin, and those comprising percolated networks of high-aspect-ratio conductive particles. Prominent examples of contiguous films exhibiting high transparency include tin-doped indium oxide (ITO), the conductive polymer poly(3,4-ethylenedioxythiophene):poly(styrene sulfonate) (PEDOT:PSS),[12–15] ultrathin films of gold,[16] and single- or few-layer graphene.[6,17,18] Examples of percolated networks include films of carbon nanotubes,[19–21] solution-grown silver[22] and copper nanowires,[3,23,24] nanowires based on electrospun templates,[25,26] patterns created by the coffee ring effect,[27] and various implementations of microcontact printing[28,29] and nanoimprint lithography.[30,31] Deposition of reduced graphene oxide sheets onto a surface can also form percolated networks;[32] these films occupy a middle ground between the contiguous and percolated categories. Transparent electrodes exhibiting either a contiguous or percolated structure are not directly interchangeable in a given application. For example, while electrodes comprising percolated networks of particles may be used

in touch screens and certain types of displays, they generally need to be combined with films of the contiguous variety in order to inject or extract charge from devices in which the semiconductor has low mobility—*i.e.*, organic light-emitting devices and solar cells.[33]

"Energy cannibalism" refers to the inputs of energy required to generate additional energy.[34] An implicit goal of all research in renewable energy technologies should be to reduce the cumulative energy demand of the product during its manufacture.[35] While ultra-thin organic solar cells have the potential to be low-cost, low-energy solutions to the growing global demand for energy—in fact, they have the highest ratio of power-to-mass of any thin-film photovoltaic technology,[36] 10 W g^{-1}—the production energy of such a device is finite, and should be minimized. According to the analysis by Anctil et al., the largest single contributor to the cumulative energy demand of an organic solar cell is the transparent electrode.[35] Sputter-deposition of ITO on polyethylene terephthalate (PET) substrates represents 39%–50% of the production energy of polymer-fullerene and small-molecule-based solar cells.[35] The contribution of printing silver contacts adds an additional 8%–11% to the cumulative energy demand, while the contribution of PEDOT:PSS (present in essentially all organic solar cells) is negligible.[35] While the correlation is not perfect, production energy tends to scale with cost, and thus reducing the energy demand of the transparent electrodes and printed contacts should help meet the "double bottom line" possible with organic solar cells.[37] That is, to generate energy inexpensively using materials and processes that do not degrade the environment by their method of extraction or their production energy manifested in increased emissions of carbon dioxide. The goal of this research is to evaluate a potentially green and inexpensive alternative to depositing and patterning

conductive electrodes based on indium, silver, specialty chemicals such as photoresist, and processing using organic solvents.

C.3 Experimental design

C.3.1 Choice of copper

We chose to fabricate transparent electrodes based on copper wires because of its price and conductivity. After silver, copper is the second-most conductive element. At a price of roughly \$7 kg^{-1},[38] it is two orders of magnitude less expensive than silver or indium, and has been so since at least 1970.[39] Additionally, its abundance in the Earth's crust is 1000 times greater than that of either silver or indium,[40] which suggests the lower price of copper will remain intact for the foreseeable future. While copper micro- and nanostructures degrade in the ambient over time by oxidation, this characteristic is shared by silver.[24] By cladding copper structures with nickel, they can be protected from oxidation.[24]

C.3.2 Poly(acrylic acid) as water-soluble lift-off resist

We chose poly(acrylic acid) (PAA) for its ability to form thin films when coated from an aqueous solution, its brittleness (that is, its amenability to patterning by mechanical abrasion) and its ability to be crosslinked by divalent metal cations in anticipation of the need to process it orthogonally to other water-soluble materials.[41,42] PAA has the advantage of being a commodity polymer with an extraordinarily low cost (~\$1 kg^{-1}),[43] which is several orders of magnitude less expensive than photoresist based on poly(methyl methacrylate) (PMMA), diazonapthoquinone-novolac (DNQ-novolac), or

epoxy (*e.g.*, SU-8). Its developer, water, is the least expensive, most environmentally benign solvent available, and thus compares favorably to the solvents used to process the above photoresists: acetone, aqueous tetramethyl ammonium hydroxide (TMAH), and propylene glycol methyl ether acetate (PGMEA). PAA readily dissolves in non-potable water used in industrial processes, thus deionized water is not required.

C.3.3 Metallic grids as transparent electrodes

We believe that grids of metallic wires in a deterministic pattern have some advantages (as well as disadvantages) when compared to randomly deposited nanowires grown from solution. Metallic grids created by a single step have no potentially resistive junctions between wires and thus no requirement to weld them together to improve conductivity.[44] Grids, moreover, are automatically percolated and do not contain isolated structures or widowed termini that do not carry current but detract from the optical transmission. The theoretical conductivity and transparency is also easily calculated from the geometry.[45] The shortcomings of grids derived from an evaporated film are that they are not easily amenable to processing from solution and that deposition under vacuum is energy intensive. Vacuum metallization does not preclude large-scale production, however. For example, biaxially oriented polyethylene terephthalate (BoPET) is metallized by physical vapor deposition and is a ubiquitous, low-cost material for food packaging (e.g., potato chip bags), and can be obtained for (<\$1 m^{-2}).[46] Roll-to-roll evaporative processing and liftoff in the context of electrodes has been demonstrated with flexographic printing, however, the features had a much lower resolution (100 μm) than is attainable with abrasion lithography.[47] It may also be possible to develop solution-

based methods of blanket deposition of conductive particles that land in the regions patterned by abrasion and that do not detach upon dissolution of the PAA in water.[48]

C.3.4 Mechanical processing

The core of the project is the use of mechanical abrasion—*i.e.*, machining—to generate patterns inexpensively. Mechanical processing by scratching with a sharp tool could be replaced by stretching, intentional cracking, or other mechanical force intended to produce percolated networks of furrows.[49–51] We tested sharp metallic (steel razor blades) and relatively softer polymeric (polypropylene picnic knives) tools for abrasion. The advantage of steel razor blades was their narrow edge. The advantage of the polypropylene knives was that there was a reduced tendency to penetrate through the PAA film and scratch the substrate. We chose these tools on the basis of cost and we are certain that purpose-fabricated cutting tools would produce a significantly higher pitch and resolution than we were able to achieve with the simple, commercial tools we chose.

C.3.5 Application in organic solar cells

As an application to evaluate the utility of mechanical abrasion as a lithographic tool, we fabricated copper grids as transparent electrodes for organic solar cells. We chose to use devices based on a bulk heterojunction of poly(3-hexylthiophene):[6,6]-phenyl C_{61} butyric acid methyl ester (P3HT:PCBM) due to its prominence in the literature.[52] We used PEDOT:PSS as a hole-transporting layer and eutectic gallium-indium as a low-work-function top electrode.[53] We found that PEDOT:PSS, when spin-coated directly on top of the grids, degraded the copper, and thus found it necessary to

evaporate a layer of nickel to protect the copper from damage. This concept was previously demonstrated by Rathmell et al. in a one-pot synthesis of cupronickel nanowires, which exhibited resistance to oxidation in ambient air.[24]

C.4 Experimental methods

C.4.1 Materials

Glass substrates were 7.5 mm × 5.0 mm × 1.0 mm microscope slides obtained from Premiere. Poly(acrylic acid) (PAA) was purchased as a 25 wt% solution in water from Alfa Aesar. PEDOT:PSS (Clevios PH1000) was purchased from Heraeus. The solid content of the PH 1000 solution was 1–1.3% and had a ratio of PEDOT to PSS of 1:2.5 by weight. (Tridecafluoro-1,1,2,2,-tetrahydrooctyl)-trichlorosilane (FOTS) was purchased from Gelest. Zonyl FS-300 (Zonyl), dimethyl sulfoxide (DMSO), ortho-dichlorobenzene (ODCB), poly(3-hexylthiophene) (P3HT), [6,6]-phenyl C_{61} butyric acid methyl ester (PCBM, >99%), and eutectic gallium-indium (EGaIn, ≥99.99%) were purchased from Sigma-Aldrich and used as received. All other solvents were purchased from Fisher Scientific or VWR International and used as received. Leitsilber 200 silver paint was purchased from Ted Pella and used as received.

C.4.2 Preparation of substrates

Glass slides were cleaned with Alconox solution (2 mg mL^{-1}), deionized water, acetone, and then isopropyl alcohol (IPA) in an ultrasonic bath for 10 min each and then rinsed and dried with compressed air. Next, the glass was plasma treated at ~30 W for 3 min at a base pressure of 200 mtorr ambient air to remove residual organic material and

activate the surface. For samples patterned by Method I, a solution of 6 wt% PAA in 18 wt% water and 76 wt% IPA was spin coated onto the glass slides at a speed of 2000 rpm (500 rpm s^{-1} ramp) for 60 s. These conditions produced a film of PAA with a thickness of ~400 nm (as measured by stylus profilometry). For samples patterned by Method II, the slides were placed in a vacuum desiccator with a glass vial containing ~100 μL of FOTS and put under house vacuum for a minimum of 3 h to passivate the surface.

C.4.3 Scoring process

We then scored the samples with a steel razor (Method I and II) or polypropylene knife (Method I only). Scoring was done by hand using a purpose-built linear motorized stage with an attached acrylic straight edge (which was used like a draftsman's T-square). The limit of the pitch is determined by the resolution of the linear motorized stage. For our experiments the apparatus permitted scratching of parallel grid lines in increments ≥100 μm. A similar apparatus which has a resolution of 500 μm could be built for ~$500, which is reasonable for laboratory-scale rapid prototyping. For this set of experiments, the film was scored with a pitch of 500 μm with the razors and 2000 μm with the polypropylene knives. While scoring with the razor in Method I, we found it difficult to prevent the razor from scratching the glass substrate beneath the water-soluble film. After scoring the entire surface in one direction, the glass was rotated 90° and then scored again to create a grid of orthogonal lines. A new scoring tool (steel razor or polypropylene knife) was used for each sample to improve repeatability of the procedure. After scoring, excess debris was blown from the substrate using a stream of compressed air. To estimate the pressure applied while scoring, we secured a sample to a balance and scored the

samples with a razor or polypropylene knife. We obtained the pressure by dividing the force measured by the balance by the area of the cutting tool in contact with the sample as measured by SEM.

C.4.4 Deposition of films

After scoring the water-soluble resist (Method I) or the glass substrate (Method II), we evaporated copper (50 nm) and nickel (10 nm) onto the surface by electron-beam evaporation. For the samples produced by Method I, the microwire grids were developed by immersion in water. To increase the diffusion of water into the water-soluble layer, ultrasonication in a water bath for at least 10 min was generally required. The remaining water-soluble layer and excess metallic film was subsequently removed by rinsing with water. For the samples produced by Method II, the microwire grids were developed by exfoliation with Scotch tape. To ensure the tape contacted the entire film surface, gentle pressure was applied with a pair of tweezers.

C.4.5 Optical transparency of copper/nickel microwire grids

The optical transparency (%T) was measured using a PerkinElmer Lambda 1050 UV-vis-NIR spectrophotometer. The wavelength range measured was 850-350 nm with a step size of 5 nm. Blank glass slides were cleaned and plasma treated under the same conditions as slides for sample preparation.

C.4.6 Sheet resistance (R_s) measurements

We measured electrical resistance by isolating rectangular strips (w = 0.5 cm, l ~

1–2 cm) from the microwire grids using a diamond scribe. We painted silver contacts on the termini of each rectangular strip. The resistance of the electrodes was measured using a Keithley 2400 SourceMeter. We measured the distance from the leading edge to leading edge of the silver paint electrical contacts with a caliper and calculated the R_s according to the relationship $R_s = R \times \frac{w}{l}$, where w and l were the widths and lengths of the rectangular regions of the microwire grids.

C.4.7 Imaging

Optical micrographs were taken using a Zeiss Axio Fluorescence Microscope. The widths of the copper/nickel microwires were calculated using the measurement tool in Adobe Photoshop. Due to the line-edge roughness, each wire was measured at seven different points (selected arbitrarily). Atomic Force Microscopy (AFM) micrographs were taken using a Veeco Scanning Probe Microscope in tapping mode. Data was analyzed with NanoScope Analysis v1.40 software (Bruker Corp.). The samples observed in AFM were 1 cm^2 cut by diamond-tipped scribe from larger glass slides after the scoring process. To remove glass debris from the surfaces, the samples for AFM were ultrasonicated in IPA for 10 min and subsequently rinsed with additional IPA and dried using compressed air. Scanning electron microscope (SEM) micrographs of the scoring tools were performed using a FEI XL30-SFEG SEM at 5 kV.

C.4.8 Fabrication of organic solar cells

We placed the developed grids in a glass container filled with IPA and then

placed the containers in a bath ultrasonicator for 20 min to remove accumulated debris. The samples were then rinsed with IPA and dried with compressed air. We subsequently deposited the PEDOT:PSS layer for both the electrodes with and without microwire grids from an aqueous solution containing 92.1 wt% Clevios PH 1000 (~0.9-1.2 wt% PEDOT:PSS), 6.9 wt% DMSO, and 1 wt% Zonyl. The concentration of DMSO was reported to be optimal for solar cell fabrication,[54] and the zonyl was added to increase the conductivity of the PEDOT:PSS.[13] The solution was filtered with a 1 μm glass microfiber (GMF) syringe filter and then spin coated at a speed of 500 rpm (100 rpm s^{-1} ramp) for 60 s, followed by 2000 rpm (750 rpm s^{-1} ramp) for 60 s, which resulted in a layer 200 nm thick. The samples were subsequently dried at 150 °C for 30 minutes under a Pyrex petri dish covered in aluminum foil to reduce dissipation of heat and to prevent dust from landing on the samples. After 30 min of drying, the samples were left to cool to room temperature for 30 minutes while still covered on the hotplate.

The photoactive layer was deposited from a solution of 1:1 by weight P3HT and PCBM in ODCB (40 mg mL^{-1}), which was stirred overnight and filtered in a 0.20 μm poly(tetrafluoroethylene) (PTFE) syringe filter. The solution was then spin coated onto the electrode layer at a speed of 500 rpm (100 rpm s^{-1} ramp) for 240 s, followed by 2000 rpm (750 rpm s^{-1} ramp) for 60 s; these conditions produced a layer 230 nm thick. A thin strip of the microwire grid/PEDOT:PSS electrode was exposed by wiping away some of the P3HT:PCBM film with chloroform so that electrical contact could be made. The samples were then immediately placed in a nitrogen-filled glovebox and annealed at 125 °C for 30 min under a Pyrex petri dish covered in aluminum foil. The substrates were then allowed to cool slowly to room temperature. To minimize exposure to ambient air

by transferring devices into and out of an evaporator in a different building, EGaIn (extruded by hand from a syringe) was used as the top contact.[55,56]

C.4.9 Photovoltaic characterization of organic solar cells

The photovoltaic properties were measured in a nitrogen-filled glovebox using a solar simulator with a 100 mW cm^{-2} flux that approximated the solar spectrum under AM 1.5G conditions (ABET Technologies 11016-U up-facing unit calibrated with a reference cell with a KG5 filter). The current density versus voltage was measured for both dark and under illumination using a Keithley 2400 SourceMeter.

C.5 Results and discussion

C.5.1 Grids produced by abrasion of water-soluble lift-off resist (Method I)

We successfully generated grids using both Method I and Method II. **Figure C.2a** shows a photograph that demonstrates the transparency of grids produced by Method II. The transparency is due to the thinness of the microwires relative to their pitch as shown in **Figure C.2b. Figure C.3a** shows a junction of copper microwires produced by scoring PAA films on glass substrates with steel razor blades. The minimum linewidth we were able to achieve was 11 μm (average linewidth was 29 ± 10 μm, N = 839, as determined by measurement of optical micrographs in Adobe Photoshop) using a razor blade with an initial edge width of less than 1 μm. From the optical micrograph in **Figure C.3a**, it is apparent that the steel razor blades also abraded the surface of the glass beneath the PAA film. We confirmed this observation by AFM (**Figure C.4**). The abrasion in the glass surface by the steel razor blades appeared to introduce substantial roughness in the

abraded regions. When measured by AFM, we found the abraded regions to have a root mean square roughness of ~10 nm compared to ~1 nm in the unabraded regions. The roughness in the abraded regions translates to the wires in the electrodes because evaporative metal deposition is a vertically conformal process. However, this surface roughness is much smaller than the height of the wires, so it is unlikely to be significantly detrimental to performance. (We exploited this roughening of the glass with direct abrasion of the glass substrates in Method II.) We also explored polymeric cutting tools. We tested the performance of a polypropylene picnic knife whose edge had a radius of curvature of approximately 40 μm, as determined by scanning electron microscopy. **Figure C.3b** shows a junction of copper wires produced using this cutting tool, which have a minimum linewidth of 246 μm (the average linewidth was 346 ± 45 μm, N = 840). The amount of pressure with the razor was estimated to be 2–11 GPa after the first score ("cycle"); the maximum pressure of the first score was estimated to be on the order of 150 GPa assuming that the blade edge was the width of a new blade; because the edge of the blade dulled with each cycle, however, this estimate was likely high (dulling is discussed below). The pressure applied by the polypropylene knife was estimated to be 80-140 kPa, which we calculated with the assumption that only one of the serrated teeth was in contact with the substrate at any given time.

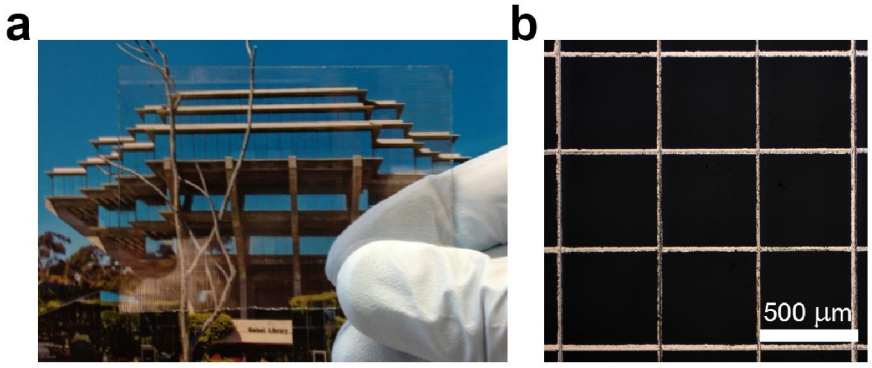

Figure C.2. Images of transparent electrodes fabricated by abrasion lithography. (a) Photograph showing the high transparency of grids produced by Method II. A reflection in the bottom left corner of the glass substrate shows the copper wires. (b) Optical micrograph showing the wires produced by Method II.

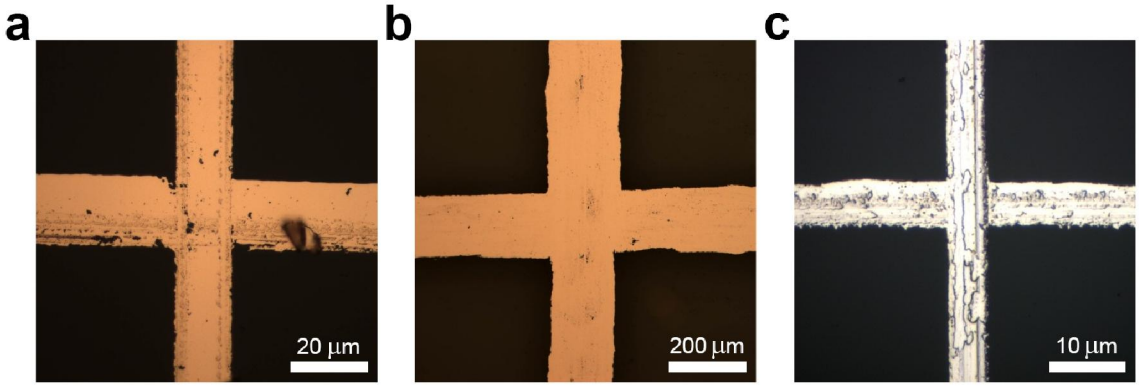

Figure C.3. Optical micrographs of junctions of copper and copper/nickel microwires. (a) A microwire junction fabricated by Method I. Surface roughness caused by the razor inadvertently abrading the substrate is apparent. (b) A microwire junction fabricated by patterned a PAA film with a polypropylene picnic knife, which was too soft to abrade the glass substrate, and thus the microwires appear to have a smoother topography. (c) A microwire junction patterned by direct abrasion of glass by a steel razor. Significant roughness generated by the razor is clearly visible.

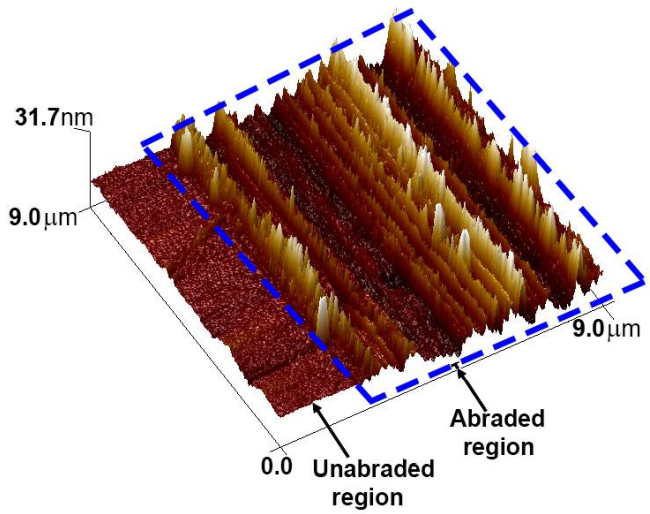

Figure C.4. 3D AFM image of glass after scoring using a steel razor. The abraded region has been roughened by the steel razor blade, while the unabraded region is relatively flat.

C.5.2 Grids produced by direct abrasion of the substrates (Method II)

During the course of developing Method I, we made the serendipitous discovery that the water-soluble lift-off resist was not necessary to produce conductive grids, and that the copper microwires patterned by direct abrasion of the substrate (Method II) could be of thinner linewidth than those produced by Method I. **Figure C.3c** shows a junction produced by direct abrasion of a glass substrate using a steel razor blade, blanket deposition of copper/nickel, and lift-off from the unabraded areas using Scotch tape. The minimum linewidth achieved was less than 5 μm (average linewidth was 17 ± 4 μm, N = 70). While the mechanism of Method I is analogous to a lift-off process in conventional lithography, the primary mechanism of Method II appears to be based, in order of importance, on three effects. The first effect is the inability of the adhesive tape to penetrate into the recessions in the substrate created by the razor blade. This supposition is supported by the observation that thicker copper films (>100 nm) lift off in the abraded

regions. The second effect is the increased roughness of the abraded regions, which increases the van der Waals force per unit area between the glass and the copper. The third effect is the scratching away of the fluorinated alkyl silane, which was used to passivate the glass in the unabraded regions to facilitate lift-off with tape.

We observed dulling of the razor blades when used on a glass substrate in both Methods I and II. After the first cycle, the razor dulled from an edge width of less than 1 μm to 10 μm; after 100 cycles, the edge width was approximately 45 μm (**Figures C.5a**, **b**). We believe applying lower pressure using an automated apparatus or using a cutting tool made of a harder material could minimize dulling. Purpose-made cutting tools composed of harder materials such as tungsten carbide or diamond would likely degrade at a much slower rate than the steel razors we evaluated.

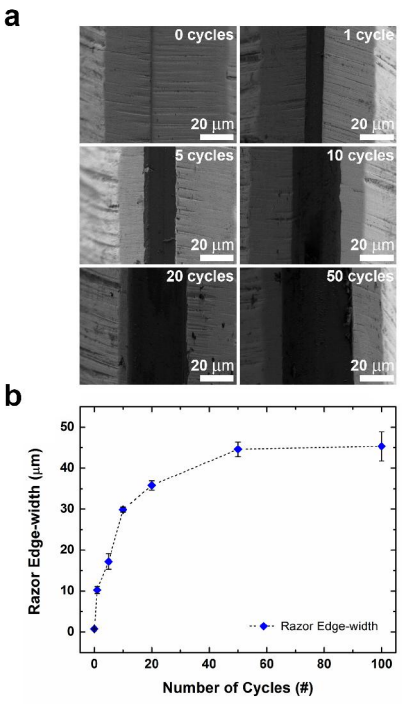

Figure C.5. Dulling of cutting tools. (a) SEM micrographs showing the progression of the dulling of a razor used in Method II, from out of box to 50 cycles. (b) The dulling of the razor plateaus at around 50 cycles.

C.5.3 Performance of copper grids as transparent electrodes

Table C.1 summarizes the pitch, linewidth, and experimental and theoretical sheet resistance, transparency, and figure-of-merit of the grids of the types depicted in **Figure C.3**. We calculated the theoretical transparency according to equation 1,

$$T = \frac{(P - L)^2}{P^2} \qquad (\mathbf{1})$$

where T is the transparency of the sample, P is the pitch of the microwire grid, and L is the average linewidth of the microwires. The theoretical sheet resistance was calculated according to the method used by Catrysse and Fan,[45]

$$R_s = \left(\frac{\rho}{t}\right) \times \left(\frac{P}{L}\right) \qquad (\mathbf{2})$$

where ρ and t are the resistivity and the thickness of the copper, respectively. We took the resistivity to be that of bulk copper, 16.8 x 10^{-9} Ω m. The figure-of-merit (FOM) was calculated according to equation 3,

$$\frac{\sigma_{dc}}{\sigma_{op}} = \frac{188}{R_s\left(\frac{1}{T^{1/2}} - 1\right)} \qquad (\mathbf{3})$$

where σ_{dc} is the dc conductivity and σ_{op} is the optical conductivity. Based on the FOM, the best devices were obtained by Method I using the polypropylene knife to pattern the films.

Deviations of the experimental sheet resistance from the theoretical sheet resistance were caused predominantly by line-edge roughness for the samples prepared by Method I and poor junctions for the samples prepared by Method II. Because these samples were made by hand, there was variability introduced by inconsistently applied pressure from cycle to cycle. The effects of these inconsistencies include breaks in

individual wires and poor junctions, as well as significant line-edge roughness. An additional explanation for breaks in the wires and poor junctions for samples prepared by Method I is a failure to completely clear the furrows of water-soluble resist. This was likely an effect of the vibrations introduced by manual scoring. For Method II, the inconsistent pressure applied by manual scoring caused variations in the depths of furrows. In some areas, the furrows were not large enough to protect the metal from exfoliation by the adhesive tape. We believe that automation of these processes would resolve these problems, in part, and thus we believe the FOM could be substantially improved as well. The calculated FOMs based on the geometry of our grids in **Table C.1** suggest that improvement should be possible.

Table C.1. Summary of the pitch, linewidth, experimental and calculated sheet resistance, transparency, and figure-of-merit of the grids of the types depicted in **Figure C.3.** Figures of merit were calculated from the average transparency and R_s.

Material		Pitch (μm)	Linewidth (μm)	Expl. Sheet Resistance (Ω sq^{-1})	Calc. Sheet Resistance (Ω sq^{-1})	Expl. Transparency (%)	Calc. Transparency (%)	Calc. Figure of Merit	Expl. Figure of Merit
PEDOT:PSS		–	–	86 ± 7	–	88.0 ± 0.3	–	33	–
Water-soluble resist, plastic knife patterned	**w/o PEDOT:PSS**	2000	346 ± 45	5.7 ± 1.6	1.93	68.7 ± 4.4	68.4	160	465
	w/ PEDOT:PSS	2000		9.9 ± 5.2	–	63.9 ± 5.2	–	76	–
Water-soluble resist, razor patterned	**w/o PEDOT:PSS**	500	29 ± 10	17 ± 7	5.76	86.2 ± 3.9	88.7	140	530
	w/ PEDOT:PSS	500		68 ± 63	–	78.0 ± 3.7	–	21	–
Direct abrasion w/razor	**w/o PEDOT:PSS**	500	17 ± 4	59 ± 40	9.8	88.5 ± 3.0	93.3	50	544

It is worth noting the increase in R_s with the addition of the PEDOT:PSS planarizing layer. This observation suggests that oxidation of the copper microwires, most likely by the sulfonic acid present in PEDOT:PSS, lowered the conductivity of the grids. This oxidation likely occurs through gaps in the microwire surface that are left unprotected by the nickel due to the surface roughness and directional nature of

evaporative deposition. We believe that this problem could be resolved by a conformal deposition process, such as sputter-coating or electroless plating with nickel.[24] (It should be noted that while a planarizing layer such as PEDOT:PSS is necessary to facilitate efficient charge collection for organic photovoltaics, it is not necessary in other applications for transparent electrodes such as touchscreens.) We calculated FOM values of metallic grid electrodes with PEDOT:PSS assuming that there was no oxidation of the electrodes.

The FOMs of grids produced by Method I were 160 and 140 for the water-soluble resist patterned by polypropylene knife and steel razor, respectively. This FOM was lower than, but still of the same order of magnitude of commercially available ITO, which had been reported to have a FOM between 400-800.[57] The theoretical FOMs in **Table C.1** suggest that if defects are minimized, the grids with the current geometry should be able to perform similarly to ITO, with FOMs of 465 (polypropylene knife patterned) and 530 (steel razor patterned) at a greatly reduced cost. With PEDOT:PSS added, due to a reduction in transparency, these FOMs drop slightly to 337 and 248 for the polypropylene knife patterned and the steel razor patterned, respectively. These values compared favorably with copper/nickel nanowire networks (transparency of 84%, R_s of 60 Ω sq^{-1}, and FOM ~34),[24] carbon nanotube networks (transparency of 90.1%, R_s of 60 Ω sq^{-1}, and FOM ~59),[20] and graphene (transparency of 90%, R_s of 30 Ω sq^{-1}, and FOM ~116).[58] Silver nanowire networks (transparency of 75%, R_s of 3.4 Ω sq^{-1}, and FOM ~357),[57] copper networks fabricated by deposition onto electrospun polymer (transparency of 90%, R_s of 2 Ω sq^{-1}, and FOM ~1738),[26] and metallic (gold) grids fabricated by photolithography (theoretical reported transparency of 90%, R_s of

0.8 Ω sq^{-1}, and FOM ~4344)[45] either performed as well or better than the electrodes reported here, but there are significant disadvantages to each of these fabrication methods. The FOM of transparent electrodes comprising of silver nanowire networks is partially limited by junction resistance.[44] Conversely, the electrodes produced by our methods can have contiguous junctions. Electrospinning is currently less scalable than the abrasion lithography methods, and abrasion lithography may have advantages over photolithography for laboratory-scale fabrication and possibly ultimately for large-area applications.

C.5.4 Performance of grids in organic solar cells

To evaluate the potential of grids produced by abrasion lithography to improve the performance of organic photovoltaic devices, we fabricated devices by depositing grids consisting of copper (50 nm) and nickel (10 nm) produced by Method I, PEDOT:PSS, P3HT:PCBM, and a top electrode of eutectic gallium indium (EGaIn). **Figure C.6a** shows plots of the average current density vs. voltage (*J-V*) of devices with and without grids ("small" device areas, ~0.1cm^2). The control samples (PEDOT:PSS only) and the samples with grids patterned by steel razor performed similarly. The average short circuit current (J_{sc}) for the control cells was 6.7 ± 1.4 mA cm^{-2} compared to 6.7 ± 1.3 mA cm^{-2} for cells with grids patterned by steel razor and 5.2 ± 1.3 mA cm^{-2} for cells with grids patterned by polypropylene knife. Additionally, the average open-circuit voltage (V_{oc}) for the control cells was 580 ± 14 mV compared to 570 ± 20 mV for the cells with grids patterned by steel razor and only 510 ± 40 mV for the cells with grids patterned by polypropylene knife. While the samples with grids patterned by steel razor

performed with the same efficiency as the control samples (1.9 ± 0.3% for the controls compared to 2.0 ± 0.3% for the cells with grids patterned by steel razor), the samples with grids patterned by polypropylene knives were about 0.6-0.7% less efficient. This effect is due to the reduced J_{sc} which we attribute to the lower transparency when compared to that of the control devices. The *J-V* curves of the cells with the highest measured efficiency (η_e) from the sample sets in **Figure C.6a** are plotted in **Figure C.6b**. These "hero" cells exhibit similar trends as the average values. Regardless of the patterning tool, the average device with grids had a reduced series resistance (R_{series}) when compared to the control devices. The average control cell had an R_{series} of 30 ± 6 Ω cm^2 compared to 20 ± 5 Ω cm^2 and 16 ± 9 Ω cm^2 for cells with grids patterned by steel razor and polypropylene knife, respectively. The reduction in R_{series} is directly attributable to the higher conductivity of copper when compared with PEDOT:PSS alone. We reasoned that with larger cells, the effect of lowered R_{series} of the devices with grids might allow them to outperform the devices without grids. To demonstrate this effect, we increased the size of the cells from ~0.1 cm^2 to ~0.5 cm^2. **Figure C.6c** shows the plots of the *J-V* curves of the larger cells with the highest η_e. This plot highlights the effect of the grids for large-area cells, namely reduced R_{series}, and increased fill factor (*FF*). We attribute the increase in *FF*, in part, to the reduced R_s of the transparent electrodes that contained grids along with PEDOT:PSS when compared to the PEDOT:PSS electrodes without grids. For these large-area cells, the *FF* of the representative PEDOT:PSS device dropped to 30% from 50% when compared with the representative smaller-area device, while the devices with the grids patterned by steel razor and by polypropylene knife only dropped to 37% from 47% and 48% from 53%, respectively. The most efficient of the

larger devices contained grids patterned by plastic picnic knives because the overall reduction in sheet resistance overcame the reduced J_{sc} due to attenuated absorption.

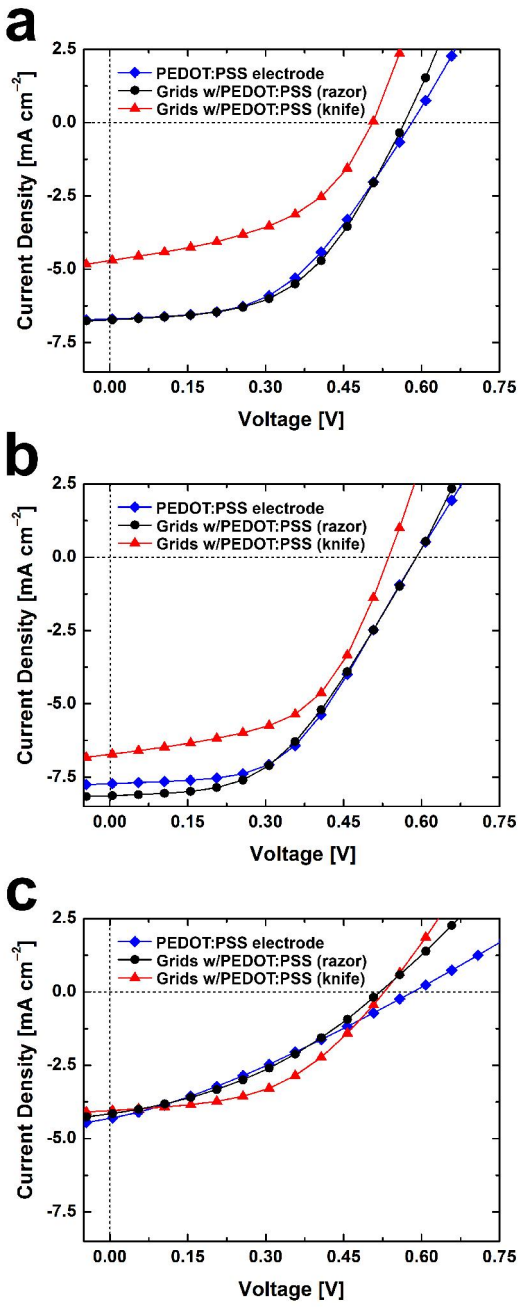

Figure C.6. *J-V* curves of P3HT:PCBM solar devices. (a) The average *J-V* curves for devices with transparent electrodes consisting of PEDOT:PSS (N = 7), PEDOT:PSS and grids patterned by polypropylene knife (N = 6), and PEDOT:PSS and grids patterned by steel razor (N = 4). (b) The *J-V* curves for the highest efficiency cells from the sample sets from (a). (c) The *J-V* curves for the highest efficiency larger cells (~0.5 cm^2 compared to ~0.1 cm^2 in (a) and (b)).

C.6 Conclusion

This paper described a simple method of fabricating grids of microwires using green, inexpensive materials. Like the use of biaxially pre-strained polymeric sheets (*i.e.*, the "shrinky-dink" method) for fabricating topographic masters for microfluidics,[59,60] the use of transparency masks for photolithography,[61] and the use of wax printing for paper-based diagnostics,[62] we believe that abrasion lithography could be a useful tool for low-cost and environmentally benign micro—and possibly nano—fabrication for rapid prototyping and generating simple patterns over large areas. The minimal tools required are methods of depositing polymeric and conductive films, and the minimal materials required are poly(acrylic acid) (the absorbent found in diapers and artificial snow) and steel razor blades (or polypropylene picnic knives). The ability to pattern by direct abrasion and exfoliation with adhesive tape (Method II) was unexpected, and may stimulate further research into low-cost methods of resist-free mechanical patterning for linewidths less than state-of-the-art. Abrasion lithography is conceptually and operationally simple and environmentally benign. While abrasion lithography as described in this paper is serial, it could be made parallel by fabricating scoring tools with multiple tips. Using multi-tipped scoring tools, abrasion lithography could become more scalable than is, for example, electrospinning, and produce better resolution than proven scalable processes like gravure printing.[63] It also presents advantages when compared to stencil masking because it is impossible to design a stencil mask whose negative areas form a crossbar geometry: the fabrication of grids from stencil masks would require two masking and deposition steps each, whereas abrasion lithography only requires one. Abrasion lithography is in principle compatible with a variety of substrates and methods

of deposition. Our initial implementation of abrasion lithography was to pattern by hand, but replacement of the manual processes with automated ones would improve the quality of the structures considerably. Roll-to-roll mechanical patterning of flexible substrates is in principle achievable and is an inviting target of future research. The goal of the project, moreover, was to demonstrate that simple processes and materials could often be used in place of sophisticated tools and specialty chemicals to generate electronic components—*i.e.*, transparent electrodes—whose figures of merit are at least of the same order of magnitude as the state-of-the-art.

Acknowledgements

This work was supported by laboratory startup funds from the University of California, San Diego. E. C. acknowledges a fellowship from the Calit2 Summer Undergraduate Research Scholars Program. The authors thank Suchol Savagatrup for helpful discussions, and Mare Ivana Diaz for help in preparing glass substrates.

Appendix C, in full, is a reprint of the material as it appears in *PLoS ONE*, 2013, 8, e83939. Adam D. Printz, Esther Chan, Celine Liong, René Martinez, and Darren J. Lipomi. The dissertation author was the primary investigator and author of this paper.

References

(1) Alcalde, B. H.; Kamp, B.; Zurutuza, A. Market Uptake of Graphene as a Disruptive Material. *P. IEEE* **2013**, *101*, 1793–1800.

(2) Dattoli, E. N.; Lu, W. ITO Nanowires and Nanoparticles for Transparent Films. *MRS Bull.* **2011**, *36*, 782–788.

(3) Rathmell, A. R.; Bergin, S. M.; Hua, Y.-L.; Li, Z.-Y.; Wiley, B. J. The Growth Mechanism of Copper Nanowires and Their Properties in Flexible, Transparent Conducting Films. *Adv. Mater.* **2010**, *22*, 3558–3563.

(4) Cao, Q.; Rogers, J. A. Ultrathin Films of Single-Walled Carbon Nanotubes for Electronics and Sensors: A Review of Fundamental and Applied Aspects. *Adv. Mater.* **2009**, *21*, 29–53.

(5) Wu, Z.; Chen, Z.; Du, X.; Logan, J. M.; Sippel, J.; Nikolou, M.; Kamaras, K.; Reynolds, J. R.; Tanner, D. B.; Hebard, A. F.; Rinzler, A. G. Transparent, Conductive Carbon Nanotube Films. *Science (80-.).* **2004**, *305*, 1273–1276.

(6) Kim, K. S.; Zhao, Y.; Jang, H.; Lee, S. Y.; Kim, J. M.; Kim, K. S.; Ahn, J.-H.; Kim, P.; Choi, J.-Y.; Hong, B. H. Large-Scale Pattern Growth of Graphene Films for Stretchable Transparent Electrodes. *Nature* **2009**, *457*, 706–710.

(7) Lee, J.-Y.; Connor, S. T.; Cui, Y.; Peumans, P. Solution-Processed Metal Nanowire Mesh Transparent Electrodes. *Nano Lett.* **2008**, *8*, 689–692.

(8) Madaria, A. R.; Kumar, A.; Zhou, C. Large Scale, Highly Conductive and Patterned Transparent Films of Silver Nanowires on Arbitrary Substrates and Their Application in Touch Screens. *Nanotechnology* **2011**, *22*, 245201.

(9) Kang, M.-G.; Kim, M.-S.; Kim, J.; Guo, L. J. Organic Solar Cells Using Nanoimprinted Transparent Metal Electrodes. *Adv. Mater.* **2008**, *20*, 4408–4413.

(10) Lewis, N.; Nocera, D. Powering the Planet: Chemical Challenges in Solar Energy Utilization. *Proc. Natl. Acad. Sci. USA* **2006**, *103*, 15729–15735.

(11) Lewis, N. S. Toward Cost-Effective Solar Energy Use. *Science (80-.).* **2007**, *315*, 798–801.

(12) Crispin, X.; Jakobsson, F. L. E.; Crispin, A.; Grim, P. C. M.; Andersson, P.; Volodin, A.; Haesendonck, C. Van; Auweraer, M. Van Der; Salaneck, W. R.; Berggren, M. The Origin of the High Conductivity of (PEDOT - PSS) Plastic Electrodes. *Chem. Mater.* **2006**, *18*, 4354–4360.

(13) Vosgueritchian, M.; Lipomi, D. J.; Bao, Z. Highly Conductive and Transparent PEDOT:PSS Films with a Fluorosurfactant for Stretchable and Flexible Transparent Electrodes. *Adv. Funct. Mater.* **2012**, *22*, 421–428.

(14) Kim, Y. H.; Sachse, C.; Machala, M. L.; May, C.; Müller-Meskamp, L.; Leo, K. Highly Conductive PEDOT:PSS Electrode with Optimized Solvent and Thermal Post-Treatment for ITO-Free Organic Solar Cells. *Adv. Funct. Mater.* **2011**, *21*, 1076–1081.

(15) Elschner, A.; Kirchmeyer, S.; Lövenich, W.; Merker, U.; Reuter, K. *PEDOT: Principles and Applications of an Intrinsically Conductive Polymer*; CRC, New York, 2010.

(16) Stec, H. M.; Williams, R. J.; Jones, T. S.; Hatton, R. A. Ultrathin Transparent Au Electrodes for Organic Photovoltaics Fabricated Using a Mixed Mono-Molecular Nucleation Layer. *Adv. Funct. Mater.* **2011**, *21*, 1709–1716.

(17) Wu, J.; Becerril, H. a.; Bao, Z.; Liu, Z.; Chen, Y.; Peumans, P. Organic Solar Cells with Solution-Processed Graphene Transparent Electrodes. *Appl. Phys. Lett.* **2008**, *92*, 263302.

(18) Choi, Y.-Y.; Kang, S. J.; Kim, H.-K.; Choi, W. M.; Na, S.-I. Multilayer Graphene Films as Transparent Electrodes for Organic Photovoltaic Devices. *Sol. Energy Mater. Sol. Cells* **2012**, *96*, 281–285.

(19) Hecht, D. S.; Hu, L.; Irvin, G. Emerging Transparent Electrodes Based on Thin Films of Carbon Nanotubes, Graphene, and Metallic Nanostructures. *Adv. Mater.* **2011**, *23*, 1482–1513.

(20) Hecht, D. S.; Heintz, A. M.; Lee, R.; Hu, L.; Moore, B.; Cucksey, C.; Risser, S. High Conductivity Transparent Carbon Nanotube Films Deposited from Superacid. *Nanotechnology* **2011**, *22*, 075201.

(21) Mirri, F.; Ma, A. W. K.; Hsu, T. T.; Behabtu, N.; Eichmann, S. L.; Young, C. C.; Tsentalovich, D. E.; Pasquali, M. High-Performance Carbon Nanotube Transparent Conductive Films by Scalable Dip Coating. *ACS Nano* **2012**, *6*, 9737–9744.

(22) Hu, L.; Kim, H. S.; Lee, J.; Peumans, P.; Cui, Y. Scalable Coating and Properties of Transparent, Flexible, Silver Nanowire Electrodes. *ACS Nano* **2010**, *4*, 2955–2963.

(23) Rathmell, A. R.; Wiley, B. J. The Synthesis and Coating of Long, Thin Copper Nanowires to Make Flexible, Transparent Conducting Films on Plastic Substrates. *Adv. Mater.* **2011**, *23*, 4798–4803.

(24) Rathmell, A. R.; Nguyen, M.; Chi, M.; Wiley, B. J. Synthesis of Oxidation-Resistant Cupronickel Nanowires for Transparent Conducting Nanowire Networks. *Nano Lett.* **2012**, *12*, 3193–3199.

(25) Wu, H.; Hu, L.; Rowell, M. W.; Kong, D.; Cha, J. J.; McDonough, J. R.; Zhu, J.; Yang, Y.; McGehee, M. D.; Cui, Y. Electrospun Metal Nanofiber Webs as High-Performance Transparent Electrode. *Nano Lett.* **2010**, *10*, 4242–4248.

(26) Wu, H.; Kong, D.; Ruan, Z.; Hsu, P.-C.; Wang, S.; Yu, Z.; Carney, T. J.; Hu, L.; Fan, S.; Cui, Y. A Transparent Electrode Based on a Metal Nanotrough Network. *Nat. Nanotechnol.* **2013**, *8*, 421–425.

(27) Layani, M.; Gruchko, M.; Milo, O.; Balberg, I.; Azulay, D.; Magdassi, S. Transparent Conductive Coatings by Printing Coffee Ring Arrays Obtained at Room Temperature. *ACS Nano* **2009**, *3*, 3537–3542.

(28) Geissler, M.; Wolf, H.; Stutz, R.; Delamarche, E.; Grummt, U.-W.; Michel, B.; Bietsch, A. Fabrication of Metal Nanowires Using Microcontact Printing. *Langmuir* **2003**, *19*, 6301–6311.

(29) Mondin, G.; Schumm, B.; Fritsch, J.; Grothe, J.; Kaskel, S. Fabrication of Micro- and Submicrometer Silver Patterns by Microcontact Printing of Mercaptosilanes and Direct Electroless Metallization. *Microelectron. Eng.* **2013**, *104*, 100–104.

(30) Kang, M.-G.; Xu, T.; Park, H. J.; Luo, X.; Guo, L. J. Efficiency Enhancement of Organic Solar Cells Using Transparent Plasmonic Ag Nanowire Electrodes. *Adv. Mater.* **2010**, *22*, 4378–4383.

(31) Chou, S. Y.; Ding, W. Ultrathin, High-Efficiency, Broad-Band, Ommni-Acceptance, Organic Solar Cells Enhanced by Plasmonic Cavity with Subwavelength Hole Array. *Opt. Express* **2013**, *21*, A60–A76.

(32) Becerril, H. A.; Mao, J.; Liu, Z.; Stoltenberg, R. M.; Bao, Z.; Chen, Y. Evaluation of Solution-Processed Reduced Graphene Oxide Films as Transparent Conductors. *ACS Nano* **2008**, *2*, 463–470.

(33) Kylberg, W.; de Castro, F. A.; Chabrecek, P.; Sonderegger, U.; Chu, B. T.-T.; Nüesch, F.; Hany, R. Woven Electrodes for Flexible Organic Photovoltaic Cells. *Adv. Mater.* **2011**, *23*, 1015–1019.

(34) Pearce, J. M. Thermodynamic Limitations to Nuclear Energy Deployment as a Greenhouse Gas Mitigation Technology. *Int. J. Nucl. Governance, Econ. Ecol.* **2008**, *2*, 113–130.

(35) Anctil, A.; Babbitt, C. W.; Raffaelle, R. P.; Landi, B. J. Cumulative Energy Demand for Small Molecule and Polymer Photovoltaics. *Prog. Photovolt Res. Appl.* **2013**, *21*, 1541–1554.

(36) Kaltenbrunner, M.; White, M. S.; Głowacki, E. D.; Sekitani, T.; Someya, T.; Sariciftci, N. S.; Bauer, S. Ultrathin and Lightweight Organic Solar Cells with High Flexibility. *Nat. Commun.* **2012**, *3*, 770.

(37) Burke, D. J.; Lipomi, D. J. Green Chemistry for Organic Solar Cells. *Energy Environ. Sci.* **2013**, *6*, 2053–2066.

(38) http://www.infomine.com/investment/metal-prices/copper/.

(39) Geological Survey, U. S. *Metal Prices in the United States Through 2010*; 2012.

(40) Alharbi, F.; Bass, J. D.; Salhi, A.; Alyamani, A.; Kim, H.-C.; Miller, R. D. Abundant Non-Toxic Materials for Thin FIlm Solar Cells.pd. *Renew. Energ.* **2011**, *36*, 2753–2758.

(41) Linder, V.; Gates, B. D.; Ryan, D.; Parviz, B. a; Whitesides, G. M. Water-Soluble Sacrificial Layers for Surface Micromachining. *Small* **2005**, *1*, 730–736.

(42) Winkleman, A.; Perez-Castillejos, R.; Lahav, M.; Narovlyansky, M.; Rodriguez, L. N. J.; Whitesides, G. M. Patterning Micron-Sized Features in a Cross-Linked Poly(acrylic Acid) Film by a Wet Etching Process. *Soft Matter* **2007**, *3*, 108–116.

(43) http://www.alibaba.com/trade/search?fsb=y&IndexArea=product_en&CatId=&SearchText=polyacrylic+acid.

(44) Garnett, E. C.; Cai, W.; Cha, J. J.; Mahmood, F.; Connor, S. T.; Greyson Christoforo, M.; Cui, Y.; McGehee, M. D.; Brongersma, M. L. Self-Limited Plasmonic Welding of Silver Nanowire Junctions. *Nat. Mater.* **2012**, *11*, 241–249.

(45) Catrysse, P. B.; Fan, S. Nanopatterned Metallic Films for Use as Transparent Conductive Electrodes in Optoelectronic Devices. *Nano Lett.* **2010**, *10*, 2944–2949.

(46) http://www.alibaba.com/trade/search?fsb=y&IndexArea=product_en&CatId=&SearchText=metallized+bopet.

(47) Lo, C.-Y.; Hiitola-Keinänen, J.; Huttunen, O.-H.; Petäjä, J.; Hast, J.; Maaninen, A.; Kopola, H.; Fujita, H.; Toshiyoshi, H. Novel Roll-to-Roll Lift-off Patterned Active-Matrix Display on Flexible Polymer Substrate. *Microelectron. Engin.* **2009**, *86*, 979–983.

(48) Chun, K.-Y.; Oh, Y.; Rho, J.; Ahn, J.-H.; Kim, Y.-J.; Choi, H. R.; Baik, S. Highly Conductive, Printable and Stretchable Composite Films of Carbon Nanotubes and Silver. *Nat. Nanotechnol.* **2010**, *5*, 853–857.

(49) Lacour, S. P.; Chan, D.; Wagner, S.; Li, T.; Suo, Z. Mechanisms of Reversible Stretchability of Thin Metal Films on Elastomeric Substrates. *Appl. Phys. Lett.* **2006**, *88*, 204103.

(50) Alaca, B. E.; Ozcan, C.; Anlas, G. Deterministic Assembly of Channeling Cracks as a Tool for Nanofabrication. *Nanotechnol.* **2010**, *21*, 055301.

(51) Elbahri, M.; Jebril, S.; Wille, S.; Adelung, R. Simple Ways to Complex Nanowires and Their Application. *Adv. Solid State Phys.* **2009**, *48*, 27–38.

(52) Li, G.; Zhu, R.; Yang, Y. Polymer Solar Cells. *Nat. Photonics* **2012**, *6*, 153–161.

(53) Pasquier, A. Du; Miller, S.; Chhowalla, M. On the Use of Ga–In Eutectic and Halogen Light Source for Testing P3HT–PCBM Organic Solar Cells. *Sol. Energy Mater. Sol. Cells* **2006**, *90*, 1828–1839.

(54) Na, S.-I.; Wang, G.; Kim, S.-S.; Kim, T.-W.; Oh, S.-H.; Yu, B.-K.; Lee, T.; Kim, D.-Y. Evolution of Nanomorphology and Anisotropic Conductivity in Solvent-Modified PEDOT:PSS Films for Polymeric Anodes of Polymer Solar Cells. *J. Mater. Chem.* **2009**, *19*, 9045–9053.

(55) Lipomi, D. J.; Tee, B. C.-K.; Vosgueritchian, M.; Bao, Z. Stretchable Organic Solar Cells. *Adv. Mater.* **2011**, *23*, 1771–1775.

(56) Lipomi, D. J.; Lee, J. A.; Vosgueritchian, M.; Tee, B. C.; Bolander, J. A.; Bao, Z. Electronic Properties of Transparent Conductive Films of PEDOT:PSS on Stretchable Substrates. *Chem. Mater.* **2012**, *24*, 373–382.

(57) De, S.; Higgins, T. M.; Lyons, P. E.; Doherty, E. M.; Nirmalraj, P. N.; Blau, W. J.; Boland, J. J.; Coleman, J. N. Silver Nanowire Networks as Flexible, Transparent, Conducting Films: Extremely High DC to Optical Conductivity Ratios. *ACS Nano* **2009**, *3*, 1767–1774.

(58) Bae, S.; Kim, H.; Lee, Y.; Xu, X.; Park, J.-S.; Zheng, Y.; Balakrishnan, J.; Lei, T.; Kim, H. R.; Song, Y. Il; Kim, Y.-J.; Kim, K. S.; Özyilmaz, B.; Ahn, J.-H.; Hong, B. H.; Iijima, S. Roll-to-Roll Production of 30-Inch Graphene Films for Transparent Electrodes. *Nat. Nanotechnol.* **2010**, *5*, 574–578.

(59) Chen, C.-S.; Breslauer, D. N.; Luna, J. I.; Grimes, A.; Chin, W.-C.; Lee, L. P.; Khine, M. Shrinky-Dink Microfluidics: 3D Polystyrene Chips. *Lab Chip* **2008**, *8*, 622–624.

(60) Grimes, A.; Breslauer, D. N.; Long, M.; Pegan, J.; Lee, L. P.; Khine, M. Shrinky-Dink Microfluidics: Rapid Generation of Deep and Rounded Patterns. *Lab Chip* **2008**, *8*, 170–172.

(61) Martinez, A. W.; Phillips, S. T.; Whitesides, G. M.; Carrilho, E. Diagnostics for the Developing World: Microfluidic Paper-Based Analytical Devices. *Anal. Chem.* **2010**, *82*, 3–10.

(62) Carrilho, E.; Martinez, A. W.; Whitesides, G. M. Understanding Wax Printing: A Simple Micropatterning Process for Paper-Based Microfluidics. *Anal. Chem.* **2009**, *81*, 7091–7095.

(63) Hrehorova, E.; Rebros, M.; Pekarovicova, A.; Bazuin, B.; Ranganathan, A.; Garner, S.; Merz, G.; Tosch, J.; Boudreau, R. Gravure Printing of Conductive Inks on Glass Substrates for Applications in Printed Electronics. *J. Disp. Technol.* **2011**, *7*, 318–324.